MULTISCALE MODELING AND EXPERIMENTAL STUDIES ON BIO-OIL UPGRADATION

A Thesis Submitted in Partial Fulfillment of the

Requirements for the Degree of

Doctor of Philosophy

by

Anand Bharti

Department of Chemical Engineering

Indian Institute of Technology Guwahati, Guwahati, India

APRIL, 2017

CERTIFICATE

It is certified that the work contained in this thesis entitled **"Multiscale Modeling and Experimental Studies on Bio-oil Upgradation"**, by Anand Bharti, has been carried out under my supervision and that this work has not been submitted elsewhere for a degree.

April 2017
IIT Guwahati

Dr. Tamal Banerjee
Professor
Department of Chemical Engineering
Indian Institute of Technology Guwahati

ACKNOWLEDGEMENTS

I would like to thank all the people who contributed in some way to the work described in this thesis and supported me to complete my PhD.

First and foremost I offer my sincerest gratitude to my PhD supervisor, **Dr. Tamal Banerjee**, for giving me opportunity to work in a very fascinating area of research. I am very grateful to Dr. Tamal Banerjee for his continuous guidance, important advices, stimulating discussions and most importantly allowing me the freedom to work in my own way. It was really an honour to work under him.

I would like to thank my Doctoral Committee members, **Dr. Vaibhav V. Goud** and **Dr. Animes Kumar Golder**, Department of Chemical Engineering and **Dr. Padma Kumar Padmanabhan**, Department of Physics, for their valuable suggestions which made the thesis successful.

I am indebted to **Dr. Kaustubha Mohanty, Dr. A K Dasmahapatra, Dr. Anugrah Singh and Dr. Pankaj Tiwari** for their research oriented teaching during my course work which helped me during my PhD. I also thank **Dr. Bishnupada Mandal**, Head, Department of Chemical Engineering, for his administrative support. Furthermore, I would like to thank other Faculty and Staff members of Department of Chemical Engineering for their valuable support during my research.

I am grateful to Central Instrument Facility, IITG for providing me the necessary support for sample analysis using Nuclear Magnetic Resonance (NMR) Spectrometer. I am particulary thankful to **Dr. G. Krishnamoorthy** (Head of the Central Instruments Facility) and **Mr. Chandan Borgohain** (Technical officer, NMR) who helped me in operating 600-MHZ NMR. I am also grateful to Analytical Laboratory, department of chemical engineering for the necessary support for various sample analysis.

My sincere thanks to **Ms. Prerna** (B.Tech, BIT Mesra) and **Mr. Abhigyan Malviya** (B.Tech, IITG). Ms. Prerna helped me in developing code for Cuckoo Search and PC-SAFT EoS while Mr. Abhigyan Malviya helped me in Monte Carlo Simulations and PC-SAFT EoS.

I deeply acknowledge my research group members **Dr. Dharamashibhai V. Rabari, Ms. Sanjukta Bhoi, Ms. Basudhrity Banerjee, Mr. Mood Mohan, Ms. Reema Biswas, Mr. Papu Kumar Naik, Mr. Debashis Kundu, Mr. Pyarimohan Dehuri, Mr. Rupesh Verma, Ms. Upasana Mahanta, Ms. Tooba Fatma, Mr. Sarvesh Namdeo, Mr. Harshit Mittal and Mr. Dhruv Gupta** for providing a co-operative research environment.

My sincere thanks to friends **Mr. Kishant Kumar, Mr. Binay Deogam, Mr. Badri Vishal, Mr. Jitendra Singh Rawat, Mr. Ranjeet Kumar Mishra, Mr. Abhishek Shukla, Mr. Proloy Das, Mr. Bikash Bindu, Mr. Kulbhusan Samal** and many more for making my stay at IIT Guwahati memorable.

Above all, I would like to thank my **late father, mother, brother, sisters as well as Dr. Tamal Banerjee's family** for their love and support which kept my morale high during the PhD. Finally, my wife **Sapna** and daughter **Saanvi** deserve a special mention for their love and persistent confidence in me.

I dedicate this thesis to *My Family*.

Anand Bharti

SYNOPSIS

Changing global climate and depletion of fossil resources are the major issues before the current generation. Consequently, the development of alternative renewable energy resources has been intensely promoted. Compared to other renewable energy sources, biomass has the potential to replace a large fraction of fossil fuels as feedstocks and thus capable to cater the energy, chemicals and materials requirement of mankind. The manufacturing facilities that produce biofuels and bio-chemicals from various biomass feedstock are called biorefineries and conceptually, this is analogous to current petroleum refinery that produces fuels and chemicals from crude oil. In order to convert biomass into valuable products within a biorefinery approach, several processes must be applied. Among them fast pyrolysis is a thermo-chemical process for the production of liquid fuel and chemicals from biomass. Bio-oil is main product of fast pyrolysis and depending on the biomass source, oxygen content remains in the range of 35-40 wt% due to several oxygen-containing components. A higher oxygen content is responsible for a lower heating value of bio-oil. But at the same time, high concentration of oxygen containing compounds make bio-oil a good raw material for the isolation of various chemicals which are attractive in the commercial sense. The first step in the recovery of chemicals from bio-oil is primary fractionation by water where bio-oil is separated into less complex fractions and then using Liquid-liquid extraction targeted chemicals can be isolated from the phases derived from bio-oil.

This thesis mainly focusses on the extraction of bio-chemicals such as acetic acid, acetol and furfural due to its large composition in bio-oil. Accurate experimental data and reliable thermodynamic models are basic requirements for such optimized extraction process design. These have been achieved through multicomponent Liquid-liquid Equilibria measurements and subsequent validation through multiscale strategies such as Perturbed-Chain Statistical Associating Fluid Theory (PC-SAFT) and Monte Carlo Simulation.

Chapter 1 gives a brief introduction on biomass conversion processes, pyrolysis, bio-oil, various routes for the upgradation of bio-oil and objective of the thesis.

The first step in the recovery of chemicals from bio-oil is extraction based separation process where water is used as a solvent. Therefore, **Chapter 2** theoretically investigates the solubility of bio-chemicals (Glycolaldehyde, Furfural, Acetic acid, Furanone) in aqueous phase in terms of intermolecular interaction energy using supermolecule approach. Initially, Stable equilibrium structures of 1:1 complexes of water with glycolaldehyde, furfural, acetic acid and furanone in gas phase were determined by second-order Møller-Plesset perturbation theory (MP2) with 6-311++G (d, p) basis set. It has been found that the most stable structure of Glycolaldehyde and Acetic acid made a cyclic complex with water and were bonded together by two H-bonds which make them unique as compared to Furanone and Furfural. Afterwards, the interaction energy is partitioned into its chemical origins (e.g. electrostatics, exchange-repulsion, polarization and charge transfer) using variational based Localized Molecular Orbital - Energy Decomposition Analysis (LMO-EDA) scheme. Finally, interaction energy is compared with available experimental solubility data. It has been demonstrated that the computed interaction energy of the chosen molecules with water predicts the correct trend of the experimentally reported solubility parameters of the corresponding molecules. In terms of solubility in water, the compounds follow the trend: Acetic acid > Glycolaldehyde > Furanone > Furfural which is the same trend as obtained experimentally from pine-derived pyrolysis oil.

The second step is the selection of potential solvent for the extraction of bio-chemicals

from aqueous phase as generated from Chapter 2. Thus, **Chapter 3** describes the experimental study on measurement of Liquid-liquid Equilibria (LLE) data at 298.15 K and at atmospheric pressure for Ionic liquids namely 1-alkyl-3-methylimidazolium bis-(trifluoromethylsulfonyl) imide ([EMIM][Tf_2N] and [BMIM][Tf_2N]) (E: Ethyl; B: Butyl) and organic solvents (ethyl acetate, *n*-propyl acetate, *n*-butyl acetate, chloroform) for extraction of acetic acid, acetol and furfural from aqueous phase. The composition is calculated using 1H NMR spectroscopy. Regeneration and reusability of ionic liquids is also reported. LLE data is then compared with available literature data for commonly used organic solvents in terms of distribution co-efficient,selectivity and solvent loss, so as to evaluate the extraction capacity of selected solvents. Considering these aspects, amyl acetate, isophorone, and [BMIM][Tf_2N] are found to be the potential solvents for the extraction of acetic acid from aqueous solution whereas [BMIM][Tf_2N] and propyl acetate are potential solvents for furfural extraction. For acetol extraction, [EMIM][Tf_2N], [BMIM][Tf_2N] and chloroform are the preferred solvents.

The third step is selection of thermodynamic models for conceptual process design of the entire extraction/regeneration processes. The next three chapters, **Chapter 4** - correlative approach, **Chapter 5** - predictive approach and **Chapter 6** - particle based simulation approach, are devoted to three different thermodynamic approaches.

Chapter 4 discusses the applicability of Cuckoo search algorithm, which is a nature inspired stochastic optimization algorithm, for estimation of binary interaction parameters of excess Gibbs free energy models such as UNIversal QUAsi-Chemical (UNIQUAC) and nonrandom two-liquid (NRTL) for liquid-liquid ternary systems involving 39 ternary systems which includes 32 IL based systems and 7 organic solvent based systems. It has been found that population size of 20 is sufficient to satisfactorily predict the LLE with high accuracy. Success rate (%SR) analysis suggested that the performance of CS mainly depends on the type of ILs and LLE systems. Specially, ternary systems containing imidazolium ILs appeared to be most challenging for parameter estimation with NRTL model. RMSD results are extremely encouraging, with deviations

in phase compositions 0.0053 (UNIQUAC) and 0.0072 (NRTL) which is 63% and 45% better than literature reported global value of 0.0145 and 0.0131 for 371 tie-lines. Three ternary systems and one quinary system were selected from literature to compare the capability of CS algorithm with genetic algorithm (GA) and particle swarm optimization (PSO) algorithm. The global %RMSD value obtained with CS algorithm was 0.14-0.85% compared to 1.0-2.0% with GA and PSO. This shows a higher efficiency for the CS algorithm in solving global optimization problems involved in the thermodynamic modeling of multicomponent systems.

In **Chapter 5**, Perturbed-chain statistical associating fluid theory (PC-SAFT) EoS which is primarily based on statistical thermodynamics, was used to model the polar and associating biochemical LLE ternary systems as studied in Chapter 3. Ethyl acetate, *n*-propyl acetate, *n*-butyl acetate and chloroform were modeled as non-associating molecules. Acetic acid, furfural, acetol, water, [EMIM][Tf_2N] and [BMIM][Tf_2N] were modeled as self-associating molecules with two association sites. Only pure component parameters were used for the prediction of ternary LLE. Binary interaction parameters k_{ij} was kept zero to keep the predictive nature of the EoS. The result shows that %RMSD for acetic acid and furfural based systems are 5.33% and 9.74% respectively. The results greatly improved with the consideration of binary interaction parameters (k_{ij}). In case of acetic acid system, %RMSD reduced to 2.43% whereas in case of furfural %RMSD reduced to 5.30%. For acetol - ionic liquids based systems, %RMSD are in the range of 5.5-8.6% which is better than organic solvent based systems which are in the range of 10.7-14.1%. The predictions were further performed with 4-association site for water and acetol; and 1-association site model for acetates with the incorporation of the binary interaction parameters (k_{ij}) between water and acetol. As a result, the overall RMSD (%) for acetate based systems reduced from 12.52% to 5.52%. This confirms the ability of PC-SAFT to model the ternary LLE systems based on pure component and binary system data.

In **Chapter 6**, particle based Gibbs Ensemble Monte Carlo molecular simulations employing the coupled-decoupled configurational-bias Monte-Carlo algorithm (CBMC)

were performed in the isobaric-isothermal (NPT) ensembles to determine the ability and limitations of the Transferable Potentials for Phase Equilibria (United-Atom) and TIP4P force fields in predicting phase equilibrium for three ternary systems: ethyl acetate-acetic acid-water, *n*-butyl acetate-acetic acid-water and [BMIM][Tf_2N]-acetic acid-water at ambient pressure. In this work, a three-box set-up, which are thermodynamically connected, is used for the NPT GEMC simulations. Two boxes are used to model the liquid phases, and the third box, filled with helium atoms, acts as transfer medium. Chemical equilibrium was maintained by transferring particles between the phases, while mechanical equilibrium with a constant external pressure bath was maintained by performing volume moves on each of the simulation boxes individually excluding the transfer box. The remaining degrees of freedom were sampled using translational, rotational, and conformational moves. It was found that the simulations agreed favorably with the experimental data for all the systems over the entire composition range and TIP4P water models may be used in conjunction with the TraPPE model to study the ternary systems.

n-Octanol is a new promising fuel which is considered as an alternative to conventional diesel. It has generated a lot of interest as recently new pathways were described to obtain *n*-Octanol from biomass or bio-oil. In **Chapter 7**, Reactive molecular dynamics (ReaxFF MD) simulation of *n*-Octanol has been performed. In order to understand the combustion characteristics of *n*-Octanol, reactive molecular dynamics (ReaxFF MD) simulation of *n*-Octanol have been performed at various temperatures (2000K-4000K) with equivalence ratios ranging from 0.5 to 2.0. From the ReaxFF MD simulations, we have found that the oxidation of *n*-Octanol is initiated mainly through two routes, (1) H-abstraction reaction by oxygen molecules and (2) the cleavage of C-C bond. It has been observed that rate of formation of CO and CO_2 are almost similar at low temperature (3000 K). With higher temperature the rate of formation of CO is more than that of CO_2. The major intermediate products found in ReaxFF MD simulations are ethylene followed by formaldehyde. A detailed reaction mechanism has been proposed for the formation of major intermediates (ethylene and formaldehyde) and final products (CO

and CO_2). Reaction mechanisms reveal that intermediates are mainly consumed by the build-up of hydroxyl and hydroperoxyl radicals. It was observed that the CO and CO_2 formation from formaldehyde and ethylene starts with the attack of molecular oxygen or hydroxyl radical or hemolytic O-H bond cleavage. Overall, a good qualitative agreement with the available experimental data in terms of product distribution has been found. The results indicate that ReaxFF MD simulations can give a detailed description of the reaction mechanism and product distribution for the combustion for oxygenated fuel such as *n*-octanol.

Chapter 8 summarizes the important findings of the present work and suggest future directions of this work.

In Summary, the thesis aims to study extraction based separation processes with the help of quantum chemical calculations, molecular simulations (Monte Carlo and ReaxFF MD), theoretical approaches (PC-SAFT EoS), optimization and experiments. The outcome of this research work will enhance the basic understanding of the extraction based processes.

Contents

List of Figures

List of Tables

Nomenclature

Abbreviations

AARD	Absolute average relative deviation
CBMC	Configurational-bias Monte Carlo
COSMO-SAC	COnductor-like Screening MOdel-Segment Activity Co-efficient
CS	Cuckoo Search
EoS	Equation of state
GA	Genetic Algorithm
GEMC	Gibbs Ensemble Monte Carlo
INT	Interaction Energy
LLE	Liquid-liquid Equilibria
LMO-EDA	Localized molecular Orbital - Energy Decomposition Analysis

MC	Monte Carlo
MCS	Monte Carlo Steps
NBO	Natural Bond Order
NCI	Non-Covalent Interactions
NMR	Nuclear Magnetic Resonance
NRTL	Non-random Two liquid
PC-SAFT	Perturbed Chain - Statistical Associating Fluid Theory
PR	Peng-Robinson
PSO	Particle Swarm Optimization
ReaxFF	Reactive Force Field
RMSD	Root Mean Square Deviation
SAPT	Symmetry-adapted perturbation theory
SPC	Simple point charge
SRK	Soave-Redlich-Kwong
TraPPE	Transferable Potentials for Phase Equilibria
UNIQUAC	UNIversal QUAsi-Chemical
VLE	Vapor-liquid Equilibria

Greek/Roman Symbols

β	Distribution coefficient
$\Delta^{A_iB_j}$	Strength of interaction between site A on molecule *i* and site B on molecule *j*
ϵ/k_B	Segment energy parameter
$\epsilon^{A_iB_i}/k$	Association energy
γ	Activity coefficient
$\kappa^{A_iB_i}$	Association volume
ω	acentric factor
Φ	Equivalence Ratio
ϕ	Fugacity coefficient
σ	Segment diameter
g_{ij}^{hs}	Radial pair distribution function for hard-sphere fluid

Ionic Liquids

[BMIM][BF_4]	1-butyl-3-methylimidazolium tetrafluoroborate
[BMIM][Tf_2N]	1-butyl-3-methylimidazolium bis(trifluoromethylsulfonyl) imide
[BMIM][TfO]	1-butyl-3-methylimidazolium trifluoromethanesulfonate

[EMIM][ESO_4]	1-ethyl-3-methylimidazolium Ethylsulfate
[EMIM][TfO]	1-ethyl-3-methylimidazolium trifluoromethanesulfonate
[HMIM][BF_4]	1-hexyl-3-methylimidazolium tetrafluoroborate
[HMIM][PF_6]	1-hexyl-3-methylimidazolium hexafluorophosphate
[OMIM][BF_4]	1-octyl-3-methylimidazolium tetrafluoroborate
[OMIM][Cl]	1-octyl-3-methylimidazolium chloride
[TDTHP][DCA]	Trihexyl(tetradecyl)-phosphonium dicyanamide
[TDTHP][DEC]	Trihexyl(tetradecyl)-phosphonium decanoate
[TDTHP][Phosph]	Trihexyl(tetradecyl)-phosphonium bis(2,4,4-trimethylpentyl) phosphinate

Others

E	Extract
k_{ij}	binary interaction parameters
m	Number of segments
R	Raffinate
x_{solute}	Mole fraction of solute
x_w	Mole fraction of water

Z	Compressibility factor
q	UNIQUAC surface area parameter
r	UNIQUAC volume parameter
S	Selectivity

CHAPTER 1

Introduction

1.1 Introduction

For over ten thousand years, humans have used biomass as primary energy source for their energy needs such as for cooking and space heating. Industrialization and mid-18^{th} century, changed the primary energy use from renewable resources to sources with a much higher energy density, such as coal and petroleum. At the same time, rapid technical progress made the industrial use of petroleum and coal economical. As a result over the past century, modern society depend heavily on fossil resources. Petroleum oil, natural gas and coal remained the world's leading fuel with 86.0% of global energy consumption in 2015 (Figure 1.1) [BP, 2016]. However the natural reserves of these fossil fuels are concentrated in a few countries and also are not renewable. At the same time, excessive consumption of fossil fuels has increased greenhouse gas emissions thereby posing a severe threat to the environment. Figure 1.2 shows an increased world carbon dioxide emission [BP, 2016]. With increasing concerns, a need for alternate energy sources is felt. These energy sources should be renewable, carbon neutral and should have the potential to replace the fossil fuels.

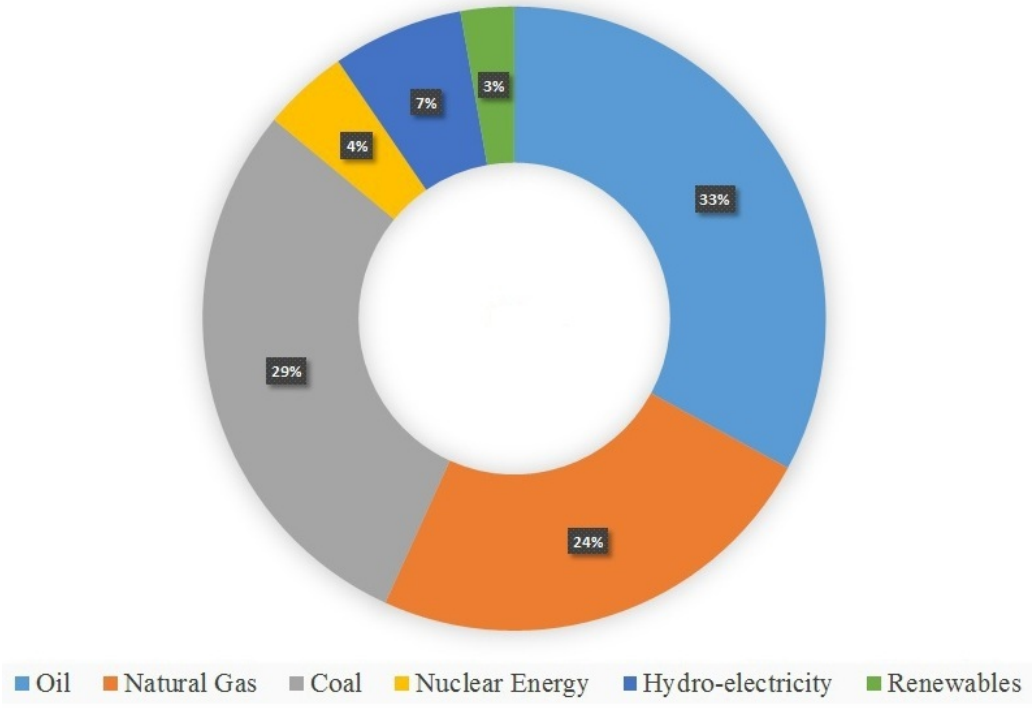

Figure 1.1.: World Energy Consumption-2015

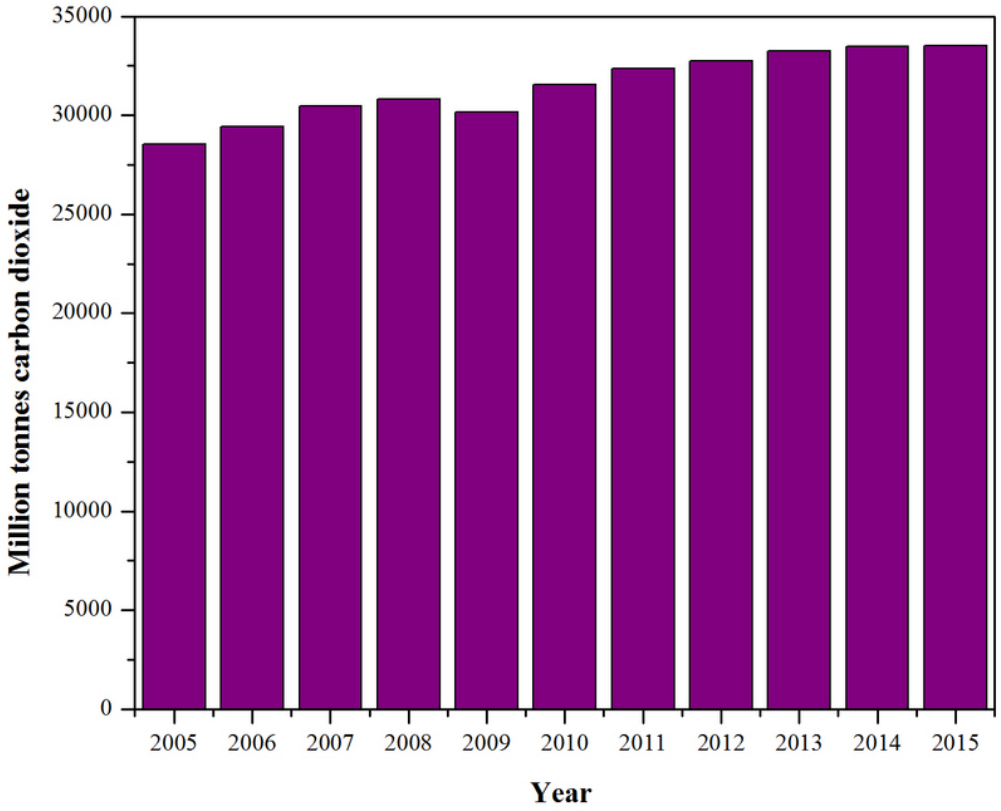

Figure 1.2.: World Carbon dioxide emmission (In Million metric tonnes)

The various alternative resources are solar, wind, hydroelectric, geothermal and biomass. Of these, biomass is the only sustainable resource for the production of fuels, chemicals and materials. Therefore, research has focusses on lignocellulosic biomass resources to meet a significant portion of energy demand [Bozell and Petersen, 2010, Gallezot, 2012, Zakzeski et al., 2010, Sims et al., 2010, Demirbas, 2009, Demirbas, 2011, Naik et al., 2010, Nigam and Singh, 2011].

1.2 Biomass conversion processes

Biomass can be converted to more useful and valuable energy forms via thermal, biochemical and mechanical processes as summarized in Figure 1.3 [Crocker, 2011]. Biological conversion is a relatively slow process and usually gives single or specific products such as ethanol or biogas. On the other side, thermal conversion gives multiple products in very short time. There are three main thermal processes available for converting biomass to a more useful form: pyrolysis, gasification and combustion as

summarized in Figure 1.4 [Crocker, 2011]. Combustion is the thermal conversion of biomass using an excess quantity of air, where the components present in the biomass are converted to their respective oxidized form. It involves the rapid oxidation of fuel to obtain energy in the form of heat which can be used for process heat or for the production of steam. Gasification converts solid biomass into syngas (CO + H_2) which can be further converted into alkanes (Fischer-Tropsch synthesis), Methanol (catalytic process) and hydrogen (water-gas shift reaction). Pyrolysis is known to convert solid biomass into liquid, gaseous and solid fraction by heating in the absence of air. The main goal of pyrolysis is to produce liquid as the primary product. The pyrolysis oil on subsequent processing can be used for heat/power generation, as biofuels and for chemical production. In comparison to combustion and gasification, pyrolysis is versatile in nature as it generates wide range of products.

1.3 Pyrolysis

Pyrolysis is the thermal decomposition of biomass, which occurs in the absence of oxygen or when significantly less oxygen is supplied than needed for complete combustion. Based on process conditions and vapor residence time, there are many variants of pyrolysis which are summarized in Table 1.1 [Crocker, 2011]. Lower process temperatures and longer vapor residence times favor the production of charcoal. High temperatures and longer residence times increase biomass conversion to gas while moderate temperatures and short vapor residence time are optimum for producing liquids. This shows considerable flexibility that can be achieved by changing process conditions during pyrolysis [Mohan et al., 2006, Bridgwater, 2012].

Fast pyrolysis for liquid production is of particular interest as liquid can be stored and transported and then subsequently used for energy and chemicals production. Fast pyrolysis is a process in which biomass is rapidly heated to high temperatures in the absence of oxygen. As a result, biomass decomposes to generate mostly vapors, aerosols and some charcoal. After cooling and condensation, a dark brown liquid, bio-oil, is formed. Thus the essential features of a fast pyrolysis process for producing liquids are:

(a) Very high heating and heat transfer rates,

(b) Controlled pyrolysis reaction temperature of $\sim$ 500 °C,

(c) Shorter vapor residence times of typically less than 2 s, and

(d) Rapid cooling of the pyrolysis vapours to give bio-oil.

The main product, bio-oil, is obtained in yields of up to 75 wt% on dry-feed basis, together with byproduct char and gas which can be used within the process, so that there are no waste streams [Mohan et al., 2006, Bridgwater, 2012, Crocker, 2011].

Table 1.1.: Typical product yields obtained by different modes of pyrolysis of wood [1]

Mode	Conditions	Liquid	Solid	Gas
Fast	$\sim$ 500 °C, short hot vapour residence time, $\sim$ 2 s	75%	12%	13%
Intermediate	$\sim$ 500 °C, hot vapour residence time, $\sim$ 10-30 s	50% (in 2-phases)	25%	25%
Carbonization	$\sim$ 400 °C, long vapour residence time, hours to days	30%	35%	35%
Gasification	$\sim$ 750-900 °C	5%	10%	85%
Torrefaction	$\sim$ 290 °C, solids residence time $\sim$ 10-60 min	0%	85%	20%

[1] [Crocker, 2011]

1.4 Bio-oil

Bio-oils are dark brown, free-flowing organic liquids that are comprised of highly oxygenated compounds. The important characteristics of bio-oil are summarized in Table 1.2. Bio-oil have a substantial amount of carboxylic acids which gives a low pH of 2-3. The low pH makes bio-oil corrosive. In addition, the strong acidity makes them extremely unstable. Bio-oil has a content of water as high as 15-30 wt%. The presence of water lowers the heating value, resulting in a lower flame temperature. Depending on the biomass and severity of the pyrolysis, the oxygen content of bio-oil is around

35-40 wt%. The high oxygen content leads to lower heating value and immiscibility with hydrocarbons. For effective use, bio-oil needs to be separated and concentrated into the compounds of similar polarities. Further for increasing the heating value for fuel use, the oxygen content must be lowered. To achieve these conditions, solvent fractionation and de-oxygenation are practiced to upgrade the bio-oil mixture [Mohan et al., 2006, Bridgwater, 2012].

Table 1.2.: Typical properties of wood derived bio-oil

Physical property	Bio-oil	Heavy fuel oil
Moisture content (wt%)	15-30	0.1
pH	2.5	-
Specific gravity	1.2	0.94
Elemental composition (wt%)		
C	54-58	85
H	5.5-7.0	11
O	35-40	1.0
N	0-0.2	0.3
HHV (MJ/Kg)	16-19	40
Viscosity, at 500 °C (cP)	40-100	180
Solids (wt%)	0.2-1.0	1
Distillation residue (wt%)	up to 50%	1

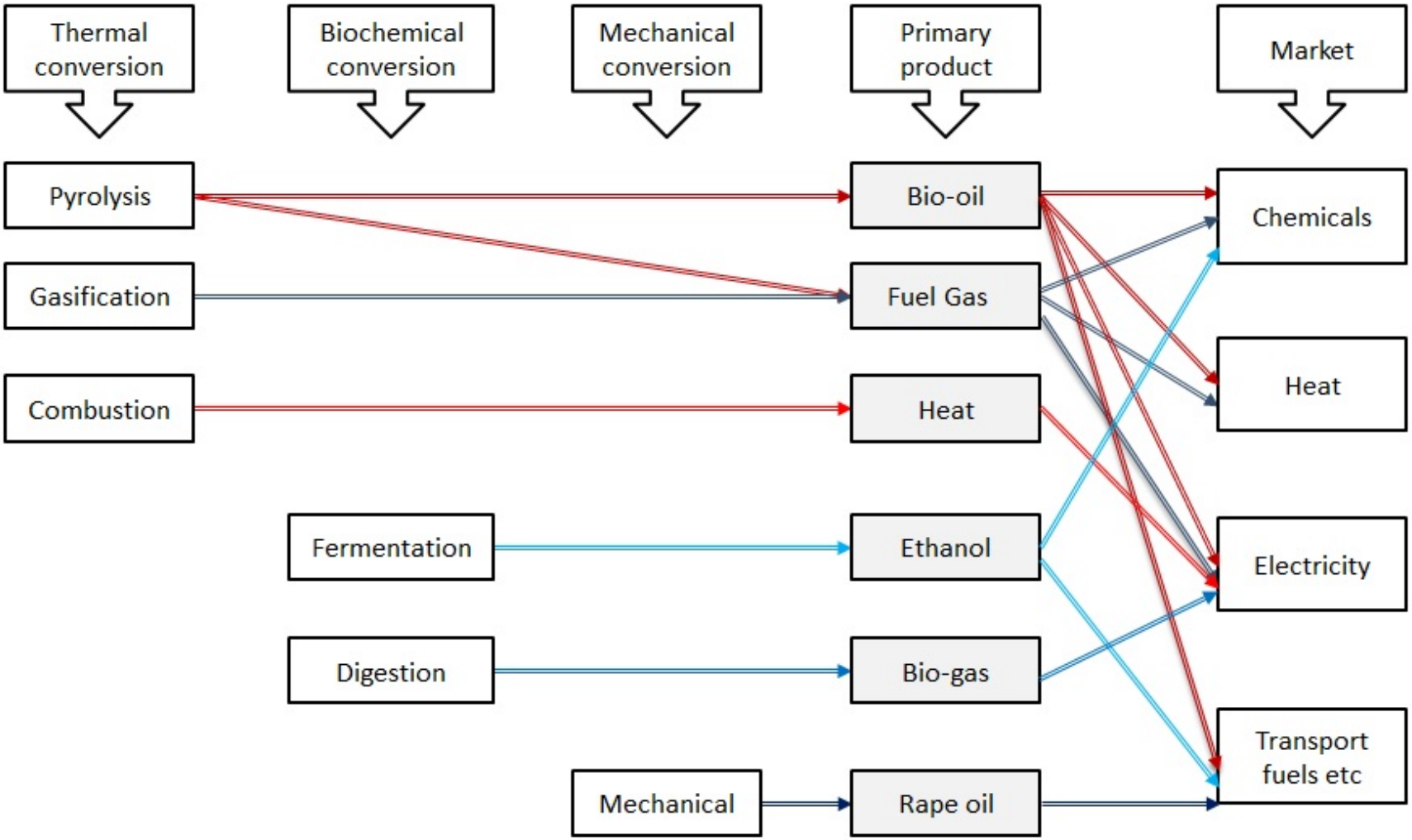

Figure 1.3.: Biomass Conversion processes, products and applications [Crocker, 2011]

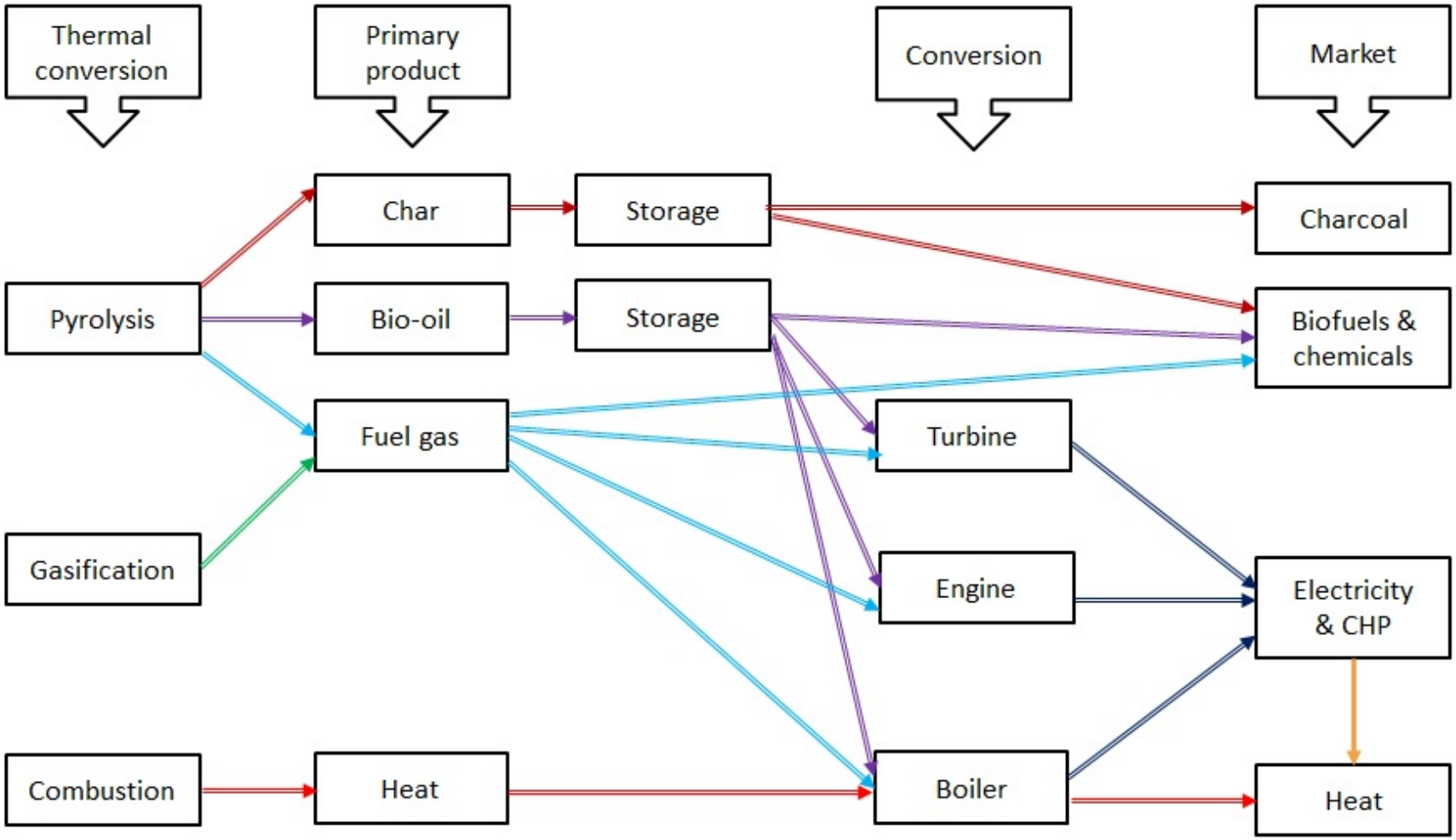

Figure 1.4.: Thermal conversion processes, products and applications [Crocker, 2011]

1.5 Upgradation of bio-oil

1.5.1. Catalytic upgrading of Bio-oil

Upgrading of bio-oil to a conventional transport fuel such as gasoline, diesel and kerosene requires full de-oxygenation. One promising option is to use bio-oil in the existing petroleum refinery. This process involves the co-feeding of bio-oil with petroleum feedstocks as shown in Figure 1.5. Petroleum refineries are already built, and use of this existing infrastructure for the production of biofuels requires little capital investment. Three options are available for using petroleum refineries to convert biomass-derived feedstocks into fuels and chemicals: 1) Fluid catalytic cracking (FCC), 2) Hydrotreating-hydrocracking, and 3) utilization of biomass-derived synthesis gas (syngas) or hydrogen. Catalytic cracking of bio-oils is regarded as a cheaper route which produces olefins and aromatics. In catalytic cracking, oxygenated molecules in bio-oil are catalytically decomposed to hydrocarbons with the removal of oxygen in the form of H_2O, CO, or CO_2. But, large amounts of coke (8-25 wt %) and poor quality of the fuels are big impediment to the process. In hydroprocessing, oxygen is removed as H_2O and CO_2 when bio-oil is hydrogenated in the presence of a catalyst. Hydro-treating of bio-oil produce diesel and gasoline range fuels, but the process needs superior techniques, complicated equipment's and excess cost due to severe process conditions (P = 150-200 bar; T= 300-400 °C).Source of hydrogen for Hydrotreating is also a big concern [Huber and Corma, 2007, Chheda et al., 2007].

1.5.2. Solvent Fractionation of Bio-oil

Bio-oil contains more than 100 oxygenated compounds. The compounds found in bio-oil have been classified into the following broad categories: Carboxylic acids, Esters, Alcohols, Ketones, Aldehydes, Oxygenates, Furans, Sugars and Phenolic compounds (Table 1.3) [Diebold, 2000]. This shows bio-oil is a good raw material for isolation of valuable chemicals. Chemicals are always attractive in the commercial sense due

to their much higher added value compared to fuels/energy products. This suggests a biorefinery concept in which optimum combinations of fuels and chemicals can be produced (Figure 1.6). In comparison to other energy sources, biomass is the only source which can be used for the mass production of chemicals [Budzianowski and Postawa, 2016, Maity, 2015a, Maity, 2015b, Parajuli et al., 2015, Kamm et al., 2006, Demirbas, 2009, Demirbas, 2011]. Acetic acid, hydroxyacetaldehyde, acetol, sugars, furans and phenolic compounds are the major chemicals present in the bio-oil. Among those abundant chemicals, this thesis mainly focusses on acetic acid, acetol and furfural due to its large composition in bio-oil mixtures.

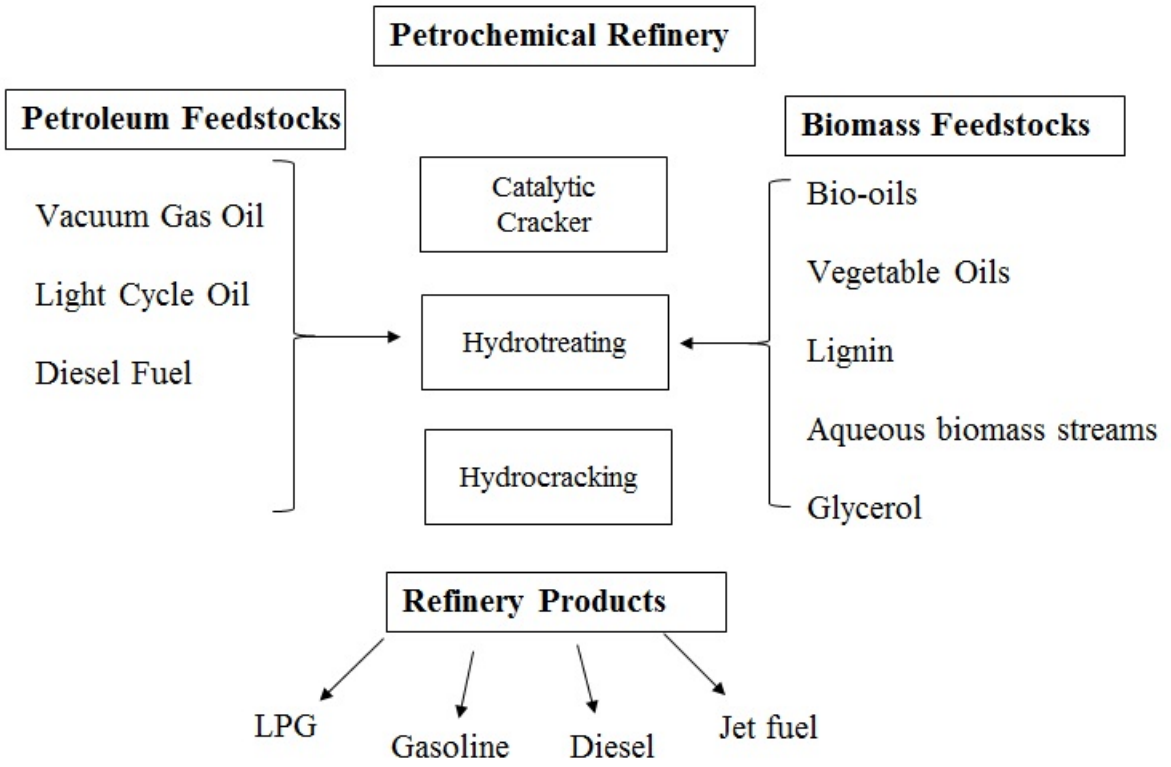

Figure 1.5.: Conversion of petroleum and biomass derived feed-stocks in a petroleum refinery [Huber and Corma, 2007]

Acetic acid is an important industrial product and the most produced acid in the world with production over eight million tons [Smejkal et al., 2005]. It is mainly used in the production of vinyl acetate monomer. Vinyl acetate is polymerised to polyvinyl acetate which are used as an adhesives or as polymers which are used for films and paints. Var-

ious esters of acetic acid such as ethyl acetate and propyl acetate are commonly used as solvents. Acetic anhydride is another product of acetic acid which is used for the conversion of cellulose to cellulose acetate and for the production of pharmaceuticals and agro-chemicals.

Acetol is another important organic material for chemical industry. It is used for the production of variety of chemical products such as propylene glycol and acrolein. Apart from it, it is also used in food industry to give aroma to foods, in cosmetic industry as skin tanning agent and in textile industry as a reduced dye [Mohamad et al., 2011]. Recent work of Li et al. [Li et al., 2013] and Albuquerque et al. [Albuquerque et al., 2015] have opened new pathways for the usage of hydroxyacetone as raw material for the production of diesel and lactic acid respectively. Li et al. [Li et al., 2013] have recently developed a new route for the synthesis of renewable diesel or jet fuel range branched alkanes by hydroxyalkylation-alkylation (HAA) of hydroxyacetone and 2-methylfuran followed by hydrodeoxygenation (HDO). Albuquerque et al. [Albuquerque et al., 2015] have reported the catalytic synthesis route for the production of lactic acid from hydroxyacetone aqueous solutions at atmospheric pressure. The conversion of hydroxyacetone to lactic acid is going to increase the usage of hydroxyacetone in near future. Lactic acid is an industrially important product with wide applications in food, pharmaceutical, cosmetic, leather, textile, and chemical industries. Currently, there is an increased demand for lactic acid as a feedstock for the production of biopolymer poly-lactic acid (PLA), which is a promising biodegradable, biocompatible, and environmentally friendly alternative to plastics derived from petrochemicals [Martinez et al., 2013, Inkinen et al., 2011, Datta and Henry, 2006, Abdel-Rahman et al., 2011].

Furfural is the promising value-added chemical which can be converted to chemicals, biofuels, and additives. Furfural alcohol is the most important chemical derived furfural, having a broad spectrum of applications. Furfural alcohol is primarily used for the production of resins for use as high-quality cores and moulds for metal casting in the foundry industry and as reactive solvent for phenolic resins. Further it is used for the synthesis of tetrahydrofurfuryl alcohol and pharmaceuticals [Mariscal et al., 2016].

The first step in the recovery of chemicals from bio-oil is primary fractionation where bio-oil is separated into less complex fractions [Sipila et al., 1998, Mohan et al., 2006, Vitasari et al., 2011]. Solvent extraction is a known potential fractionation method. Bio-oils are easily separated into an aqueous top phase and an organic bottom phase by adding water to bio-oil. Aqueous top phase mainly contains polar compounds such as acetic acid, acetol, while organic bottom phase contains lignin-containing fractions. Both phases can be further processed separately to extract value added chemicals.

Table 1.3.: Chemical composition of bio-oil (in wt%) [Diebold, 2000]

Acids	**low**	**high**	**Esters**	**low**	**high**	**Ketones**	**low**	**high**
Formic	0.3	9.1	Methyl formate	0.1	0.9	Acetone	2.8	2.8
Acetic	0.5	12.0	Butyrolactone	0.1	0.9	2-Butanone	0.3	0.9
Propanoic	0.1	1.8	others	0.3	1.4	Others	1.1	2.5
Hydroxyacetic	0.1	0.9	*total*	**0.5**	**3.2**	*total*	**4.2**	**6.2**
Others	0.9	2.6	**Alcohols**			**Guaiacols**		
total	**1.9**	**26.4**	Methanol	0.4	2.4	Isoeugenol	0.1	7.2
Aldehydes			Ethanol	0.6	1.4	Eugenol	0.1	2.3
Formaldehyde	0.1	3.3	Ethylene glycol	0.7	2.0	others	2.0	5.6
Acetaldehyde	0.1	8.5	*total*	**1.7**	**5.8**	*total*	**2.2**	**15.1**
Ethanedial	0.9	4.6	**Phenols**			**Syringols**		
2-Propenal	0.6	0.9	Phenol	0.1	3.8	2,6-DiOMe phenol	0.7	4.8
Others	0.6	1.0	2-Ethylphenol	0.1	1.3	Propyl syringol	0.1	1.5
total	**2.3**	**18.3**	Others	2.6	7.5	Syringaldehyde	0.1	1.5
Sugars			*total*	**2.8**	**12.6**	others	0.5	1.1
Levoglucosan	0.4	1.4	**Furans**			*total*	**1.4**	**8.9**
Glucose	0.4	1.3	Furfural alcohol	0.1	5.2	**Misc.**		
fructose	0.7	2.9	Furfural	0.1	1.1	Hydroxyacetaldehyde	0.9	13.0
D-xylose	0.1	1.4	2-Furanone	0.1	1.1	Acetol	0.7	7.4
Cellobiosan	0.6	3.2	Others	1.1	3.8	Others	1.6	5.4
Others	3.2	3.2	*total*	**1.4**	**11.2**	*total*	**3.2**	**25.8**
total	**5.4**	**13.4**						

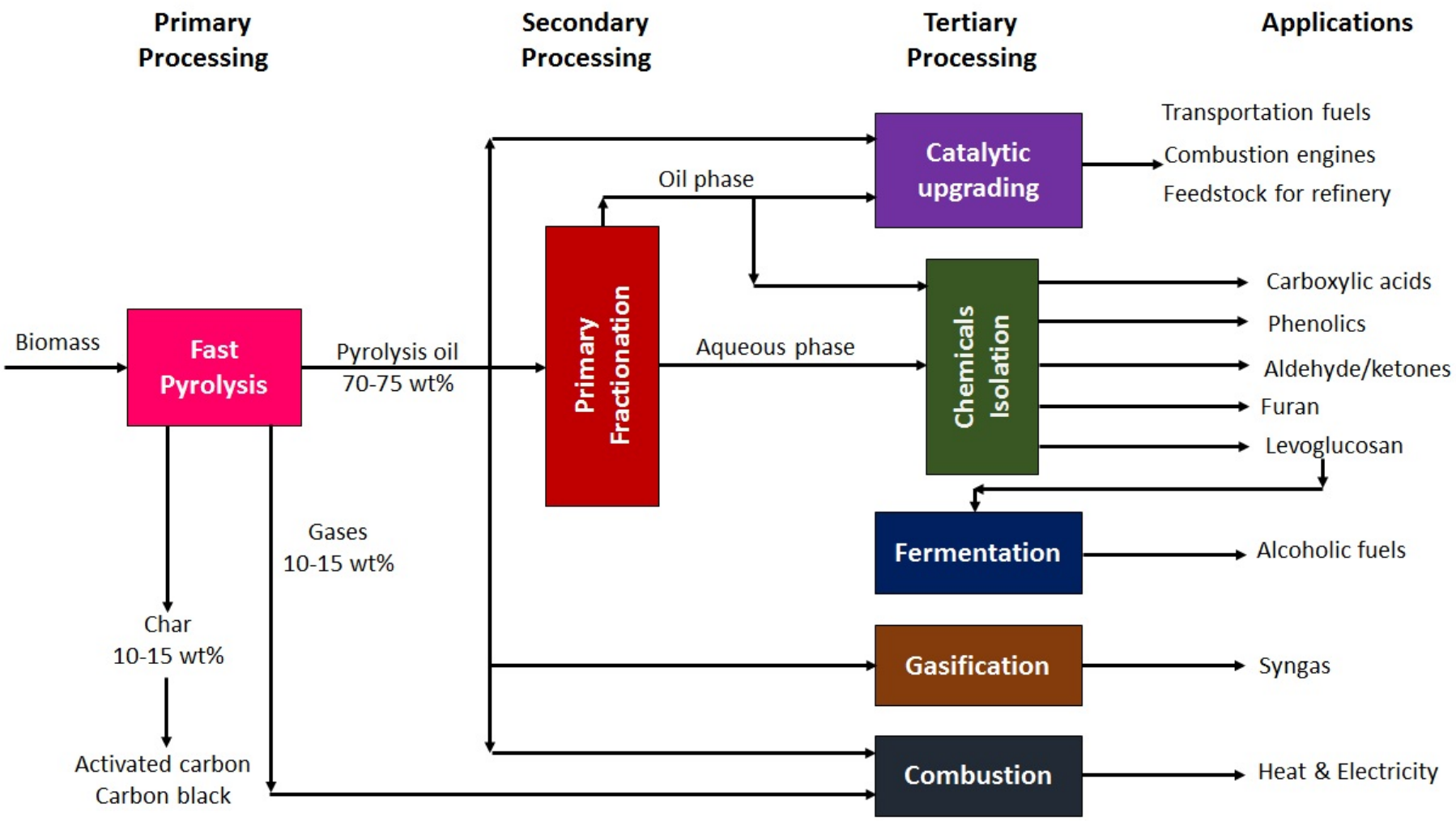

Figure 1.6.: Bio-oil based biorefinery

1.6 Objective of the Thesis

This research aims to study extraction-based separation process to isolate bio-chemicals from aqueous phase. Correct experimental data and reliable thermodynamic models are basic requirements for optimized process design. In this thesis, both these aspects are addressed. Schematic outline of the thesis is shown in Figure 1.7.

The first step in the recovery of chemicals from bio-oil is extraction based separation process where water is used as a solvent. Therefore, **Chapter 2** theoretically investigates the solubility of bio-oil chemicals in aqueous media in terms of intermolecular interaction energy using supermolecule approach. In addition, the interaction energy is partitioned into its chemical origins (e.g. electrostatics, exchange-repulsion, polarization and charge transfer) using variational based Localized molecular Orbital - Energy Decomposition Analysis (LMO-EDA) scheme. Finally interaction energy is compared with available experimental solubility data.

The second step is selection of solvent for extraction of bio-chemicals from aqueous phase generated from Step-1. Thus, **Chapter 3** describes the experimental study on measurement of Liquid-liquid Equilibria (LLE) data at 298.15 K and at atmospheric pressure for Ionic liquids and organic solvents for extraction of acetic acid, acetol and furfural from aqueous phase. The composition is calculated using ^{1}H NMR spectroscopy. Regeneration and reusability of ionic liquids is also reported. LLE data is then compared with available literature data for commonly used organic solvents in terms of distribution co-efficient and selectivity, so as to evaluate the extraction capacity of selected solvents.

The third step is selection of thermodynamic models for conceptual process design of the entire extraction/regeneration processes. The next three chapters, **Chapter 4** - correlative approach, **Chapter 5** - predictive approach and **Chapter 6** - particle based simulation approach, are devoted to three different thermodynamic approaches.

Chapter 4 discusses the applicability of Cuckoo search algorithm for estimation of binary interaction parameters from excess Gibbs free energy models such as NRTL and UNIQUAC regressed via experimental LLE data. In addition, performance of Cuckoo search is compared with Genetic algorithm (GA) and Particle Swarm Optimization (PSO) algorithm in solving global optimization problems involved in the thermodynamic modeling of multi-component systems.

Chapter 5 focuses on the modeling of polar and associating biochemical systems using Perturbed Chain - Statistical Associating Fluid Theory (PC-SAFT) equation of state. The PC-SAFT EoS is used to predict the phase equilibria of biochemical systems studied in chapter 3. We examine the manner in which different association schemes can be used to model the polar systems.

In **Chapter 6**, particle based Monte Carlo (MC) simulation is used to study the liquid-liquid phase equilibria. Gibbs Ensemble Monte Carlo simulation (GEMC) employing the configurational-bias Monte Carlo algorithm (CBMC) is performed in the isobaric-isothermal (NPT) ensemble. Existing force field parameters, Transferable Potentials for Phase Equilibria (TraPPE) and TIP4P, is used to determine its ability in predicting the phase equilibrium for acetic acid based ternary systems.

In **Chapter 7**, Reactive Molecular Dynamics (ReaxFF MD) is further carried out to understand the combustion characteristics of a potential biofuel, *n*-octanol. Simulation is carried out at temperatures ranging from 2000 to 4000 K and equivalence ratios from 0.5 to 2.0. Detailed reaction mechanism and product distribution for the combustion of *n*-octanol is investigated and compared with available experimental data.

Chapter 8 summarizes the important findings of the present work and suggest future directions of this work.

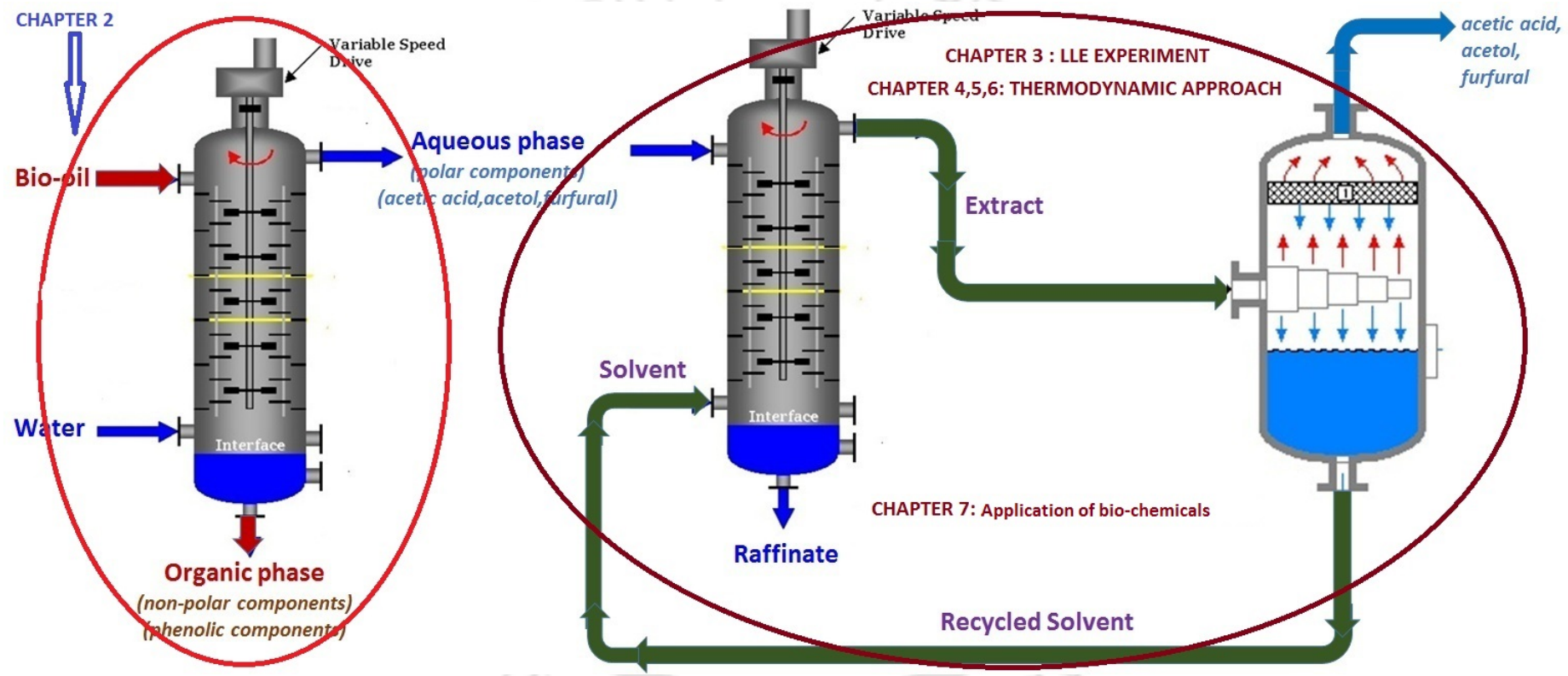

Figure 1.7.: Schematic outline of thesis

REFERENCES

[BP, 2016] (2016). Bp statistical review of world energy, bp.com/statisticalreview.

[Abdel-Rahman et al., 2011] Abdel-Rahman, M. A., Tashiro, Y., and Sonomoto, K. (2011). Lactic acid production from lignocellulose-derived sugars using lactic acid bacteria: Overview and limits. *Journal of Biotechnology*, 156:286–301.

[Albuquerque et al., 2015] Albuquerque, E. M., Borges, L., and Fraga, M. A. (2015). Lactic acid production from aqueous-phase selective oxidation of hydroxyacetone. *Journal of Molecular Catalysis A: Chemical*, 400:64–70.

[Bozell and Petersen, 2010] Bozell, J. J. and Petersen, G. R. (2010). Technology development for the production of biobased products from biorefinery carbohydrates-the us department of energy's "top 10" revisited. *Green Chemistry*, 12:539–554.

[Bridgwater, 2012] Bridgwater, A. V. (2012). Review of fast pyrolysis of biomass and product upgrading. *Biomass and Bioenergy*, 38:68–94.

[Budzianowski and Postawa, 2016] Budzianowski, W. M. and Postawa, K. (2016). Total chain integration of sustainable biorefinery systems. *Applied Energy*, 184:1432–1446.

[Chheda et al., 2007] Chheda, J. N., Huber, G. W., and Dumesic, J. A. (2007). Liquid-

phase catalytic processing of biomass-derived oxygenated hydrocarbons to fuels and chemicals. *Angew. Chem. Int. Ed.*, 46:7164–7183.

[Crocker, 2011] Crocker, M., editor (2011). *Thermochemical Conversion of Biomass to Liquid Fuels and Chemicals*. RSC Energy and Environment Series. The Royal Society of Chemistry, UK.

[Datta and Henry, 2006] Datta, R. and Henry, M. (2006). Review lactic acid: recent advances in products, processes and technologies - a review. *J. Chem. Technol. Biotechnol.*, 81:1119–1129.

[Demirbas, 2011] Demirbas, A. (2011). Competitive liquid biofuels from biomass. *Applied Energy*, 88:17–28.

[Demirbas, 2009] Demirbas, M. F. (2009). Biorefineries for biofuel upgrading: A critical review. *Applied Energy*, 86:S151–S161.

[Diebold, 2000] Diebold, J. P. (2000). A review of the chemical and physical mechanisms of the storage stability of fast pyrolysis bio-oils,nrel/sr-570-27613. Technical report.

[Gallezot, 2012] Gallezot, P. (2012). Conversion of biomass to selected chemical products. *Chem. Soc. Rev.*, 41:1538–1558.

[Huber and Corma, 2007] Huber, G. W. and Corma, A. (2007). Synergies between bio- and oil refineries for the production of fuels from biomass. *Angew. Chem. Int. Ed.*, 46:7184–7201.

[Inkinen et al., 2011] Inkinen, S., Hakkarainen, M., Albertsson, A., and Sodergard, A. (2011). From lactic acid to poly(lactic acid)(pla): Characterization and analysis of pla and its precursors. *Biomacromolecules*, 12:523–532.

[Kamm et al., 2006] Kamm, B., Gruber, P. R., and Kamm, M., editors (2006).

Biorefineries-Industrial Processes and Products: Status Quo and Future Directions. Wiley-VCH Verlag GmbH and Co. KGaA.

[Li et al., 2013] Li, G., Li, N., Li, S., Wang, A., Cong, Y., Wang, X., and Zhang, T. (2013). Synthesis of renewable diesel with hydroxyacetone and 2-methyl-furan. *Chem. Commun.*, 49:5727–5729.

[Maity, 2015a] Maity, S. K. (2015a). Opportunities, recent trends and challenges of integrated biorefinery: Part i. *Renew. Sustain. Energy Rev.*, 43:1427–1445.

[Maity, 2015b] Maity, S. K. (2015b). Opportunities, recent trends and challenges of integrated biorefinery: Part ii. *Renew. Sustain. Energy Rev.*, 43:1446–1466.

[Mariscal et al., 2016] Mariscal, R., Maireles-Torres, P., Ojeda, M., Sadaba, I., and Granados, M. L. (2016). Furfural: a renewable and versatile platform molecule for the synthesis of chemicals and fuels. *Energy Environ. Sci.*, 9:1144–1189.

[Martinez et al., 2013] Martinez, F. A. C., Balciunas, E. M., Salgado, J. M., Gonzalez, J. M. D., Convertic, A., and d. Oliveiraa, R. P. (2013). Lactic acid properties, applications and production: A review. *Trends in Food Science and Technology*, 30:70–83.

[Mohamad et al., 2011] Mohamad, M. H., Awang, R., and Yunus, W. M. (2011). A review of acetol: Application and production. *American Journal of Applied Sciences*, 8:1135–1139.

[Mohan et al., 2006] Mohan, D., Jr., C. U. P., and Steele, P. H. (2006). Pyrolysis of wood/biomass for bio-oil: A critical review. *Energy and Fuels*, 20:848–889.

[Naik et al., 2010] Naik, S. N., Goud, V. V., K.Rout, P., and Dalai, A. K. (2010). Production of first and second generation biofuels: A comprehensive review. *Renewable and Sustainable Energy Reviews*, 14:578–597.

[Nigam and Singh, 2011] Nigam, P. S. and Singh, A. (2011). Production of liquid bio-

fuels from renewable resources. *Progress in Energy and Combustion Science*, 37:52–68.

[Parajuli et al., 2015] Parajuli, R., Dalgaard, T., Jørgensen, U., Adamsen, A. P. S., Knudsen, M. T., Birkved, M., Gylling, M., and Schjørring, J. K. (2015). Biorefining in the prevailing energy and materials crisis: a review of sustainable pathways for biorefinery value chains and sustainability assessment methodologies. *Renew. Sustain. Energy Rev.*, 43:244–263.

[Sims et al., 2010] Sims, R. E. H., Mabee, W., Saddler, J. N., and Taylor, M. (2010). An overview of second generation biofuel technologies. *Bioresource Technology*, 101:1570–1580.

[Sipila et al., 1998] Sipila, K., Kuoppala, E., Fagernas, L., and Oasmaa, A. (1998). Characterization of biomass-based flash pyrolysis oils. *Biomass and Bioenergy*, 14:103–113.

[Smejkal et al., 2005] Smejkal, Q., Linke, D., and Baerns, M. (2005). Energetic and economic evaluation of the production of acetic acid via ethane oxidation. *Chemical Engineering and Processing: Journal of Biotechnology*, 44:421–428.

[Vitasari et al., 2011] Vitasari, C. R., Meindersma, G. W., and de Haan, A. B. (2011). Water extraction of pyrolysis oil: The first step for the recovery of renewable chemicals. *Bioresource Technology*, 102:7204–7210.

[Zakzeski et al., 2010] Zakzeski, J., Bruijnincx, P. C. A., Jongerius, A. L., and Weckhuysen, B. M. (2010). The catalytic valorization of lignin for the production of renewable chemicals. *Chem. Rev.*, 110:3552–3599.

CHAPTER 2

Solubility Prediction of Bio-Oil derived Chemicals in Aqueous media

2.1 Introduction

Fractionation of bio-oil with water is the easiest method which transforms bio-oil into two fractions: an aqueous top phase and an organic bottom phase. The bottom phase mainly contains lignin-containing fractions, while top layer is enriched with carbohydrate derived compounds [Sipila et al., 1998, Mohan et al., 2006]. Both phases can be processed separately to extract value added chemicals. Vitasari et al. [Vitasari et al., 2011] have studied the effects of stirring rate and water-to-oil ratio on the extraction of Glycolaldehyde, Acetic acid, Acetol, Furfural, Furanone, Levoglucosan, Syringol and Guaiacol from forest residue-derived bio-oil and pine-derived bio-oil. Based on experimental observation, they concluded that the distribution coefficient of a compound in aqueous phase depends on its polarity and solubility. However the mechanism of distribution of compounds into two phases has not been studied in detail.

It is a known fact that intermolecular forces acting between water and compounds present in bio-oil are primarily responsible for the solubility of compounds in water. The magnitude of the intermolecular force decides the relative solubility of the compounds in water. Various experimental studies have been carried out for different bio systems, but many difficulties prevent the detailed understanding of the nature of these forces. In this scenario Ab initio quantum chemistry calculation plays an important role in understanding the nature of such interactions. The most simple and conventional method to calculate the interaction energy between different molecules in a system is the supermolecule approach [Morokuma, 1971, Kitaura and Morokuma, 1976, Ziegler and Rauk, 1977, Stevens and Fink, 1987, Frey and Davidson, 1989, Glendening and Streitwieser, 1994, Chen and Gordon, 1996, van der Vaart and Merz, 1999, Khaliullin et al., 2007, Wu et al., 2009, Mitoraj et al., 2009, Mo et al., 2011, Su and Li, 2009, Kumar et al., 2013] in which the interaction energy of a pair of molecules is calculated as the difference between the energy of the pair and the energy of the individual molecules.

Many methods have been developed over the years to partition this total interaction

energy (INT) into various meaningful energy terms. These methods employ either the variational or the perturbation approach. The symmetry-adapted perturbation theory (SAPT) is one of the most widely used schemes in perturbation approach [Szalewicz and Jeziorski, 1979, Chałasiński and Szcześniak, 1988, Jeziorski et al., 1994]. Density functional theory based SAPT methods such as DFT-SAPT and DF-DFT-SAPT have also been developed [Heßelmann and Jansen, 2002a, Heßelmann and Jansen, 2002b, Heßelmann and Jansen, 2003, Heßelmann et al., 2005]. Some of the widely used schemes based on the variational approach include the Kitaura-Morokuma (KM) scheme [Morokuma, 1971, Kitaura and Morokuma, 1976] which forms the basis for many of the other energy decomposition schemes.

The KM scheme partitions the interaction energy into electrostatic (ES), exchange (EX), polarization energy (POL), charge transfer (CT) and MIX components. The different components of the interaction terms are defined as follows: (a) electrostatic: the classical coulombic interaction between occupied molecular orbitals (MO's) which does not cause mixing of MO's; (b) exchange: the interaction between occupied MO's which causes electron exchange between molecules; (c) polarization: the interaction which causes the mixing between the occupied and vacant MO's within each molecule; (d) charge transfer: the interaction which causes intermolecular transfer of electrons from the occupied MO's of one molecule to the vacant MO's of the other and vice versa. Localized Molecular Orbital-Energy Decomposition Analysis (LMO-EDA) scheme developed by Su et al. [Su and Li, 2009] is an extension and modification of the KM scheme. The advantage of this method over KM scheme is that high-level quantum chemistry methods such as MP2, CCSD and CCSD (T) can be used with it and thus makes it a robust model. LMO-EDA divides the total interaction energy (INT) into Electrostatic Energy (ES), Exchange Energy (EX), Repulsion Energy (REP), Polarization Energy (POL), and dispersion Energy (DISP) terms. In such a scheme there is no change in Electrostatic Energy (ES). However the sum of EX and REP terms of LMO-EDA is same as the EX term of KM scheme. Similarly the Polarization Energy (POL) of LMO-EDA is equal to the sum of POL, CT and MIX terms of KM scheme. The DISP term then simply becomes

the difference between the MP2 and HF interaction energies.

Due to its simplicity and robustness, the LMO-EDA scheme has been widely used for various weak and strong interactions [Yu, 2013, Ma et al., 2013, Singh et al., 2014, Shen et al., 2012, Thellamurege and Hirao, 2013, Semrouni et al., 2013, El-Hamdi et al., 2013].Yu [Yu, 2013] has studied the intermolecular interactions between HCOOH and C_6H_6 with the LMO-EDA method and found that the dispersion energies are as important as the electrostatic energies for the total interaction energies of the five HCOOH $\cdots$ C_6H_6 complexes. Ma et al. [Ma et al., 2013] have investigated the hydrogen bonding interactions in HXeCCH $\cdots$ H2O and HXeCCH $\cdots$ HF complexes by Ab initio calculation. They also carried out LMO-EDA analysis and observed that the dominant stabilizing forces are exchange energies and electrostatic interactions in all the complexes. However it was found that the polarization and dispersion interactions play a minor role to the stabilization of these complexes. Singh et al. [Singh et al., 2014] have investigated the competition between a very weak n $\rightarrow \pi^*_{Ar}$ interaction and a very strong hydrogen bond (N-H $\cdots$ N) interaction present in the complexes of 7-azaindole with a series of 2,6-substituted fluoropyridines by Ab initio calculation. The conclusion obtained from Ab initio calculation was supported by LMO-EDA analysis that the increase in the dispersion component is much more rapid compared to that of the electrostatic component with an increase in fluorination of the fluoropyridine ring. The report of solubility parameters of Bio-Oil derived chemicals from EDA calculation in the literature is sparse. Recently Garrec et al. [Garrec et al., 2014] obtained the relative partition of peroxyl radical intermediate and hydroperoxide derivatives using a Universal Solvation Model (SMD). Further the authors conducted classical MD simulations for a hydrated phosphatidylcholine (DLPC) bilayer containing a small number of oxidized lipids.

Thus, in this chapter solubility of selected bio-oil molecules in water has been estimated. Further the natural bond orbital (NBO) analysis was employed to confirm the hydrogen bonding interaction in these complexes. Thereafter the computed interaction energies were regarded as the measurement for the solubility of the bio-oil molecules in water. Finally based on interaction energy, solubility ranking of the compounds in water

was confirmed and compared with the available experimental solubility parameters.

2.2 Theory and Methods

2.2.1. Energy Decomposition Analysis

Intermolecular forces are interaction forces between molecules that hold molecules together. Intermolecular forces are significantly weaker than the chemical bond but a thorough understanding and most importantly quantification of these forces are of utmost importance as these forces play an important role in determining the properties of the systems. In supermolecule approach,the interaction energy is expressed as follows:

$$\text{Interaction Energy (INT)} = \text{Energy of the complex} - \text{(Energy of the monomer-1 + Energy of the monomer-2)} \quad (2.1)$$

In the Localized Molecular Orbital-Energy Decomposition Analysis (LMO-EDA) method, interaction energy in terms of component energy terms is expressed as [Su and Li, 2009]

$$\Delta E = \Delta E^{ES} + \Delta E^{EX} + \Delta E^{REP} + \Delta E^{POL} + \Delta E^{DISP} \quad (2.2)$$

2.2.2. Computational Details

For H-bonded complexes, the proper selection of the level of theory and basis set is important for the structure optimization of the complexes as well as for the estimation of interaction energy between the molecules in the complexes. For reliable description of such systems, higher level of theory such as second-order MP2 or advanced correlated methods is required. Methods such as coupled-cluster singles, doubles and noniterative triples [CCSD (T)] along with large basis sets are useful as Hartree-Fock method does not consider electron correlation. Second-order MP2 calculations with moderately large basis sets can provide reasonably good results at reasonable cost for such calculations. Muller et al. [Müller et al., 2004] have shown that at MP2 level, the

smaller 6-31+G(d,p) and 6-311++G(d,p) basis sets predict hydrogen bond lengths which are in excellent agreement with the estimated complete basis set (CBS) limit for 2-pyridone dimer. MP2/6-311++G(d,p) predicted binding energy was also in good agreement with the MP2 CBS limit. Therefore, in this work geometries of the complexes have been optimized at second order MP2 with 6-311++G(d,p) basis set.
Diffuse functions are also important for reliable calculation of interaction energy of H-bonded systems [Foresman and Frisch, 1996]. Therefore, basis sets with diffuse and polarization functions have been selected as they are expected to provide accurate information of the weakly bonded systems. Geometry optimization of all the complexes has been carried out using Gaussian 03 program [Frisch et al., 2004]. A frequency optimization was done in Gaussian 03 to detect the presence of any imaginary frequencies. Total interaction energy as well as energy decomposition analysis has been done by Localized Molecular Orbital method using quantum chemistry package GAMESS, USA [Schmidt et al., 1993]. LMO-EDA analysis was carried out at the MP2/6-311++G(d,p) level on optimized geometries. Interaction energies of various complexes were corrected from the basis set superposition error (BSSE) using the counterpoise method of Boys and Bernardi [Boys and Bernardi, 1970]. For better understanding of the interactions, natural charges for different complexes have been calculated by natural bond orbital (NBO) method available in the Gaussian 03 software [Glendening et al.,]. We now proceed with the geometry optimization where we first discuss the individual component and thereafter for mixtures. As the procedure is same for all compounds and mixtures, we have reported the optimization of Glycolaldehyde as a pure component and subsequently Glycolaldehyde-water as a complex in next section. The detailed structures of all other individual components along with its complexes are given in Appendix A.

2.3 Results and Discussion

2.3.1. Glycolaldehyde and water complex

Glycolaldehyde monomer has four conformers: Cis cis (Cc), Cis trans (Ct), Trans trans (Tt), and Trans gauche (Tg) [Senent, 2004, Ratajczyk et al., 2004, Carbonniere and

Pouchan, 2012, Aspiala et al., 1986, Carroll et al., 2013, Aviles-Moreno et al., 2006]. In Cc and Ct conformers hydroxyl O and carbonyl O are on the same side of C-C single bond whereas in Tt and Tg conformers, hydroxyl O and carbonyl O are on the opposite side of C-C single bond. The optimized equilibrium geometry along with important geometrical parameters and total energies are reported in Appendix-A. The four conformers can be best described by two dihedral angles: O1-C1-C2-O2 and H1-O1-C1-C2. The calculated dihedral angles are Cc (0, 0), Ct (0,-180), Tt (177,175) and Tg (160.5,-70.9). Based on the optimized geometries, the relative order of energy with respect to Cc conformer is 11.14 kJ/mol, 11.95 kJ/mol and 19.28 kJ/mol for Tt, Tg and Ct conformers respectively. This indicates that Cc conformer is the most stable which is in accordance with the previous findings [Senent, 2004, Ratajczyk et al., 2004, Carbonniere and Pouchan, 2012, Aspiala et al., 1986, Carroll et al., 2013, Aviles-Moreno et al., 2006]. From the optimized geometry, we may infer that Cc conformer is the most stable due to the formation of an intramolecular hydrogen bond between carbonyl O and hydroxyl H with H-bond length (HBL) of 2.103 Å which is very much in agreement with the reported value of 2.0661 Å calculated at MP2 theory with cc-pVQZ basis sets [Senent, 2004].

Starting with optimized geometries of Glycolaldehyde and various possible orientation of water molecule around it, twelve numbers of different complexes have been found. In the present work, Cc-water complexes have been labeled by letter Cc-n; Ct-water complexes by letter Ct-n; Tt-water complexes by letter Tt-n; and Tg-water complexes by letter Tg-n where n is serial number [see Figures 2.1-2.12 for optimized geometries]. From the optimized equilibrium geometry, we can say that the interaction between Glycolaldehyde and water is due to the presence of the carbonyl and hydroxyl groups in the Glycolaldehyde; and O and H atoms present in the water molecule. These interactions are due to the formation of hydrogen bonds. H-bonding interactions have been classified into very strong, strong and weak [Desiraju and Steiner, 2006]. The strength of the very strong H-bonding interactions ranges from 15 to 40 kcal/mol with H-bond length 1.2-1.5 Å and bond angle 175-180°. For the strong and weak H-bonds,

the strength varies from 4-15 and < 4 kcal/mol respectively. For the strong H-bonding interactions, bond length ranges from 1.5-2.2 Å with bond angle 130-180°, whereas interactions in which H-bond length varies from 2.0-3.0 Å are termed as weak H-bonding interactions. The van der Waals cut-off criterion requires that in a hydrogen bond H$\cdots$A, bond length must be smaller than the sum of the H and A van der Waals radii. For the H$\cdots$ O H-bond, this criterion says H-bond length must be smaller than 2.72 Å (vdW radii of H = 1.20 Å and vdW radii of O = 1.52 Å). In the following discussions, we consider the existence of an H-bond when the bond length is less than 2.2 Å. Apart from the cut-off H-bond length, two features of H-bonds will also be considered. First, there is a significant charge transfer from the proton acceptor (Y) to the proton donor (X-H). Second, formation of the X-H$\cdots$ Y, H-bond results in weakening of the X-H bond and this weakening is accompanied by bond elongation [Hobza and Havlas, 2000].

In Cc-1 complex, two hydrogen bonds are formed: One between the carbonyl O and H_{H2O} with H-bond length (HBL) of 2.085 Å and the second one between hydroxyl H and O_{H2O} having HBL 1.874 Å. In Cc-2 complex, two H-bonds are formed: One Intramolecular between hydroxyl H and carbonyl O with HBL 2.104 Å and the second one between carbonyl O and H_{H2O} with HBL 2.041 Å. In Cc-3 complex, two H-bonds are formed: One intramolecular between hydroxyl H and carbonyl O with HBL 2.083 Å and the second one between carbonyl O and H_{H2O} with HBL 1.965 Å. In Cc-4 complex, two H-bonds are formed: One between hydroxyl H and O_{H2O} with HBL 1.922 Å. and the second one between carbonyl O and H_{H2O} with HBL 2.275 Å. In Ct-1, Ct-2 and Ct-3 complexes, H-bond is formed between carbonyl O and H_{H2O} with HBL 1.985 Å; between hydroxyl H and O_{H2O} with HBL 1.899 Å; and between hydroxyl O and H_{H2O} with HBL 1.975 Å respectively. In Tt-1, Tt-2 and Tt-3 complexes H-bond is formed between carbonyl O and H_{H2O} with HBL 1.989 Å ; between hydroxyl O and H_{H2O} with HBL 1.980 Å; and between hydroxyl H and O_{H2O} with HBL 1.893 Å respectively. In Tg-1 and Tg-2 complexes H-bond is formed between carbonyl O and H_{H2O} with HBL 2.010 Å; and between hydroxyl O and H_{H2O} with HBL 1.967 Å respectively.

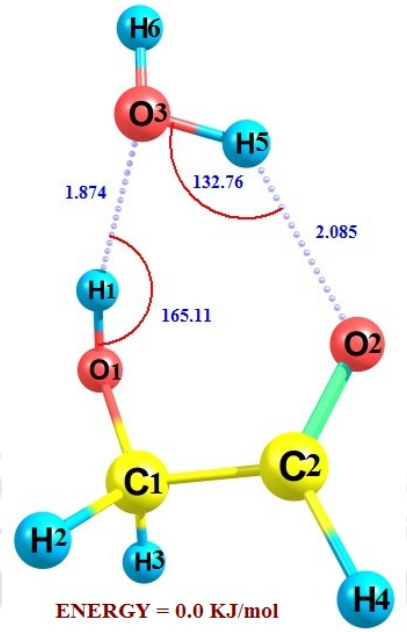

Figure 2.1.: Optimized equilibrium geometry of Glycolaldehyde-water complex Cc-1.

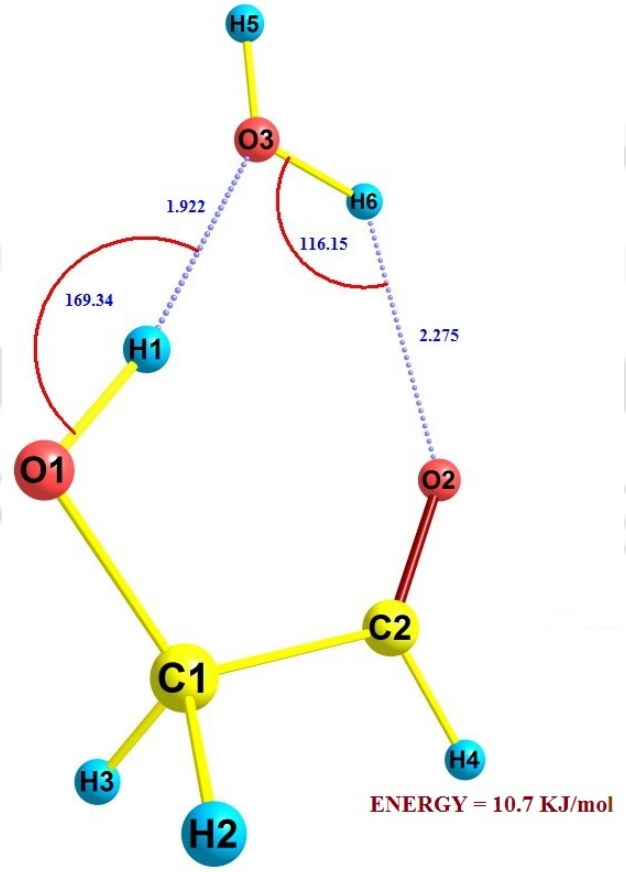

Figure 2.2.: Optimized equilibrium geometry of Glycolaldehyde-water complex Cc-4 (Energy w.r.t. Cc-1).

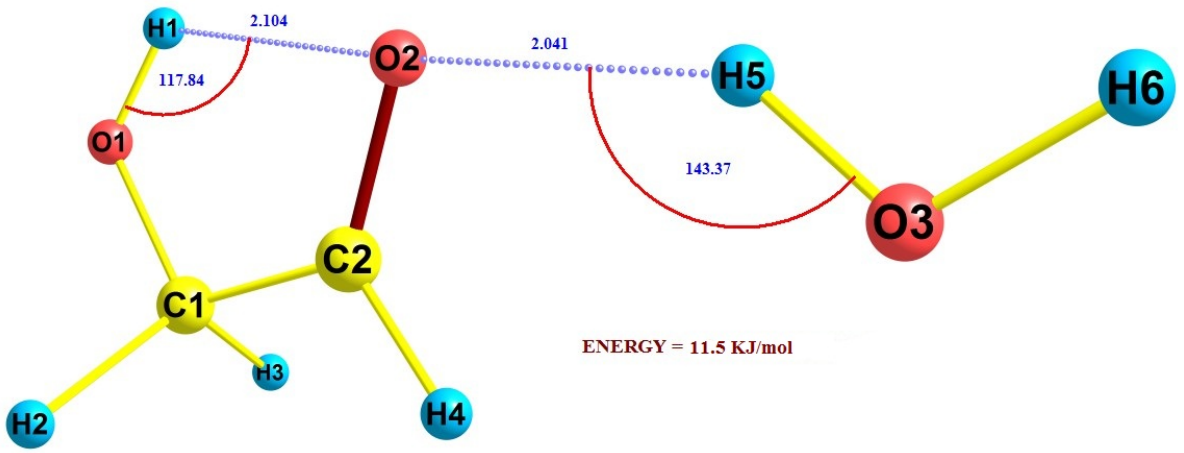

Figure 2.3.: Optimized equilibrium geometry of Glycolaldehyde-water complex Cc-2 (Energy w.r.t. Cc-1).

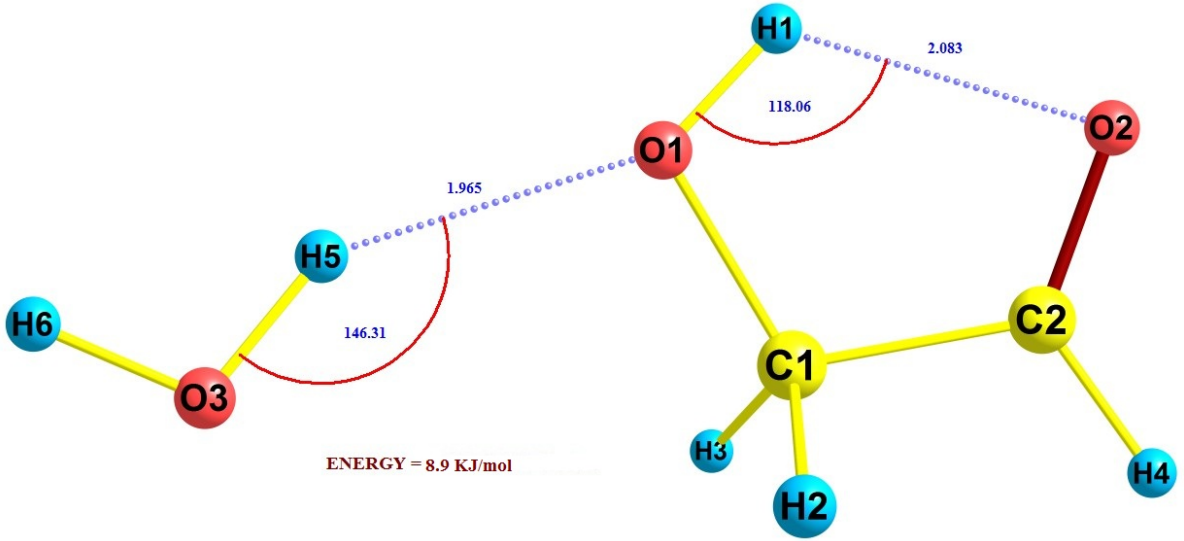

Figure 2.4.: Optimized equilibrium geometry of Glycolaldehyde-water complex Cc-3 (Energy w.r.t. Cc-1).

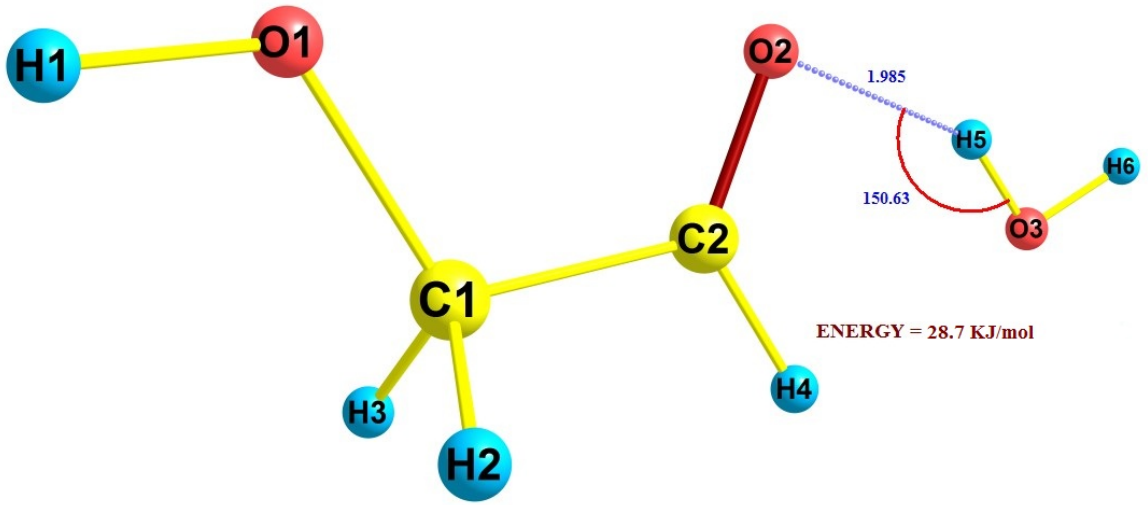

Figure 2.5.: Optimized equilibrium geometry of Glycolaldehyde-water complex Ct-1 (Energy w.r.t. Cc-1).

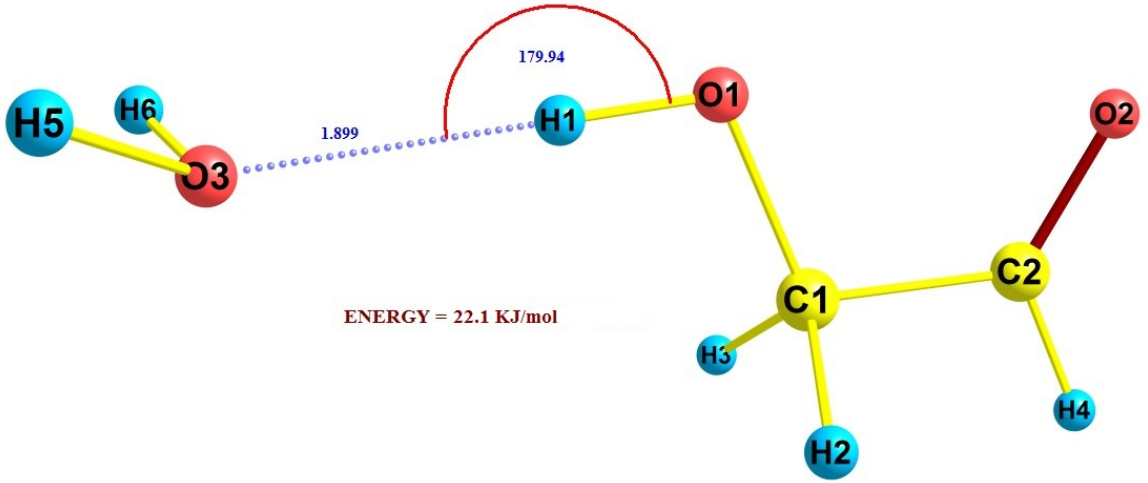

Figure 2.6.: Optimized equilibrium geometry of Glycolaldehyde-water complex Ct-2 (Energy w.r.t. Cc-1).

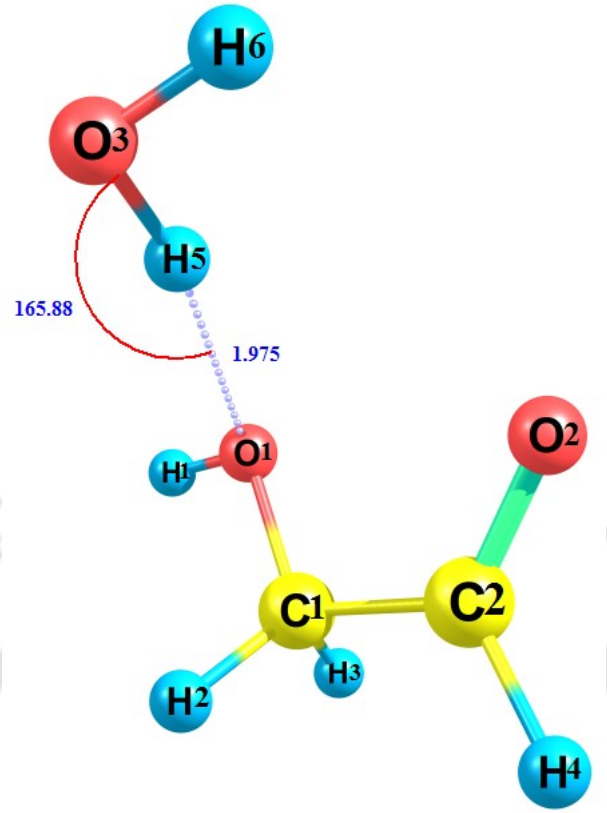

Figure 2.7.: Optimized equilibrium geometry of Glycolaldehyde-water complex Ct-3 (Energy w.r.t. Cc-1).

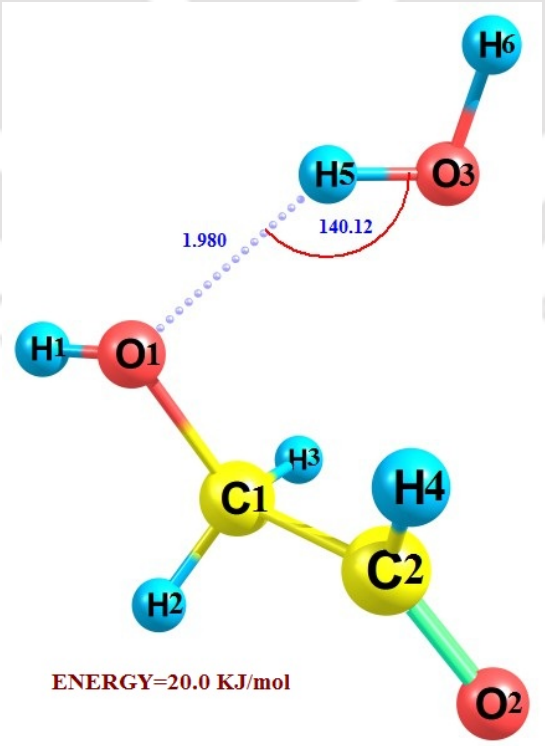

Figure 2.8.: Optimized equilibrium geometry of Glycolaldehyde-water complex Tt-2 (Energy w.r.t. Cc-1).

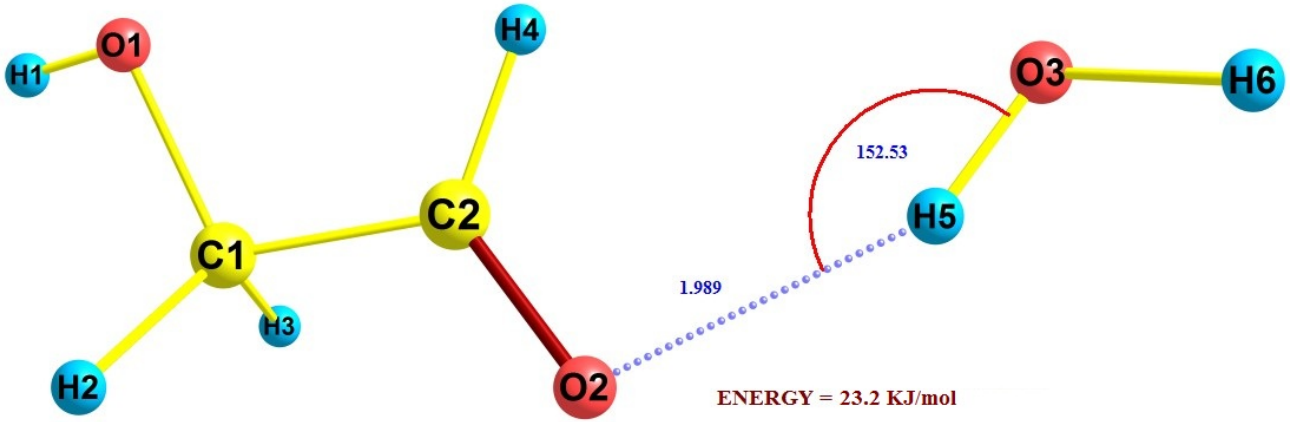

Figure 2.9.: Optimized equilibrium geometry of Glycolaldehyde-water complex Tt-1 (Energy w.r.t. Cc-1).

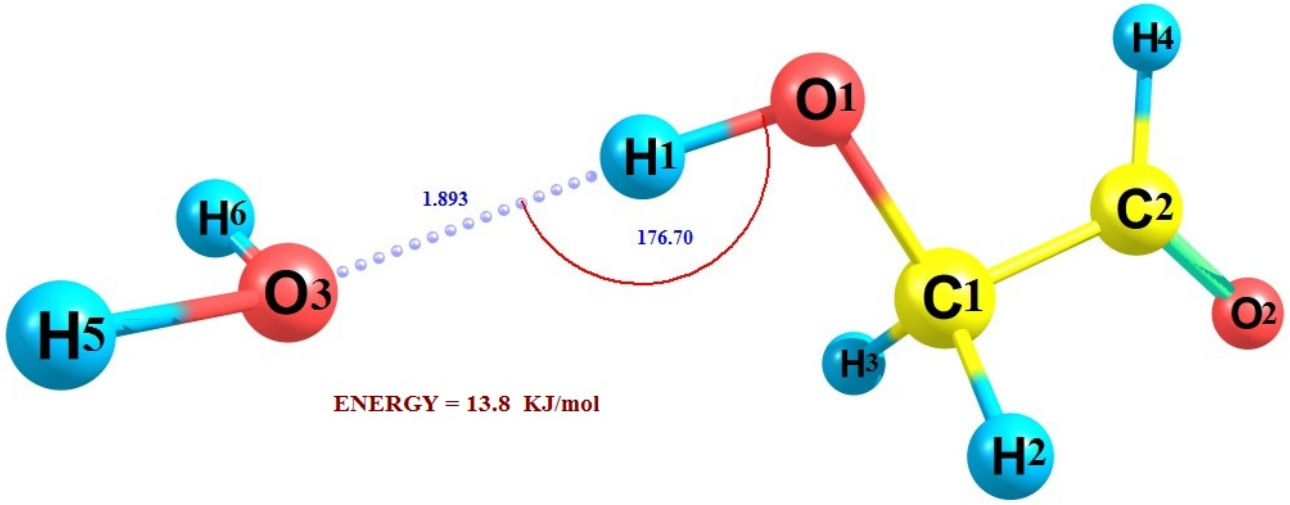

Figure 2.10.: Optimized equilibrium geometry of Glycolaldehyde-water complex Tt-3 (Energy w.r.t. Cc-1).

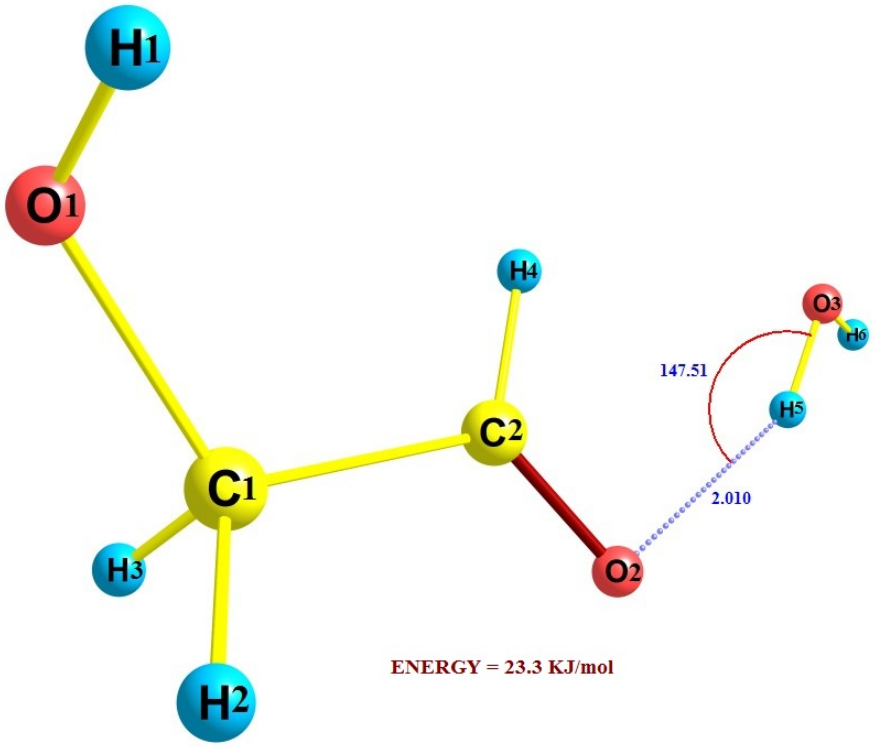

Figure 2.11.: Optimized equilibrium geometry of Glycolaldehyde-water complex Tg-1 (Energy w.r.t. Cc-1).

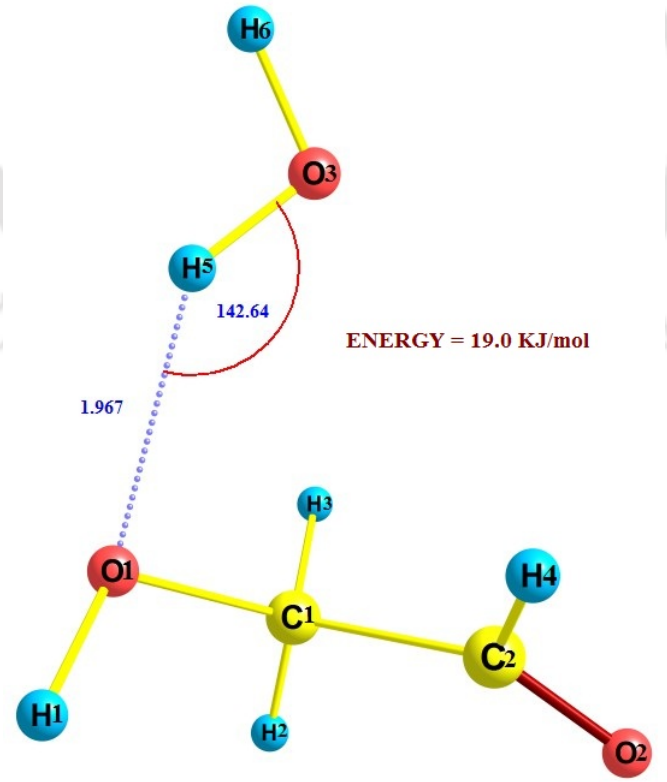

Figure 2.12.: Optimized equilibrium geometry of Glycolaldehyde-water complex Tg-2 (Energy w.r.t. Cc-1).

The H-bond formations are evident by the bond elongation of O-H group of Glycolaldehyde and of water molecule. In Cc-1, Hydroxyl O-H bond increases from 0.967 Å to 0.970 Å whereas in water it increases from 0.960 Å to 0.965 Å. The changes in lengths of O-H bonds upon complex formation are reported in Appendix-A. Based on the calculated bond lengths, we may say that the H-bond between hydroxyl H and O_{H2O} (Cc-1, Tt-3 and Ct-2 conformers) is stronger than that between carbonyl O and H_{H2O} and between hydroxyl O and H_{H2O}. This nature can be further examined by calculating the natural charges.

The natural charges are calculated for each complex using natural Bond Order (NBO) method. The changes of the natural charges in atoms upon complex formation and the net charge transfer (CT) from the proton acceptor toward the proton donor are compiled in Table 2.1.

Table 2.1.: Natural charges by Natural Bond Order (NBO) for Glycolaldehyde and water complexes.

complex		charges
Cc-1	Glycolaldehyde	-0.010
	Water	+0.010
Cc-2	Glycolaldehyde	+0.007
	Water	-0.007
Cc-3	Glycolaldehyde	+0.006
	Water	-0.006
Cc-4	Glycolaldehyde	-0.007
	Water	+0.007
Ct-1	Glycolaldehyde	+0.010
	Water	-0.010
Ct-2	Glycolaldehyde	-0.010
	Water	+0.010
Ct-3	Glycolaldehyde	+0.008
	Water	-0.008
Tt-1	Glycolaldehyde	+0.010
	Water	-0.010
Tt-2	Glycolaldehyde	+0.005
	Water	-0.005
Tt-3	Glycolaldehyde	-0.011
	Water	+0.011
Tg-1	Glycolaldehyde	+0.009
	Water	-0.009
Tg-2	Glycolaldehyde	+0.006
	Water	-0.006

In Cc-1, charge transfer occurs in two directions: from carbonyl O to H_{H2O} and from O_{H2O} to H_{OH}. However the overall charge on water has increased by +0.010e and the same amount of negative charge appears on Glycolaldehyde in Cc-1. This indicates that there is a net charge transfer from water to Glycolaldehyde. NBO analysis can also be used for the determination of the strength of the individual $H_{OH} \cdots O_{H2O}$ and $H_{H2O} \cdots O_{CO}$ interactions. In $H_{OH} \cdots O_{H2O}$ interaction, charge transfer occurs from the lone pair of oxygen of O_{H2O} to the anti-bonding orbital of OH group of the Glycolaldehyde where as in $H_{H2O} \cdots O_{CO}$ interaction, charge transfer occurs from lone pair of oxygen of O_{CO} to the anti-bonding orbital of OH group of the water. The NBO interaction energy is given by the second order perturbative energy $E^{(2)}_{i\rightarrow j}$ where i and j denote the donor and acceptor orbitals, respectively. The $E^{(2)}_{i\rightarrow j}$ values for $H_{OH} \cdots O_{H2O}$ and $H_{H2O} \cdots O_{CO}$ interactions are 11.31 kcal/mol and 2.17 kcal/mol respectively. The magnitude of the interaction energy shows $H_{OH} \cdots O_{H2O}$ interaction is stronger than $H_{H2O} \cdots O_{CO}$ interaction. Similarly, in Cc-2, charge on Glycolaldehyde has increased by +0.007e and the same amount of negative charge has appeared on water which indicates net charge transfer from Glycolaldehyde to water. Similarly for all complexes, charge transfer process is consistent with H-bond formation. Therefore, changes in bond length and charge analysis confirm the H-bond formation between Glycolaldehyde and water.

The Non-Covalent Interactions (NCI) index was recently developed by Johnson et al. [Johnson et al., 2010, Contreras-García et al., 2011], primarily for the identification of H-bond interactions. This visualization approach is based on electron densities and its derivatives. The NCI index is a 2D plot of reduced density gradient (RDG) and the electron density. A sudden change in the RDG is seen for a weak interaction when present between interacting atoms of the molecules. NCI plot for Cc-1 complex (Figure 2.13) has been drawn using freely available software Multiwfn [Lu and Chen, 2012]. Noncovalent interaction (NCI) plot for Glycolaldehyde-water complex Cc-1 is shown in Figure 2.13. Noncovalent interactions are characterized by low density and reduced gradient values. The interaction types are identified by the values of sign$(\lambda_2)\rho$ in these regions.

Large negative values of sign$(\lambda_2)\rho$ are indicative of attractive interactions (hydrogen bonding) while values near zero indicate very weak van der Waals interaction [Johnson et al., 2010, Contreras-García et al., 2011]. In Figure 2.13, there are three different spikes which correspond to three different non-covalent interactions. Peaks appeared at q = 0.007 au for vdW and q = -0.017 au & q = -0.026 au for hydrogen bonds. Two different hydrogen peaks are in consistent with the optimized geometry (Figure 2.1) and second order perturbative energy $E^{(2)}_{i\rightarrow j}$ values.

Based on total energy of optimized geometries (Table A.2 of Appendix A), we can conclude that complex Cc-1 is the most stable. This result is very much in agreement with the experimental data reported by Aviles-Moreno et al. [Aviles-Moreno et al., 2006] based on rotational spectrum as obtained using a molecular beam Fourier transform microwave spectrometer. The experiments confirmed the identity of the experimentally detected conformer as being complex Cc-1 and which was well supported by ab initio calculations.

Thus, based on the geometry optimization by Ab initio quantum chemistry method, we can get information about the most stable complex out of the many possible complexes. For H-bonded system, we can also get information about the number of H-bonds in the complex as well as H-bond lengths. However the geometry optimization method does not give a clear idea about the various forces that hold together these assemblies and govern its stability. Therefore, to get more insight into the nature of interactions as well as for quantification of the interactions, Localized Molecular Orbital-Energy Decomposition Analysis (LMO-EDA) has been carried out for all the complexes of Glycolaldehyde and water [see Annexure-A]. The Localized Molecular Orbital Energy Decomposition Analysis (LMO-EDA) shows that the electrostatic energy is the main driving force for the formation of the complexes while sum contributions of exchange-repulsion term are not favorable for the formation of complexes. Polarization energy and dispersion energy terms make a small contribution for the formation of complexes. The dispersion energy for Cc-2 (+0.06 kcal/mol), Ct-1 (+0.02 kcal/mol), Tt-1 (+0.05 kcal/mol) and Tg-1 (+0.01 kcal/mol) is positive whereas without BSSE, dispersion energies are

-0.67 kcal/mol, -0.89 kcal/mol, -0.85 kcal/ mol and -0.88 kcal/mol respectively. As mentioned by Su et al. [Su and Li, 2009], this may be caused by the differences in the intra- and intermolecular correlation energy on going from non-interacting to interacting systems which may be dependent on the basis set and distance. Based on the interaction energies (INT) values (Table A.7 of Annexure A), it can be conformed that among all complexes, interaction between Glycolaldehyde and water is the strongest in Cc-1 complex. Therefore, based on total energy and interaction energy, we can conclude that complex Cc-1 (Figure 2.1) is more stable. The interaction energy values (INT of Eq. (1)) are in the range of -4.0 to -7.5 kcal/mol (Table A.7 of Annexure A). These are different to the energies of the complex (first term of right hand side of Eq. (1)). While the 'Energy of the complex' refers to the stability of the individual conformer, the interaction energy predicts the stability for the entire system. This implies greater the negative values, higher the energy require to disassemble the complex.

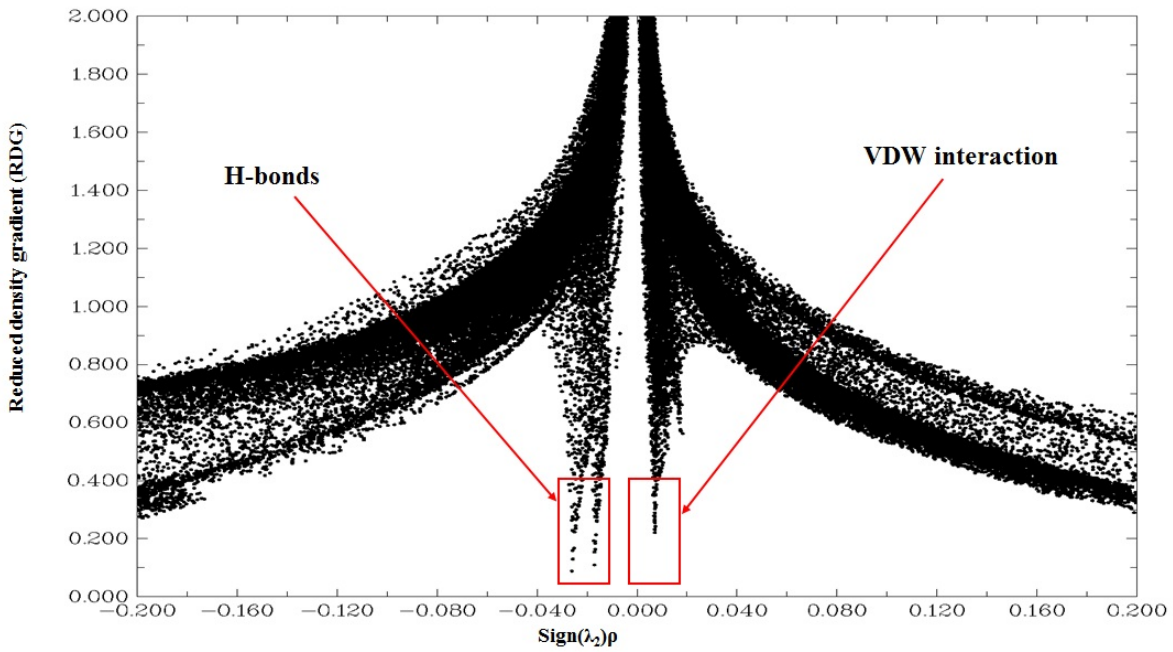

Figure 2.13.: NCI plot for Glycolaldehyde-water complex Cc-1.

2.3.2. Furfural-water, Acetic acid-water and Furanone-water complexes

Similar to the above discussions, the complexes of Furfural-water [Rivelino et al., 2002, Rogojerov et al., 2005, Ashish and Ramasami, 2008] (Appendix A), Acetic acid-

water [Senent, 2001, Maçôas et al., 2004, Maçôas et al., 2003] (Appendix A) and Furanone-water [Rao, 1976] (Appendix A) have been optimized and compared with the existing literature [Rivelino et al., 2002, Rogojerov et al., 2005, Ashish and Ramasami, 2008, Senent, 2001, Maçôas et al., 2004, Maçôas et al., 2003, Rao, 1976]. The optimized equilibrium geometries of the most stable complexes are shown in Figures 2.14-2.16. Based on the optimized geometries, energy order of Furfural-water complexes was predicted as FURC-1 < FURC-2 < FURC-3 < FURT-1 < FURT-2 < FURT-3, which indicates that cis-OO complexes are more stable than trans-OO complexes, whereas trans-OO monomer is more stable than cis-OO monomer and FURC-1 (Figure 2.14) is the most stable complex. For acetic acid complexes the order of energy is AAT-1 < AAT-2 < AAT-3 < AAC-3 < AAC-2 < AAC-1 < AAC-4 which indicates that trans complexes are more stable than cis complexes and conformer AAT-1 (Figure 2.15) is the most stable complex among all the complexes of acetic acid and water [Appendix A]. In the similar manner the decreasing order for furanone-water is 2(5H)-FUR-2 < 2(5H)-FUR-3 < 2(5H)-FUR-1 < 2 (3H)- FUR-1 < 2(3H)-FUR-2 < 2(3H)-FUR-3 < 3(2H)-FUR-1 < 3(2H)-FUR-2 which indicates 2(5H)-FUR-2 (Figure 2.16) is the most stable complex.

2.3.3. Inferences from interaction energies and its relation with distribution coefficients

The interaction energies between acetic acid-water, glycolaldehyde-water, furanone-water and furfural-water have been tabulated for the most stable complexes in Table 2.2 and shown in Figure 2.17. The relatively large ΔE^{EX} and ΔE^{REP} for acetic acid-water indicate that there is a significant orbital overlap between acetic acid and water molecules in the complex. The relatively smaller values of ΔE^{POL} suggest that the orbitals of water molecule undergo moderate changes in their shapes in the complex formation process. This is necessary to maximize the H-bond strength. Based on the interaction energy with water, the compounds follow the following trend: Acetic acid (-8.44 kcal/mol) > Glycolaldehyde (-7.46 kcal/mol) > Furanone (-6.08 kcal/mol) >

Furfural (-4.84 kc al/mol). On comparing the individual energy terms, they follow the same trend as followed by total interaction energy as shown in Figure 2.17, that is (Acetic acid: ΔE^{ES}; ΔE^{EX}; ΔE^{REP}; ΔE^{POL}) > (Glycolaldehyde: ΔE^{ES}; ΔE^{EX}; ΔE^{REP}; ΔE^{POL}) > (Furanone: ΔE^{ES}; ΔE^{EX}; ΔE^{REP}; ΔE^{POL}) > (Furfural: ΔE^{ES}; ΔE^{EX}; ΔE^{REP}; ΔE^{POL}). The H-bond length in the compounds also follows the same trend: Acetic acid (HBL = 1.804 Å) < Glycolaldehyde (HBL = 1.874 Å) < Furanone (HBL = 1.972 Å) < Furfural (HBL = 1.98 Å).

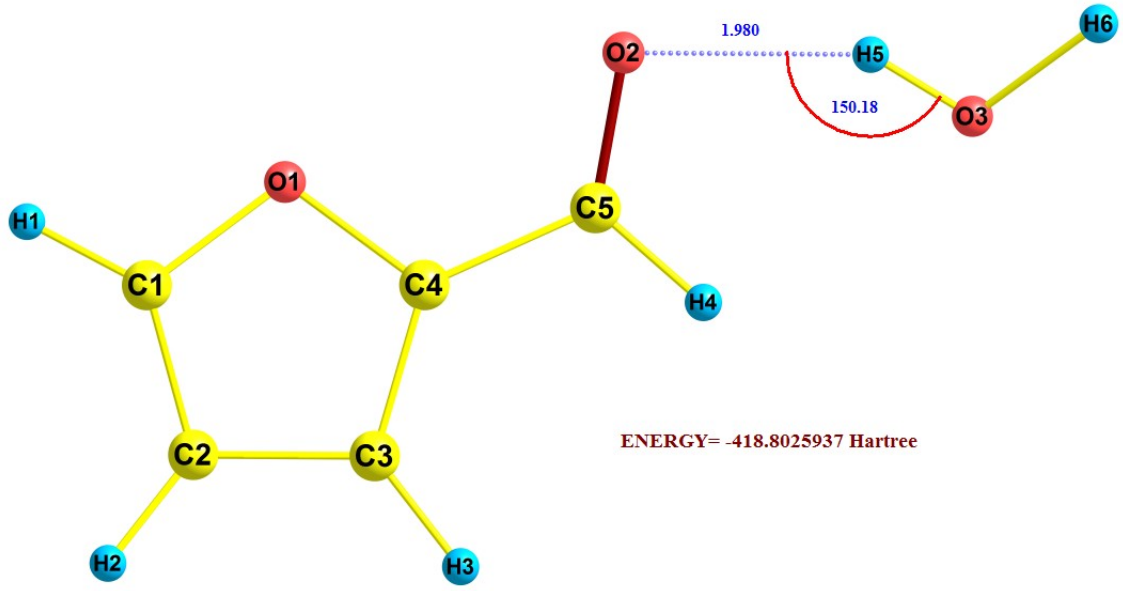

Figure 2.14.: Optimized equilibrium geometry of Furfural-water complex FURC-1.

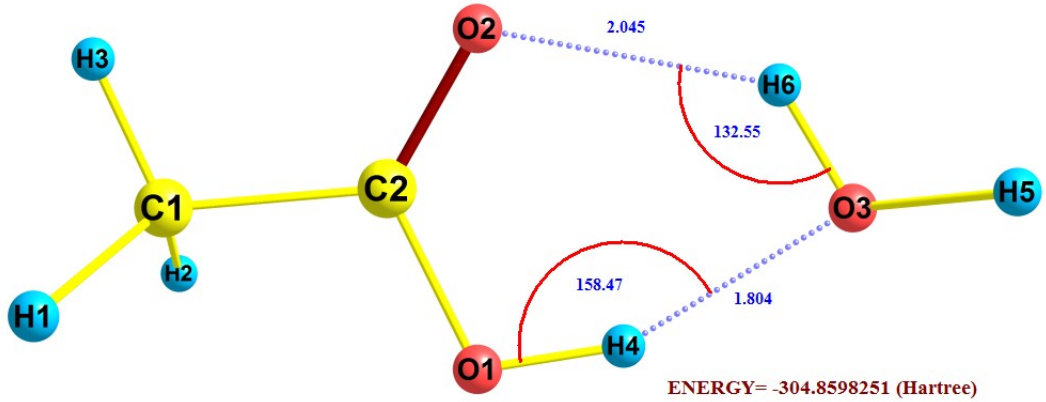

Figure 2.15.: Optimized equilibrium geometry of acetic acid-water complex AAT-1.

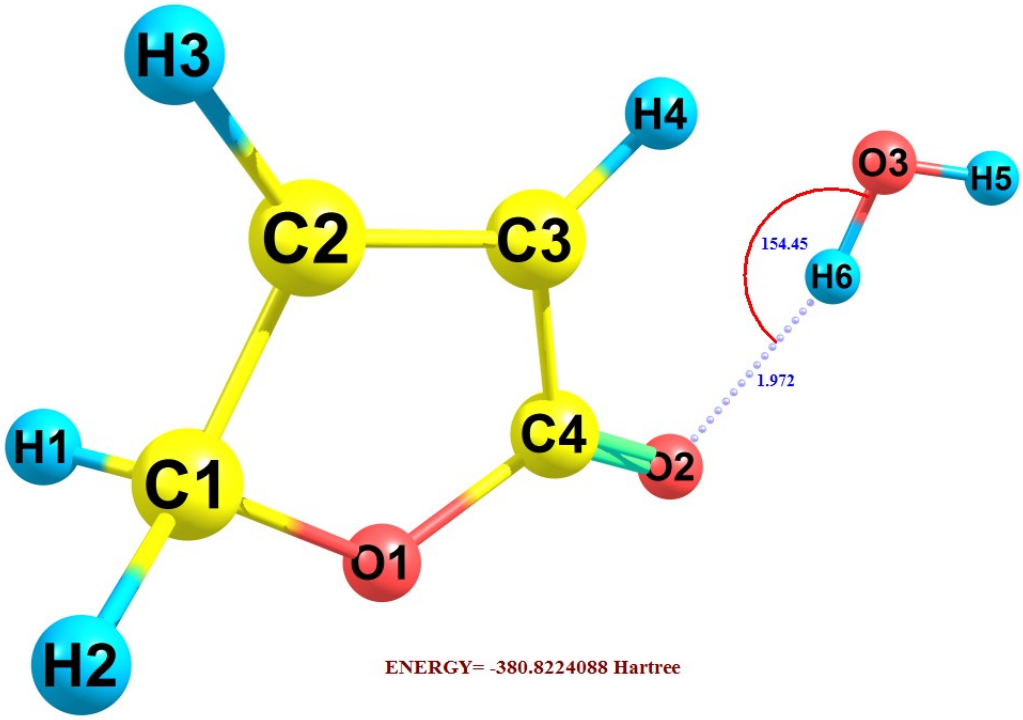

Figure 2.16.: Optimized equilibrium geometry of Furanone-water complex 2(5H) FUR-2.

Acetic acid and glycolaldehyde arrange as a cyclic complex with water bound together by two H-bonds which make them unique compared to furanone and furfural. The larger negative energy values show larger interaction with water. This trend shows how readily the complex could be separated into individual molecules. It means for the separation of acetic acid and water molecules from the complex we need more energy as compared to others.

In terms of solubility, which is dependent on intermolecular forces, the stronger the attractions between solute and solvent molecules, the greater the solubility. It means, in terms of solubility in water, compounds will follow the following trend:

Acetic acid > Glycolaldehyde > Furanone > Furfural

The available experimental results of Vitasari et al. [Vitasari et al., 2011] show that for the pine-derived pyrolysis oil, the experimental trend of the distribution coefficient starts with acetic acid (2.37) and is followed by glycolaldehyde (2.21), furanone (0.82), and furfural (0.44). This is a similar trend as was observed from the trend obtained via interaction energies. Overall based on the present study in which intermolecular

interactions between molecules have been calculated in gas phase, we can conclude that solubility of acetic acid in water will be higher followed by Glycolaldehyde. This is then followed by the solubility of furanone and furfural. The gas phase predicted solubility is very much in agreement with the experimental results that is solubility of acetic acid and Glycolaldehyde is higher than furanone and furfural in water. Thus, water fractionation process may be used for the extraction of value added chemicals such as acetic acid and glycolaldehyde in aqueous phase and the Localized Molecular Orbital-Energy Decomposition Analysis (LMO-EDA) may open a pathway for computing the trend of distribution coefficients when experimental data are not available.

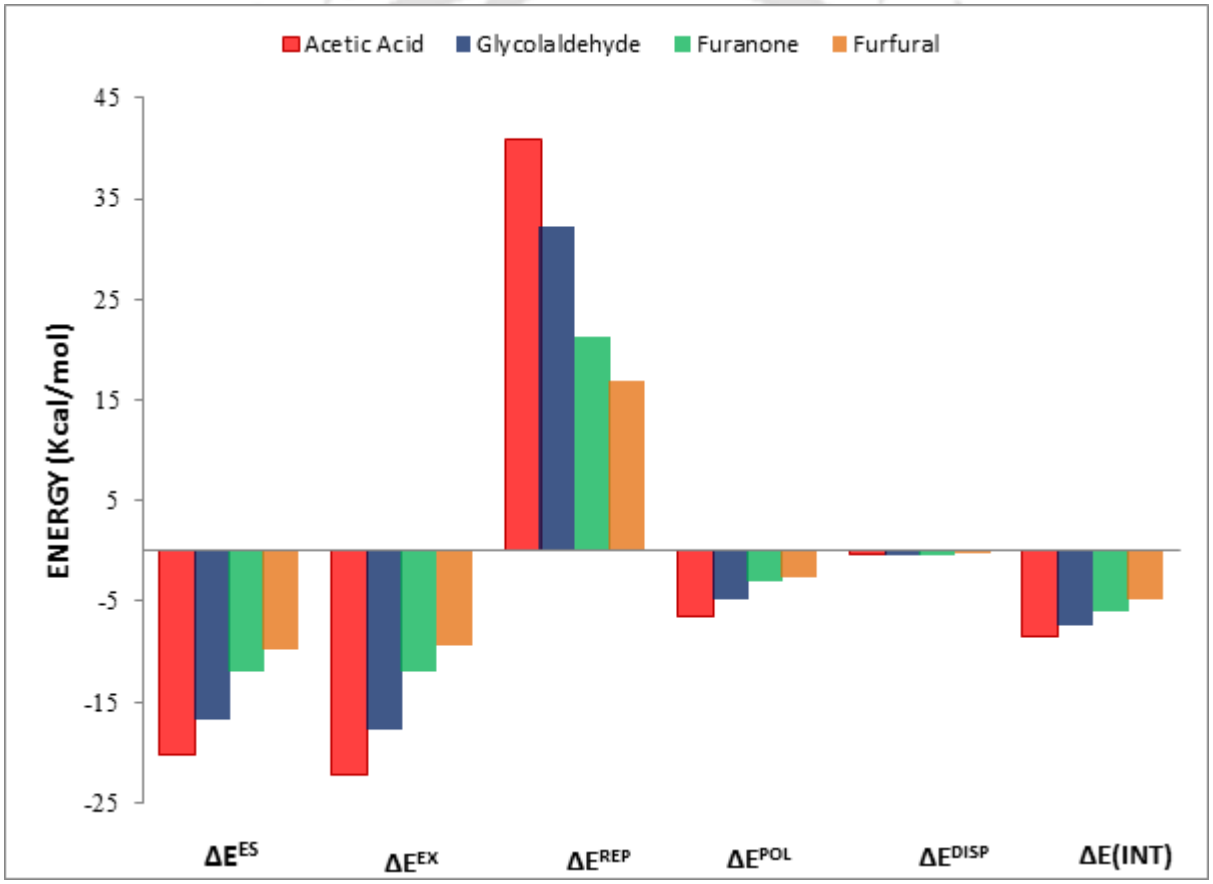

Figure 2.17.: Interaction Energy for Acetic acid-water, Glycolaldehyde-water, Furanone-water, Furfural-water

Table 2.2.: Results of Localized Molecular Orbital-Energy Decomposition Analysis (LMO-EDA) for Acetic acid, Glycolaldehyde, Furanone and Furfural in water complexes carried out at MP2/6-311++G** Level [all values are in Kcal/mol]

	ΔE^{ES}	ΔE^{EX}	ΔE^{REP}	ΔE^{POL}	ΔE^{DISP}	ΔE(INT)	Distribution coefficient
Acetic acid	-20.14	-22.25	40.96	-6.59	-0.42	-8.44	2.37
Glycolaldehyde	-16.67	-17.76	32.23	-4.79	-0.47	-7.46	2.21
Furanone	-11.93	-11.91	21.18	-3.04	-0.38	-6.08	0.82
Furfural	-9.76	-9.45	16.87	-2.52	0.02	-4.84	0.44

2.4 Conclusions

The current work reports the computational study on solubility prediction of bio-oil derived chemicals in aqueous media by Localized Molecular Orbital-Energy Decomposition Analysis (LMO-EDA). This work computed the structures of 1:1 complexes of water with glycolaldehyde, furfural, acetic acid and furanone using MP2 theory. Afterward, the Energy Decomposition Analysis (EDA) was performed on the lowest energy conformer of each of the complexes using LMO method. It has been demonstrated that the computed interaction energy, electrostatic component of the interaction energy of the chosen molecules with water predicts the correct trend of the experimentally reported solubility parameters of the corresponding molecules. In terms of solubility in water, the compounds follow the trend:

Acetic acid > Glycolaldehyde > Furanone > Furfural

which is approximately the same trend as obtained experimentally from pine-derived pyrolysis oil.

REFERENCES

[Ashish and Ramasami, 2008] Ashish, H. and Ramasami, P. (2008). Rotational barrier and thermodynamical parameters of furfural, thiofurfural, and selenofurfural in the gas and solution phases: Theoretical study based on density functional theory method. *Molecular Physics*, 106:175–185.

[Aspiala et al., 1986] Aspiala, A., Murto, J., and Stén, P. (1986). Ir-induced conformer interconversion processes of glycolaldehyde in low-temperature matrices, and ab initio calculations on the energetics and vibrational frequencies of the conformers. *Chemical Physics*, 106:399–412.

[Aviles-Moreno et al., 2006] Aviles-Moreno, J.-R., Demaison, J., and Huet, T. (2006). Conformational flexibility in hydrated sugars: The glycolaldehyde-water complex. *Journal of the American Chemical Society*, 128:10467–10473.

[Boys and Bernardi, 1970] Boys, S. and Bernardi, F. (1970). The calculation of small molecular interactions by the differences of separate total energies. some procedures with reduced errors. *Molecular Physics*, 19:553–566.

[Carbonniere and Pouchan, 2012] Carbonniere, P. and Pouchan, C. (2012). Modelization of vibrational spectra beyond the harmonic approximation from an iterative

variation-perturbation scheme: The four conformers of the glycolaldehyde. *Theoretical Chemistry Accounts*, 131:1–8.

[Carroll et al., 2013] Carroll, P. B., McGuire, B. A., Zaleski, D. P., Neill, J. L., Pate, B. H., and Weaver, S. L. W. (2013). The pure rotational spectrum of glycolaldehyde isotopologues observed in natural abundance. *Journal of Molecular Spectroscopy*, 284–285:21 – 28.

[Chałasiński and Szcześniak, 1988] Chałasiński, G. and Szcześniak, M. (1988). On the connection between the supermolecular møller-plesset treatment of the interaction energy and the perturbation theory of intermolecular forces. *Molecular Physics*, 63:205–224.

[Chen and Gordon, 1996] Chen, W. and Gordon, M. (1996). Energy decomposition analyses for many-body interaction and applications to water complexes. *Journal of Physical Chemistry*, 100:14316–14328.

[Contreras-García et al., 2011] Contreras-García, J., Johnson, E. R., Keinan, S., Chaudret, R., Piquemal, J.-P., Beratan, D. N., and Yang, W. (2011). Nciplot: A program for plotting noncovalent interaction regions. *Journal of Chemical Theory and Computation*, 7:625–632.

[Desiraju and Steiner, 2006] Desiraju, G. and Steiner, T. (2006). *The Week Hydrogen Bond in Structural Chemistry and Biology*. Oxford University Press, Oxford.

[El-Hamdi et al., 2013] El-Hamdi, M., El Bakouri El Farri, O., Salvador, P., Abdelouahid, B., El Begrani, M., Poater, J., and Solà, M. (2013). Analysis of the relative stabilities of ortho, meta, and para mcly(xc 4h4)(ph3)2 heterometallabenzenes (m = rh, ir; x = n, p; y = cl and m = ru, os; x = n, p; y = co). *Organometallics*, 32:4892–4903.

[Foresman and Frisch, 1996] Foresman, J. B. and Frisch, A. (1996). *Exploring Chem-*

istry with Electronic Structure Methods,second ed.,. Gaussian, Inc., Pittsburgh, PA.

[Frey and Davidson, 1989] Frey, R. and Davidson, E. (1989). Energy partitioning of the self-consistent field interaction energy of scco. *The Journal of Chemical Physics*, 90:5555–5562.

[Frisch et al., 2004] Frisch, M., Trucks, G., Schlegel, H., Scuseria, G., Robb, M., Cheeseman, J., Jr., J. M., Vreven, T., Kudin, K., Burant, J., Millam, J., Iyengar, S., Tomasi, J., Barone, V., Mennucci, B., Cossi, M., Scalmani, G., Rega, N., Petersson, G., Nakatsuji, H., Hada, M., Ehara, M., Toyota, K., Fukuda, R., Hasegawa, J., Ishida, M., Nakajima, T., Honda, Y., Kitao, O., Nakai, H., Klene, M., Li, X., Knox, J., Hratchian, H., Cross, J., Adamo, C., Jaramillo, J., Gomperts, R., Stratmann, R., Yazyev, O., Austin, A., Cammi, R., Pomelli, C., Ochterski, J., Ayala, P., Morokuma, K., Voth, G., Salvador, P., Dannenberg, J., Zakrzewski, V., Dapprich, S., Daniels, A., Strain, M., Farkas, O., Malick, D., Rabuck, A., Raghavachari, K., Foresman, J., Ortiz, J., Cui, Q., Baboul, A., Clifford, S., Cioslowski, J., Stefanov, B., Liu, G., Liashenko, A., Piskorz, P., Komaromi, I., Martin, R., Fox, D., Keith, T., Al-Laham, M., Peng, C., Nanayakkara, A., Challacombe, M., Gill, P., Johnson, B., Chen, W., Wong, M., Gonzalez, C., and Pople, J. (2004). *Gaussian 03, Revision C.02*. Gaussian, Inc., Wallingford, CT.

[Garrec et al., 2014] Garrec, J., Monari, A., Assfeld, X., Mir, L., and Tarek, M. (2014). Lipid peroxidation in membranes: The peroxyl radical does not "float". *Journal of Physical Chemistry Letters*, 5:1653–1658.

[Glendening et al.,] Glendening, E., Reed, A., Carpenter, J., and Weinhold, F. Nbo version 3.1.

[Glendening and Streitwieser, 1994] Glendening, E. D. and Streitwieser, A. (1994). Natural energy decomposition analysis: An energy partitioning procedure for molecular interactions with application to weak hydrogen bonding, strong ionic, and moderate donor–acceptor interactions. *The Journal of Chemical Physics*, 100:2900–2909.

[Heßelmann and Jansen, 2002a] Heßelmann, A. and Jansen, G. (2002a). First-order intermolecular interaction energies from kohn-sham orbitals. *Chemical Physics Letters*, 357:464–470.

[Heßelmann and Jansen, 2002b] Heßelmann, A. and Jansen, G. (2002b). Intermolecular induction and exchange-induction energies from coupled-perturbed kohn-sham density functional theory. *Chemical Physics Letters*, 362:319–325.

[Heßelmann and Jansen, 2003] Heßelmann, A. and Jansen, G. (2003). Intermolecular dispersion energies from time-dependent density functional theory. *Chemical Physics Letters*, 367:778–784.

[Heßelmann et al., 2005] Heßelmann, A., Jansen, G., and Schütz, M. (2005). Density-functional theory-symmetry-adapted intermolecular perturbation theory with density fitting: A new efficient method to study intermolecular interaction energies. *The Journal of Chemical Physics*, 122:014103.

[Hobza and Havlas, 2000] Hobza, P. and Havlas, Z. (2000). Blue-shifting hydrogen bonds. *Chemical Reviews*, 100:4253–4264.

[Jeziorski et al., 1994] Jeziorski, B., Moszynski, R., and Szalewicz, K. (1994). Perturbation theory approach to intermolecular potential energy surfaces of van der waals complexes. *Chemical Reviews*, 94:1887–1930.

[Johnson et al., 2010] Johnson, E. R., Keinan, S., Mori-Sánchez, P., Contreras-García, J., Cohen, A. J., and Yang, W. (2010). Revealing noncovalent interactions. *Journal of the American Chemical Society*, 132:6498–6506.

[Khaliullin et al., 2007] Khaliullin, R., Cobar, E., Lochan, R., Bell, A., and Head-Gordon, M. (2007). Unravelling the origin of intermolecular interactions using absolutely localized molecular orbitals. *Journal of Physical Chemistry A*, 111:8753–8765.

[Kitaura and Morokuma, 1976] Kitaura, K. and Morokuma, K. (1976). A new energy decomposition scheme for molecular interactions within the hartree-fock approximation. *International Journal of Quantum Chemistry*, 10:325–340.

[Kumar et al., 2013] Kumar, R. M., Vijay, D., Sastry, G. N., and Subramanian, V. (2013). *Concepts and Methods in Modern Theoretical Chemistry: Electronic Structure and Reactivity pp. 313-343 (Chapter 15)*. CRC Press Taylor and Francis Group, United Kingdom.

[Lu and Chen, 2012] Lu, T. and Chen, F. (2012). Multiwfn: A multifunctional wavefunction analyzer. *Journal of Computational Chemistry*, 33:580–592.

[Ma et al., 2013] Ma, L., Huang, Z., Niu, X., Shen, T., and Guo, L. (2013). A theoretical study on the hydrogen bonding interactions in hxecch...y (y=h2o and hf) complexes. *Computational and Theoretical Chemistry*, 1017:14–21.

[Maçôas et al., 2004] Maçôas, E., Khriachtchev, L., Fausto, R., and Räsänen, M. (2004). Photochemistry and vibrational spectroscopy of the trans and cis conformers of acetic acid in solid ar. *Journal of Physical Chemistry A*, 108:3380–3389.

[Maçôas et al., 2003] Maçôas, E., Khriachtchev, L., Pettersson, M., Fausto, R., and Räsänen, M. (2003). Rotational isomerism in acetic acid: The first experimental observation of the high-energy conformer. *Journal of the American Chemical Society*, 125:16188–16189.

[Mitoraj et al., 2009] Mitoraj, M. P., Michalak, A., and Ziegler, T. (2009). A combined charge and energy decomposition scheme for bond analysis. *Journal of Chemical Theory and Computation*, 5:962–975.

[Müller et al., 2004] Müller, A., Losada, M., and Leutwyler, S. (2004). Ab initio benchmark study of (2-pyridone)2, a strongly bound doubly hydrogen-bonded dimer. *The Journal of Physical Chemistry A*, 108:157–165.

[Mo et al., 2011] Mo, Y., Bao, P., and Gao, J. (2011). Energy decomposition analysis based on a block-localized wavefunction and multistate density functional theory. *Physical Chemistry Chemical Physics*, 13:6760–6775.

[Mohan et al., 2006] Mohan, D., Pittman Jr., C., and Steele, P. (2006). Pyrolysis of wood/biomass for bio-oil: A critical review. *Energy and Fuels*, 20:848–889.

[Morokuma, 1971] Morokuma, K. (1971). Molecular orbital studies of hydrogen bonds. iii. c=o···h–o hydrogen bond in h2co···h2o and h2co···2h2o. *The Journal of Chemical Physics*, 55:1236–1244.

[Rao, 1976] Rao, Y. (1976). Recent advances in the chemistry of unsaturated lactones. *Chemical Reviews*, 76:625–694.

[Ratajczyk et al., 2004] Ratajczyk, T., Pecul, M., Sadlej, J., and Helgaker, T. (2004). Potential energy and spin-spin coupling constants surface of glycolaldehyde. *Journal of Physical Chemistry A*, 108:2758–2769.

[Rivelino et al., 2002] Rivelino, R., Coutinho, K., and Canuto, S. (2002). A monte carlo-quantum mechanics study of the solvent-induced spectral shift and the specific role of hydrogen bonds in the conformational equilibrium of furfural in water. *Journal of Physical Chemistry B*, 106:12317–12322.

[Rogojerov et al., 2005] Rogojerov, M., Keresztury, G., and Jordanov, B. (2005). Vibrational spectra of partially oriented molecules having two conformers in nematic and isotropic solutions: Furfural and 2-chlorobenzaldehyde. *Spectrochimica Acta - Part A: Molecular and Biomolecular Spectroscopy*, 61:1661–1670.

[Schmidt et al., 1993] Schmidt, M. W., Baldridge, K. K., Boatz, J. A., Elbert, S. T., Gordon, M. S., Jensen, J. H., Koseki, S., Matsunaga, N., Nguyen, K. A., Su, S., Windus, T. L., Dupuis, M., and Montgomery, J. A. (1993). General atomic and molecular electronic structure system. *Journal of Computational Chemistry*, 14:1347–1363.

[Semrouni et al., 2013] Semrouni, D., Isley, W., Clavaguéra, C., Dognon, J.-P., Cramer, C., and Gagliardi, L. (2013). Ab initio extension of the amoeba polarizable force field to fe 2+. *Journal of Chemical Theory and Computation*, 9:3062–3071.

[Senent, 2004] Senent, M. (2004). Ab initio study of the torsional spectrum of glycolaldehyde. *Journal of Physical Chemistry A*, 108:6286–6293.

[Senent, 2001] Senent, M. L. (2001). Ab initio determination of the torsional spectra of acetic acid. *Molecular Physics*, 99:1311–1321.

[Shen et al., 2012] Shen, T., Huang, Z., Guo, L., and Wang, H. (2012). An ab initio study on the insertion of radon atoms into hypohalous acids. *Inorganica Chimica Acta*, 386:68–72.

[Singh et al., 2014] Singh, S. K., Kumar, S., and Das, A. (2014). Competition between n [rightward arrow] [small pi]ar* and conventional hydrogen bonding (n-h[three dots, centered]n) interactions: an ab initio study of the complexes of 7-azaindole and fluorosubstituted pyridines. *Phys. Chem. Chem. Phys.*, 16:8819–8827.

[Sipila et al., 1998] Sipila, K., Kuoppala, E., Fagernas, L., and Oasmaa, A. (1998). Characterization of biomass-based flash pyrolysis oils. *Biomass and Bioenergy*, 14:103–113.

[Stevens and Fink, 1987] Stevens, W. J. and Fink, W. H. (1987). Frozen fragment reduced variational space analysis of hydrogen bonding interactions. application to the water dimer. *Chemical Physics Letters*, 139:15 – 22.

[Su and Li, 2009] Su, P. and Li, H. (2009). Energy decomposition analysis of covalent bonds and intermolecular interactions. *The Journal of Chemical Physics*, 131:014102.

[Szalewicz and Jeziorski, 1979] Szalewicz, K. and Jeziorski, B. (1979). Symmetry-adapted double-perturbation analysis of intramolecular correlation effects in weak

intermolecular interactions: The he-he interaction. *Molecular Physics*, 38:191–208.

[Thellamurege and Hirao, 2013] Thellamurege, N. and Hirao, H. (2013). Water complexes of cytochrome p450: Insights from energy decomposition analysis. *Molecules*, 18:6782–6791.

[van der Vaart and Merz, 1999] van der Vaart, A. and Merz, K. M. (1999). Divide and conquer interaction energy decomposition. *The Journal of Physical Chemistry A*, 103:3321–3329.

[Vitasari et al., 2011] Vitasari, C., Meindersma, G., and de Haan, A. (2011). Water extraction of pyrolysis oil: The first step for the recovery of renewable chemicals. *Bioresource Technology*, 102:7204–7210.

[Wu et al., 2009] Wu, Q., Ayers, P. W., and Zhang, Y. (2009). Density-based energy decomposition analysis for intermolecular interactions with variationally determined intermediate state energies. *The Journal of Chemical Physics*, 131:164112.

[Yu, 2013] Yu, F. (2013). Intermolecular interactions of formic acid with benzene: Energy decomposition analyses with ab initio mp2 and double-hybrid density functional computations. *International Journal of Quantum Chemistry*, 113:2355–2360.

[Ziegler and Rauk, 1977] Ziegler, T. and Rauk, A. (1977). On the calculation of bonding energies by the hartree fock slater method: I. the transition state method. *Theoretica chimica acta*, 46:1–10.

CHAPTER 3

Liquid-Liquid Equilibria (LLE): Experiments

3.1 Introduction

Lignocellulosic biomass has received enormous attention as a renewable energy resource as they can improve energy security and reduce carbon emissions [Ralph et al., 2010, Demirbas, 2009, Demirbas, 2011, S.N.Naik et al., 2010, Nigam and Singh, 2011]. Last decade saw considerable research in fast pyrolysis process for the production of liquid fuel and chemicals from biomass. Fast pyrolysis of biomass produces 60-75 wt% of liquid bio-oil, 15-25 wt% of solid char and 10-20 wt% of noncondensable gases depending on the feedstock used [Bridgwater, 2003, Czernik and Bridgwater, 2004, Mohan et al., 2006, Bridgwater, 2012]. Several chemicals have been identified in bio-oil of which the most abundant and of interest are: glycolaldehyde (0.9-13 wt%), acetic acid (0.5-12 wt%), formic acid (0.3-9.1 wt%), acetol (0.7-7.4 wt%), furfural alcohol (0.1-5.2 wt%) and furfural (0.1-1.1 wt%) [J.P.Diebold, 2000]. Due to high concentration of the value-added chemical compounds, production of chemicals from bio-oil has received considerable interest.

Fractionation of bio-oil with water is the easiest method which transforms bio-oil in to two fractions: an aqueous top phase enriched in carbohydrate derived chemicals and an organic bottom phase containing lignin-containing fractions. Both phases can be further processed separately to extract value added chemicals [Mohan et al., 2006, Sipila et al., 1998]. Vitasari et al. have studied the effects of stirring rate and water-to-oil ratio on the extraction of various chemicals from forest-residue derived bio-oil and pine-derived bio-oil and found that water extraction is indeed a very useful method to extract 80-90% polar compounds [Vitasari et al., 2011]. The aqueous phase derived from bio-oil is a good feed for the extraction of acetic acid, levoglucosan and sugar compounds. Tri-n-octylamine (TOA) has been found to be a promising extractant for the extraction of acetic acid from bio-oil [Mahfud et al., 2008]. By optimizing the extraction process, acetic acid extraction efficiencies of 93% has been achieved using 50 vol% TOA in octane and 23 wt% bio-oil in THF. However a key drawback of this process resulted in the transfer of high amounts of TOA to the pyrolysis oil phase. In another work , acetic acid

has been extracted from an aqueous phase derived from bio-oil [Mahfud et al., 2008]. The extraction efficiency was 75% using toluene as the TOA diluent. In contrast to the experiments with bio-oil, TOA was not detected in the aqueous phase. Rasrendra et al. have also demonstrated that reactive extraction is an attractive method to obtain organic acids from an aqueous stream derived from pyrolysis oil [Rasrendra et al., 2011]. They found that TOA and 2-ethylhexanol are the preferred extract and diluent respectively. At equilibrium conditions, 86% acetic acid recovery was obtained using 40 wt% TOA in 2-ethylhexanol in batch mode at room temperature. Bennett et al. have further extracted levoglucosan from bio-oil by optimizing the water-to-oil ratio and operating temperature [Bennett et al., 2009]. Optimal selection of water-to-oil ratio yielded an aqueous phase containing levoglucosan concentration of up to 87 g/l i.e., a yield of 7.8 wt% of the bio-oil at 34 °C. Similarly, extraction of bio-oil with water followed by $CH_2Cl_2/CHCl_3$ effectively separated sugar and sugar derivatives from aromatics. Further acid-treatment in methanol converted the sugar into levulinic acid/ester and sugar derivative into fuel derivatives [Hu et al., 2012].

Mantilla et al. have studied the extraction of phenolic compounds from bio-oil by two consecutive liquid-liquid extraction stages [Mantilla et al., 2015]. The first liquid-liquid extraction was performed with dichloromethane which ensured that the phenolic fraction was present only in one phase of the bio-oil; and the second extraction with ethyl acetate maximized the phenol composition in the organic fraction. Wei et al. have studied the liquid-liquid extraction of bio-oil with several solvents (hexane, petroleum ether and chloroform) [Wei et al., 2014]. In comparison to raw bio-oil, the solvent phase had high concentrations (85%) of phenols and guaiacols, while no sugar and very low acid and alcohol contents were detected, which were left in the water phases. Yang et al. proposed a solvent combination of n-hexane, ethyl acetate and Tetrahydrofuran to sequentially extract and separate the bio-oil in to three fraction of different applications, i.e., light oil (26.13%), mid-weight oil (54.19%), and heavy oil (19.68%) [Yang et al., 2014]. Light oil contains low-molecular weight compounds, which can be used to extract chemicals such as phenols. Mid-weight oil was found to comprise aromatic

oligomers while heavy oil was found to be rich in alkanes. Park et al. also studied the separation of bio-oil components by adding water, organic solvents (hexadecane and octane), and sodium hydroxide [Park et al., 2016]. Acetic acid and phenolic compounds were extracted in aqueous and organic phases, respectively. In summary, the organic solvents extracted a higher fraction of chemicals from bio-oil in combined mode, than in sequential extraction. However, organic solvents partitioned into the aqueous phase in combined extraction.

In most of the processes as described above, a significant portion of solvents was found in the raffinate phase or the aqueous rich phase. This necessitates the use of novel solvents which can serve two purposes namely negligible concentration in the aqueous phase; and higher selectivity and distribution for bio-oil derived chemicals. The last decade saw great amount of interest in a new class of liquid materials termed as ionic liquids (ILs). ILs are organic salts made of bulky nonsymmetrical organic cations and organic/inorganic anions and are liquid below 100°C. The physical and chemical properties of ionic liquids can be tuned as per application by selecting the cationic or the anionic constituent. Therefore, ILs are regarded as "designer solvents". Due to its unique properties, ILs have a variety of applications in synthesis, catalysis, separation technologies, lubrication, analytical and electrolytes [Marsh et al., 2004, Berthod et al., 2008, Werner et al., 2010, Plechkovaa and Seddon, 2008].

Therefore, in this chapter, we report the LLE data for the extraction of acetic acid and furfural from aqueous solution using 1-butyl-3-methylimidazolium bis(trifluoromethylsulfonyl)imide [BMIM][Tf_2N] as solvent. We also report the LLE data for the extraction of acetol from aqueous solution using both conventional solvents (chloroform/ethyl acetate/*n*-propyl acetate/*n*-butyl acetate) and Ionic Liquids ([EMIM][Tf_2N] and [BMIM][Tf_2N]) for which no such data have previously been reported in literature. All LLE data have been reported at 298.15 K and at atmospheric pressure.

3.2 Experiments

3.2.1. Chemicals and Materials

Acetol (95%, CAS: 116-09-6), *n*-propyl acetate (99%, CAS: 109-60-4) and *n*-butyl acetate (>99%, CAS: 123-86-4) were purchased from Alfa Aesar, UK. Acetic acid (>99%, CAS: 64-19-7), ethyl acetate (99.5%, CAS: 141-78-6) and chloroform (>99%, stabilized with 0.7-1.0 % ethanol) were purchased from Merck, India. Furfural (>99%, CAS: 98-01-1) was purchased from SRL Pvt., Ltd., India. Ionic liquids, 1-Ethyl-3-Methylimidazolium bis (trifluoromethylsulfonyl) imide (>98%, CAS: 174899-82-2), 1-Butyl-3-Methylimidazolium bis (trifluoromethylsulfonyl) imide (>98%, CAS: 174899-83-3) and Dimethyl Sulfoxide-d6 (DMSO-d6, 99.8%) were purchased from Merck, Germany. All the chemicals were analytical grade and used without further purification (Table 3.1). Millipore water was used in all the experiments. The purities of all the materials were checked by density measurement and ^{1}H NMR spectroscopy. Analysis of peaks of ^{1}H NMR spectroscopy indicated negligible impurities. For reducing the water content and volatile compounds to negligible values, vacuum (0.1Pa) for at least 48h were applied to the IL prior to the measurements.

3.2.2. Density Measurement

The density of all the chemicals were measured with an Anton-Paar DMA 4500 M digital oscillating U-tube density meter. Millipore water was used for the calibration of density meter at 293.15 K. The temperature was within $\pm$ 0.01 K during each measurement. Density measurements were carried out at temperatures ranging from 293.15 K to 333.15 K at atmospheric pressure. Repeatability for the standard deviation in the density measurement was 10^{-5} g/cm^3. Experimentally measured densities are reported in Table 3.2.

3.2.3. Liquid-Liquid Equilibria Experiments

In each LLE experiment, a known quantity of water, acetic acid/acetol/furfural and solvent were added in a 15-30 ml size glass vial. Components were added in such a composition that heterogeneous solutions were formed. Parafilm was used to seal the glass vials to avoid any evaporation loss. These sealed glass vials were kept in a thermostatic shaker bath (Dailhan Lab, China) which was operated at 150 RPM and 298.15K (Uncertainty of $\pm$ 0.01K). The samples were stirred for 3 hours at isothermal condition and then kept undisturbed for 12 hours to ensure the equilibrium. Two clear phases were found to appear i.e. water rich phase and solvent rich phase. The samples from each phase were then collected using syringe (needle size 0.45 x 13 mm; Hindustan Syringes & Medical devices Ltd., Faridabad, India) for compositional analysis.

3.2.4. Composition Analysis

^{1}H-nuclear magnetic resonance (NMR) spectroscopy was used for the composition analysis. ^{1}H-NMR spectrum provides the information regarding the number of different types of hydrogen atoms present in the molecule as well as the electronic environment for the different types of hydrogen. Each group of chemically equivalent hydrogen gives rise to a unique peak in the NMR spectrum. Further different groups provide different chemical shift within the NMR spectra. The number of hydrogen atoms corresponding to each peak is identified by the integration (relative area) of the peak for each group.Thus, the area under each peak is proportional to the number of hydrogen atoms within the peak. This is used for the determination of the composition of each component present in the mixture. In this work, ^{1}H-NMR spectra were recorded by both 400 MHz (Varian) and 600 MHz (Bruker) NMR spectrometers. NMR spectra are recorded in solution and it is assumed that solvent protons do not interfere with the compound spectra. Therefore, deuterated solvents are used for NMR. In this work, deuterated dimethyl sulfoxide (DMSO-D_6), was used.

Table 3.1.: Chemicals Source, Purification Method, Purity and Analysis Method

Sl. no.	Chemical Name	Source	Purification Method	Purity (Mass fraction)	Analysis Method
1	Acetic acid	Merck, India	None	> 0.99	density method and ^{1}H NMR[a]
2	Furfural	SRL Pvt. Ltd., India	None	> 0.99	density method and ^{1}H NMR
3	Acetol	Alfa Aesar, UK	None	0.95	density method and ^{1}H NMR
4	Ethyl acetate	Merck, India	None	0.995	density method and ^{1}H NMR
5	*n*-propyl acetate	Alfa Aesar, UK	None	0.99	density method and ^{1}H NMR
6	*n*-butyl acetate	Alfa Aesar, UK	None	> 0.99	density method and ^{1}H NMR
7	Chloroform	Merck, India	None	> 0.99	density method and ^{1}H NMR
8	[EMIM][Tf_2N][b]	Merck, Germany	Vacuum drying	> 0.98	density method and ^{1}H NMR
9	[BMIM][Tf_2N][c]	Merck, Germany	Vacuum drying	> 0.98	density method and ^{1}H NMR
10	DMSO-D_6	Merck, Germany	None	0.998	None

[a] ^{1}H NMR = ^{1}H Nuclear Magnetic Resonance spectroscopy

[b] [EMIM][Tf_2N] = 1-Ethyl-3-Methylimidazolium bis (trifluoromethylsulfonyl) imide

[c] [BMIM][Tf_2N] = 1-Butyl-3-Methylimidazolium bis (trifluoromethylsulfonyl) imide

Table 3.2.: Density(ρ) of acetic acid, acetol, furfural, ethyl acetate, *n*-propyl acetate, *n*-butyl acetate, chloroform, [EMIM][Tf_2N] and [BMIM][Tf_2N] as a function of temperature at atmospheric pressure (p = 0.1 Mpa)

Acetic acid		**Acetol**	
T (K)	ρ **(g/**cm^3**)**	**T (K)**	ρ **(g/**cm^3**)**
293.15	1.04975	293.15	1.08013
298.15	1.04407	298.15	1.07492
303.15	1.03839	303.15	1.06967
308.15	1.03272	308.15	1.06431
313.15	1.02705	313.15	1.05871
Ethyl acetate		318.15	1.05313
293.15	0.90048	323.15	1.04755
298.15	0.89436	328.15	1.04201
303.15	0.88819	333.15	1.03662
308.15	0.88198	***n*-butyl acetate**	
313.15	0.87573	293.15	0.88061
***n*-propyl acetate**		298.15	0.87545
293.15	0.88780	303.15	0.87027
298.15	0.88219	308.15	0.86508
303.15	0.87656	313.15	0.85986
308.15	0.87090	**Chloroform**	
313.15	0.86521	293.15	1.4800
Furfural		298.15	1.4710
298.15		303.15	1.4605
313.15		313.15	1.4415
[EMIM][Tf_2N]		**[BMIM][Tf_2N]**	
293.15	1.5326	293.15	1.4495
298.15	1.5277	298.15	1.4447
303.15	1.5227	303.15	1.4400
308.15	1.5180	308.15	1.4352
313.15	1.5128	313.15	1.4305

A sample of 0.10 ml from each phase was collected using 1 ml syringe (needle size 0.45 x 13 mm; Hindustan Syringes & Medical devices Ltd., Faridabad, India) and mixed with 0.5 ml of NMR solvent (DMSO-d_6) in NMR tube (thrift grade, Sigma Aldrich). The tube was placed on Spinix Vortex Shaker (TARSONS) for mixing the sample and NMR solvent. Then, tubes were placed in NMR spectrophotometer and reference peak for NMR solvent was recorded (2.5 ppm for DMSO-d_6). In each NMR spectroscopy experiment, a free induction decay (fid) data file is generated. All fid files were analysed using a freeware namely, ACD/NMR Processor Academic Edition software (www.acdlabs.com) for the calculation of mole-fraction of each component in respective phase. Peaks were analyzed for the calculation of mole fraction of each component in respective phase.

^{1}H NMR peak values for all the components studied in this work are reported in Figure 3.1. Methyl group of acetic acid showed a peak at 1.9 ppm which was considered for the quantification of acetic acid in both the phases. Peak at 5.0 ppm and 1.16 ppm was used for the quantification of acetol and ethyl acetate respectively. Peak at 0.85 ppm due to three H-atoms was used for the quantification of *n*-propyl acetate and *n*-butyl acetate. Chloroform ($CHCl_3$) spectra has single peak at 8.26 due to single H-atom which was used for the composition estimation of chloroform. NMR spectra of furfural showed four different peaks. Peak at 8.0 ppm due to single H-atom was used for the quantification of furfural in both the phases. Peak at 9.0 ppm due to single H-atom was used for the quantification of [EMIM][Tf_2N] and [BMIM][Tf_2N]. The water in DMSO-d_6 showed peak at 3.3-4.0 ppm.

To verify the reliability of ^{1}H NMR spectroscopy, solutions of known compositions of IL-acetic acid-water was prepared and analyzed by ^{1}H NMR spectroscopy. The results obtained were in good agreement with the known compositions ($\pm$ 0.001 mole fraction). Further we have carried out the composition analysis for binary mixtures of [BMIM][Tf_2N]-water at T = 298.15 K and atmospheric pressure.^{1}H-NMR spectrum of water phase is dominated by water peak where the mole fraction of IL is 0.004 (Figure 3.2). In a similar manner the mole fraction of water in IL-phase is 0.3169 (Figure 3.3). These values are tabulated in Table 3.3 and compared with existing experimental

data. The comparison clearly shows the reliability of ^{1}H-NMR determined composition. Further the water mole fractions in both the phases were confirmed by a Karl Fisher Titrator (MetroOhm 787 KF Titrino).

Table 3.3.: Benchmarking Studies of IL-Water mixtures using ^{1}H-NMR spectroscopy at T = 298.15 K and pressure p = 0.1 Mpa

	water in IL-phase		
[BMIM][Tf_2N]	This Work	1/2	3
Mole fraction	0.3169	0.2700 (0.23-0.31)	0.2568
	IL in water phase		
Mole fraction	0.0004	0.0003	0.0003

1 = [Crosthwaite et al., 2004]

2 = [Chapeaux et al., 2007]

3 = [Freire et al., 2008]

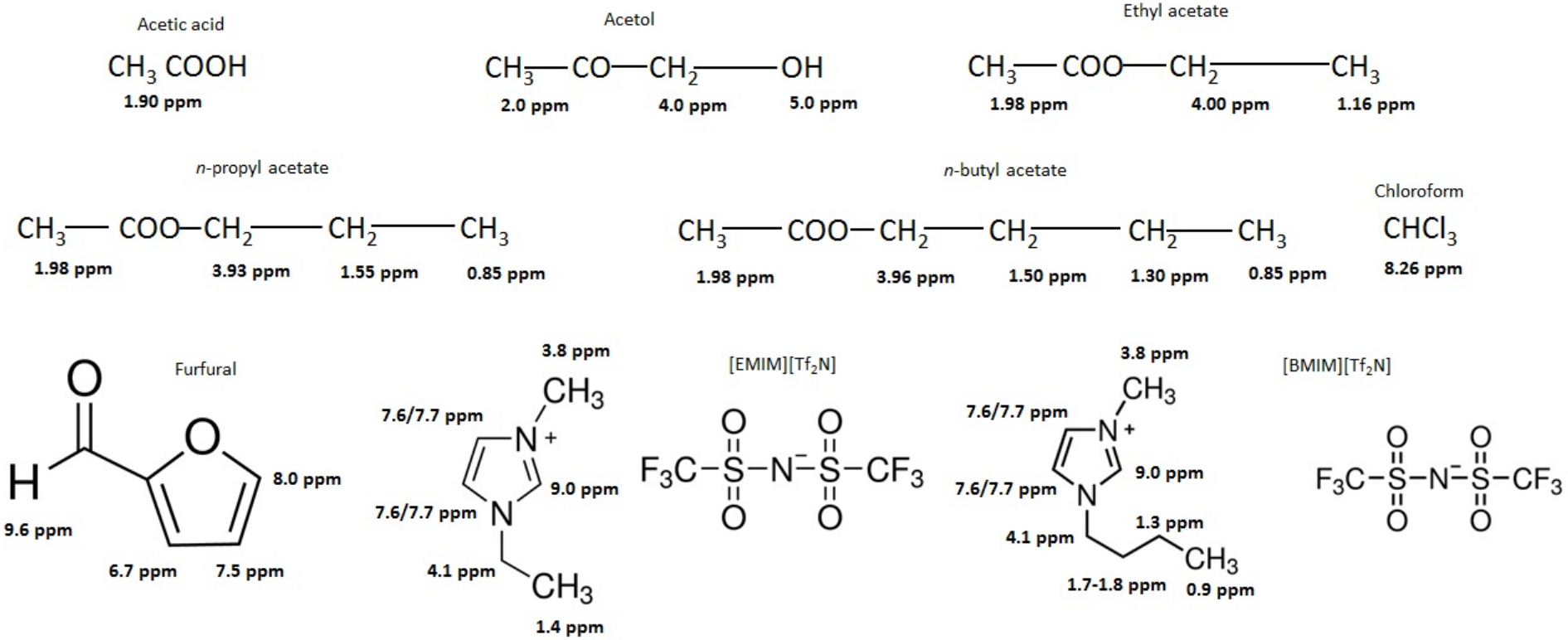

Figure 3.1.: ^{1}H NMR peak values (in ppm) of chemical compounds studied in this work.

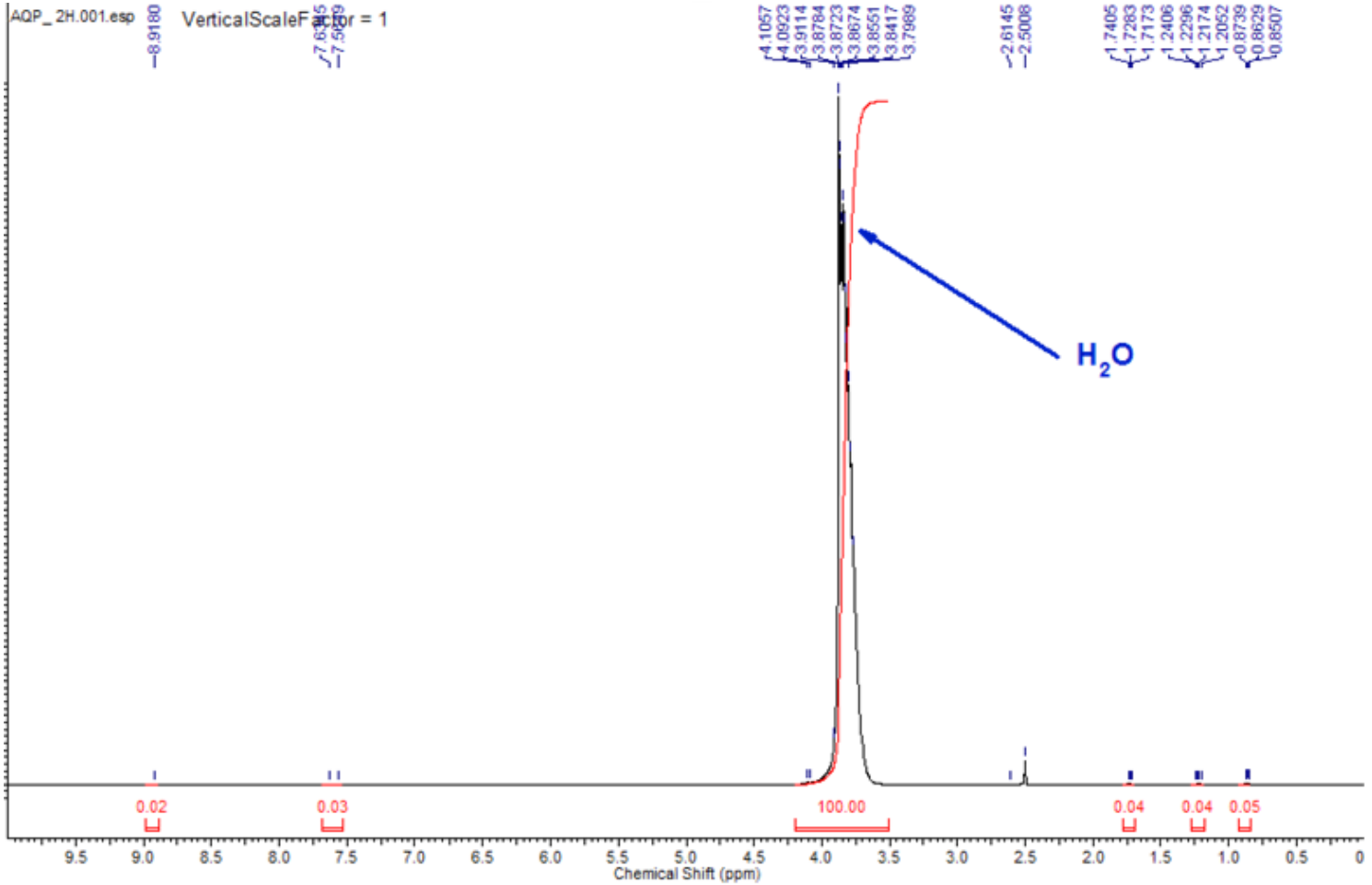

Figure 3.2.: ^{1}H NMR spectra of water rich-Phase for [BMIM][Tf_2N] + WATER

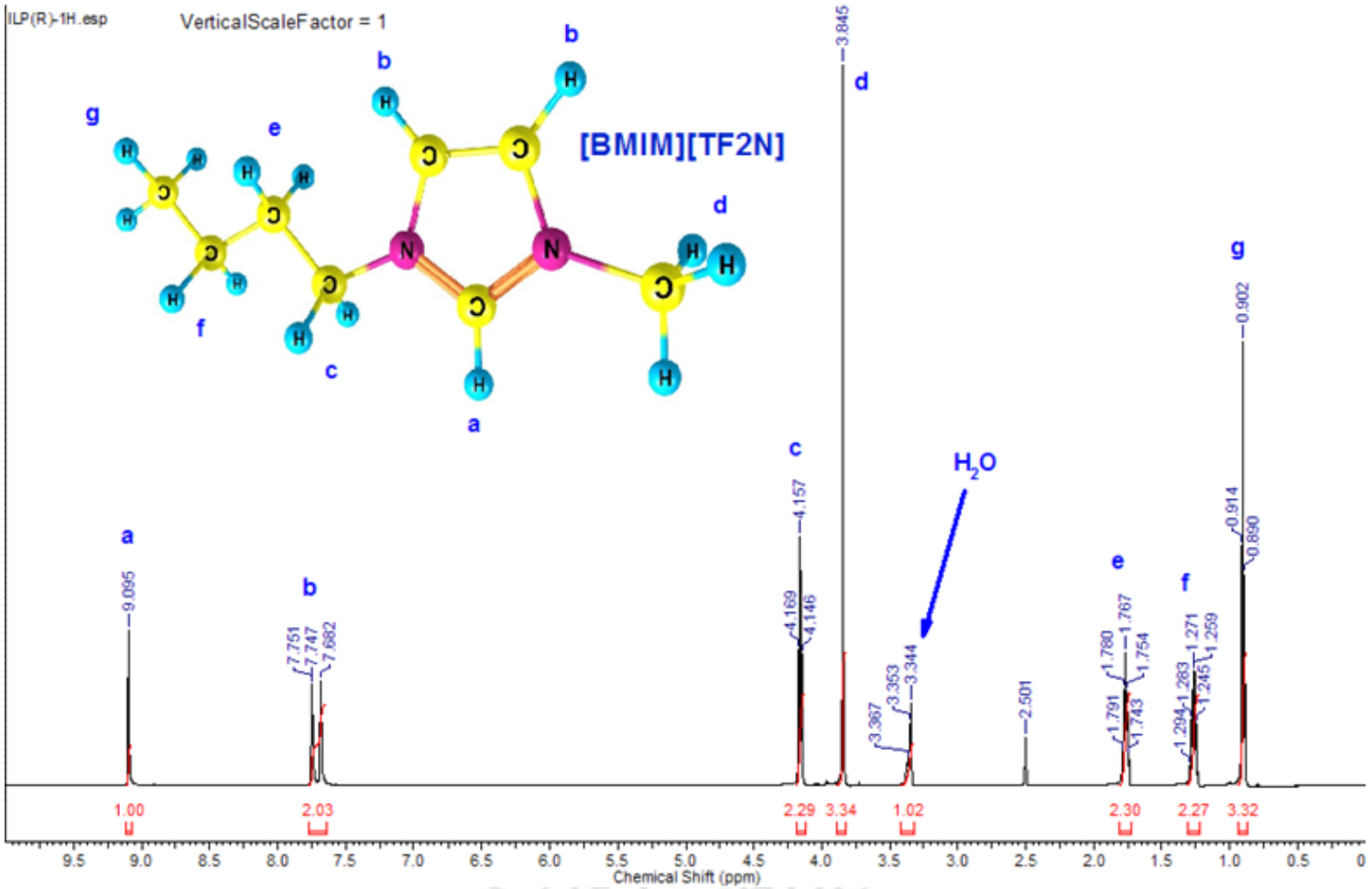

Figure 3.3.: ^{1}H NMR spectra of IL rich-Phase for [BMIM][Tf_2N] + WATER

3.3 Results and Discussions

The extraction effectiveness of a solvent is generally expressed in terms of distribution coefficient (β) and selectivity (S). Distribution coefficient (β) and selectivity (S) are defined as:

$$\beta = \frac{x^E_{solute}}{x^R_{solute}} \tag{3.1}$$

$$\mathrm{S} = \frac{x^E_{solute}/x^R_{solute}}{x^E_w/x^R_w} \tag{3.2}$$

where x_{solute} and x_w are the mole fractions of solute (i.e., acetic acid or furfural or acetol) and water, respectively. Superscripts E and R indicate the extract and the raffinate phases, respectively. Distribution co-efficient gives a measure of the affinity of the solute for the two phases. The distribution coefficient for a solute should be large enough so that a lower solvent (S)/feed (F) ratio is required. Similarly, selectivity parameter must be greater than unity for a useful extraction operation.

3.3.1. [BMIM][Tf_2N] - acetic acid - water system

The experimental LLE data of [BMIM][Tf_2N]/acetic acid/water system was measured at 298.15 K under atmospheric pressure. The experimental LLE data of the system along with distribution coefficients and selectivities is reported in Table 3.4. The experimental LLE ternary diagram for the system is shown in Figure 3.4. The experimental data showed that distribution coefficient was in the range of 1.84-2.65, while selectivity was in the range of 4.22-7.43. Selectivity value grater than one implies that the extraction of acetic acid by [BMIM][Tf_2N] is possible. Another significant aspect is the fact that the quantity of ionic liquid in raffinate phase is zero which will result in lower process operating cost. Another important finding is that [BMIM][Tf_2N] can be used to extract acetic acid for mole fractions lesser than 0.15. LLE data also revealed that selectivity decreases with increase in the acetic acid concentration in water. Furthermore, the water solubility in extract phase generally increased with increase in concentration of acetic acid in the ionic liquid. This is due to the fact that as the concentration of acetic

acid increases, the hydrogen bonding capacity of the mixture also increases. This allows the water molecules to interact within the system even in the presence of hydrophobic ionic liquids. Finally, the performance of [BMIM][Tf_2N] was also compared with other solvents (ethyl acetate, *n*-propyl acetate, butyl acetate, amyl acetate, 2-methyl ethyl acetate, 2-methyl propyl acetate, isophorone, MTBE) as reported in literature in terms of distribution coefficient and selectivity [Colombo et al., 1999, Xiao et al., 2006, Toikka et al., 2014, Wang et al., 2007b, Wang et al., 2007a, Miao et al., 2007]. This is shown in Figure 3.5. The highest acetic acid distribution coefficients were found for isophorone whereas distribution coefficients were almost same for other solvents. The selectivity for [BMIM][Tf_2N] was lower than other solvents. On the contrary, the mole fraction(%) of [BMIM][Tf_2N] in raffinate phase was close to zero; whereas for other solvents it was in the range of 0.42-12.04 %. Thus, a high concentration of solvent in raffinate phase may add to extra capital and energy cost. Considering both the aspects, Amyl acetate, Isophorone and [BMIM][Tf_2N] are potential solvents for the extraction of acetic acid from aqueous solution.

Table 3.4.: Experimental Tie Lines data for the system [BMIM][Tf_2N] (1) - acetic acid (2) - water (3) at T = 298.15 K and p = 0.1 Mpa.

Sl.	**Extract phase**			**Raffinate phase**			**Distribution**	**Selec-**
No.	X_1	X_2	X_3	X_1	X_2	X_3	**Co-efficient(β)**	**tivity(S)**
1	0.6317	0.0335	0.3348	0.0000	0.0156	0.9844	2.15	6.31
2	0.5917	0.0592	0.3491	0.0000	0.0223	0.9777	2.65	7.43
3	0.5854	0.0780	0.3366	0.0000	0.0337	0.9663	2.31	6.64
4	0.5541	0.1043	0.3416	0.0000	0.0457	0.9543	2.28	6.38
5	0.4594	0.1446	0.3960	0.0000	0.0684	0.9316	2.11	4.97
6	0.4408	0.1620	0.3972	0.0000	0.0881	0.9119	1.84	4.22

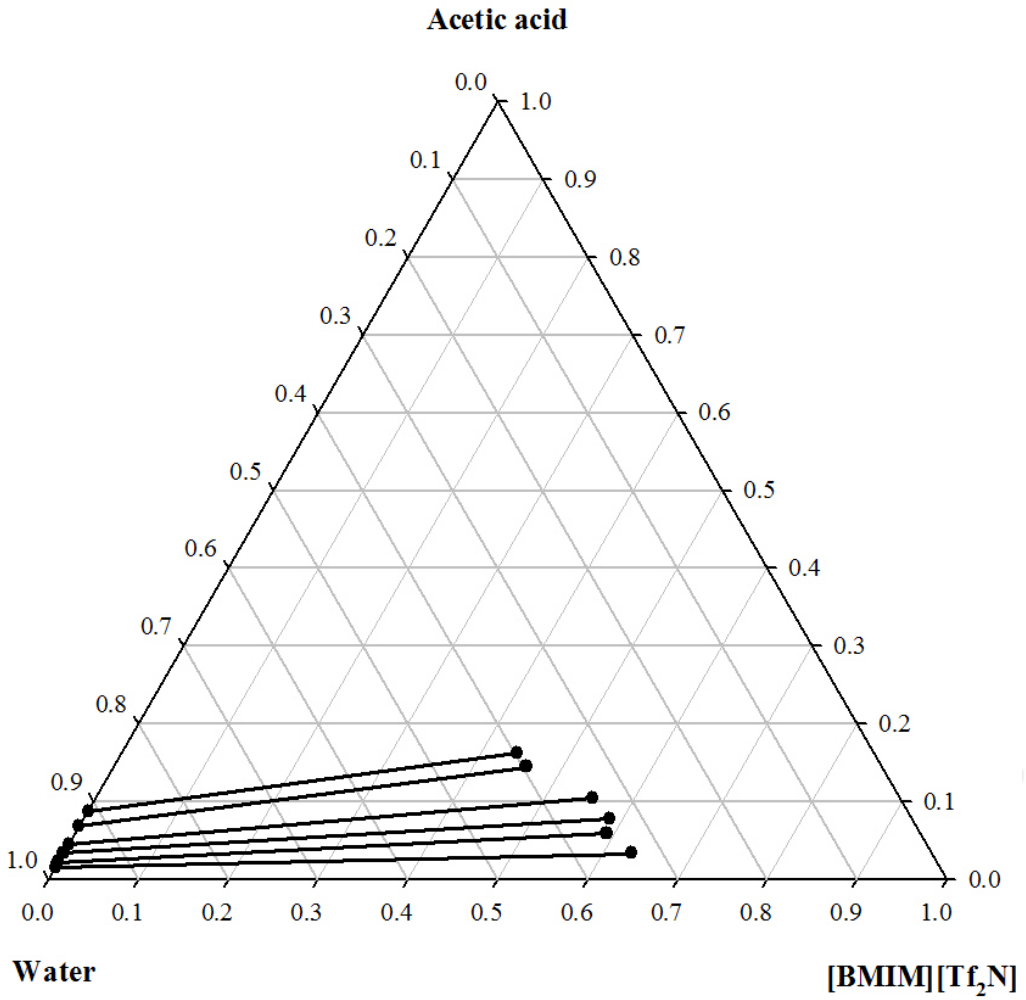

Figure 3.4.: Experimental tie lines for the ternary system: [BMIM][Tf_2N]-acetic acid-water at 298.15 K and 1 atm.

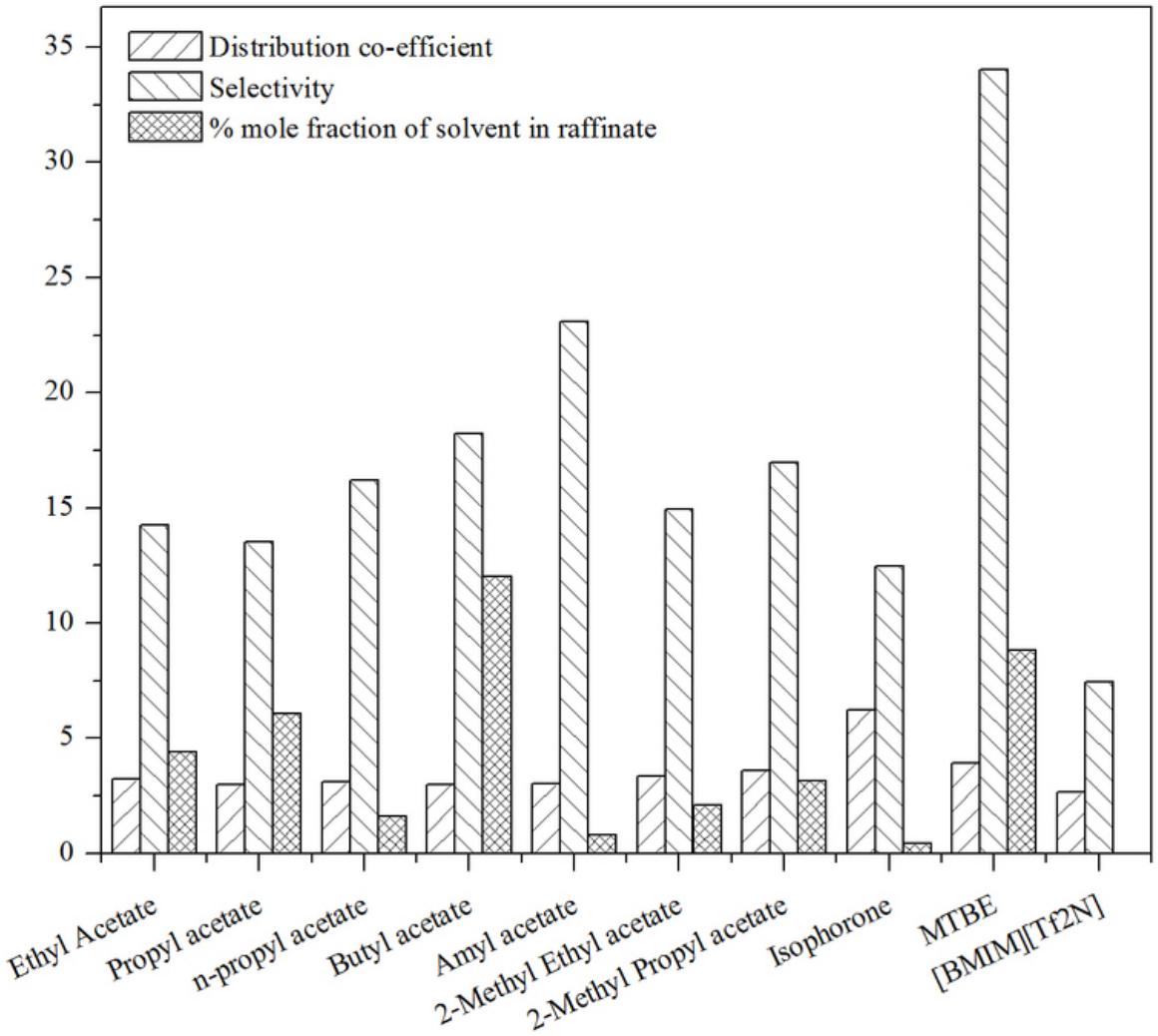

Figure 3.5.: Distribution co-efficient, Selectivity and % mole fraction of solvent in raffinate for acetic acid based ternary system: Present work Vs. Lit.

3.3.2. [EMIM][Tf_2N]/[BMIM][Tf_2N]/chloroform/ethyl acetate/ n-propyl acetate/ n-butyl acetate - acetol - water systems

The experimental LLE data of [EMIM][Tf_2N]/acetol/water, [BMIM][Tf_2N]/acetol/water, chloroform/acetol/water, ethyl acetate/acetol/water, *n*-propyl acetate/acetol/water, and *n*-butyl acetate/acetol/water systems were measured at 298.15 K under atmospheric pressure. The experimental LLE data of these systems along with distribution coefficients and selectivities are reported in Tables 3.5-3.10. The experimental LLE ternary diagram for these systems are shown in Figures 3.6-3.11 and Figure 3.12 shows the com-

parison between the various solvents. Distribution coefficients are in the range of 0.85-1.09 for ethyl acetate, 0.62-0.91 for *n*-propyl acetate, 0.55-0.75 for *n*-butyl acetate, 1.11-1.57 for chloroform, 1.98-2.69 for [EMIM][Tf_2N] and 1.80-2.23 for [BMIM][Tf_2N]. This suggests acetol can be extracted more effectively from aqueous solution using [EMIM][Tf_2N] and [BMIM][Tf_2N]. Selectivity are in the range of 1.72-4.44 for ethyl acetate, 1.92-5.01 for *n*-propyl acetate, 3.01-6.70 for *n*-butyl acetate, 2.96-25.89 for chloroform, 3.89-6.75 for [EMIM][Tf_2N] and 3.37-6.12 for [BMIM][Tf_2N]. For all solvents, selectivity value is grater than one which means that extraction of acetol is possible by all the studied solvents. The highest acetol distribution coefficients were found for [EMIM][Tf_2N] and [BMIM][Tf_2N] whereas distribution coefficients were approximately one for all other solvents. The selectivity was higher for chloroform followed by [EMIM][Tf_2N] and [BMIM][Tf_2N]. Mole fraction (%) of solvent in raffinate for ethyl acetate, *n*-propyl acetate, *n*-butyl acetate, chloroform, [EMIM][Tf_2N] and [BMIM][Tf_2N] were 9.30%, 6.72%, 3.17%, 1.84%, 0.37% and 0.00% respectively. This implies that the latter two namely the IL's may be useful for solvent extraction at ambient condition as trace quantity of ionic liquid in raffinate phase will result in lower process operating cost. For all liquid mixtures, total miscibility was found at high acetol concentrations (> 30 mol%). Overall, [EMIM][Tf_2N], [BMIM][Tf_2N] and chloroform are potential solvents for the extraction of acetol from aqueous solution.

Table 3.5.: Experimental Tie Lines data for the system [EMIM][Tf_2N] (1) - acetol (2) - water (3) at $T = 298.15$ K and $p = 0.1$ Mpa.

Sl.	**Extract phase**			**Raffinate phase**			**Distribution**	**Selec-**
No.	X_1	X_2	X_3	X_1	X_2	X_3	**Co-efficient(β)**	**tivity(S)**
1	0.5587	0.0503	0.3910	0.0000	0.0187	0.9813	2.69	6.75
2	0.4951	0.0990	0.4059	0.0000	0.0400	0.9600	2.48	5.85
3	0.4202	0.1513	0.4285	0.0000	0.0717	0.9283	2.11	4.57
4	0.3636	0.2037	0.4327	0.0037	0.0933	0.9030	2.18	4.56
5	0.3087	0.2469	0.4444	0.0000	0.1250	0.8750	1.98	3.89

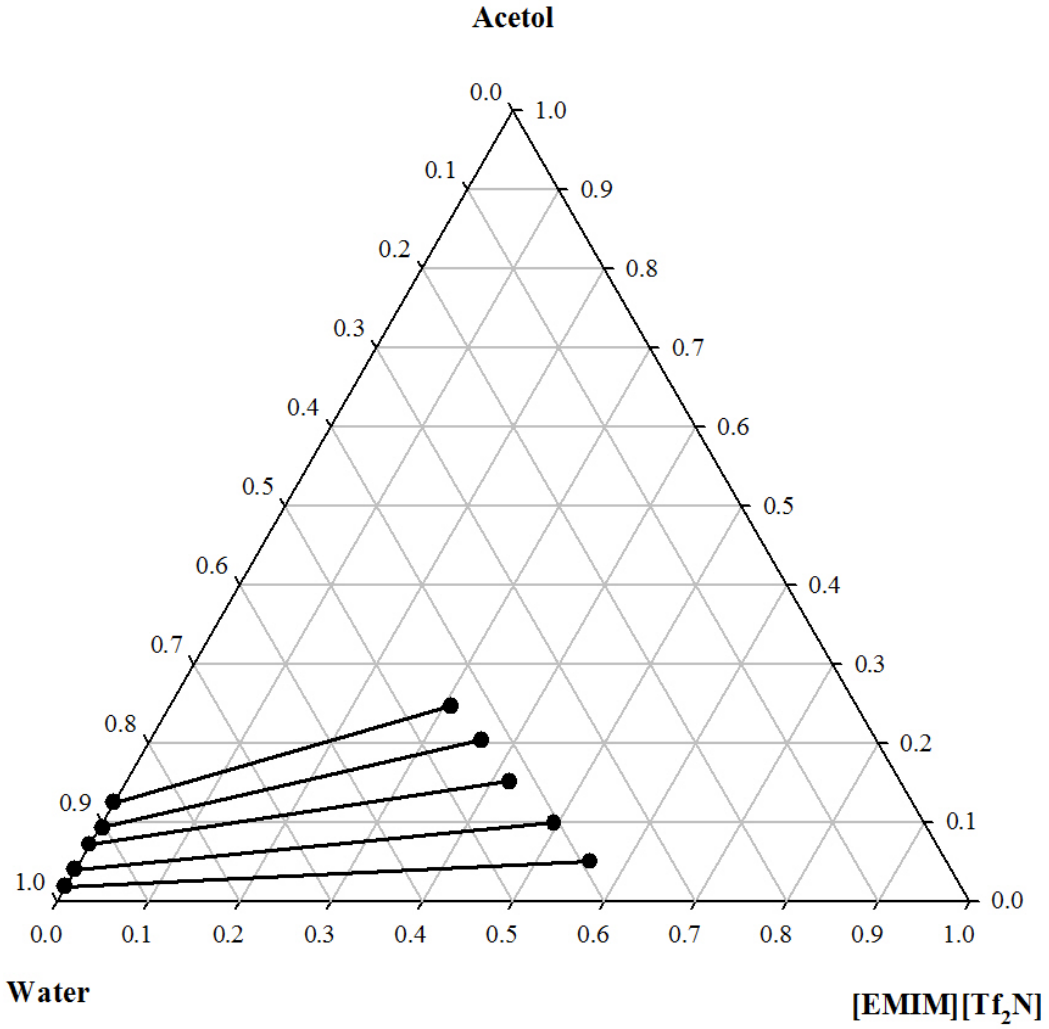

Figure 3.6.: Experimental tie lines for the ternary system: [EMIM][Tf_2N]-acetol -water at 298.15 K and 1 atm.

Table 3.6.: Experimental Tie Lines data for the system [BMIM][Tf_2N] (1) - acetol (2) - water (3) at T = 298.15 K and p = 0.1 Mpa.

Sl.	Extract phase			Raffinate phase			Distribution	Selec-
No.	X_1	X_2	X_3	X_1	X_2	X_3	Co-efficient(β)	tivity(S)
1	0.5327	0.1225	0.3448	0.0000	0.0549	0.9451	2.23	6.12
2	0.4878	0.1659	0.3463	0.0000	0.0771	0.9229	2.15	5.73
3	0.4240	0.2304	0.3456	0.0000	0.1050	0.8950	2.19	5.68
4	0.3431	0.2744	0.3825	0.0000	0.1307	0.8693	2.10	4.77
5	0.2726	0.3170	0.4104	0.0000	0.1579	0.8421	2.01	4.12
6	0.2260	0.3390	0.4350	0.0000	0.1880	0.8120	1.80	3.37

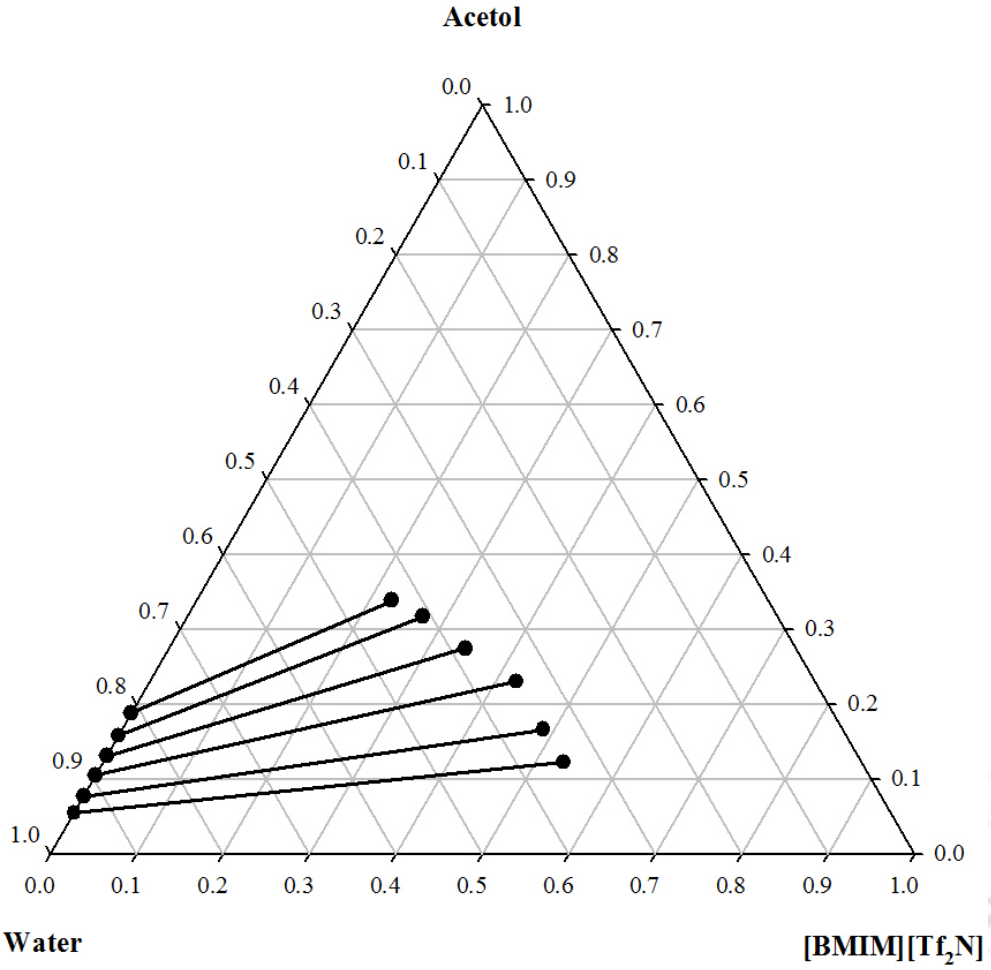

Figure 3.7.: Experimental tie lines for the ternary system: [BMIM][Tf_2N]-acetol -water at 298.15 K and 1 atm.

Table 3.7.: Experimental Tie Lines data for the system Chloroform (1) - acetol (2) - water (3) at $T = 298.15$ K and $p = 0.1$ Mpa.

Sl.	Extract phase			Raffinate phase			Distribution	Selec-
No.	X_1	X_2	X_3	X_1	X_2	X_3	Co-efficient(β)	tivity(S)
1	0.9050	0.0543	0.0407	0.0000	0.0490	0.9510	1.11	25.89
2	0.7752	0.1163	0.1085	0.0000	0.0823	0.9177	1.41	11.95
3	0.7246	0.1812	0.0942	0.0000	0.1267	0.8733	1.43	13.26
4	0.6006	0.2462	0.1532	0.0000	0.1570	0.8430	1.57	8.63
5	0.5181	0.3057	0.1762	0.0000	0.1953	0.8047	1.57	7.15
6	0.3861	0.3436	0.2703	0.0117	0.2331	0.7552	1.47	4.12
7	0.2840	0.3722	0.3438	0.0184	0.2628	0.7188	1.42	2.96

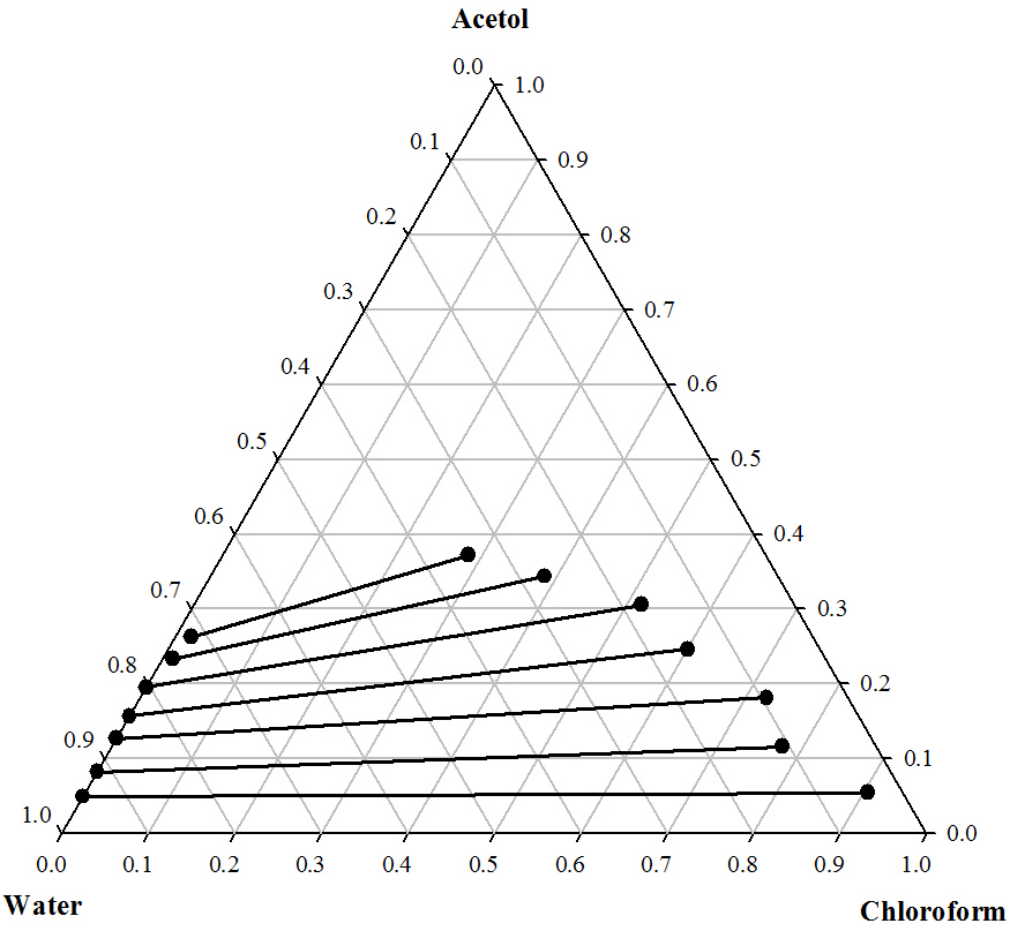

Figure 3.8.: Experimental tie lines for the ternary system: Chloroform-acetol-water at 298.15 K and 1 atm.

Table 3.8.: Experimental Tie Lines data for the system ethyl acetate (1) - acetol (2) - water (3) at $T = 298.15$ K and $p = 0.1$ Mpa.

Sl.	Extract phase			Raffinate phase			Distribution	Selec-
No.	X_1	X_2	X_3	X_1	X_2	X_3	Co-efficient(β)	tivity(S)
1	0.8005	0.0149	0.1846	0.0139	0.0176	0.9685	0.85	4.44
2	0.7214	0.0544	0.2242	0.0050	0.0582	0.9368	0.93	3.91
3	0.6858	0.0838	0.2304	0.0214	0.0772	0.9014	1.09	4.25
4	0.6125	0.1131	0.2744	0.0375	0.1061	0.8564	1.07	3.33
5	0.4980	0.1533	0.3487	0.0166	0.1610	0.8224	0.95	2.25
6	0.4112	0.1792	0.4086	0.0930	0.1847	0.7223	0.97	1.72

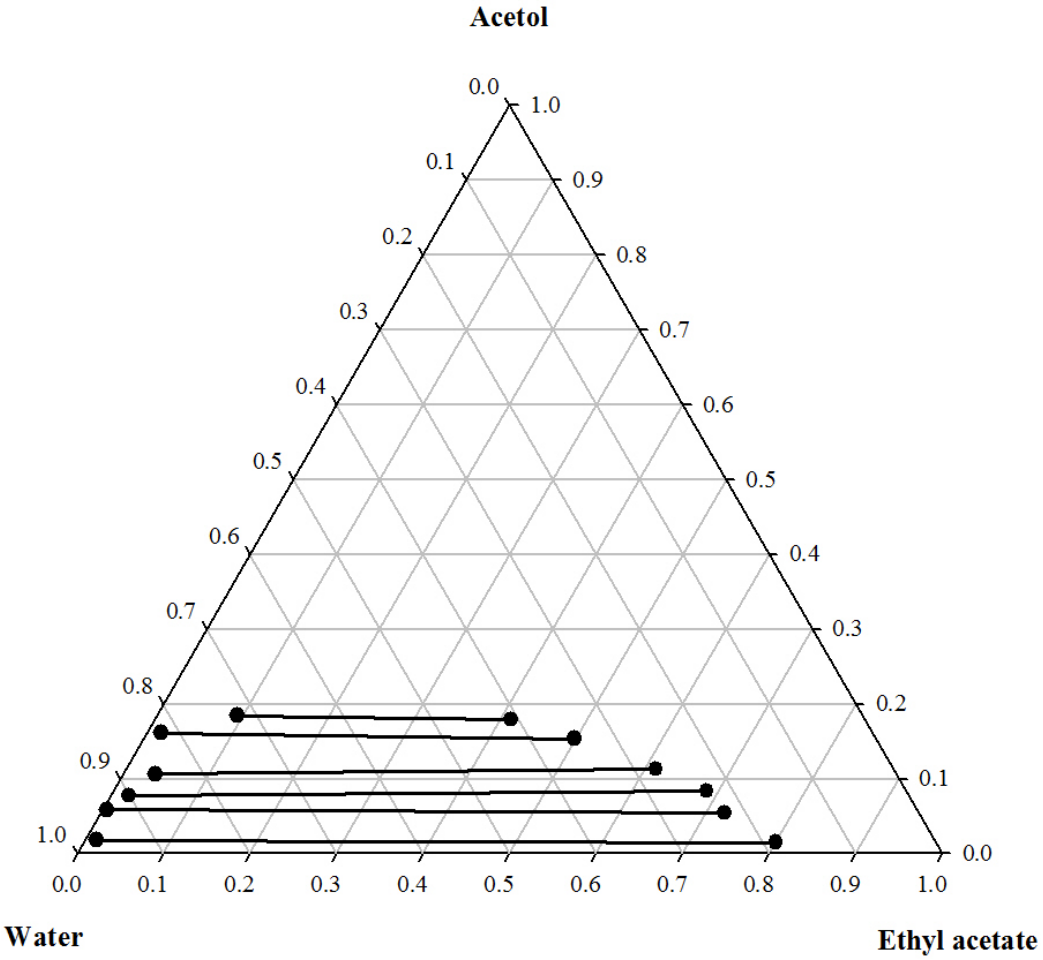

Figure 3.9.: Experimental tie lines for the ternary system: Ethyl acetate-acetol- water at 298.15 K and 1 atm.

Table 3.9.: Experimental Tie Lines data for the system *n*-propyl acetate (1) - acetol (2) - water (3) at $T = 298.15$ K and $p = 0.1$ Mpa.

Sl.	Extract phase			Raffinate phase			Distribution	Selec-
No.	X_1	X_2	X_3	X_1	X_2	X_3	Co-efficient(β)	tivity(S)
1	0.8493	0.0304	0.1203	0.0164	0.0492	0.9344	0.62	4.80
2	0.8005	0.0673	0.1322	0.0283	0.0896	0.8821	0.75	5.01
3	0.7114	0.1152	0.1734	0.0104	0.1417	0.8479	0.81	3.98
4	0.6405	0.1501	0.2094	0.0170	0.1824	0.8006	0.82	3.15
5	0.5657	0.1901	0.2442	0.0276	0.2230	0.7494	0.85	2.62
6	0.4336	0.2586	0.3078	0.0672	0.2840	0.6488	0.91	1.92

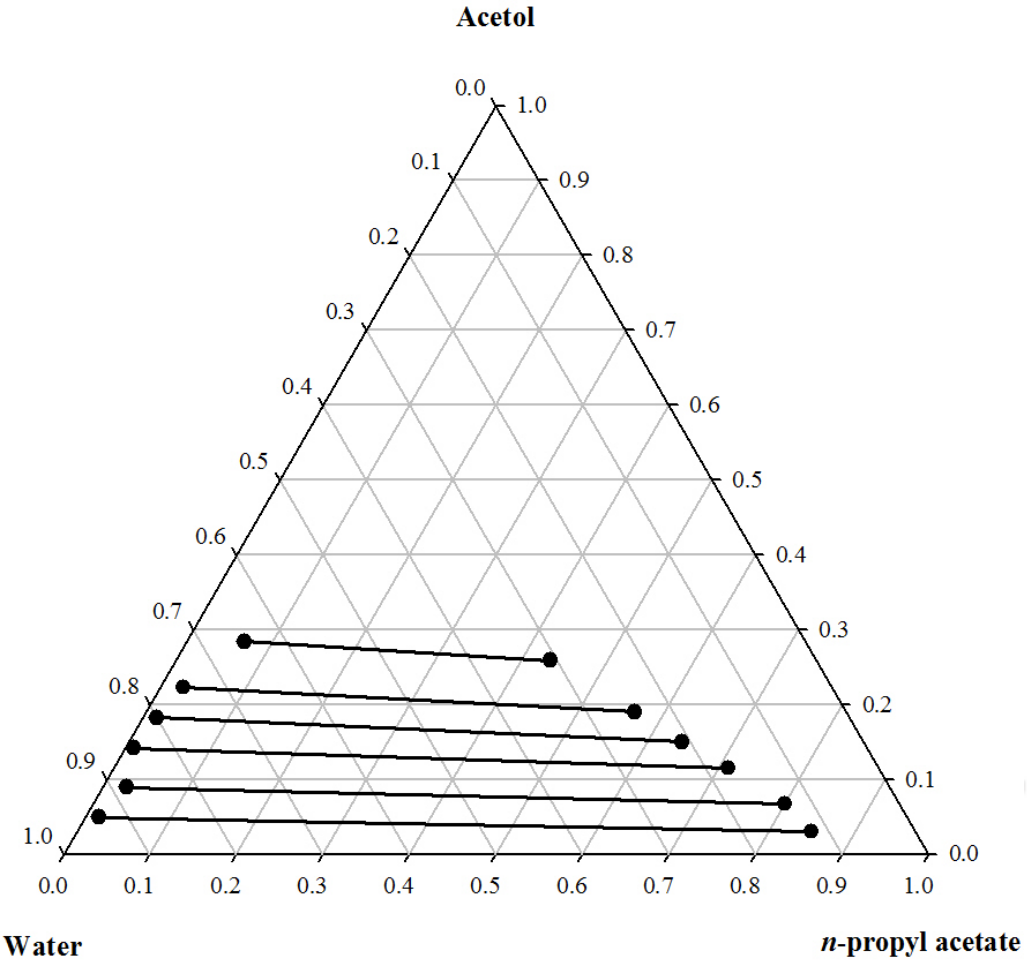

Figure 3.10.: Experimental tie lines for the ternary system: *n*-propyl acetate-acetol -water at 298.15 K and 1 atm.

Table 3.10.: Experimental Tie Lines data for the system *n*-butyl acetate (1) - acetol (2) - water (3) at $T = 298.15$ K and $p = 0.1$ Mpa.

Sl. No.	Extract phase X_1	X_2	X_3	Raffinate phase X_1	X_2	X_3	Distribution Co-efficient(β)	Selec-tivity(S)
1	0.8944	0.0289	0.0767	0.0117	0.0526	0.9357	0.55	6.70
2	0.8411	0.0626	0.0963	0.0317	0.1000	0.8683	0.63	5.64
3	0.8066	0.0946	0.0988	0.0130	0.1499	0.8371	0.63	5.35
4	0.7589	0.1286	0.1125	0.0090	0.1926	0.7984	0.67	4.74
5	0.6984	0.1604	0.1412	0.0095	0.2364	0.7541	0.68	3.62
6	0.6697	0.1949	0.1354	0.0166	0.2923	0.6911	0.67	3.40
7	0.5976	0.2381	0.1643	0.0243	0.3173	0.6584	0.75	3.01

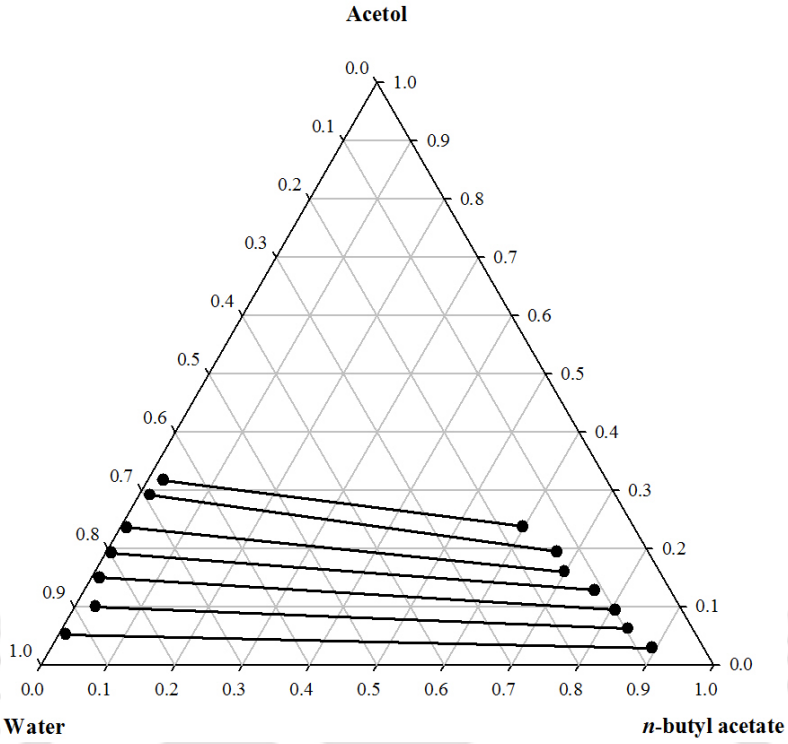

Figure 3.11.: Experimental tie lines for the ternary system: *n*-butyl acetate-acetol -water at 298.15 K and 1 atm.

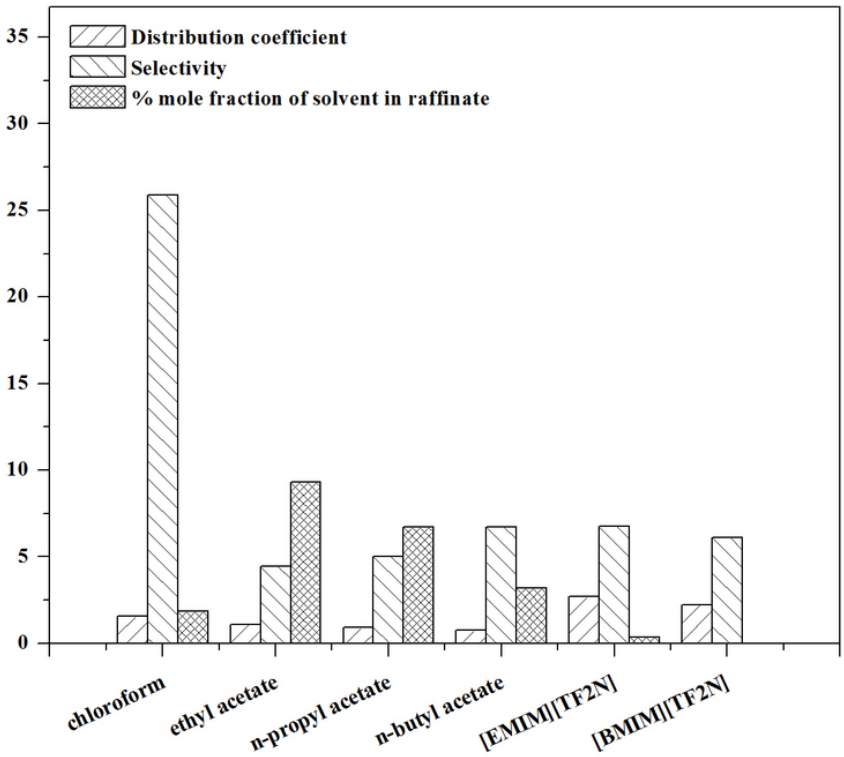

Figure 3.12.: Distribution co-efficient, Selectivity and % mole fraction of solvent in raffinate for acetol based ternary system: Present work Vs. Literature.

3.3.3. [BMIM][Tf_2N] - furfural - water

The experimental LLE data of [BMIM][Tf_2N]/furfural/water system was measured at 298.15 K under atmospheric pressure. The experimental LLE data of the system along with distribution coefficients and selectivities is reported in Table 3.11. The experimental LLE ternary diagram for the system is shown in Figure 3.13. The experimental data measured the distribution coefficient which was in the range of 84.79-164.88; while selectivity in the range of 315.83-543.85. Selectivity value grater than unity implies a possible extraction of furfural by [BMIM][Tf_2N]. Another significant aspect is the fact that the quantity of ionic liquid in raffinate phase is zero which will again result into lower process operating cost. Another important finding is that [BMIM][Tf_2N] can be an effective solvent at close to 0.50 mole fraction of furfural. Finally, the performance of [BMIM][Tf_2N] was also compared with other solvents (ethyl acetate, propyl acetate, 1-butanol, tert-pentanol) as reported in literature in terms of distribution coefficient and selectivity [de Almeida et al., 2012, Mannisto et al., 2016] and shown in Figure 3.14. The highest furfural distribution coefficients were found for propyl acetate followed by [BMIM][Tf_2N]. Similarly, selectivity also followed the same trend i.e. propyl acetate followed by [BMIM][Tf_2N]. However mole fraction(%) of [BMIM][Tf_2N] in raffinate phase was close to zero; whereas for other solvents it was in the range of 0.10-2.55 %. Overall, [BMIM][Tf_2N] and propyl acetate are potential solvents for the extraction of furfural from aqueous solution.

3.3.4. Regeneration of Ionic Liquids

Most ionic liquids exhibit negligible vapor pressure as well as high thermal and chemical stabilities. These properties make usage of ionic liquids as solvents economical as regeneration can be easily carried out and the same solvent can be reutilized with insignificant quantity loss. Figure 3.15 shows the TG/DTG curves of [BMIM][Tf_2N]. The curve clearly shows that [BMIM][Tf_2N] remains in liquid phase till 350° C. In present work ionic liquids, [BMIM][Tf_2N] and [EMIM][Tf_2N], were regenerated several times

(more than 10) and it was found the its property remain the same after each regeneration. Figure 3.16 shows the ^{1}H NMR plot of regenerated [BMIM][Tf_2N] after acetic acid extraction. No peak was detected at 1.90 ppm due to methyl group of acetic acid.

Table 3.11.: Experimental Tie Lines data for the system [BMIM][Tf_2N] (1) - furfural (2) - water (3) at $T = 298.15$ K and $p = 0.1$ Mpa.

Sl.	**Extract phase**			**Raffinate phase**			**Distribution**	**Selec-**
No.	X_1	X_2	X_3	X_1	X_2	X_3	**Co-efficient(β)**	**tivity(S)**
1	0.5653	0.1319	0.3028	0.0004	0.0008	0.9988	164.88	543.85
2	0.4617	0.2210	0.3173	0.0002	0.0022	0.9976	100.45	315.83
3	0.3400	0.3840	0.2760	0.0002	0.0036	0.9962	106.67	385.00
4	0.2873	0.4986	0.2141	0.0004	0.0055	0.9941	90.65	420.92
5	0.1913	0.5681	0.2406	0.0000	0.0067	0.9933	84.79	350.05

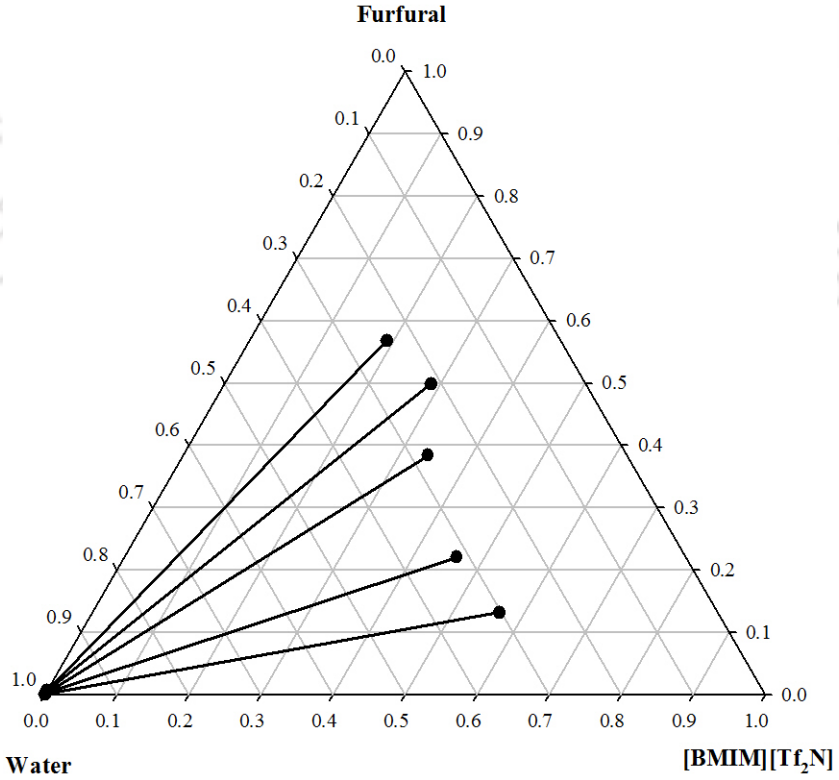

Figure 3.13.: Experimental tie lines for the ternary system: [BMIM][Tf_2N]-furfural -water at 298.15 K and 1 atm.

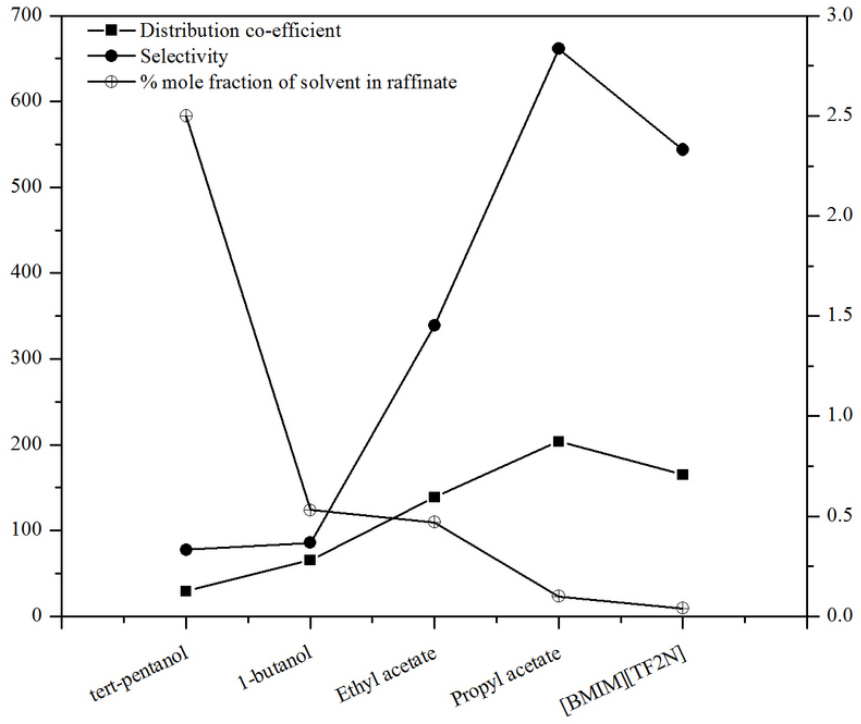

Figure 3.14.: Distribution co-efficient, Selectivity and % mole fraction of solvent in raffinate for furfural based ternary system: Present work Vs. Literature.

3.4 Conclusions

In this work conventional organic solvents (ethyl acetate, *n*-propyl acetate, *n*-butyl acetate, chloroform) as well as ionic liquids, 1-ethyl-3-methylimidazolium bis (trifluoromethylsulfonyl) imide ([EMIM][Tf_2N]) and 1-butyl-3-methylimidazolium bis (trifluoromethylsulfonyl) imide ([BMIM][Tf_2N]), were investigated for the extraction of acetic acid, hydroxyacetone and furfural from aqueous solution. Based on distribution coefficient, selectivity and mole fraction (%) of solvent in raffinate phase, Amyl acetate, Isophorone and [BMIM][Tf_2N] were found to be the potential solvents for the extraction of acetic acid. On a similar note, [EMIM][Tf_2N] and [BMIM][Tf_2N] were found to be the most effective solvent for hydroxyacetone extraction; while [BMIM][Tf_2N] and propyl acetate were preferred solvents for furfural. Compared to organic solvents, composition of ionic liquids in raffinate phase was found to be negligible which eventually reduce the capital and energy cost of the overall process.

Note: see **Appendix B** for ^{1}H NMR plots of the studied systems.

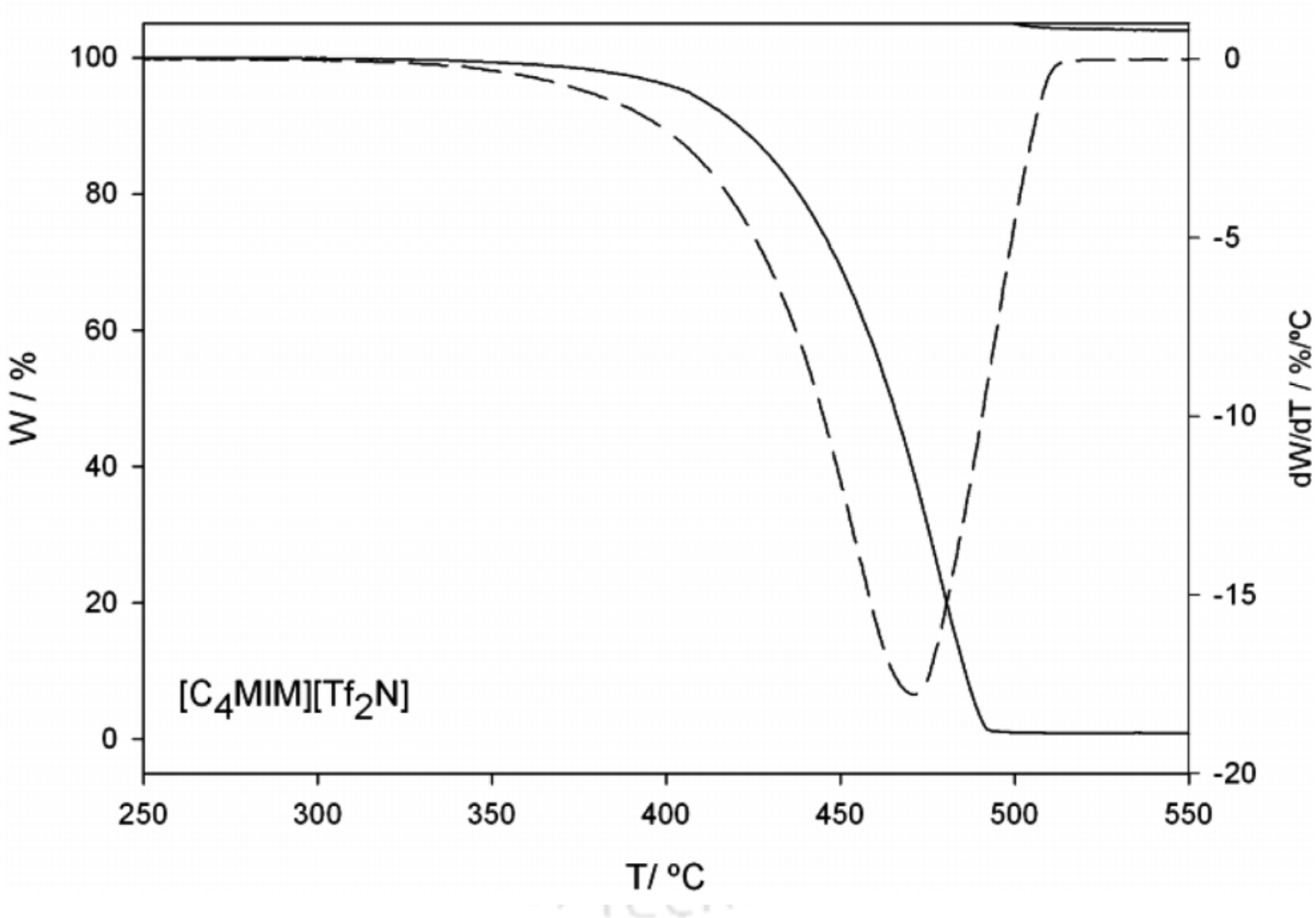

Figure 3.15.: TG and DTG curves of [BMIM][Tf_2N] [Villanueva et al., 2013]

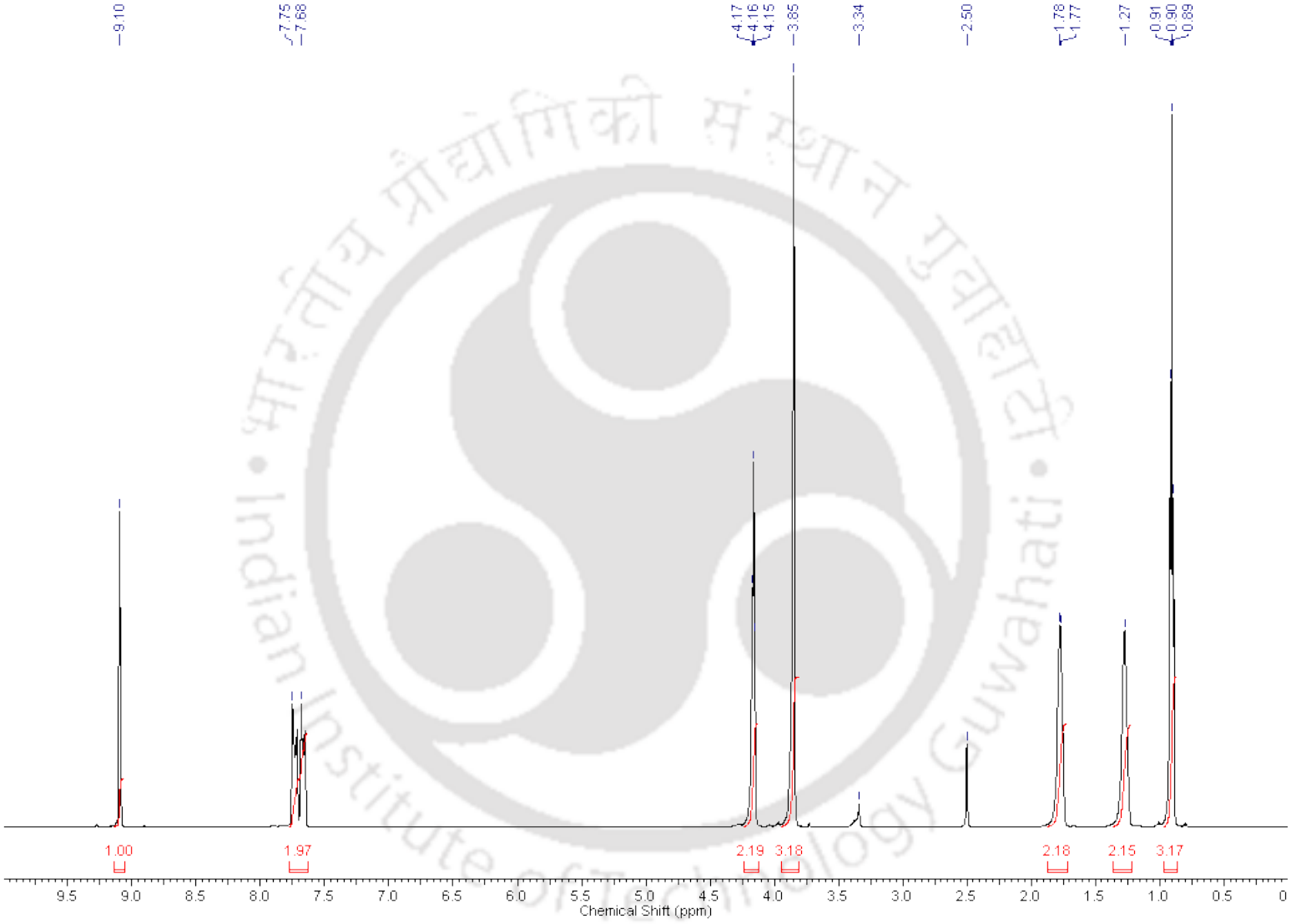

Figure 3.16.: ^{1}H NMR spectrum of regenerated [BMIM][Tf_2N]

REFERENCES

[Bennett et al., 2009] Bennett, N. M., Helle, S. S., and Duff, S. J. (2009). Extraction and hydrolysis of levoglucosan from pyrolysis oil. *Bioresour. Technol.*, 100:6059–6063.

[Berthod et al., 2008] Berthod, A., Ruiz-Angel, M., and Carda-Broch, S. (2008). Ionic liquids in separation techniques. *J. Chromatogr. A*, 1184:6–18.

[Bridgwater, 2003] Bridgwater, A. (2003). Renewable fuels and chemicals by thermal processing of biomass. *Chem. Eng. J.*, 91:87–102.

[Bridgwater, 2012] Bridgwater, A. (2012). Review of fast pyrolysis of biomass and product upgrading. *Biomass and Bioenergy*, 38:68–94.

[Chapeaux et al., 2007] Chapeaux, A., Simoni, L. D., Stadtherr, M. A., and Brennecke, J. F. (2007). Liquid phase behavior of ionic liquids with water and 1-octanol and modeling of 1-octanolwater partition coefficients. *J. chem. Eng. Data*, 52:2462–2467.

[Colombo et al., 1999] Colombo, A., Battilana, P., Ragaini, V., and Bianchi, C. L. (1999). Liquid-liquid equilibria of the ternary systems water + acetic acid + ethyl acetate and water + acetic acid + isophorone (3,5,5-trimethyl-2-cyclohexen-1-one).

J. Chem. Eng. Data, 44:35–39.

[Crosthwaite et al., 2004] Crosthwaite, J. M., Aki, S. N., Maginn, E. J., and Brennecke, J. F. (2004). Liquid phase behavior of imidazolium-based ionic liquids with alcohols. *J. Phys. Chem. B*, 108:5113–5119.

[Czernik and Bridgwater, 2004] Czernik, S. and Bridgwater, A. (2004). Overview of applications of biomass fast pyrolysis oil. *Energy Fuels*, 18:590–598.

[de Almeida et al., 2012] de Almeida, B. F., Waldrigui, T. M., de C. Alves, T., de Oliveira, L. H., and Aznar, M. (2012). Experimental and calculated liquid-liquid equilibrium data for water + furfural + solvents. *Fluid Phase Equilibria*, 334:97–105.

[Demirbas, 2011] Demirbas, A. (2011). Competitive liquid biofuels from biomass. *Applied Energy*, 88:17–28.

[Demirbas, 2009] Demirbas, M. F. (2009). Biorefineries for biofuel upgrading: A critical review. *Applied Energy*, 86:S151–S161.

[Freire et al., 2008] Freire, M. G., Carvalho, P. J., Gardas, R. L., Marrucho, I. M., Santos, L. M., and Coutinho, J. A. (2008). Mutual solubilities of water and the [$c_n$mim][tf_2n] hydrophobic ionic liquids. *J. Phys. Chem. B*, 112:1604–1610.

[Hu et al., 2012] Hu, X., Mourant, D., Gunawan, R., Wu, L., Wang, Y., Lievens, C., and Li, C.-Z. (2012). Production of value-added chemicals from bio-oil via acid catalysis coupled with liquid–liquid extraction. *RSC Adv.*, 2:9366–9370.

[J.P.Diebold, 2000] J.P.Diebold (2000). A review of the chemical and physical mechanisms of the storage stability of fast pyrolysis bio-oils,nrel/sr-570-27613. Technical report.

[Mahfud et al., 2008] Mahfud, F., Geel, F. V., Venderbosch, R., and Heeres, H. (2008).

Acetic acid recovery from fast pyrolysis oil. an exploratory study on liquid-liquid reactive extraction using aliphatic tertiary amines. *Sep. Sci. Technol.*, 43:3056–3074.

[Mannisto et al., 2016] Mannisto, M., Pokki, J.-P., Creati, A., Voisin, A., Zaitseva, A., and Alopaeus, V. (2016). Ternary and binary lle measurements for solvent (4-methyl-2-pentanone and 2-methyl-2-butanol) + furfural + water between 298 and 401 k. *J. Chem. Eng. Data*, 61:903–911.

[Mantilla et al., 2015] Mantilla, S., Manrique, A., and Maradei, P. (2015). Methodology for extraction of phenolic compounds of bio-oil from agricultural biomass wastes. *Waste Biomass Valor*, 6:371–383.

[Marsh et al., 2004] Marsh, K. N., Boxall, J. A., and Lichtenthaler, R. (2004). Room temperature ionic liquids and their mixtures-a review. *Fluid Phase Equilibria*, 219:93–98.

[Miao et al., 2007] Miao, X., Zhang, H., Wang, T., and He, M. (2007). Liquid-liquid equilibria of the ternary system water + acetic acid + methyl tert-butyl ether. *J. Chem. Eng. Data*, 52:789–793.

[Mohan et al., 2006] Mohan, D., Jr., C. U. P., and Steele, P. H. (2006). Pyrolysis of wood/biomass for bio-oil: A critical review. *Energy and Fuels*, 20:848–889.

[Nigam and Singh, 2011] Nigam, P. S. and Singh, A. (2011). Production of liquid biofuels from renewable resources. *Progress in Energy and Combustion Science*, 37:52–68.

[Park et al., 2016] Park, L., Ren, S., Yiacoumi, S., Ye, X., Borole, A., and Tsouris, C. (2016). Separation of switchgrass bio oil by water organic solvent addition and ph adjustment. *Energy and Fuels*, 30:2164–2173.

[Plechkovaa and Seddon, 2008] Plechkovaa, N. and Seddon, K. (2008). Applications

of ionic liquids in the chemical industry. *Chem. Soc. Rev.*, 37:123–150.

[Ralph et al., 2010] Ralph, E., W.M.Sims, Jack, N., and Saddler, M. T. (2010). An overview of second generation biofuel technologies. *Bioresource Technology*, 101:1570–1580.

[Rasrendra et al., 2011] Rasrendra, C., Girisuta, B., van de Bovenkamp, H., Winkelman, J., Leijenhorst, E., Venderbosch, R., Windt, M., Meier, D., and Heeres, H. (2011). Recovery of acetic acid from an aqueous pyrolysis oil phase by reactive extraction using tri-n-octylamine. *Chem. Eng. J.*, 176-177:244–252.

[Sipila et al., 1998] Sipila, K., Kuoppala, E., Fagernas, L., and Oasmaa, A. (1998). Characterization of biomass-based flash pyrolysis oils. *Biomass and Bioenergy*, 14:103–113.

[S.N.Naik et al., 2010] S.N.Naik, V.Goud, V., K.Rout, P., and K.Dalai, A. (2010). Production of first and second generation biofuels: A comprehensive review. *Renewable and Sustainable Energy Reviews*, 14:578–597.

[Toikka et al., 2014] Toikka, M., Samarov, A., and Toikka, A. (2014). Solubility, liquid-liquid equilibrium and critical states for the system acetic acid + n-propanol + n-propyl acetate + water at 293.15 k and 303.15 k. *Fluid Phase Equilibria*, 375:66–72.

[Villanueva et al., 2013] Villanueva, M., Coronas, A., Garca, J., and Salgado, J. (2013). *Ind. Eng. Chem. Res.*, 52:15718–15727.

[Vitasari et al., 2011] Vitasari, C., Meindersma, G., and de Haan, A. (2011). Water extraction of pyrolysis oil: The first step for the recovery of renewable chemicals. *Bioresource Technology*, 102:7204–7210.

[Wang et al., 2007a] Wang, L., Cheng, Y., and Li, X. (2007a). Liquid-liquid equilibria for acetic acid + water + amyl acetate and acetic acid + water + 2-methyl ethyl

acetate ternary systems. *J. Chem. Eng. Data*, 52:2171–2173.

[Wang et al., 2007b] Wang, L., Cheng, Y., Xiao, X., and Li, X. (2007b). Liquid-liquid equilibria for the ternary systems acetic acid + water + butyl acetate and acetic acid + water + 2-methyl propyl acetate at 304.15 k, 332.15 k, and 366.15 k. *J. Chem. Eng. Data*, 52:1255–1257.

[Wei et al., 2014] Wei, Y., Lei, H., Wang, L., Zhu, L., Zhang, X., Liu, Y., Chen, S., and Ahring, B. (2014). Liquid-liquid extraction of biomass pyrolysis bio-oil. *Energy and Fuels*, 28:1207–1212.

[Werner et al., 2010] Werner, S., Haumann, M., and Wasserscheid, P. (2010). Ionic liquids in chemical engineering. *Annu. Rev. Biomol. Eng.*, 1:203–230.

[Xiao et al., 2006] Xiao, X., Wang, L., Ding, G., and Li, X. (2006). Liquid-liquid equilibria for the ternary system water + acetic acid + propyl acetate. *J. Chem. Eng. Data*, 51:582–583.

[Yang et al., 2014] Yang, X., Lyu, H., Chen, K., Zhu, X., Zhang, S., and Chen, J. (2014). Selective extraction of bio oil from hydrothermal liquefaction of salix psammophila by organic solvents with different polarities through multistep extraction separation. *BioResources*, 9:5219–5233.

CHAPTER 4

Cuckoo Search Algorithm for the Prediction of Multicomponent Liquid-Liquid Equilibria

4.1 Introduction

Liquid-liquid extraction is an important separation technology, with a wide range of applications in chemical, petrochemical and pharmaceutical industries. Liquid-liquid Equilibrium (LLE) data of multi-component systems are essential for proper understanding of the extraction process and for the designing and optimization of separation processes. Excess Gibbs free energy models, such as NRTL [Renon and Prausnitz, 1968] and UNIversal QUAsi-Chemical (UNIQUAC) [Abrams and Prausnitz, 1975] models are commonly used to predict the LLE as they provide good agreement with experimental data [Aznar, 2007, Banerjee et al., 2005, Santiago et al., 2009, Vatani et al., 2012]. For LLE prediction, each of these models require binary interaction parameters. These parameters are generally estimated from the known experimental LLE data by the optimization of an objective function. Mathematically the aim of optimization is to find the set of inputs that either maximizes or minimizes the output of the objective function. The objective function is highly non-convex having multiple local optima. For Liquid-Liquid phase equilibria, finding the global optimum (reliable interaction parameters) thus becomes a necessary requirement for the correct LLE prediction.

Nature inspired metaheuristic algorithms are becoming increasingly popular to solve global optimization problems. They work remarkably efficiently and have many advantages over traditional, deterministic methods and thus have been applied in almost all areas of science, engineering and industry [Yang and Deb, 2014]. Nature inspired metaheuristic algorithms are broadly classified into Evolutionary Algorithms (Genetic Algorithm (GA), Differential Evolution (DE)), Physical Algorithms (Simulated Annealing (SA), Harmonic Search (HS)), Swarm Intelligence (Particle Swarm optimization (PSO) , Ant Colony Optimization (ACO)), Bio-inspired Algorithms (Artificial Immune System) and others (Cuckoo Search (CS) Algorithm, Bat Algorithm) [Nanda and Panda, 2014]. Genetic Algorithm remains one of the most widely used optimization algorithms in modern nonlinear optimization. It is based on natural selection process that mimics biological evolution. Simulated Annealing is a trajectory based search algorithm

which mimics the annealing process in material processing. Particle Swarm Optimization (PSO) is inspired by the swarm intelligence of fish and birds [Yang, 2010].

The application of Nature inspired metaheuristic algorithms for solving phase equilibrium calculations (PEC), phase stability (PS) problems and parameter estimation (PE) has grown considerably in recent years. Srinivas and Rangaiah [Srinivas and Rangaiah, 2007] have applied differential evolution with tabu list (DETL) for phase equilibrium (VLE, LLE, VLLE) and parameter estimation problems. It was found that the performance of DETL was better as compared to DE and tabu list (TS). Further Bonilla-Petriciolet et al. [Petriciolet et al., 2010] have evaluated the performance of SA, GA, DE, DETL and PSO for modeling several binary VLE data using local composition models and found that DE and DETL perform better than other algorithms in terms of success rate for parameter estimation. Bonilla-Petricioleta and J.G. Segovia-Hernandez [Petriciolet and Hernández, 2010] have also tested different variants of PSO for performing phase stability and equilibrium calculations in both reactive and non-reactive systems. Their results showed that classical PSO with constant cognitive and social parameters was a reliable method and offered the best performance. Zhang et al. [Zhang et al., 2011b] have also evaluated the performance of three stochastic algorithms, unified bare-bones particle swarm optimization (UBBPSO), integrated differential evolution (IDE) and IDE without tabu list and radius (IDE_N), and compared their performance for phase equilibrium and phase stability problems. Overall, IDE was found to perform better in terms of global success rate and faster convergence rate for the phase equilibrium problems. H. Zhang et al. [Zhang et al., 2011a] have further applied IDE algorithm for parameter estimation in VLE modeling problems. Compared to other stochastic algorithms such as SA, PSO, DE, and DETL, IDE was found to be reliable (higher global success rate) for solving these modeling problems. Fateen et al. [Fateen et al., 2012] have also evaluated the performance of three global optimization algorithms, Covariant Matrix Adaptation-Evolution Strategy (CMA-ES), Shuffled Complex Evolution (SCE) and Firefly Algorithm (FA), for phase and chemical equilibrium calculations. The phase equilibrium problems include both multi-component systems with

and without chemical reactions. FA was found to be the most reliable among the three techniques, whereas CMA-ES can find the global minimum reliably and accurately even with a smaller number of iterations. Fernandez-Vargas et al. [Fernández-Vargas et al., 2013] have applied an improved version of Ant colony optimization (ACO) algorithm, named as ACO with feasible region selection (ACOFRS), to perform thermodynamic calculations i.e. parameter estimation, phase equilibrium calculations and phase stability analysis for liquid-liquid and vapor-liquid equilibrium multicomponent systems. It was concluded that ACOFRS is an alternative method for performing global optimization in phase equilibrium calculations of multicomponent systems and it outperformed other stochastic optimization methods such as PSO, DE and GA for solving VLE parameter estimation problems.

Apart from the phase equilibrium calculations (PEC) and phase stability (PS) problems, stochastic global optimization methods has also been applied for estimation of binary interaction parameters in multicomponent LLE systems. Singh et al. [Singh et al., 2005] utilized GA to estimate the binary interaction parameters for NRTL and UNIQUAC models in multicomponent LLE systems and demonstrated that their performance was better than inside variance estimation method (IVEM) and the techniques applied in ASPEN and DECHEMA. Sahoo et al. [Sahoo et al., 2006] calculated the interaction parameters for NRTL model in ternary, quaternary and quinary LLE systems based on GA and showed that the results obtained using GA were better than other techniques in literature. Ferrari et al. [Ferrari et al., 2009] applied SA and PSO algorithms for parameter estimation of NRTL and UNIQUAC models for binary and multicomponent LLE systems and showed that both algorithms were capable of modeling liquid-liquid equilibrium data. Merzougui et al. [Merzougui et al., 2011] used a hybrid algorithm i.e. a combination of GA and Levenberg-Marquardt (LM) method, for parameter estimation with NRTL and UNIQUAC models for six LLE systems and found good correlation with experimental data. Vatani et al. [Vatani et al., 2012] also performed the liquid-liquid equilibria calculation for 20 different IL based ternary LLE systems by NRTL and two-suffix Margules models with binary interaction parameters

calculated using Genetic Algorithm (GA). A harmony search algorithm was used by Merzougui et al. [Merzougui et al., 2012] to calculate the interaction parameters of NRTL model for twenty ternary liquid-liquid systems. Kabouche et al. [Kabouche et al., 2012] have used SA, GA, Nelder-Mead Simplex (NMS), SA-NMS (hybrid) and GA-NMS (hybrid) to estimate interactions parameters of NRTL and UNIQUAC models for LLE systems. The hybrid algorithm namely GA-NMS showed the best performance in terms of RMSD with minimum number of iterations among the others. Bonilla-Petriciolet et al. [Bonilla-Petriciolet et al., 2013] have recently analyzed the capabilities of seven stochastic global optimization methods, SA, GA, DE, PSO, HS, DETL and bare bones PSO (BBPSO), to model mean activity coefficients in aqueous solutions of quaternary ammonium salts at 25 °C using the electrolyte NRTL model. The results indicated that SA, DETL and BBPSO offer better performance for solving parameter estimation problems involved in the modeling of thermodynamic properties of ionic liquids (ILs).

Besides the well-known methods, the investigations on nature inspired optimization algorithms are still currently under development. Cuckoo Search (CS) is one of the latest nature-inspired metaheuristic algorithms developed by Yang and Deb [Yang and Deb, 2009]. It is a population-based method which mimics the breeding behaviour such as brood parasitism of certain cuckoo species. This algorithm is enhanced by the so-called Levy flights. Recent studies have shown that CS is potentially far more efficient than other algorithms in many applications. It has been applied in many areas [Fister et al., 2013] which includes applied thermodynamic calculations. Bhargava et al. [Bhargava et al., 2013] have applied CS algorithm for solving phase stability, phase equilibrium and reactive phase equilibrium problems. They found that CS offers a reliable performance for solving these thermodynamic calculations and is better than other metaheuristics for phase equilibrium modeling. Fateen and Petriciolet [Fateen and Bonilla-Petriciolet, 2014a] have compared the reliability and efficiency of eight promising nature inspired metaheuristic algorithms for the solution of nine difficult phase stability and phase equilibrium problems. These algorithms are the cuckoo search (CS), intelligent firefly (IFA), bat (BA), artificial bee colony (ABC), MAKHA, a hybrid between

monkey algorithm and krill herd algorithm, covariance matrix adaptation evolution strategy (CMAES), magnetic charged system search (MCSS), and bare bones particle swarm optimization (BBPSO). The results clearly showed that CS is the most reliable of all tested optimization methods as it successfully solved all thermodynamic problems tested in the study. Fateen and Petriciolet [Fateen and Bonilla-Petriciolet, 2014b] have also applied Gradient-Based Cuckoo Search (GBCS) algorithm for solving several challenging phase stability problems and analyzed its performance at different numerical effort levels. The GBCS was found to perform better than the original CS algorithm. In comparison with other stochastic optimization, GBCS proved to be the most reliable without any reduction in efficiency.

Till date the computation using CS algorithm is scarce for multicomponent phase equilibria problems. In a recent work by Jaime-Leal et al. [Jaime-Leal et al., 2015], CS algorithm was used to predict the binary phase equilibrium data for aqueous quaternary ammonium IL mixtures. In their work the mean activity coefficients of quaternary ammonium IL's was predicted using the e-NRTL model. The results obtained were very encouraging with a global success rate of $\sim$ 86% with CS as compared to $\sim$ 77% with other stochastic methods. However computation with ternary, quaternary or quinary systems are not available in the literature. Keeping this limitation in mind, we have attempted to predict the multicomponent LLE data for both IL and organic solvent systems.

In our study, binary interaction parameters of UNIQUAC and NRTL models were estimated using CS algorithm for 39 ternary systems which includes 32 IL based systems and 7 organic solvent based systems. Apart from it, UNIQUAC and NRTL models interaction parameters were also estimated for 8 bio-chemicals (acetic acid/furfural/acetol) based LLE ternary systems studied in the present work. The results (root mean square deviation) thus obtained were compared with those reported in the literature. In the concluding section, three quaternary systems and one quinary system were selected to compare the performance of CS with GA and PSO algorithms.

4.2 Theory and Calculation

4.2.1. Cuckoo Search (CS)

Cuckoo search (CS) is a natured-inspired metaheuristic search algorithm, based on the reproduction behaviour of cuckoos, which has been recently developed by Yang and Deb [Yang and Deb, 2009, Yang and Deb, 2013]. Specific egg laying and breeding behaviour of some cuckoos species is the basis of this optimization algorithm. The cuckoo is the brood parasite, which never builds their own nests. They lay their eggs in the nest of other species, leaving host species to care for its eggs. If these eggs are discovered by the host bird, it will either throw out the cuckoo egg or abandon the nest to start afresh. Some species of cuckoos have learnt to mimic the colour and pattern of their own eggs so as to match that of their hosts. This reduces the probability of the eggs being abandoned and therefore, increases their re-productivity. To implement these concepts, the CS employ three idealised rules where: (a) eggs are laid one at a time and then dumped randomly in a host nest;(b) the nest having better eggs or solutions are carried over to next generation; and (c) the host bird usually find an alien egg within a probability of unity. However if an alien egg is found, the host bird can either throw the egg away or abandon the nest, and build a completely new nest.

The above rules are valid for single objective optimization problem. For multi-objective optimization problems with K different objectives, the first and last rule need modification. Here each cuckoo lays K eggs at a time (Rule a) and thus a new nest with K eggs are built (Rule c). From implementation point of view, each egg in a nest represents a solution, and a cuckoo egg represents a new solution. The aim is to use the potentially better solution (cuckoo egg) to replace the not-so-good solution (egg) in the nests. The steps of the algorithm are as follows:

Step-1: Initialization of CS algorithm parameters

The following parameters are defined: number of nests (n), discovery probability (p_a), lower and upper bounds and maximum number of generations/iterations ($iter_{max}$).

Step-2: Generation of initial population of nests of host birds

The initial population of the nests are generated randomly between the lower bound and upper bound.

Step-3: Generation of new solutions/eggs by Lévy flights

In this step, all the host eggs except the best one are replaced by new cuckoo eggs if objective function corresponding to each new cuckoo egg is better than the corresponding existing host egg objective function. A new solution is generated by Lévy flight as below

$$y_i^{(t+1)} = {y_i}^{(t)} + \alpha.S.({y_i}^{(t)} - {y_{best}}^{(t)}).(rand) \tag{4.1}$$

where α is the step size parameter, *rand* is a random number from a standard normal distribution, y_i^t is the i^{th} nest current position, y_{best}^t is the current best nest and *S* is a random walk based on the Lévy flights. In CS algorithm, Lévy flights are used to explore the unknown, large-scale search space as it is more efficient than the Brownian random walks. The Lévy flight essentially provides a random walk whose random step length is drawn from a Lévy distribution (equation 4.2).

$$L\acute{e}vy \sim \mathrm{u} = \mathrm{t}^{-1-\beta}, (1 < \beta \leq 2) \tag{4.2}$$

This has an infinite variance with an infinite mean. In this work, a Lévy flight has been performed for generating new solution according to Mantegna algorithm [Yang, 2014]. In Mantegna's algorithm, the step length *S* is calculated by

$$s = \frac{u}{|v|^{1/\beta}} \tag{4.3}$$

where β is considered to be 1.5 and *u* and *v* are drawn from normal distributions. It takes the form:

$$u \sim N(0, \sigma_u^2), \qquad v \sim N(0, \sigma_v^2) \tag{4.4}$$

where

$$\sigma_u = \left\{ \frac{\Gamma(1+\beta)\sin(\pi\beta/2)}{\Gamma[(1+\beta)/2]\beta 2^{(\beta-1)/2}} \right\}^{1/\beta}, \qquad \sigma_v = 1 \tag{4.5}$$

Here Γ is the standard Gamma function.

Step-4: Discovery of alien eggs

In this step, the alien eggs discovery is performed for each egg by generating a random number *rand* $\in 0, 1$ and comparing it with discovery probability p_a such as:

$$y_i^{(t+1)} \leftarrow y_i^{(t)} \qquad if \quad rand \leq p_a, \tag{4.6}$$

$$y_i^{(t+1)} \leftarrow y_i^{(t)} + \zeta(y_j^t - y_k^t) \qquad if \quad rand > p_a \tag{4.7}$$

where y_j^t and y_k^t are two different solutions selected randomly by random permutation and ζ is a random number drawn from a uniform distribution.

Step-5: Termination criterion

The maximum number of iterations or tolerance criterion may be used as termination criterion of the algorithm. In this work, maximum number of iterations has been used as termination criterion. The pseudo-code and the flow diagram of the CS algorithm are shown in Figure 4.1 and Figure 4.2 respectively.

begin

Objective function $f(x), x = (x_1, ..., x_d)^T$

Generate initial population of

n *host nests* x_i *(i=1,2,....,n)*

while(*t* < *MaxGeneration*) or (*stop criterion*)

Get a cuckoo randomly by Lévy flights

evaluate its quality/fitness F_i

Choose a nest among n *(say, j) randomly*

if($F_i < F_j$),

replace j by the new solution;

end

A fraction (p_a) *of worse nests*

are abandoned and new ones are built;

Keep the best solutions

(or nests with quality solutions);

Rank the solutions and find the current best

end

Postprocess results and visualization

end

Figure 4.1.: Pseudo code of Cuckoo Search (CS) Algorithm.

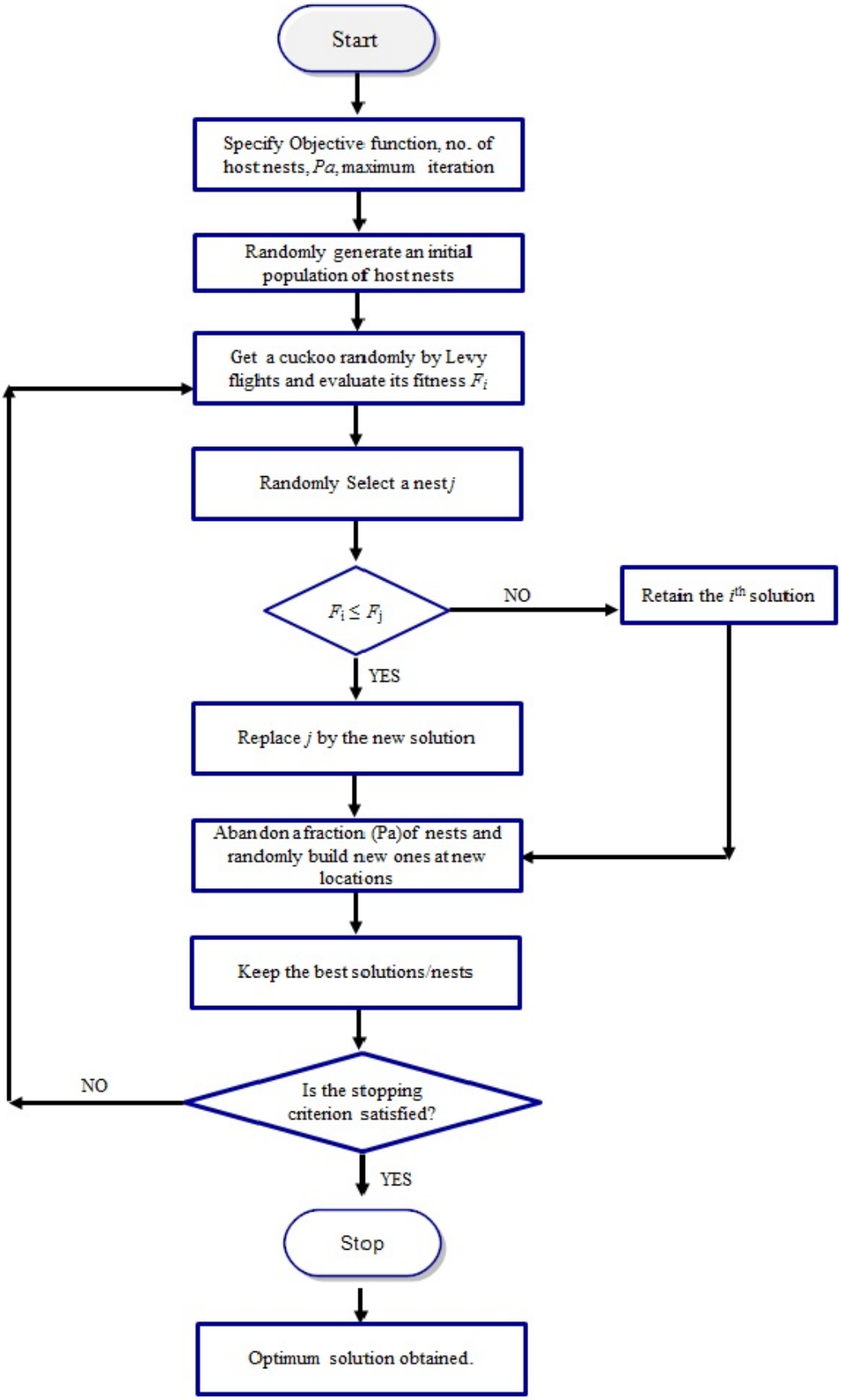

Figure 4.2.: Flow diagram of Cuckoo Search Algorithm.

4.2.2. UNIQUAC Model and NRTL Model

In UNIQUAC model, the activity coefficient, γ_i , of component *'i'* in the multicomponent system is given by:

$$\ln \gamma_i = \ln\left(\frac{\Phi_i}{x_i}\right) + \frac{z}{2} q_i \ln\left(\frac{\theta_i}{\Phi_i}\right) + l_i - \frac{\Phi_i}{x_i}\sum_{j=1}^{c} x_j l_j + q\left(1 - \ln\sum_{j=1}^{c}\theta_j\tau_{ji} - \sum_{j=1}^{c}\frac{\theta_j\tau_{ij}}{\sum_{k=1}^{c}\theta_k\tau_{kj}}\right) \tag{4.8}$$

$$with, \tau_{ij} = \exp(-\frac{A_{ij}}{T}), \quad \theta_i = \frac{q_i x_i}{\sum_k q_k x_k}, \tag{4.9}$$

$$\Phi_i = \frac{r_i x_i}{\sum_k r_k x_k}, \quad l_i = \frac{z}{2}(r_k - q_k) + 1 - r_k \tag{4.10}$$

where z is lattice coordination number (z=10), r_i and q_i are, respectively the volume and surface area of the pure component *i*, x_i is the mole fraction of component *i* and τ_{ij} is interaction parameter between component *i* and *j*.

The structure parameters *'r'* and *'q'* for the compounds have been taken from our previous work [Banerjee et al., 2005, Varma et al., 2011, Rabari and Banerjee, 2013, Rabari and Banerjee, 2014, Bharti and Banerjee, 2015] and literature [Santiago et al., 2009, González et al., 2010, Feng et al., 2015, Luo et al., 2015].

In NRTL model, the activity coefficient, γ_i , of component *'i'* in the ternary system is given by:

$$\ln \gamma_i = \frac{\sum_{j=1}^{c}\tau_{ji}G_{ji}x_j}{\sum_{l=1}^{c}G_{li}x_l} + \sum_{j=1}^{c}\frac{x_j G_{ij}}{\sum_{l=1}^{c}G_{lj}x_l}\left[\tau_{ij} - \frac{\sum_{r=1}^{c}x_r\tau_{rj}G_{rj}}{\sum_{l=1}^{c}G_{lj}x_l}\right] \tag{4.11}$$

$$G_{ji} = \exp(-\alpha_{ji}\tau_{ji}), \quad \tau_{ji} = \frac{g_{ji} - g_{ii}}{RT}, \quad \alpha_{ji} = \alpha_{ij} \tag{4.12}$$

where *g* is an energy parameter characterizing the interaction of species *i* and *j*, x_i is the mole fraction of component *i* and α the non-randomness parameter. Although α can be treated as an adjustable parameter, but in this study α was set equal to 0.2 which is a value prescribed for hydrocarbons.

4.2.3. Liquid-Liquid Equilibria Modeling

The thermodynamic equilibrium condition for multicomponent liquid-liquid system can be described by the following expression:

$$\gamma_i^I x_i^I = \gamma_i^{II} x_i^{II} \text{ (i} = 1, 2, 3, ...) \tag{4.13}$$

where γ_i, the activity coefficient of component *i* in a phase (I or II) is predicted using the NRTL model. x_i^I and x_i^{II} represents the mole fraction of component *i* in phase I and II respectively. The compositions of the extract and raffinate phases are calculated using a flash algorithm(Figure 4.3) as described by the modified Rashford-Rice Algorithm [Seader, 2006]. The optimum binary interaction parameters are those which minimize the difference between the experimental and calculated compositions and are given by the relation

$$F_{obj} = \sum_{k=1}^{m} \sum_{i=1}^{c} \sum_{l=I}^{II} \left(x_{ik}^l - \hat{x}_{ik}^l \right)^2 \tag{4.14}$$

The RMSD values, which provide a measure of the accuracy of the correlations, were calculated according to the following expression:

$$RMSD = \left(\frac{F_{obj}}{2mc} \right)^{1/2} = \left[\sum_{k=1}^{m} \sum_{i=1}^{c} \sum_{l=I}^{II} \frac{\left(x_{ik}^l - \hat{x}_{ik}^l \right)^2}{2mc} \right]^{1/2} \tag{4.15}$$

where, *m* refers the number of tie lines and *c* refers to the number of components. Here x_{ik}^l and $\hat{x}_{il}^k$ are the experimental and predicted values of mole fraction for component *i* for the k^{th} tie line in phase *l*,respectively. Figure 4.3 shows the flow diagram of the total algorithm used in this work for the calculation of binary interaction parameters. (MATLAB Code of Cuckoo Search algorithm along with Flash algorithm is in **Appendix C**).

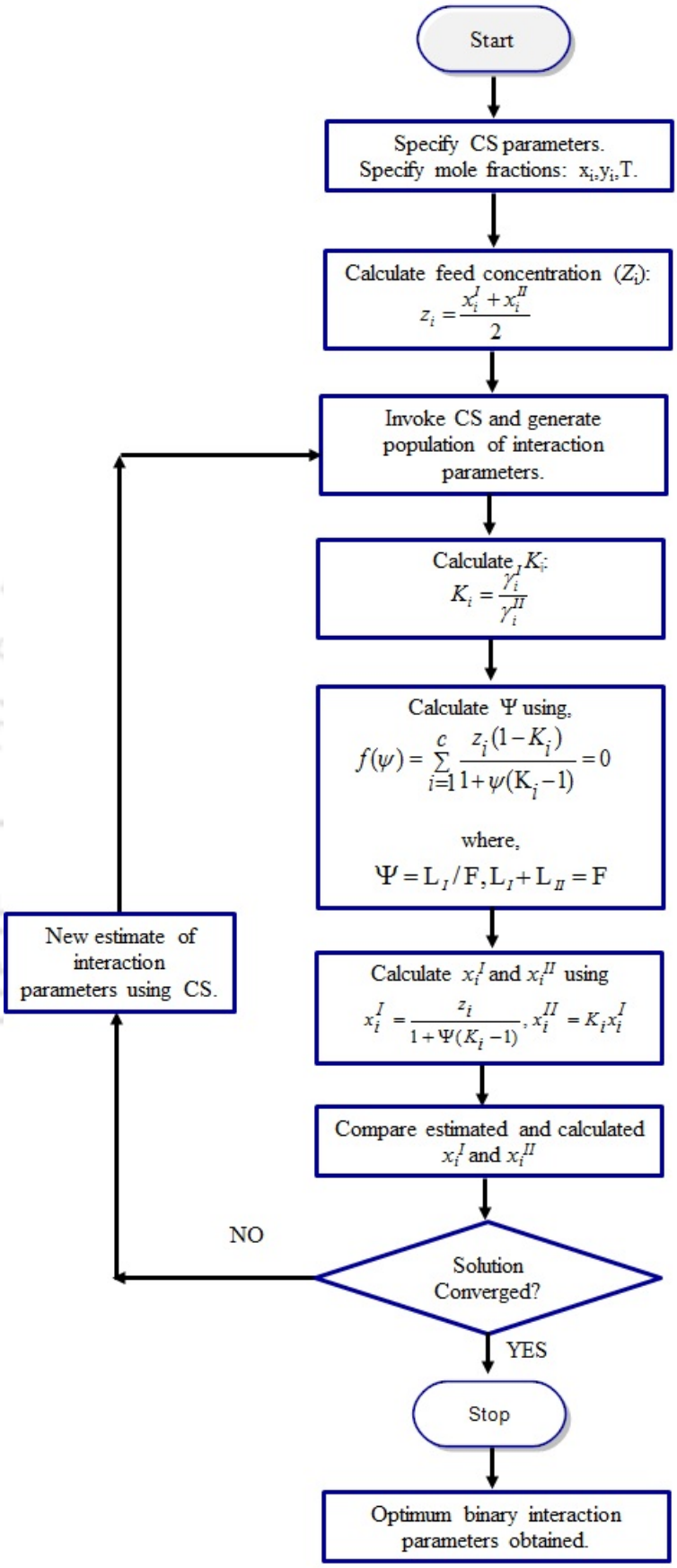

Figure 4.3.: Flow diagram of the Flash algorithm used for LLE modelling.

4.3 Results and Discussions

Thirty two IL and seven organic based ternary systems were selected from literature to test our approach with CS. They were correlated with both UNIQUAC and NRTL models with interaction parameters estimated by the CS algorithm. The systems used in this work are given in Table 4.1 and Table 4.2 respectively. The structure parameters *'r'* and *'q'* for all compounds studied in this work has been reported in Table 4.3 and Table 4.4. System no 1, [OMIM][Cl] + Ethanol + TAEE has been used for benchmarking study.

4.3.1. Effect of Bounds

The effect of the value of bounds on RMSD values have been considered and shown in Table 4.5 for UNIQUAC and Table 4.6 for NRTL model for system 1. A population size of 20 was used for the benchmarking system. Maximum number of iterations of 2000 was used as the stopping condition. Based on the recommendations of Yang and Deb [Yang and Deb, 2009], p_a of 0.25 was used. For each bound, 30 numerical trials have been carried out with random initial values of interaction parameters. It can be inferred from Table 4.5 and Table 4.6 that the RMSD values are minimum at a bound of -1000 to +1000 for UNIQUAC model and -100 to +100 for NRTL model. All the parameters were found to lie within the same range. Keeping this in mind, we have chosen the lower and upper bounds for estimation of interaction parameters for all the systems.

4.3.2. Maximum Number of Iterations and Population size

The effect of the maximum number of iterations and population size on RMSD values have been considered and shown in Figure 4.4. For UNIQUAC model, population size of 20 and maximum iteration of 1000 is sufficient to give a very good RMSD value. A further increase in population size and iteration was not able to improve the solution (Figure 4.4a). For NRTL model, population size of 20 and maximum iteration of 1500 was able to give a very high RMSD value (Figure 4.4b).

Table 4.1.: Ionic Liquid-based Ternary Systems Studied in this Work

System No.	System Name	Temperature (K)	Tie-Line	Reference
1	[OMIM][Cl] + ethanol + TAEE	298.15	11	[Arce et al., 2004a]
2	[BMIM][TfO] + ethanol + TAEE	298.15	9	[Arce et al., 2004b]
3	[BMIM][TfO] + ethanol + ETBE	298.15	8	[Arce et al., 2006a]
4	[EMIM][TfO] + ethanol + ETBE	298.15	9	[Arce et al., 2006b]
5	[C_8MIM][BF_4] + thiophene + i-octane	298.15	11	[Alonso et al., 2007]
6	[C_8MIM][BF_4] + cyclohexane + hexane	298.15	10	[Alonso et al., 2007]
7	[C_8MIM][BF_4] + thiophene + n-heptane	298.15	10	[Alonso et al., 2008]
8	[C_8MIM][BF_4] + thiophene + n-dodecane	298.15	12	[Alonso et al., 2008]
9	[C_8MIM][BF_4] + thiophene + n-hexadecane	298.15	11	[Alonso et al., 2008]
10	[HMIM][BF_4] + benzene + heptane	298.15	12	[Letcher and Reddy, 2005]
11	[HMIM][BF_4] + benzene + hexadecane	298.15	9	[Letcher and Reddy, 2005]
12	[HMIM][PF_6] + benzene + heptane	298.15	12	[Letcher and Reddy, 2005]
13	[OMIM][Cl] + benzene + heptane	298.15	5	[Letcher and Deenadayalu, 2003]
14	[HMIM][BF_4] + ethanol + hexene	298.15	12	[Letcher and Reddy, 2004]
15	[HMIM][BF_4] + ethanol + heptene	298.15	8	[Letcher and Reddy, 2004]
16	[HMIM][PF_6] + ethanol + hexene	298.15	13	[Letcher and Reddy, 2004]

17	[HMIM][PF_6] + ethanol + heptene	298.15	13	[Letcher and Reddy, 2004]
18	[HMIM][BF_4] + benzene + dodecane	298.15	7	[Letcher and Reddy, 2005]
19	[HMIM][PF_6] + benzene + dodecane	298.15	7	[Letcher and Reddy, 2005]
20	[BMIM][BF_4] + benzene + heptane	298.15	8	[Revelli et al., 2010]
21	[BMIM][BF_4] + thiophene + heptane	298.15	9	[Revelli et al., 2010]
22	[TDTHP][DCA] + 1-butanol + water	298.15	8	[Rabari and Banerjee, 2014]
23	[TDTHP][DEC] + 1-butanol + water	298.15	8	[Rabari and Banerjee, 2014]
24	[TDTHP][Phosph] + 1-propanol + water	298.15	8	[Rabari and Banerjee, 2013]
25	[TDTHP][Phosph] + 1-butanol + water	298.15	8	[Rabari and Banerjee, 2013]
26	[Emim][ESO_4] + benzene + hexane	298.15	8	[García et al., 2009]
27	[Emim][ESO_4] + benzene + cyclohexane	298.15	9	[González et al., 2010]
28	[Emim][ESO_4] + benzene + methylcyclohexane	298.15	10	[González et al., 2010]
29	[Emim][ESO_4] + benzene + cyclooctane	298.15	9	[González et al., 2010]
30	[BMIM][Tf_2N] + ethanol + water	283.20	13	[Cháfer et al., 2015]
31	[BMIM][Tf_2N] + ethanol + water	303.20	10	[Cháfer et al., 2015]
32	[BMIM][Tf_2N] + ethanol + water	323.20	8	[Cháfer et al., 2015]
		Total Tie-lines	**305**	

Table 4.2.: Organic solvent based Ternary Systems Studied in this Work

System No.	System Name	Temperature(K)	Tie-Line	Reference
1	Formamide + indole +2-methylnaphthalene	308.15	12	[Feng et al., 2015]
2	Ethylene Glycol + indole +2-methylnaphthalene	308.15	12	[Feng et al., 2015]
3	Monoethanolamine + indole + 2-methylnaphthalene	308.15	10	[Feng et al., 2015]
4	2-Methoxy-2-methylpropane + propionic acid + water	298.2	8	[Luo et al., 2015]
5	2-Methoxy-2-methylpropane + propionic acid + water	323.2	8	[Luo et al., 2015]
6	2-Methoxy-2-methylpropane + butyric acid + water	298.2	8	[Luo et al., 2015]
7	2-Methoxy-2-methylpropane + butyric acid + water	323.2	8	[Luo et al., 2015]
		Total Tie-lines	**66**	

Table 4.3.: Abbreviation and Full Name of Ionic Liquids Used in this Work along with UNIQUAC Volume and Surface Area Structural Parameters

Abbreviation	Full name of ionic liquid	r	q	Reference
[OMIM][Cl]	1-octyl-3-methylimidazolium chloride	11.993	7.886	[Banerjee et al., 2005]
[BMIM][TfO]	1-butyl-3-methylimidazolium trifluoromethanesulfonate	12.460	7.518	[Banerjee et al., 2005]
[OMIM][BF_4]	1-octyl-3-methylimidazolium tetrafluoroborate	13.187	8.357	[Banerjee et al., 2005]
[HMIM][BF_4]	1-hexyl-3-methylimidazolium tetrafluoroborate	11.658	7.388	[Banerjee et al., 2005]
[HMIM][PF_6]	1-hexyl-3-methylimidazolium hexafluorophosphate	12.869	8.166	[Banerjee et al., 2005]
[BMIM][BF_4]	1-butyl-3-methylimidazolium tetrafluoroborate	10.057	6.368	[Banerjee et al., 2005]
[TDTHP][DCA]	Trihexyl(tetradecyl)-phosphonium dicyanamide	8.37	5.81	[Rabari and Banerjee, 2014]
[TDTHP][DEC]	Trihexyl(tetradecyl)-phosphonium decanoate	8.77	5.96	[Rabari and Banerjee, 2014]
[TDTHP][Phosph]	Trihexyl(tetradecyl)-phosphonium bis(2,4,4-trimethylpentyl) phosphinate	9.834	6.258	[Rabari and Banerjee, 2013]
[BMIM][Tf_2N]	1-butyl-3-methylimidazolium bis(trifluoromethylsulfonyl) imide	11.964	9.753	[Bharti and Banerjee, 2015]
[EMIM][ESO_4]	1-ethyl-3-methylimidazolium Ethylsulfate	8.3927	6.6260	[Varma et al., 2011]
[EMIM][TfO]	1-ethyl-3-methylimidazolium trifluoromethanesulfonate	7.6193	6.075	[Santiago et al., 2009]

Table 4.4.: UNIQUAC Volume and Surface Area Structural Parameters of Compounds Used in this Work

Solvent	r	q	Reference
Tert-amyl ethyl ether (TAEE)	6.68	4.512	[Banerjee et al., 2005]
Ethanol	2.112	1.95	[Banerjee et al., 2005]
i-octane	5.986	4.642	[Banerjee et al., 2005]
Water	0.92	1.42	[Banerjee et al., 2005]
Hexane	4.594	3.621	[Banerjee et al., 2005]
n-heptane	5.292	4.152	[Banerjee et al., 2005]
Benzene	3.295	2.611	[Banerjee et al., 2005]
1-hexene	4.339	3.448	[Banerjee et al., 2005]
1-heptene	5.032	3.983	[Banerjee et al., 2005]
n-dodecane	8.5462	7.096	[Santiago et al., 2009]
n-hexadecane	11.2438	9.256	[Santiago et al., 2009]
Ethyl tert-butyl Ether (ETBE)	5.1726	4.388	[Santiago et al., 2009]
Thiophene	2.8569	2.140	[Santiago et al., 2009]
1-butanol	3.92	3.67	[Rabari and Banerjee, 2014]
1-propanol	3.2499	3.128	[Rabari and Banerjee, 2014]
Methylcyclohexane	4.72	3.776	[González et al., 2010]
Cyclooctane	5.395	4.32	[González et al., 2010]
Cyclohexane	4.0464	3.24	[González et al., 2010]
Formamide	1.6928	1.644	[Feng et al., 2015]
Indole	4.282	2.692	[Feng et al., 2015]
2-methylnaphthalene	5.7158	4.008	[Feng et al., 2015]
Ethylene glycol	2.4088	2.248	[Feng et al., 2015]
Monoethanolamine	2.5735	2.36	[Feng et al., 2015]
Propionic acid	2.8768	2.612	[Luo et al., 2015]
2-methoxy-2-methylpropane	4.0678	3.632	[Luo et al., 2015]
Butyric acid	3.5512	3.152	[Luo et al., 2015]

Table 4.5.: Effect of Bounds on RMSD for System 1: [OMIM][Cl] + Ethanol + TAEE Using UNIQUAC Model

Bounds		RMSD			Hitting Bound	
Lower	**Upper**	**Min.**	**Avg.**	**Max.**	**Lower**	**Upper**
-100	100	0.0336	0.0336	0.0336	Yes	Yes
-200	200	0.0226	0.0226	0.0226	Yes	Yes
-500	500	0.0058	0.0058	0.0058	No	Yes
-1000	1000	0.0058	0.0058	0.0058	No	No
-1500	1500	0.0058	0.0058	0.0058	No	Yes
-2000	2000	0.0057	0.0058	0.0058	No	Yes

Table 4.6.: Effect of Bounds on RMSD for System 1: [OMIM][Cl] + Ethanol + TAEE Using NRTL Model

Bounds		RMSD			Hitting Bound	
Lower	**Upper**	**Min.**	**Avg.**	**Max.**	**Lower**	**Upper**
-100	100	0.0031	0.0047	0.0110	No	No
-200	200	0.0033	0.0066	0.0146	No	Yes
-500	500	0.0041	0.0108	0.0253	No	Yes
-1000	1000	0.0041	0.0120	0.0213	No	Yes
-1500	1500	0.0045	0.0144	0.0223	No	Yes
-2000	2000	0.0052	0.0150	0.0223	No	Yes

Keeping this in mind, we have chosen 20 as the population size for all systems and 1000 and 1500 as the maximum number of iterations respectively for UNIQUAC and NRTL model for the estimation of interaction parameters in all systems. After the benchmarking with the above system, CS has been applied on the other ternary systems. For each system, 30 trials has been carried out with random initial values of Population and the lowest RMSD along with the corresponding interaction parameters were then selected as the final result.

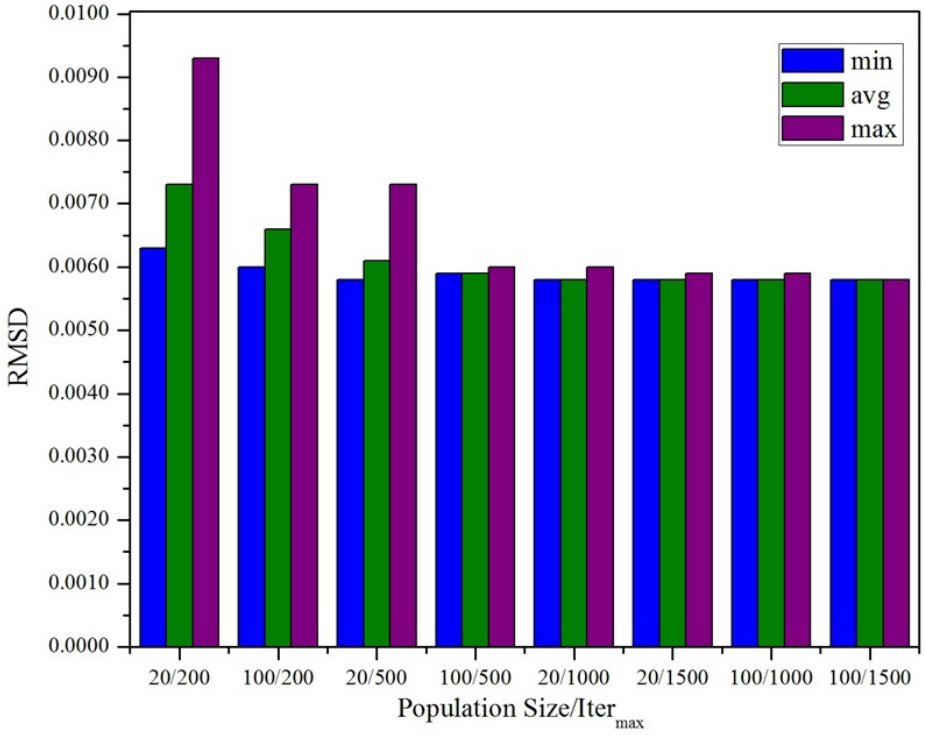

(a)

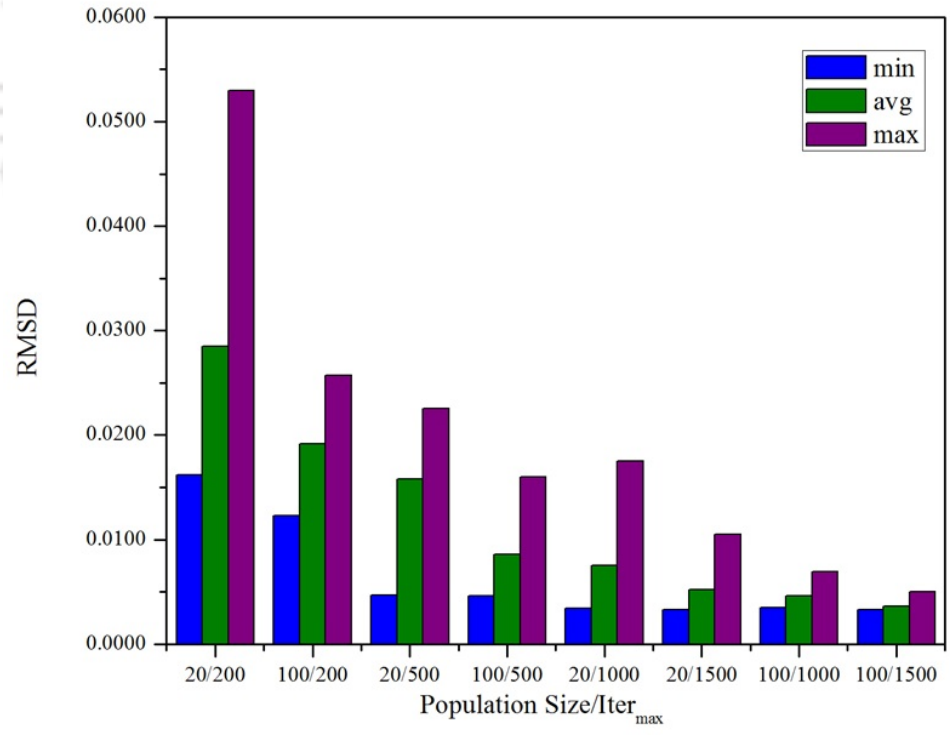

(b)

Figure 4.4.: Effect of population size and $Iter_{max}$ on RMSD for system 1(benchmarking system) using (a) UNIQUAC model and (b) NRTL model

4.3.3. Comparison with Reported Data

The convergence plots of CS for few selected imidazolium and phosphonium based systems have been shown in Figure 4.5a-d. For imidazolium based ILs (Figure 4.5a), the objective function value reduces to the order of 10^{-3} in approximately 60 iterations with UNIQUAC model. For phosphonium ILs (Figure 4.5b) with UNIQUAC model, the objective function value reduces to the order of 10^{-3} in approximately 100, 250 and 350 iterations respectively for [Phosph], [DCA] and [DEC] anions. With NRTL model, imidazolium ILs (Figure 4.5c)used more number of iterations as compared to phosphonium ILs (Figure 4.5d) in order to obtain a function value with order of 10^{-3}.

Figure 4.6a-d shows the convergence plots of CS for imidazolium and phosphonium ILs with respect to maximum number of iterations ($Iter_{max}$). For each $Iter_{max}$, 30 different trials has been carried out and the obtained minimum value of objective function has been assigned as F_{obj}. F^*_{obj} is the global optimum calculated using CS with $iter_{max}$ = 5000. From the plot, it is clear that the performance of CS improves with increment of $Iter_{max}$. In particular, CS is very reliable for finding the global solution with high precision for phosphonium ILs as compared to imidazolium ILs. This is due to the fact that the solution were within 10^{-7}-10^{-8} of the global minimum for phosphonium ILs with UNIQUAC model. On the other hand, CS was able to find the global minimum with a tolerance of 10^{-6}-10^{-7} for imidazolium ILs with UNIQUAC model. Again with NRTL model, CS could converge to the global minimum within a tolerance of 10^{-3}-10^{-5} for imidazolium ILs and 10^{-6}-10^{-7} for phosphonium ILs.

For the calculation of Success Rate (SR) of CS, following criterion has been considered:$F_{obj} - F^*_{obj} \leq \epsilon$ where ϵ is tolerance. Table 4.7 and Table 4.8 shows the %SR of CS with different tolerance values and stopping conditions. It is clear that %SR of CS increased with increments of $Iter_{max}$ and decreased with increment of tolerance values. With UNIQUAC model, %SR for imidazolium ILs are in the range of 23-87% ($iter_{max}$=2000) whereas for phosphonium ILs >90% ($iter_{max}$=2000) at tolerance value of 10^{-5} is obtained.

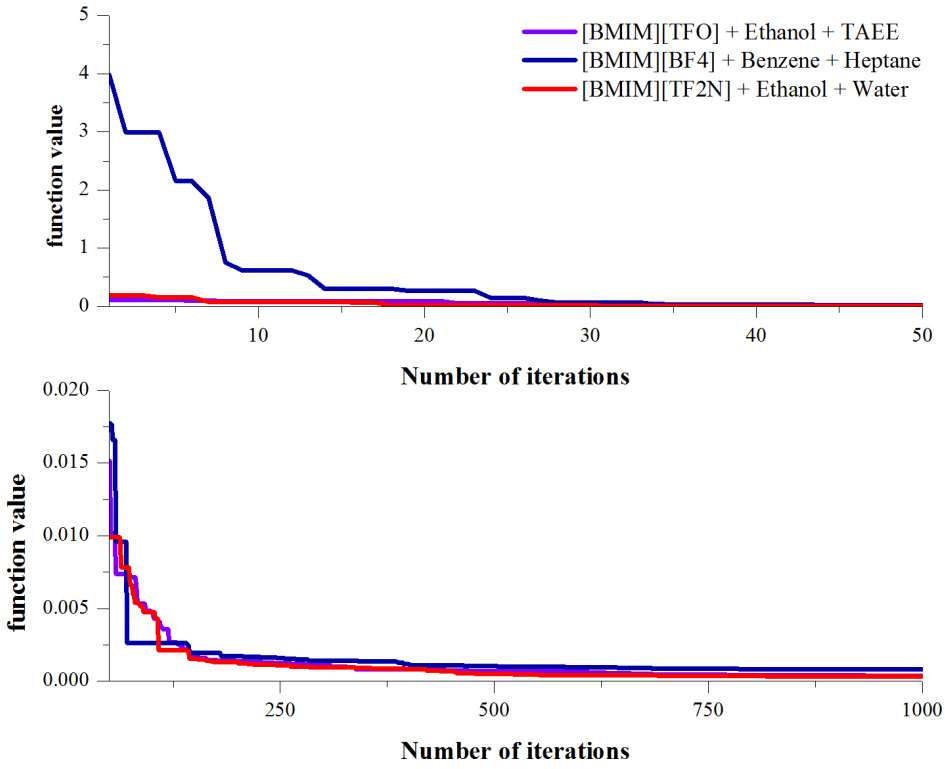

(a)

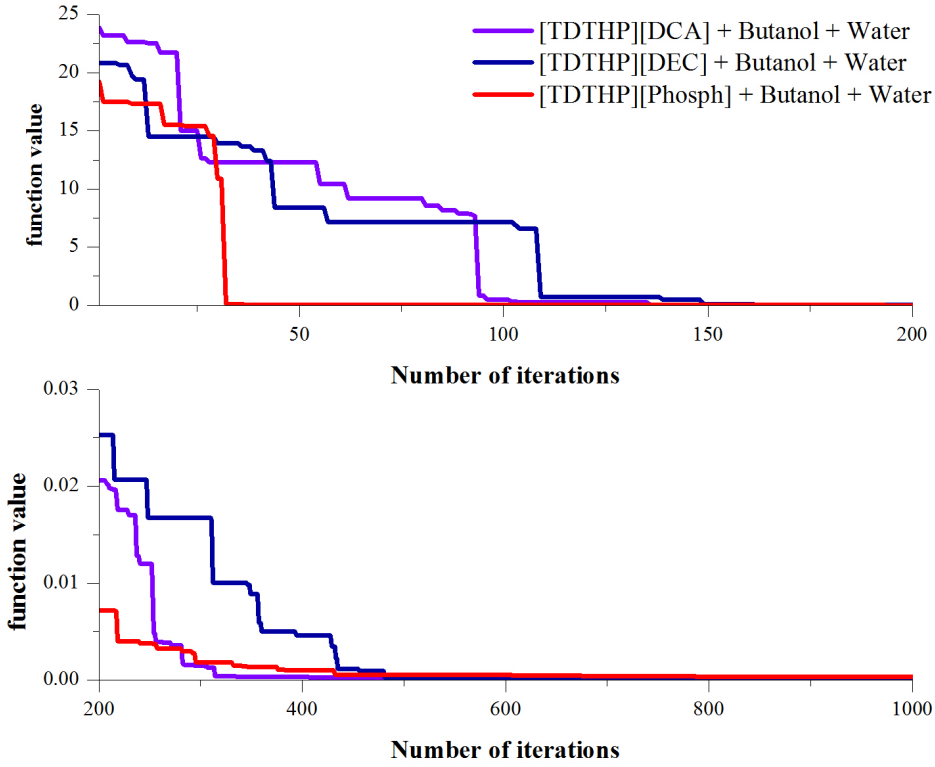

(b)

Figure 4.5.: Convergence plots of CS for selected (a) imidazolium-based ternary systems with UNIQUAC model (N=20, $Iter_{max}$ = 1000), (b) phosphonium-based ternary systems with UNIQUAC model (N=20, $Iter_{max}$ = 1000).

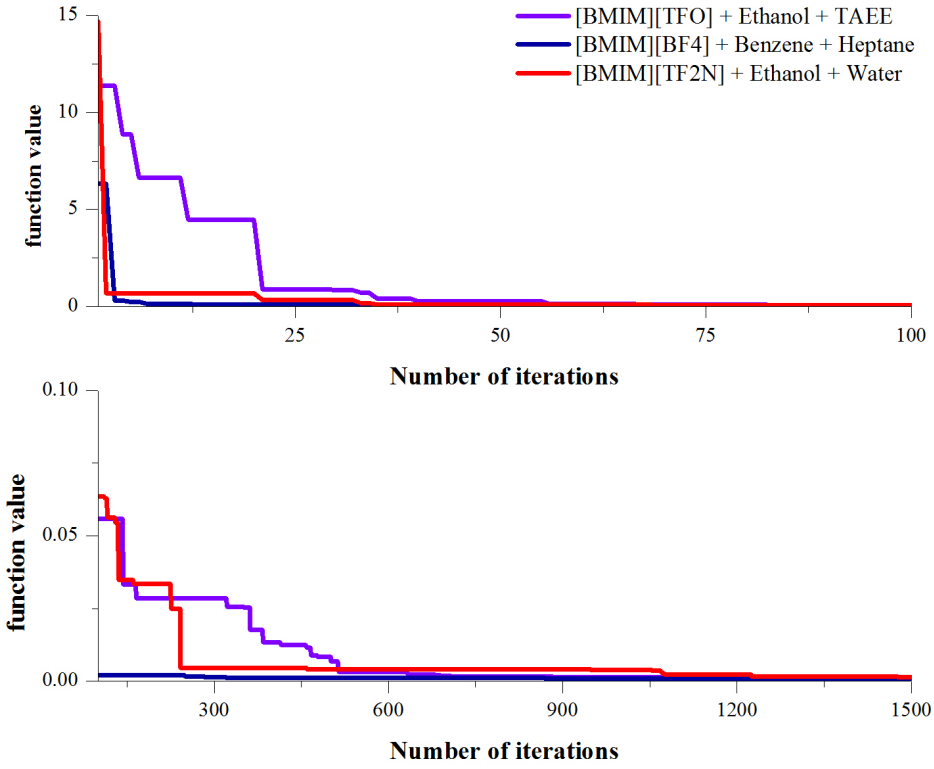

(c)

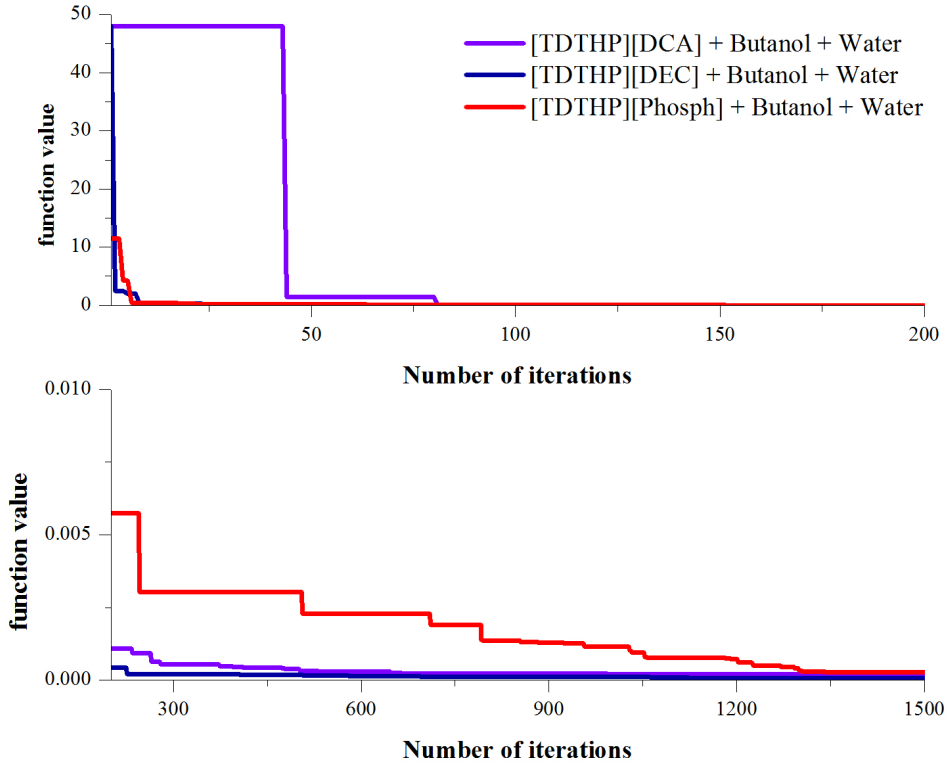

(d)

Figure 4.5.: Convergence plots of CS for selected (c) imidazolium-based ternary systems with NRTL model (N=20, $Iter_{max}$ = 1000), (d) phosphonium-based ternary systems with NRTL model (N=20, $Iter_{max}$ = 1000).

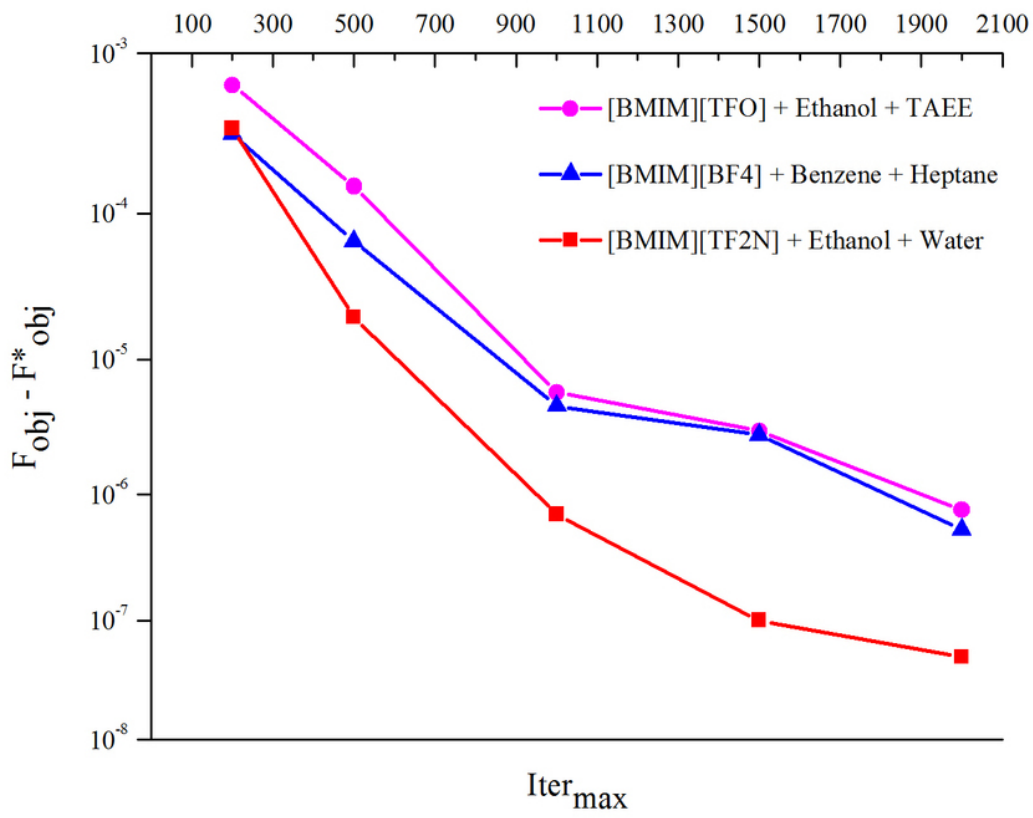

(a)

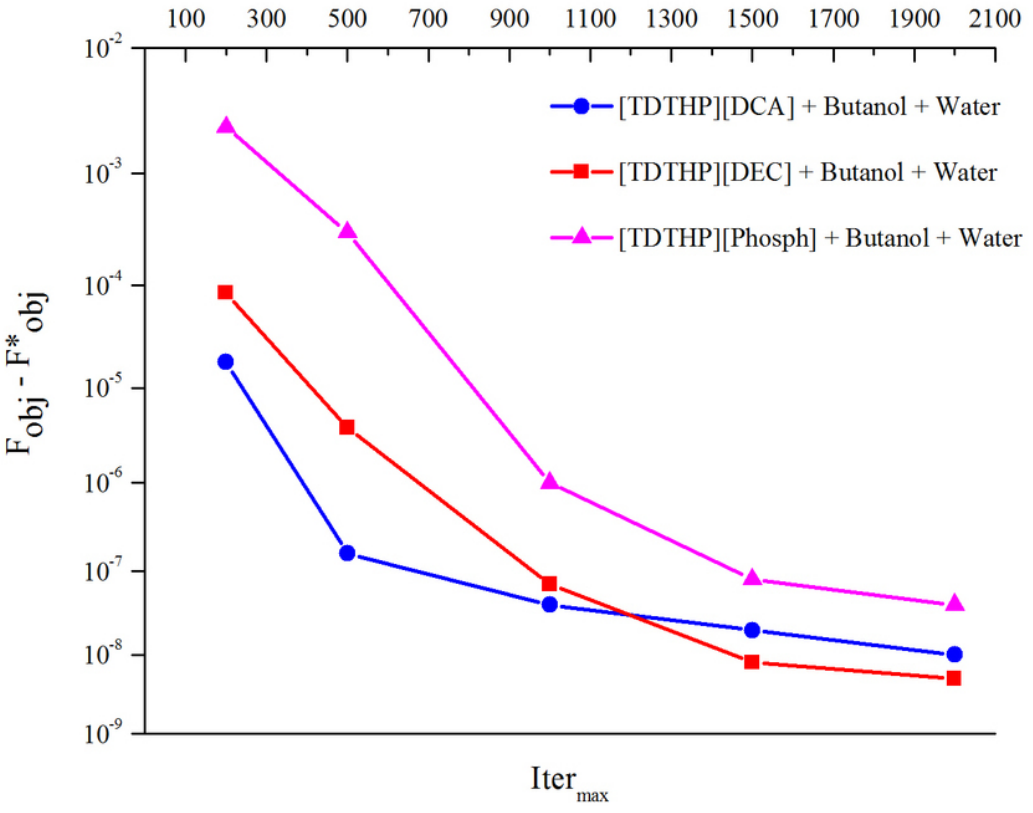

(b)

Figure 4.6.: Convergence plots of CS for selected (a) imidazolium-based ternary systems with UNIQUAC model w.r.t $Iter_{max}$, (b) phosphonium-based ternary systems with UNIQUAC model w.r.t $Iter_{max}$.

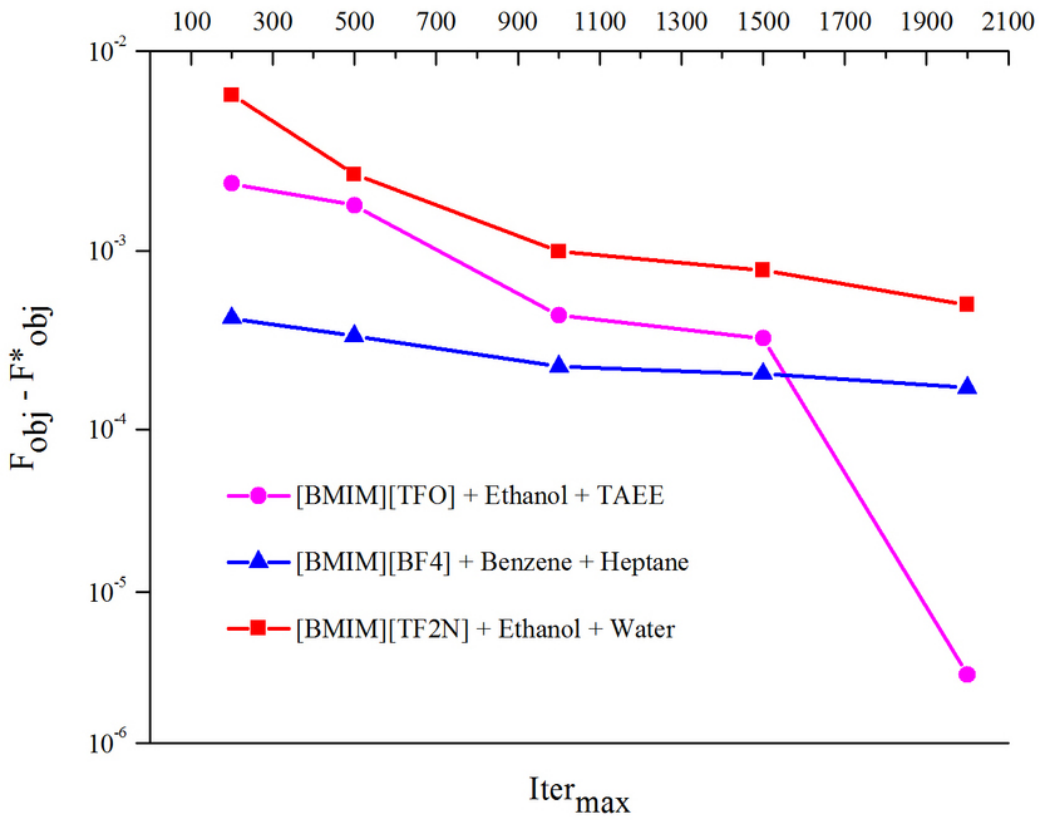

(c)

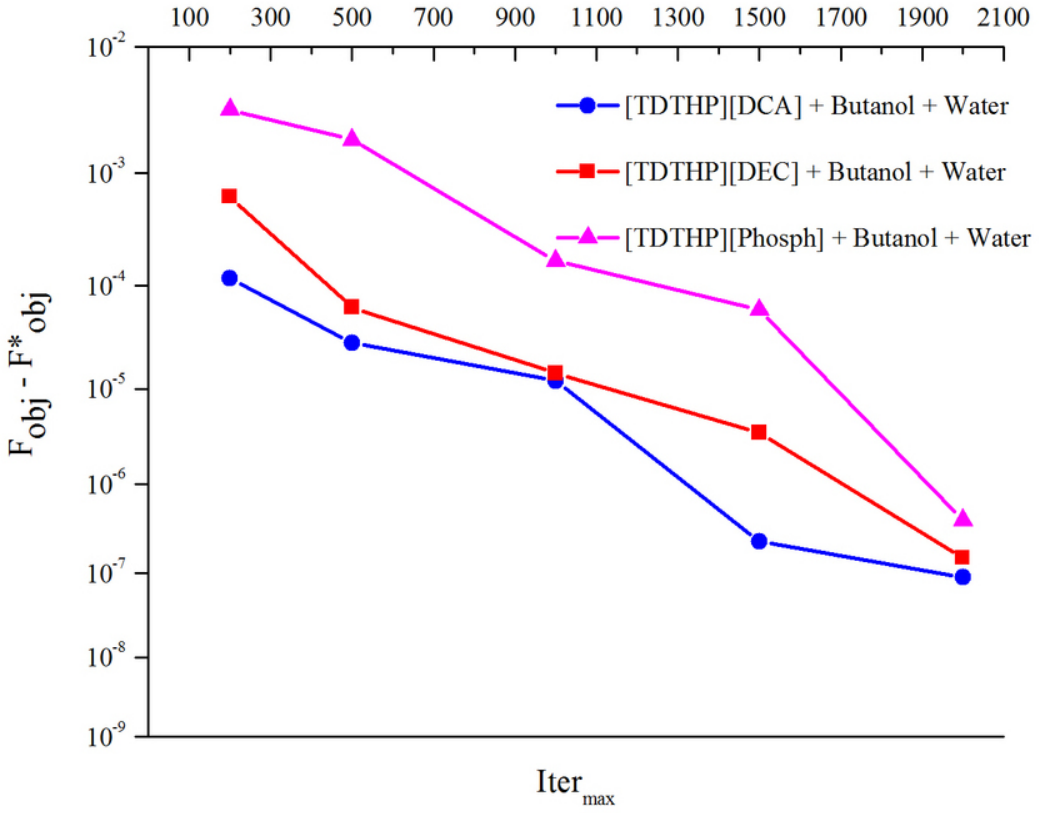

(d)

Figure 4.6.: Convergence plots of CS for selected (c) imidazolium-based ternary systems with NRTL model w.r.t $Iter_{max}$, (d) phosphonium-based ternary systems with NRTL model $Iter_{max}$.

Table 4.7.: Success Performance (%SR) of CS with UNIQUAC Model for Selected Ternary Systems

Tolerance (ϵ)	$\mathrm{Iter}_{\max}$	**SYS-2***	**SYS-20***	**SYS-30***	**SYS-22***	**SYS-23***	**SYS-25***
1.0E-3	200	3.3	50.0	53.3	73.3	36.7	0.0
	500	76.7	93.3	100.0	100.0	93.3	33.3
	1000	100.0	100.0	100.0	100.0	100.0	96.7
	1500	100.0	100.0	100.0	100.0	100.0	100.0
	2000	100.0	100.0	100.0	100.0	100.0	100.0
1.0E-4	200	0.0	0.0	0.0	33.3	3.3	0.0
	500	0.0	6.7	23.3	100.0	36.7	0.0
	1000	26.7	40.0	63.3	100.0	93.3	50.0
	1500	26.7	76.7	83.3	100.0	96.7	86.7
	2000	40.0	96.7	93.3	100.0	96.7	96.7
1.0E-5	200	0.0	0.0	0.0	0.0	0.0	0.0
	500	0.0	0.0	0.0	53.3	6.7	0.0
	1000	3.3	6.7	23.3	90.0	76.7	26.7
	1500	3.3	23.3	60.0	96.7	96.7	76.7
	2000	23.3	86.7	70.0	96.7	96.7	90.0

* SYS = Refers to systems of Table 4.1.

Table 4.8.: Success Performance (%SR) of CS with NRTL Model for Selected Ternary Systems

Tolerance (ϵ)	$\mathrm{Iter}_{\max}$	**SYS-2***	**SYS-20***	**SYS-30***	**SYS-22***	**SYS-23***	**SYS-25***
1.0E-3	200	0.0	16.7	0.0	86.7	13.3	0.0
	500	0.0	76.7	0.0	100.0	90.0	0.0
	1000	6.7	100.0	3.3	100.0	96.7	13.3
	1500	13.3	100.0	3.3	100.0	100.0	73.3
	2000	36.7	100.0	10.0	100.0	100.0	76.7
1.0E-4	200	0.0	0.0	0.0	0.0	0.0	0.0
	500	0.0	0.0	0.0	70.0	10.0	0.0
	1000	0.0	0.0	0.0	96.7	60.0	0.0
	1500	0.0	0.0	0.0	100.0	83.3	23.3
	2000	13.3	0.0	0.0	100.0	86.7	46.7
1.0E-5	200	0.0	0.0	0.0	0.0	0.0	0.0
	500	0.0	0.0	0.0	0.0	0.0	0.0
	1000	0.0	0.0	0.0	0.0	0.0	0.0
	1500	0.0	0.0	0.0	16.7	10.0	0.0
	2000	3.3	0.0	0.0	23.3	20.0	3.3

* SYS = Refers to systems of Table 4.1.

With NRTL model having maximum number of iterations as 2000, success rate in % for imidazolium ILs are in the range of 0-3.3% whereas for phosphonium ILs they are in the range of 3.3-23.3% with a tolerance value of 10^{-5}. This implies that CS gave a lower order of success in the parameter estimation of imidazolium ILs especially with NRTL model. Thus CS can be a recommended tool for imidazolium as well as phosphonium ILs with UNIQUAC model.

The RMSD values calculated using CS algorithm have been compared with the RMSD

values reported in literature and tabulated in Table 4.9-4.12. For IL based liquid-liquid ternary systems, global RMSD value with CS are 0.0056 (Table 4.9) and 0.0076 (Table 4.11) for UNIQUAC and NRTL model respectively. This is 64% and 45% better than literature reported global value of 0.0156 and 0.0139 for 305 tie-lines. For organic solvent based liquid-liquid ternary systems, global RMSD value with CS is 0.0036 (Table 4.10) and 0.0048 (Table 4.12) for UNIQUAC and NRTL model respectively. This again is 53% and 43% better than literature reported global value of 0.0077 and 0.0085 for 66 tie-lines. The overall RMSD values with CS are 0.0053 and 0.0072 for UNIQUAC and NRTL models respectively for 371 tie-lines. So in a nutshell this again is 63% and 45% better than literature reported global value of 0.0145 and 0.0131. These results are extremely satisfactory when compared to the deviation reported by Santiago et al. [Santiago et al., 2009] and Aznar [Aznar, 2007]. It is also about the same order of magnitude as reported by Vatani et al. [Vatani et al., 2012]. Santiago et al. [Santiago et al., 2009] further correlated LLE data of fifty ternary systems involving twelve different IL's, comprising 408 experimental tie-lines, by the UNIQUAC model with global deviation of 1.75%. Aznar [Aznar, 2007] correlated LLE data for 24 IL based ternary systems (184 tie-lines) by NRTL model and found global root mean square (RMS) deviations of 1.4%. Both Aznar [Aznar, 2007] and Santiago et al. [Santiago et al., 2009] estimated the interaction parameters using the Simplex method. Vatani et al. [Vatani et al., 2012] performed the liquid-liquid equilibria calculation for 20 different IL based ternary systems by NRTL model with binary interaction parameters calculated using Genetic Algorithm (GA). The overall RMSD value was 0.39% for 169 tie-lines.

In order to confirm our capability with CS, a comparison with GA and PSO algorithms was made for quaternary and quinary system. Three quaternary systems, Ethanol + Water + Pentane + Hexane; Ethanol + Water + Pentane + Cyclohexane; Ethanol + Water + Hexane + Cyclohexane and one quinary system, Ethanol + Water + Pentane + Hexane + Cyclohexane, as studied by Khansary and Sani [Khansary and Sani, 2014] were selected for the same. The experimental data for the above mentioned systems has been taken from Huang et al. [yung Huang et al., 2010]. For each system, 20 trials

has been carried out and the lowest RMSD along with the corresponding interaction parameters were selected as the final result and reported in Table 4.13 and Table 4.14. For quaternary system, CS gave RMSD (%) values in the range of 0.14-0.44% against 1.0% for GA and PSO (Table 4.13). Whereas for quinary system, CS gave RMSD (%) values 0.85% against 2.0% for GA and PSO (Table 4.14). This clearly shows CS algorithm is a reliable tool to correlate LLE data and even in some cases, it is superior to GA and PSO algorithms.

4.3.4. Bio-Chemicals based ternary systems

Lastly, interaction parameters were estimated for following bio-chemicals based ternary systems studied in this work: [BMIM][Tf_2N] (1) + acetic acid (2) + water (3); [BMIM]-[Tf_2N] (1) + furfural (2) + water (3); Ethyl acetate (1) + acetol (2) + water (3); *n*-propyl acetate (1) + acetol (2) + water (3); *n*-butyl acetate (1) + acetol (2) + water (3); Chloroform (1) + acetol (2) + water (3); [EMIM][Tf_2N] (1) + acetol (2) + water (3); [BMIM][Tf_2N] (1) + acetol (2) + water (3). UNIQUAC structure parameters for the components are reported in Table 4.4 and Table 4.15. Using UNIQUAC model, the root mean square deviation (RMSD) values were in the range of 0.0019-0.0075 (Table 4.16) while with NRTL model it was in the range of 0.0026-0.0063 (Table 4.17). These RMSD values indicate both models were able to correlate the experimental tie-line data.

4.4 Conclusions

In summary based on %SR and RMSD analyses, it can be concluded that CS algorithm gave good result in terms of both success rate and number of iterations especially for UNIQUAC model. LLE systems containing imidazolium ILs appears to be challenging for parameter estimation for higher precision. Further studies should be focused on the performance improvement of CS algorithm to get result with good precision using low numerical effort. Thus it can be concluded that the UNIQUAC and NRTL models, with interaction parameters estimated by CS algorithm, was able to correlate the LLE data successfully.

Table 4.9.: UNIQUAC Binary Interaction Parameters and RMSD Values for Ionic Liquid-based Ternary Systems

System	Binary Interaction Parameters(K)						RMSD	RMSD	
no.	A_{12}	A_{21}	A_{13}	A_{31}	A_{23}	A_{32}	(this work)	(lit.)	Reference
1	-2.19	-152.95	29.59	190.74	-246.23	716.64	0.0058	0.0101	[Santiago et al., 2009]
2	383.19	-297.74	-36.77	460.98	-207.15	421.52	0.0027	0.0038	[Santiago et al., 2009]
3	458.01	-171.18	-129.45	378.98	-155.56	643.72	0.0040	0.0063	[Santiago et al., 2009]
4	521.19	-171.8	-55.47	627.24	-194.46	685.15	0.0019	0.0071	[Santiago et al., 2009]
5	-102.40	274.03	-84.97	470.6	69.84	81.16	0.0054	0.0114	[Santiago et al., 2009]
6	234.72	-29.42	-39.30	367.97	-111.45	173.95	0.0045	0.0064	[Santiago et al., 2009]
7	26.52	155.76	10.41	184.19	-21.85	201.47	0.0049	0.0130	[Santiago et al., 2009]
8	164.99	64.04	-174.63	546.85	14.5	160.35	0.0080	0.0236	[Santiago et al., 2009]
9	224.53	30.55	-157.4	415.66	5.13	159.24	0.0113	0.0246	[Santiago et al., 2009]
10	-119.60	305.63	-58.91	497.37	80.19	-22.81	0.0088	0.0241	[Santiago et al., 2009]
11	473.07	-84.94	680.35	155.92	83.05	135.69	0.0119	0.0276	[Santiago et al., 2009]
12	-223.05	600.06	-18.37	362.53	209.49	-141.47	0.0064	0.0228	[Santiago et al., 2009]
13	124.42	64.5	96.73	137.73	263.34	-93.08	0.0109	0.0300	[Santiago et al., 2009]
14	315.17	-18.63	-39.89	417.74	-53.43	606.5	0.0055	0.0089	[Santiago et al., 2009]
15	231.76	3.71	-9.68	320.92	-67.76	587.51	0.0066	0.0091	[Santiago et al., 2009]

16	160.06	27.14	94.61	142.4	281.60	-73.26	0.0059	0.0203	[Santiago et al., 2009]
17	104.98	72.94	-23.9	327.07	170.11	10.73	0.0051	0.0215	[Santiago et al., 2009]
18	-136.50	392.82	-42.74	206.13	378.99	-190.76	0.0058	0.0243	[Santiago et al., 2009]
19	-210.73	966	0.12	120.51	994.64	-278.94	0.0089	0.0406	[Santiago et al., 2009]
20	-59.60	201.92	138.04	352.36	211.81	-93.32	0.0041	0.0058	[Revelli et al., 2010]
21	29.38	137.11	131.42	417.88	69.07	131.67	0.0016	0.0042	[Revelli et al., 2010]
22	-438.36	2666.98	2426.07	-104.39	2225.62	-24.24	0.0024*	0.0048	[Rabari and Banerjee, 2014]
23	-315.99	-70.82	2544.94	-312.03	2750.69	-88.1	0.0014*	0.0055	[Rabari and Banerjee, 2014]
24	-179.89	82.36	925.72	-249.73	504.79	-4.65	0.0017	0.0031	[Rabari and Banerjee, 2013]
25	-405.21	775.64	640.95	-189.43	2698.66	-69.92	0.0027*	0.0056	[Rabari and Banerjee, 2013]
26	23.22	157.91	280.22	251.85	-21.95	105.26	0.0011	0.0020	[García et al., 2009]
27	-126.89	613.09	122.98	399.26	58.47	-29.55	0.0016	0.0060	[González et al., 2010]
28	-81.46	429.31	146.08	382.4	-22.88	83.91	0.0010	0.0040	[González et al., 2010]
29	18.00	201.37	86.38	445.91	-10.37	86.24	0.0011	0.0020	[González et al., 2010]
30	668.94	-36.16	599.96	-72.44	95.63	396.95	0.0021	0.0014	[Cháfer et al., 2015]
31	319.61	-105.95	594.27	-86.88	822.94	-219.49	0.0014	0.0017	[Cháfer et al., 2015]
32	237.67	121.16	674.04	-130.94	319.46	78.34	0.0017	0.0015	[Cháfer et al., 2015]
					Global	**RMSD**	**0.0056**	**0.0156**	

Table 4.10.: UNIQUAC binary interaction parameters and RMSD values for organic solvent based ternary systems

System	Binary interaction parameters(K)						RMSD	RMSD	
no.	A_{12}	A_{21}	A_{13}	A_{31}	A_{23}	A_{32}	(this work)	(lit.)	Reference
1	-458.86	2871.24	-78.55	1192.58	61.51	75.51	0.0036*	0.0084	[Feng et al., 2015]
2	-184.45	597.67	-16.58	833.18	-3.34	175.78	0.0045	0.0086	[Feng et al., 2015]
3	-328.81	2823.1	-169.54	866.8	-76.79	417.34	0.0062*	0.0070	[Feng et al., 2015]
4	112.27	-47.37	489.39	59.04	-90.84	284.71	0.0015	0.0087	[Luo et al., 2015]
5	522.14	-286.47	420.67	149.94	-42.64	171.08	0.0016	0.0074	[Luo et al., 2015]
6	557.99	-278.58	675.88	53.52	-83.29	299.54	0.0018	0.0042	[Luo et al., 2015]
7	577.05	-301.10	552.05	135.49	-21.14	222.64	0.0011	0.0083	[Luo et al., 2015]
					Global	**RMSD**	**0.0036**	**0.0077**	

*lower bound = - 3000 and upper bound = + 3000.

Table 4.11.: NRTL Binary Interaction Parameters and RMSD Values for Ionic Liquid-based Ternary Systems

System	Binary Interaction Parameters(K)						RMSD	RMSD	
no.	τ_{12}	τ_{21}	τ_{13}	τ_{31}	τ_{23}	τ_{32}	(this work)	(lit.)	Reference
1	28.39	18.57	-3.11	85.37	7.00	2.28	0.0033	0.0067	[Arce et al., 2004a]
2	26.67	19.63	2.62	44.79	9.11	2.97	0.0044	0.0031	[Arce et al., 2004b]
3	-1.00	17.93	3.75	57.9	6.94	2.43	0.0037	0.0058	[Arce et al., 2006b]
4	25.40	20.24	2.47	89.37	7.21	2.99	0.0058	0.0047	[Arce et al., 2006a]
5	97.55	0.81	4.12	2.16	5.04	1.21	0.0122	0.0071	[Alonso et al., 2007]
6	21.34	18.59	4.54	-2.78	6.09	2.68	0.0062	0.0061	[Alonso et al., 2007]
7	27.92	0.32	3.74	3.53	5.57	19.7	0.0121	0.0171	[Alonso et al., 2008]
8	85.64	1.24	3.43	3.37	5.46	80.02	0.0132	0.0231	[Alonso et al., 2008]
9	-0.87	22.20	4.33	25.76	4.86	1.55	0.0174	0.0277	[Alonso et al., 2008]
10	11.72	19.83	21.51	87.99	5.43	8.07	0.0072	0.0180	[Letcher and Reddy, 2005]
11	43.92	23.70	3.63	15.27	10.8	-55.95	0.0128	0.0160	[Letcher and Reddy, 2005]
12	28.32	1.05	21.86	80.23	5.99	0.59	0.0053	0.0150	[Letcher and Reddy, 2005]
13	3.51	36.42	21.38	2.97	4.60	1.48	0.0070	0.0040	[Letcher and Deenadayalu, 2003]
14	-2.61	3.49	7.96	2.74	37.49	35.75	0.0095	0.0050	[Letcher and Reddy, 2004]
15	84.11	72.12	3.34	18.60	8.68	3.32	0.0084	0.0090	[Letcher and Reddy, 2004]

16	2.00	5.44	20.43	1.58	78.7	20.02	0.0085	0.0220	[Letcher and Reddy, 2004]
17	67.19	2.38	2.97	2.87	18.47	-82.02	0.0111	0.0370	[Letcher and Reddy, 2004]
18	20.31	1.41	16.12	22.24	3.79	34.87	0.0041	0.0060	[Letcher and Reddy, 2005]
19	21.13	1.43	16.47	21.8	3.79	33.64	0.0064	0.0040	[Letcher and Reddy, 2005]
20	86.52	4.32	6.07	12.6	35.19	0.69	0.0046	0.0236	[Revelli et al., 2010]
21	0.10	5.34	24.57	1.22	5.63	54.01	0.0036	0.0027	[Revelli et al., 2010]
22	-3.13	74.27	17.31	97.84	8.30	4.32	0.0020	0.0012	[Rabari and Banerjee, 2014]
23	-4.74	32.49	17.64	91.26	6.43	3.8	0.0012	0.0014	[Rabari and Banerjee, 2014]
24	-1.59	21.65	1.16	16.67	5.53	2.91	0.0040	0.0015	[Rabari and Banerjee, 2013]
25	84.25	35.13	-7.19	16.52	8.44	3.16	0.0024	0.0028	[Rabari and Banerjee, 2013]
26	2.24	3.31	43.18	55.11	6.83	1.96	0.0011	0.0018	[García et al., 2009]
27	92.53	1.55	13.83	70.15	5.72	0.32	0.0016	0.0020	[González et al., 2010]
28	86.19	2.12	13.63	79.35	5.29	0.45	0.0010	0.0030	[González et al., 2010]
29	48.84	26.27	13.72	74.38	6.23	0.42	0.0020	0.0020	[González et al., 2010]
30	30.19	0.53	0.21	16.91	9.79	75.05	0.0043	0.0030	[Cháfer et al., 2015]
31	-45.39	22.26	0.27	17.83	9.29	-44.5	0.0024	0.0023	[Cháfer et al., 2015]
32	58.67	21.85	-0.18	4.64	11.41	29.56	0.0026	0.0019	[Cháfer et al., 2015]
					Global	**RMSD**	**0.0076**	**0.0139**	

Table 4.12.: NRTL binary interaction parameters and RMSD values for organic solvent based ternary systems

System	Binary Interaction Parameters(K)						RMSD	RMSD	
no.	τ_{12}	τ_{21}	τ_{13}	τ_{31}	τ_{23}	τ_{32}	(this work)	(lit.)	Reference
1	0.5	18.86	69.19	70.7	5.77	2.20	0.0032	0.0041	[Feng et al., 2015]
2	-75.12	20.88	2.49	1.99	11.28	67.72	0.0041	0.0053	[Feng et al., 2015]
3	-3.21	4.92	6.29	98.67	37.61	2.59	0.0076	0.0162	[Feng et al., 2015]
4	1.56	2.81	65.81	7.71	25.71	2.43	0.0036	0.0081	[Luo et al., 2015]
5	0.51	3.12	13.22	12.35	33.26	3.23	0.0037	0.0054	[Luo et al., 2015]
6	-7.91	2.66	98.17	2.83	20.39	36.13	0.0042	0.0072	[Luo et al., 2015]
7	-2.09	3.23	65.23	82.79	31.15	3.14	0.0058	0.0074	[Luo et al., 2015]
					Global	**RMSD**	**0.0048**	**0.0085**	

Table 4.13.: Comparison of CS with GA and PSO algorithm for Quaternary Systems

System	Model	Temp		CS		RMSD%		
		K	*i-j*	τ_{ij}	τ_{ji}	CS	GA*	PSO*
Ethanol(1)	NRTL	293.15	1-2	-49.75	-94.25	0.31	1.267	1.233
Water(2)			1-3	11.21	29.51			
Hexane(3)			1-4	10.98	60.45			
Cyclohexane(4)			2-3	2.62	39.45			
			2-4	1.03	-41.04			
			3-4	73.65	71.04			
Ethanol(1)	NRTL	303.15	1-2	95.13	55.17	0.26		
Water(2)			1-3	30.28	2.52			
Hexane(3)			1-4	-43.75	4.40			
Cyclohexane(4)			2-3	53.28	4.69			
			2-4	8.48	4.55			
			3-4	-1.38	60.03			
Ethanol(1)	NRTL	308.15	1-2	39.69	51.06	0.44		
Water(2)			1-3	42.06	2.47			
Hexane(3)			1-4	37.53	2.39			
Cyclohexane(4)			2-3	39.62	4.25			
			2-4	29.86	6.74			

			3-4	31.87	-44.12			
Ethanol(1)	NRTL	293.15	1-2	71.52	-91.38	0.14	1.032	1.112
Water(2)			1-3	-94.29	-89.42			
Pentane(3)			1-4	17.79	-89.10			
Cyclohexane(4)			2-3	-16.17	4.16			
			2-4	60.84	5.81			
			3-4	-64.59	90.90			
Ethanol(1)	NRTL	303.15	1-2	79.21	81.28	0.31		
Water(2)			1-3	36.99	2.37			
Pentane(3)			1-4	70.35	2.50			
Cyclohexane(4)			2-3	32.06	3.63			
			2-4	2.21	50.12			
			3-4	71.95	31.19			
Ethanol(1)	NRTL	308.15	1-2	54.91	38.80	0.33		
Water(2)			1-3	-77.47	2.14			
Pentane(3)			1-4	-92.07	2.66			
Cyclohexane(4)			2-3	88.93	4.11			
			2-4	23.63	4.21			
			3-4	28.67	-29.60			
Ethanol(1)	NRTL	293.15	1-2	86.22	-74.37	0.27	1.021	1.031

Water(2)			1-3	-78.62	-72.31	
Pentane(3)			1-4	52.55	-32.82	
Hexane(4)			2-3	78.20	4.70	
			2-4	-79.86	60.47	
			3-4	-83.83	72.96	
Ethanol(1)	NRTL	303.15	1-2	-1.85	58.42	0.34
Water(2)			1-3	3.16	-68.27	
Pentane(3)			1-4	2.98	-7.83	
Hexane(4)			2-3	2.48	2.79	
			2-4	62.65	8.41	
			3-4	-4.39	1.63	
Ethanol(1)	NRTL	308.15	1-2	-94.95	-84.66	0.37
Water(2)			1-3	11.72	43.44	
Pentane(3)			1-4	13.74	-5.05	
Hexane(4)			2-3	2.12	-71.55	
			2-4	1.29	-90.86	
			3-4	92.89	70.49	

* [Khansary and Sani, 2014]

Table 4.14.: Comparison of CS with GA and PSO algorithm for Quinary Systems

System	**Model**	**Temp**		**CS**		**RMSD**		
		K	***i-j***	τ_{ij}	τ_{ji}	**CS**	**GA***	**PSO***
Ethanol (1)	NRTL	303.15	1-2	-47.78	15.78	0.85	2.11	2.07
Water (2)			1-3	-80.29	49.33			
Pentane (3)			1-4	-70.43	28.75			
Hexane (4)			1-5	-56.56	-86.43			
Cyclohexane (5)			2-3	27.71	-42.10			
			2-4	27.35	-43.29			
			2-5	95.84	26.65			
			3-4	-72.19	-81.97			
			3-5	-72.54	-12.76			
			4-5	-69.12	20.29			
Ethanol (1)	NRTL	308.15	1-2	82.87	36.80	0.83		
Water (2)			1-3	64.09	96.85			
Pentane (3)			1-4	-77.3	2.24			
Hexane (4)			1-5	-60.06	25.66			
Cyclohexane (5)			2-3	-7.81	22.34			
			2-4	-91.92	87.86			
			2-5	-52.69	53.04			
			3-4	-92.02	-14.27			
			3-5	-63.84	2.14			
			4-5	3.46	-16.67			

* [Khansary and Sani, 2014]

Table 4.15.: UNIQUAC Volume and Surface Area Structural Parameters of Compounds Used in this Work

Solvent	**r**	**q**
acetol*	2.87409	2.612
ethyl acetate*	3.47858	3.116
n-propyl acetate*	4.15293	3.656
n-butyl acetate*	4.82729	4.196
chloroform*	2.8675	2.412
[EMIM][Tf_2N]**	10.1066	8.059

*Aspen Plus V8.8 data bank (Aspen Technology Inc., USA).

** [Santiago et al., 2010]

Table 4.16.: UNIQUAC binary interaction parameters and RMSD values for bio-oil chemicals based ternary systems

System	Binary interaction parameters(K)						RMSD	
no.	A_{12}	A_{21}	A_{13}	A_{31}	A_{23}	A_{32}	(this work)	Reference
1	-266.06	-335.82	248.66	127.29	-273.86	-682.32	0.0075	This work
2	-357.32	928.03	510.23	-86.744	631.0	-52.788	0.0043	This work
3	997.14	-78.80	242.88	211.38	-52.38	862.96	0.0058	This work
4	-129.66	350.13	414.87	138.76	-176.09	76.35	0.0048	This work
5	-246.15	988.58	573.56	57.03	-35.63	-144.88	0.0052	This work
6	-279.79	220.43	377.38	739.81	-213.20	10.70	0.0065	This work
7	449.41	84.57	431.86	-74.84	256.65	291.06	0.0019	This work
8	301.20	0.84	525.33	-74.97	315.80	37.67	0.0028	This work

1 = [BMIM][Tf_2N] (1) + acetic acid (2) + water (3); 2 = [BMIM][Tf_2N] (1) + furfural (2) + water (3); 3 = Ethyl acetate (1) + acetol (2) + water (3); 4 = *n*-propyl acetate (1) + acetol (2) + water (3); 5 = *n*-butyl acetate (1) + acetol (2) + water (3); 6 = Chloroform (1) + acetol (2) + water (3); 7 = [EMIM][Tf_2N] (1) + acetol (2) + water (3); 8 = [BMIM][Tf_2N] (1) + acetol (2) + water (3)

Table 4.17.: NRTL binary interaction parameters and RMSD values for bio-oil chemicals based ternary systems

System	Binary Interaction Parameters(K)						RMSD	
no.	τ_{12}	τ_{21}	τ_{13}	τ_{31}	τ_{23}	τ_{32}	(this work)	Reference
1	-1.8201	16.52	10.582	14.226	39.995	33.466	0.0036	This work
2	1.6956	-2.7893	143.356	11.332	16.523	4.1444	0.0026	This work
3	99.38	2.30	3.06	26.09	2.96	0.37	0.0031	This work
4	-52.17	2.00	3.09	24.66	1.62	-92.96	0.0026	This work
5	-15.14	2.54	3.29	27.29	3.29	27.29	0.0040	This work
6	20.39	0.79	23.57	6.16	1.17	28.10	0.0063	This work
7	29.18	0.59	-0.47	10.00	12.29	-38.59	0.0035	This work
8	5.56	1.86	27.24	10.25	-49.59	11.21	0.0029	This work

1 = [BMIM][Tf_2N] (1) + acetic acid (2) + water (3); 2 = [BMIM][Tf_2N] (1) + furfural (2) + water (3); 3 = Ethyl acetate (1) + acetol (2) + water (3); 4 = *n*-propyl acetate (1) + acetol (2) + water (3); 5 = *n*-butyl acetate (1) + acetol (2) + water (3); 6 = Chloroform (1) + acetol (2) + water (3); 7 = [EMIM][Tf_2N] (1) + acetol (2) + water (3); 8 = [BMIM][Tf_2N] (1) + acetol (2) + water (3)

REFERENCES

[Abrams and Prausnitz, 1975] Abrams, D. S. and Prausnitz, J. M. (1975). Statistical thermodynamics of liquid mixtures: A new expression for the excess gibbs energy of partly or completely miscible systems. *AIChE Journal*, 21:116–128.

[Alonso et al., 2007] Alonso, L., Arce, A., Francisco, M., Rodr'iguez, O., and Soto, A. (2007). Gasoline desulfurization using extraction with [c8mim][bf4] ionic liquid. *AIChE Journal*, 53:3108–3115.

[Alonso et al., 2008] Alonso, L., Arce, A., Francisco, M., and Soto, A. (2008). Solvent extraction of thiophene from n-alkanes (c7, c12, and c16) using the ionic liquid [c8mim][bf4]. *The Journal of Chemical Thermodynamics*, 40:966–972.

[Arce et al., 2006a] Arce, A., Rodr'iguez, H., and Soto, A. (2006a). Effect of anion fluorination in 1-ethyl-3-methylimidazolium as solvent for the liquid extraction of ethanol from ethyl tert-butyl ether. *Fluid Phase Equilibria*, 242:164–168.

[Arce et al., 2006b] Arce, A., Rodr'iguez, H., and Soto, A. (2006b). Purification of ethyl tert-butyl ether from its mixtures with ethanol by using an ionic liquid. *Chemical Engineering Journal*, 115:219–223.

[Arce et al., 2004a] Arce, A., Rodríguez, O., and Soto, A. (2004a). Experimental determination of liquid-liquid equilibrium using ionic liquids:tert-amyl ethyl ether + ethanol + 1-octyl-3-

methylimidazolium chloride system at 298.15 k. *Journal of Chemical & Engineering Data*, 49:514–517.

[Arce et al., 2004b] Arce, A., Rodríguez, O., and Soto, A. (2004b). tert-amyl ethyl ether separation from its mixtures with ethanol using the 1-butyl-3-methylimidazolium trifluoromethanesulfonate ionic liquid:liquid-liquid equilibrium. *Industrial & Engineering Chemistry Research*, 43:8323–8327.

[Aznar, 2007] Aznar, M. (2007). Correlation of (liquid + liquid) equilibrium of systems including ionic liquids. *Brazilian Journal of Chemical Engineering*, 24:143–149.

[Banerjee et al., 2005] Banerjee, T., Singh, M. K., Sahoo, R. K., and Khanna, A. (2005). Volume, surface and uniquac interaction parameters for imidazolium based ionic liquids via polarizable continuum model. *Fluid Phase Equilibria*, 234:64–76.

[Bhargava et al., 2013] Bhargava, V., Fateen, S., and Bonilla-Petriciolet, A. (2013). Cuckoo search: A new nature-inspired optimization method for phase equilibrium calculations. *Fluid Phase Equilibria*, 337:191–200.

[Bharti and Banerjee, 2015] Bharti, A. and Banerjee, T. (2015). Enhancement of bio-oil derived chemicals in aqueous phase using ionic liquids: Experimental and cosmo-sac predictions using a modified hydrogen bonding expression. *Fluid Phase Equilibria*, 400:27–37.

[Bonilla-Petriciolet et al., 2013] Bonilla-Petriciolet, A., Fateen, S., and Rangaiah, G. (2013). Assessment of capabilities and limitations of stochastic global optimization methods for modeling mean activity coefficients of ionic liquids. *Fluid Phase Equilibria*, 340:15–26.

[Cháfer et al., 2015] Cháfer, A., de la Torre, J., Font, A., and Lladosa, E. (2015). Liquid-liquid equilibria of water + ethanol + 1-butyl-3-methylimidazolium bis(trifluoromethanesulfonyl)imide ternary system: Measurements and correlation at different temperatures. *Journal of Chemical & Engineering Data*, 60:2426–2433.

[Fateen and Bonilla-Petriciolet, 2014a] Fateen, S. and Bonilla-Petriciolet, A. (2014a). On the

effectiveness of the nature-inspired metaheuristic algorithms for performing phase equilibrium thermodynamic calculations. *Sci. World J.*, 2014.

[Fateen and Bonilla-Petriciolet, 2014b] Fateen, S.-E. K. and Bonilla-Petriciolet, A. (2014b). A note on effective phase stability calculations using a gradient-based cuckoo search algorithm. *Fluid Phase Equilibria*, 375:360–366.

[Fateen et al., 2012] Fateen, S.-E. K., Bonilla-Petriciolet, A., and Rangaiah, G. P. (2012). Evaluation of covariance matrix adaptation evolution strategy, shuffled complex evolution and firefly algorithms for phase stability, phase equilibrium and chemical equilibrium problems. *Chemical Engineering Research and Design*, 90:2051–2071.

[Feng et al., 2015] Feng, Y., Yang, E., Dang, L., and Wei, H. (2015). Liquid-liquid phase equilibrium for ternary mixtures of formamide (or ethylene glycol, or monoethanolamine) + indole + 2-methylnaphthalene at 308.15 k. *Fluid Phase Equilibria*, 398:10–14.

[Fernández-Vargas et al., 2013] Fernández-Vargas, J. A., Bonilla-Petriciolet, A., and Segovia-Hernández, J. G. (2013). An improved ant colony optimization method and its application for the thermodynamic modeling of phase equilibrium. *Fluid Phase Equilibria*, 353:121–131.

[Ferrari et al., 2009] Ferrari, J. C., Nagatani, G., Corazza, F. C., Oliveira, J. V., and Corazza, M. L. (2009). Application of stochastic algorithms for parameter estimation in the liquid-liquid phase equilibrium modeling. *Fluid Phase Equilibria*, 280:110 – 119.

[Fister et al., 2013] Fister, I., J., Fister, D., and Fister, I. (2013). A comprehensive review of cuckoo search: variants andhybrids. *Int. J. Mathematical Modelling and Numerical Optimisation*, 4:387–409.

[García et al., 2009] García, J., Fernández, A., Torrecilla, J. S., Oliet, M., and Rodríguez, F. (2009). Liquid-liquid equilibria for hexane + benzene + 1-ethyl-3-methylimidazolium ethylsulfate at (298.2, 313.2 and 328.2) k. *Fluid Phase Equilibria*, 282:117–120.

[González et al., 2010] González, E. J., Calvar, N., Gonzalez, B., and Domínguez, A. (2010).

Liquid extraction of benzene from its mixtures using 1-ethyl-3-methylimidazolium ethylsulfate as a solvent. *Journal of Chemical & Engineering Data*, 55(11):4931–4936.

[Jaime-Leal et al., 2015] Jaime-Leal, J., Bonilla-Petriciolet, A., Bhargava, V., and Fateen, S. (2015). Nonlinear parameter estimation of e-nrtl model for quaternary ammonium ionic liquids using cuckoo search. *Chemical Engineering Research and Design*, 93:464–472.

[Kabouche et al., 2012] Kabouche, A., Boultif, A., Abidi, A., and Gherraf, N. (2012). Interaction parameter estimation in liquid-liquid phase equilibrium modeling using stochastic and hybrid algorithms. *Fluid Phase Equilibria*, 336:113–121.

[Khansary and Sani, 2014] Khansary, M. A. and Sani, A. H. (2014). Using genetic algorithm (ga) and particle swarm optimization (pso) methods for determination of interaction parameters in multicomponent systems of liquid-liquid equilibria. *Fluid Phase Equilibria*, 365:141–145.

[Letcher and Deenadayalu, 2003] Letcher, T. M. and Deenadayalu, N. (2003). Ternary liquid-liquid equilibria for mixtures of 1-methyl-3-octyl-imidazolium chloride + benzene + an alkane at t=298.2 k and 1 atm. *The Journal of Chemical Thermodynamics*, 35:67–76.

[Letcher and Reddy, 2004] Letcher, T. M. and Reddy, P. (2004). Ternary liquid-liquid equilibria for mixtures of 1-hexyl-3-methylimidozolium (tetrafluoroborate or hexafluorophosphate) + ethanol + an alkene at t=298.2 k. *Fluid Phase Equilibria*, 219:107–112.

[Letcher and Reddy, 2005] Letcher, T. M. and Reddy, P. (2005). Ternary (liquid + liquid) equilibria for mixtures of 1-hexyl-3-methylimidazolium (tetrafluoroborate or hexafluorophosphate) + benzene + an alkane at t=298.2 k and p=0.1 {MPa}. *The Journal of Chemical Thermodynamics*, 37:415–421.

[Luo et al., 2015] Luo, L., Liu, D., Li, L., and Chen, Y. (2015). Phase equilibria of (water + propionic acid or butyric acid + 2-methoxy-2-methylpropane) ternary systems at 298.2 k and 323.2 k. *Fluid Phase Equilibria*, 403:30–35.

[Merzougui et al., 2011] Merzougui, A., Hasseine, A., Kabouche, A., and Korichi, M.

(2011). Lle for the extraction of alcohol from aqueous solutions with diethyl ether and dichloromethane at 293.15 k, parameter estimation using a hybrid genetic based approach. *Fluid Phase Equilibria*, 309:161–167.

[Merzougui et al., 2012] Merzougui, A., Hasseine, A., and Laiadi, D. (2012). Application of the harmony search algorithm to calculate the interaction parameters in liquid-liquid phase equilibrium modeling. *Fluid Phase Equilibria*, 324:94–101.

[Nanda and Panda, 2014] Nanda, S. J. and Panda, G. (2014). A survey on nature inspired metaheuristic algorithms for partitional clustering. *Swarm and Evolutionary Computation*, 16:1–18.

[Petriciolet and Hernández, 2010] Petriciolet, A. B. and Hernández, J. G. S. (2010). A comparative study of particle swarm optimization and its variants for phase stability and equilibrium calculations in multicomponent reactive and non-reactive systems. *Fluid Phase Equilibria*, 289:110–121.

[Petriciolet et al., 2010] Petriciolet, A. B., Rangaiah, G. P., and Hernández, J. G. S. (2010). Evaluation of stochastic global optimization methods for modeling vapor-liquid equilibrium data. *Fluid Phase Equilibria*, 287:111–125.

[Rabari and Banerjee, 2013] Rabari, D. and Banerjee, T. (2013). Biobutanol and n-propanol recovery using a low density phosphonium based ionic liquid at t = 298.15 k and p = 1 atm. *Fluid Phase Equilibria*, 355:26–33.

[Rabari and Banerjee, 2014] Rabari, D. and Banerjee, T. (2014). Experimental and theoretical studies on the effectiveness of phosphonium-based ionic liquids for butanol removal at t = 298.15 k and p = 1 atm. *Industrial & Engineering Chemistry Research*, 53(49):18935–18942.

[Renon and Prausnitz, 1968] Renon, H. and Prausnitz, J. M. (1968). Local compositions in thermodynamic excess functions for liquid mixtures. *AIChE Journal*, 14:135–144.

[Revelli et al., 2010] Revelli, A.-L., Mutelet, F., and Jaubert, J. (2010). Extraction of benzene

or thiophene from n-heptane using ionic liquids. nmr and thermodynamic study. *The Journal of Physical Chemistry B*, 114:4600–4608.

[Sahoo et al., 2006] Sahoo, R. K., Banerjee, T., Ahmad, S. A., and Khanna, A. (2006). Improved binary parameters using {GA} for multi-component aromatic extraction: {NRTL} model without and with closure equations. *Fluid Phase Equilibria*, 239:107–119.

[Santiago et al., 2009] Santiago, R., Santos, G. R., and Aznar, M. (2009). Uniquac correlation of liquid-liquid equilibrium in systems involving ionic liquids: The dft-pcm approach. *Fluid Phase Equilibria*, 278:54–61.

[Santiago et al., 2010] Santiago, R. S., Santos, G. R., and Aznar, M. (2010). Uniquac correlation of liquid-liquid equilibrium in systems involving ionic liquids: The dft-pcm approach. part ii. *Fluid Phase Equilibria*, 293:66–72.

[Seader, 2006] Seader, J. D.and Henley, E. J. (2006). *Separation Process Principles*. John Wiley & Sons,.

[Singh et al., 2005] Singh, M. K., Banerjee, T., and Khanna, A. (2005). Genetic algorithm to estimate interaction parameters of multicomponent systems for liquid-liquid equilibria. *Computers & Chemical Engineering*, 29:1712–1719.

[Srinivas and Rangaiah, 2007] Srinivas, M. and Rangaiah, G. P. (2007). Differential evolution with tabu list for global optimization and its application to phase equilibrium and parameter estimation problems. *Industrial & Engineering Chemistry Research*, 46:3410–3421.

[Varma et al., 2011] Varma, N. R., Ramalingam, A., and Banerjee, T. (2011). Experiments, correlations and cosmo-rs predictions for the extraction of benzothiophene from n-hexane using imidazolium-based ionic liquids. *Chemical Engineering Journal*, 166:30–39.

[Vatani et al., 2012] Vatani, M., Asghari, M., and Vakili-Nezhaad, G. (2012). Application of genetic algorithm to the calculation of parameters for {NRTL} and two-suffix margules models in ternary extraction ionic liquid systems. *Journal of Industrial and Engineering Chemistry*, 18:1715 – 1720.

[Yang, 2010] Yang, X. (2010). *Engineering Optimization: An Introduction with Metaheuristic Applications*. John Wiley & Sons, Hoboken, NJ.

[Yang, 2014] Yang, X. (2014). *Nature-Inspired Optimization Algorithms*. Elsevier.

[Yang and Deb, 2009] Yang, X.-S. and Deb, S. (2009). Cuckoo search via levy flighrs. *In Proceedings of World Congress on Nature & Biologically Inspired Computing (NaBIC 2009), December 9-11, 2009, Coimbatore, India; IEEE Publications: New York*, pages 210–214.

[Yang and Deb, 2013] Yang, X.-S. and Deb, S. (2013). Multiobjective cuckoo search for design optimization. *Comput. Oper. Res.*, 40:1616–1624.

[Yang and Deb, 2014] Yang, X.-S. and Deb, S. (2014). Cuckoo search: recent advances and applications. *Neural Computing and Applications*, 24:169–174.

[yung Huang et al., 2010] yung Huang, C., yu Chung, P., Tseng, I.-M., and sun Lee, L. (2010). Measurements and correlations of liquid-liquid-equilibria of the mixtures consisting of ethanol, water, pentane, hexane, and cyclohexane. *The Open Thermodynamics Journal*, 4:102–118.

[Zhang et al., 2011a] Zhang, H., Rangaiah, G. P., and Bonilla-Petriciolet, A. (2011a). Integrated differential evolution for global optimization and its performance for modeling vaporr-liquid equilibrium data. *Industrial & Engineering Chemistry Research*, 50:10047–10061.

[Zhang et al., 2011b] Zhang, H., Vargas, J. A. F., Rangaiah, G. P., Petriciolet, A. B., and Hernández, J. G. S. (2011b). Evaluation of integrated differential evolution and unified bare-bones particle swarm optimization for phase equilibrium and stability problems. *Fluid Phase Equilibria*, 310:129–141.

CHAPTER 5

Perturbed Chain - Statistical Associating Fluid Theory (PC-SAFT) Equation of state: Liquid-liquid Equilibria

5.1 Introduction

Cubic equations of state are classical high pressure models. Such cubic EOS are still the primary choice of models for petrochemicals, gas processing and air separation. The van der Waals equation of state was the first equation capable of representing vapor-liquid coexistence [Wei and Sadus, 2000].

$$Z = \frac{V}{V-b} - \frac{a}{RTV} \tag{5.1}$$

where *Z* is the compressibility factor, *T* is temperature, *V* is volume, and *R* is the molar universal gas constant. The parameter "*a*" is a measure of the attractive forces between the molecules, and the parameter "*b*" is the covolume occupied by the molecules. The van der Waals equation can be regarded as a "hard-sphere (repulsive) + dispersion (attractive)" term equation of state. It gives a qualitative description of the vapor and liquid phases and phase transitions, but it is not accurate for critical properties and phase equilibria calculations. The van der Waals equation has been superseded by a large number of other, more accurate equations of state. The most important model for the modification of the van der Waals equation of state is the Redlich-Kwong equation. It retains the original van der Waals hard-sphere term with the addition of a temperature-dependent attractive term [Redlich and Kwong, 1949].

$$Z = \frac{V}{V-b} - \frac{a}{RT^{1.5}(V+b)} \tag{5.2}$$

Soave suggested replacing the term $a/T^{1.5}$ with a more general temperature-dependent term *a(T)* [Soave, 1972].

$$Z = \frac{V}{V-b} - \frac{a(T)}{RT(V+b)} \tag{5.3}$$

where

$$a(T) = 0.4274\left(\frac{R^2T_c^2}{P_c}\right)\left\{1 + m\left[1 - \left(\frac{T}{T_c}\right)^{0.5}\right]\right\}^2 \tag{5.4}$$

$$m = 0.480 + 1.57\omega - 0.176\omega^2; b = 0.08664\frac{RT_c}{P_c} \tag{5.5}$$

where T_c is critical temperature, P_c is critical pressure and ω is acentric factor which is the measure of the non-sphericity of the molecule:

$$\omega = -logP_r^{sat} - 1.00 \tag{5.6}$$

Here P_r^{sat} is the reduced vapor pressure and evaluated at T_r (reduced temperature) = 0.7.

Peng and Robinson redefined *a(T)* as [Peng and Robinson, 1976]:

$$a(T) = 0.45724\left(\frac{R^2T_c^2}{P_c}\right)\left\{1 + k\left[1 - \left(\frac{T}{T_c}\right)^{0.5}\right]\right\}^2 \tag{5.7}$$

$$k = 0.37464 + 1.5422\omega - 0.26922\omega^2; b = 0.07780\frac{RT_c}{P_c} \tag{5.8}$$

They also proposed a different expression

$$Z = \frac{V}{V-b} - \frac{a(T)V}{RT[V(V+b)+b(V-b)]} \tag{5.9}$$

Soave-Redlich-Kwong and Peng-Robinson are hence known as two-parameter models. Extension to mixtures requires mixing rules for the two parameters of the EoS, the energy parameter (*a*) and the co-volume one (*b*). Van der Waals one-fluid (vdW1f) mixing rules and classical combining rules have received widespread application [Wei and Sadus, 2000]. The van der Waals one fluid (vdW1f) mixing rules are given by the equations:

$$a = \sum_{i=1}^{n}\sum_{j=1}^{n} x_i x_j a_{ij} \tag{5.10}$$

$$b = \sum_{i=1}^{n}\sum_{j=1}^{n} x_i x_j b_{ij} \tag{5.11}$$

The mixing rules actually represent the interactions between the components in the mixture. They depend not only on the pure fluid parameters but also on the cross-parameters such as a_{12} and b_{12}. For cross-parameters following combining rules are used:

$$a_{ij} = \sqrt{a_i a_j}(1 - k_{ij}) \tag{5.12}$$

$$b_{ij} = \frac{b_i + b_j}{2}(1 - l_{ij}) \tag{5.13}$$

where k_{ij} and l_{ij} are binary interaction parameters correcting for the deviations of the mixture parameters from the means of the pure-component parameters.

SRK and PR with the mixing and combining rules had been used for years and still widely used in the oil and petroleum industry for modeling hydrocarbons and gas-hydrocarbon mixtures. However, there are many systems where cubic EoS have been proven to be unsuccessful such as for mixtures with polar and hydrogen bonding fluids such as water, alcohols and acids. In general, LLE is not very well correlated with cubic EoS even for non-polar systems. Results are poor for complex, multicomponent VLE and LLE, especially in the presence of associating compounds [Kontogeorgis and Folas, 2010]. The reason for not so good prediction for polar and associating components is inherent in cubic EoS. In terms of *Z*, cubic EoS can be written as:

$$Z = Z^{Rep.} + Z^{Att.} \tag{5.14}$$

$Z^{Rep.}$ is repulsive contribution due to hard-sphere nature whereas $Z^{Att.}$ is attractive contribution due to dispersive nature. Cubic EoS only considers the dispersive intermolecular interactions and don't consider specific intermolecular interactions such as hydrogen bonding which are present in polar and associating components. This led to poor prediction of phase equilibria for complex systems in which components have tendency to form hydrogen bonds.

The limitations of cubic EoS have led to the development of the following:

1. *activity coefficient models* based on group contributions e.g. UNIFAC which offered a solution to the thermodynamic modeling of complex systems at low pressures [Fredenslund et al., 1975],

2. *improved mixing rules* for cubic equations of state such as EoS/G^E mixing rules which allowed cubic EoS to be used for describing highly non-ideal systems using information from activity coefficient model such as UNIFAC, NRTL [Abrams and Prausnitz, 1975] or UNIQUAC [Renon and Prausnitz, 1968], and

3. *improved non-cubic EoS* primarily based on Statistical Thermodynamics especially after 1990 with the development of Statistical Associating Fluid Theory (SAFT) [Chapman et al., 1989] and Cubic-Plus-Accociation (CPA) equations of state [Kontogeorgis et al., 1996]. In the context of the thesis we shall be focussing on the latter namely PC-SAFT EoS, since the mixtures have

water, acid and acetol. The former namely activity co-efficient models have already been devised in Chapter 4. We shall now initially discuss the PC-SAFT EoS with its basic equations and terminology.

5.2 PC-SAFT EoS

Associating systems are those, which contain compounds capable of hydrogen bonding e.g. alcohols, water and acids. Phase equilibria of complex associating systems is important in many applications. Over the last two decades, a variety of models to account for the effects of hydrogen bonding in solutions have been proposed. These are called *association models*. The hydrogen bonding formation in the same molecule is called self-association while forming of hydrogen bonding between two different molecules is called cross-association. All developed models can be classified in three main families: (1) chemical theories, (2) lattice-fluid theories, and (3) perturbation theories. Our work is focussed on Perturbed Chain - Statistical Associating Fluid Theory (PC-SAFT) which is a theoretically derived model based on perturbation theories [Kontogeorgis and Folas, 2010].

Based on Wertheim's thermodynamic perturbation theory of first order [Wertheim, 1984a, Wertheim, 1984b, Wertheim, 1986b, Wertheim, 1986c, Wertheim, 1986a, Wertheim, 1987], Chapman et al. [Chapman et al., 1989, Chapman et al., 1990] proposed molecularly based equation of state for chain molecules, referred to as statistical associating fluid theory (SAFT) . In SAFT approach, molecules are assumed to consist of equal-sized hard spherical segments. The attractive forces (dispersive attraction) are added to each segment and interactions are described by any appropriate potential. Thereafter one or more chain sites are added to each segment and chain molecules are formed by bonding at chain sites. Finally, specific association sites are added in the chain such that two chains can associate through attractive interaction. Each of these steps contributes to the Helmholtz free energy change. Therefore, in SAFT equation of state, the residual Helmholtz energy per molecule for a pure component has hard sphere ($\tilde{a}^{hs}$), dispersion ($\tilde{a}^{disp}$), chain ($\tilde{a}^{chain}$), and association ($\tilde{a}^{assoc}$) contributions and written as:

$$\tilde{a}^{res} = \tilde{a}^{hs} + \tilde{a}^{disp} + \tilde{a}^{chain} + \tilde{a}^{assoc} \tag{5.15}$$

where $\tilde{a}^{res}$ is the residual Helmholtz free energy of the system ($\tilde{a}^{res} = \tilde{a}^{total}$ - $\tilde{a}^{ideal}$) and $\tilde{a} = A/NkT$. In Equation 6.1, the sum of the first two terms is the hard-sphere-chain reference system accounting for molecular repulsion and chain connectivity while the last two terms is the perturbation accounting for molecular attraction and for association due to specific interactions respectively. Figure 5.6 shows the steps for the formation of chain molecules and association complexes from hard spheres as per SAFT model.

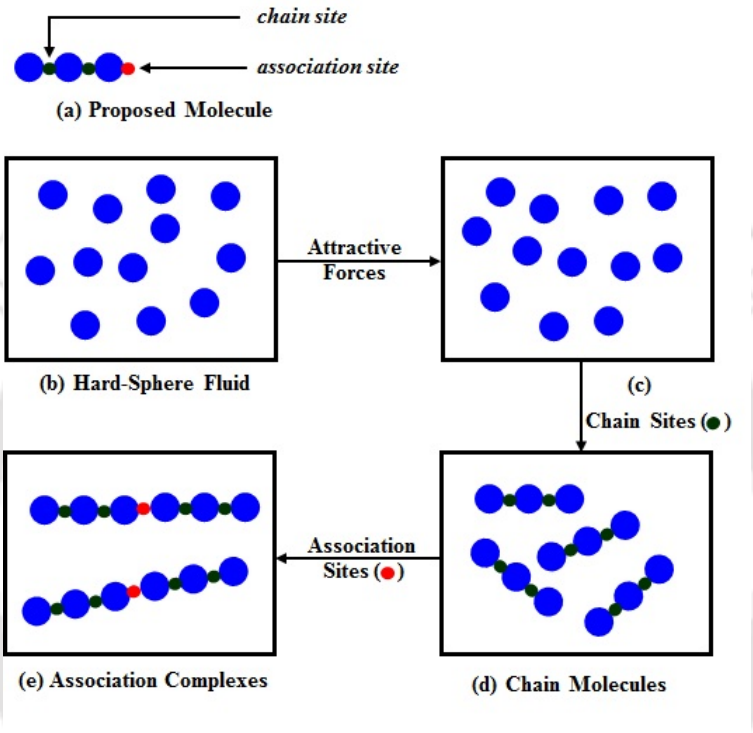

Figure 5.1.: Steps to form chain molecules and association complexes from hard spheres in the SAFT model [Fu and Sandler, 1995]

Gross and Sadowski developed a variant, namely the Perturbed Chain - Statistical Associating Fluid Theory (PC-SAFT) Equation of State. Using hard-chain reference fluid and applying a perturbation theory for chain molecules, Gross and Sadowski derived a dispersion expression for chain molecules [Gross and Sadowski, 2001, Gross and Sadowski, 2002]. PC-SAFT uses the hard-chain fluid as the reference system, whereas in SAFT, a hard-sphere fluid is considered as a reference system. In this EoS, molecules are assumed to be chains composed of hard spheres, which repel each other. The attractive forces among molecules are accounted by adding perturbation terms to the reference system which includes dispersive forces and specific associative interactions (Figure 5.2). The residual Helmholtz energy is calculated as the Helmholtz energy

of the reference system ($\tilde{a}^{hc}$) superposed with the Helmholtz energy of perturbation, that is, dispersion ($\tilde{a}^{disp}$) and association ($\tilde{a}^{assoc}$):

$$\tilde{a}^{res} = \tilde{a}^{hc} + \tilde{a}^{disp} + \tilde{a}^{assoc} \tag{5.16}$$

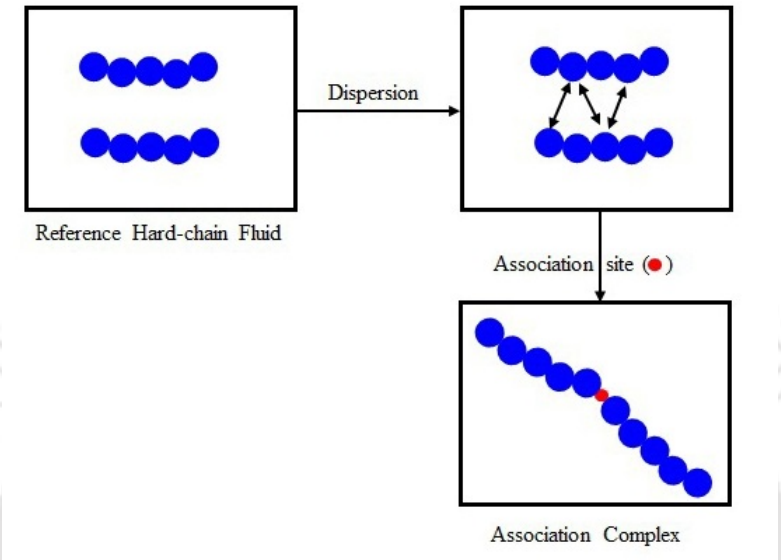

Figure 5.2.: Procedure to form a molecule in the PC-SAFT model

Hard-chain contribution: The Helmholtz energy of the hard-chain reference term is given as

$$\widetilde{a}^{hc} = \overline{m}\widetilde{a}^{hs} - \sum_i x_i(m_i - 1)\ln(g_{ii}^{hs}(d_{ii})) \tag{5.17}$$

where x_i is the mole fraction of chains of component *i*, m_i is the number of segments in a chain and the mean segment number in the mixture is defined as:

$$\overline{m} = \sum_i x_i m_i \tag{5.18}$$

The Helmholtz energy for the hard-sphere segments is given on a per-segment basis as:

$$\widetilde{a}^{hs} = \frac{1}{\xi_o}\left[\frac{3\xi_1\xi_2}{(1-\xi_3)} + \frac{\xi_2^3}{\xi_3(1-\xi_3)^2} + \left(\frac{\xi_2^3}{\xi_3^2} - \xi_o\right)\ln(1-\xi_o)\right] \tag{5.19}$$

The radial pair distribution function for the hard-sphere fluid is given by:

$$g_{ij}^{hs}(d_{ij}) = \frac{1}{1-\xi_3} + \left(\frac{d_i d_j}{d_i + d_j}\right)\frac{3\xi_2}{(1-\xi_3)^2} + \left(\frac{d_i d_j}{d_i + d_j}\right)^2 \frac{2\xi_2^2}{(1-\xi_3)^3} \tag{5.20}$$

and ξ_n is defined as:

$$\xi_n = \tfrac{\pi}{6}\rho \sum_i x_i m_i d_i^n \qquad n \in \{0,1,2,3\} \tag{5.21}$$

The temperature-dependent segment diameter is obtained as:

$$d_i\,(T) = \sigma_i \left[1 - 0.12\exp\left(\frac{-3\xi_i}{kT}\right)\right] \tag{5.22}$$

where σ_i is the temperature-independent segment diameter and ϵ_i/k is the depth of the pair-potential.

Dispersion contribution: The dispersion contribution to the Helmholtz energy is given by

$$\widetilde{a}^{disp} = -2\pi\rho I_1\,(\eta, \overline{m})\,\overline{m^2\epsilon\sigma^3} - \pi\rho\overline{m}C_1 I_2\,(\eta, \overline{m})\,\overline{m^2\epsilon^2\sigma^3} \tag{5.23}$$

with

$$C_1 = \left[1 + \overline{m}\frac{8\eta - 2\eta^2}{(1-\eta)^4} + \left((1-\overline{m})\frac{20\eta - 27\eta^2 + 12\eta^3 - 2\eta^4}{[(1-\eta)(2-\eta)]^2}\right)\right]^{-1} \tag{5.24}$$

and

$$\overline{m^2\epsilon\sigma^3} = \sum_i \sum_j x_i x_j m_i m_j \left(\frac{\epsilon_{ij}}{kT}\right)\sigma_{ij}^3 \tag{5.25}$$

$$\overline{m^2\epsilon^2\sigma^3} = \sum_i \sum_j x_i x_j m_i m_j \left(\frac{\epsilon_{ij}}{kT}\right)^2 \sigma_{ij}^3 \tag{5.26}$$

Power series I_1 and I_2 depend only on density and segment number according to the following equations:

$$I_1(\eta,\overline{m}) = \sum_{i=0}^{6} a_i(\overline{m})\,\eta^i \quad ; \quad I_2(\eta,\overline{m}) = \sum_{i=0}^{6} b_i(\overline{m})\,\eta^i \tag{5.27}$$

where the coefficients $a_i(m)$ and $b_i(m)$ are functions of the segment number:

$$a_i(\overline{m}) = a_{oi} + \frac{(\overline{m}-1)}{\overline{m}}a_{1i} + \frac{(\overline{m}-1)}{\overline{m}}\frac{(\overline{m}-2)}{\overline{m}}a_{2i} \tag{5.28}$$

$$b_i(\overline{m}) = b_{oi} + \frac{(\overline{m}-1)}{\overline{m}}b_{1i} + \frac{(\overline{m}-1)}{\overline{m}}\frac{(\overline{m}-2)}{\overline{m}}b_{2i} \tag{5.29}$$

Association contribution: The association contribution to the Helmholtz energy is given as

$$\widetilde{a}^{assoc} = \sum_i x_i \left[\sum_{A_i}\left(\ln X^{A_i} - \frac{X^{A_i}}{2}\right) + \frac{M_i}{2}\right] \tag{5.30}$$

where X^{A_i} is the fraction of the free molecules i that are not bonded at the association site A:

$$X^{A_i} = \left(1 + \rho.\sum_j x_j \sum_{B_j} X^{B_j}\Delta^{A_iB_j}\right)^{-1} \tag{5.31}$$

with

$$\Delta^{A_iB_j} = g_{ij}^{hs}(d_{ij}).\kappa^{A_iB_j}.d_{ij}^3.\left(exp\left(\frac{\epsilon^{A_iB_j}}{kT}\right) - 1\right) \tag{5.32}$$

where M_i is number of association sites on molecule i and $\Delta^{A_iB_j}$ is strength of interaction between site A on molecule i and site B on molecule j. The combining rules suggested by Wolbach ans Sandler

$$\epsilon^{A_iB_j} = \frac{1}{2}\left(\epsilon^{A_iB_i} + \epsilon^{A_jB_j}\right) \tag{5.33}$$

$$\kappa^{A_iB_j} = \sqrt{\kappa^{A_iB_i}\kappa^{A_jB_j}}\left(\frac{\sqrt{\sigma_{ii}\sigma_{jj}}}{0.5\left(\sigma_{ii}+\sigma_{jj}\right)}\right)^3 \tag{5.34}$$

was used [Wolbach and Sandler, 1998].

In terms of compressibility factor Z, the EoS is given as the sum of the ideal gas contribution ($Z^{id} = 1$), the hard-chain contribution (Z^{hc}), the dispersion (attractive) contribution (Z^{disp}) and the contribution due to associating interactions (Z^{assoc}). Thus,

$$Z = Z^{id} + Z^{hc} + Z^{disp} + Z^{assoc} \tag{5.35}$$

The expression for all the above terms are given in Appendix D.

5.3 Results and Discussions

5.3.1. Parameterization of PC-SAFT EoS

In PC-SAFT approach, non-associating molecules are represented by three parameters: m, number of segments; σ, the segment diameter; and ϵ/k_B, the segment energy parameter. The self-associating molecules require two additional parameters: the association energy $\epsilon^{A_iB_i}/k$ and association volume $\kappa^{A_iB_i}$ which determine the associating interactions between the association site A_i and B_i of a pure component i. Acetic acid, furfural, water, [EMIM][Tf_2N], [BMIM][Tf_2N] and acetol were assigned two association sites (2B association scheme [Huang and Radosz, 1990]) whereas ethyl acetate, *n*-propyl acetate, *n*-butyl acetate and chloforom were considered to be nonassociating in nature. In 2B association scheme [Huang and Radosz, 1990],

$$\Delta^{AA} = \Delta^{BB} = 0; \Delta^{AB} \neq 0; X^A = X^B = \frac{-1 + (1 + 4\rho\Delta)^{1/2}}{2\rho\Delta} \tag{5.36}$$

For each pure component, parameters were estimated by regressing the experimental liquid density data using Genetic algorithm as per the non-linear equation 5.37. Acetic acid, acetol, ethyl acetate, *n*-propyl acetate and *n*-butyl acetate densities are reported in Table 3.2 which was used for PC-SAFT parameter estimation; whereas densities of furfural, chloroform , [EMIM][Tf_2N] and [BMIM][Tf_2N] were taken from literature [Clara et al., 2010, Tariq et al., 2010].

The objective function used for regression was:

$$\mathrm{OF} = \sum_{i=1}^{n_{pts}} \left(1 - \frac{\rho_i^{calc}}{\rho_i^{exp}}\right)^2 \tag{5.37}$$

This takes into account the deviations between calculated (ρ_i^{calc}) and experimental (ρ_i^{exp}) liquid densities. The percentage absolute average relative deviation (%AARD) between the experimentally obtained and calculated densities was determined according to the following expression%:

$$AARD(\%) = \frac{100}{n_{pts}} \sum_{i=1}^{n_{pts}} \left|1 - \frac{\rho_i^{calc}}{\rho_i^{exp}}\right| \tag{5.38}$$

The Flow diagram of the algorithm used for the estimation of pure component PC-SAFT parameters are shown in Figure 5.3. The optimization algorithm has been coded in MATLAB ® 2014b. Figures 5.4 and 5.5 show the resulting density-temperature diagrams for the all the components considered in this work. The average absolute deviation (AAD,%) of the density for all the components is in the range of 0.003-0.129 % (Table 5.1) which concludes that the density is well correlated for all the components. Pure component PC-SAFT parameters for all the components are reported in Table 5.1. In case of ionic liquids, [EMIM][Tf_2N] and [BMIM][Tf_2N], the associating parameters (κ^{AB} and ϵ^{AB}/k) were taken from literature [Chan et al., 2012]. In case of water, all the PC-SAFT parameters were taken from literature [Gross and Sadowski, 2002].

5.3.2. PC-SAFT modeling of ternary liquid-liquid systems

LLE calculations of a multi-component system are based on equal fugacity values,f_i, of all components, i, in phases I and II are performed using the relation

$$x_i^I \phi_i^I = x_i^{II} \phi_i^{II} \tag{5.39}$$

where x_i and ϕ_i are the mole fraction and fugacity coefficient, respectively, of component i. Fugacity coefficient of the components were calculated using PC-SAFT EoS. The expression for calculating the fugacity coefficient for component i is given in Appendix D.

The Flow diagram of the algorithm used for LLE prediction is shown in Figure 5.6 with the algorithm coded in MATLAB ® 2014b. Only pure component parameters were used for the pre-

diction of ternary LLE. Binary interaction parameters between each component (k_{ij}) was kept zero so as to keep the predictive nature of the EoS. To check the accuracy of inhouse developed code, comparison was made with Aspen Plus V8.8 (Aspen Technology Inc., USA) results. For this purpose, one ternary system, [BMIM][Tf_2N] + acetic acid + water, was selected. The deviation between the experimental and the predicted data was evaluated in terms of root mean square deviation (RMSD,%) which was calculated using the expression:

$$\mathrm{RMSD} = \left[\sum_{k=1}^{m} \sum_{i=1}^{c} \sum_{l=I}^{II} \frac{\left(x_{ik}^{l} - \widehat{x}_{ik}^{l}\right)^2}{2mc} \right]^{1/2} \tag{5.40}$$

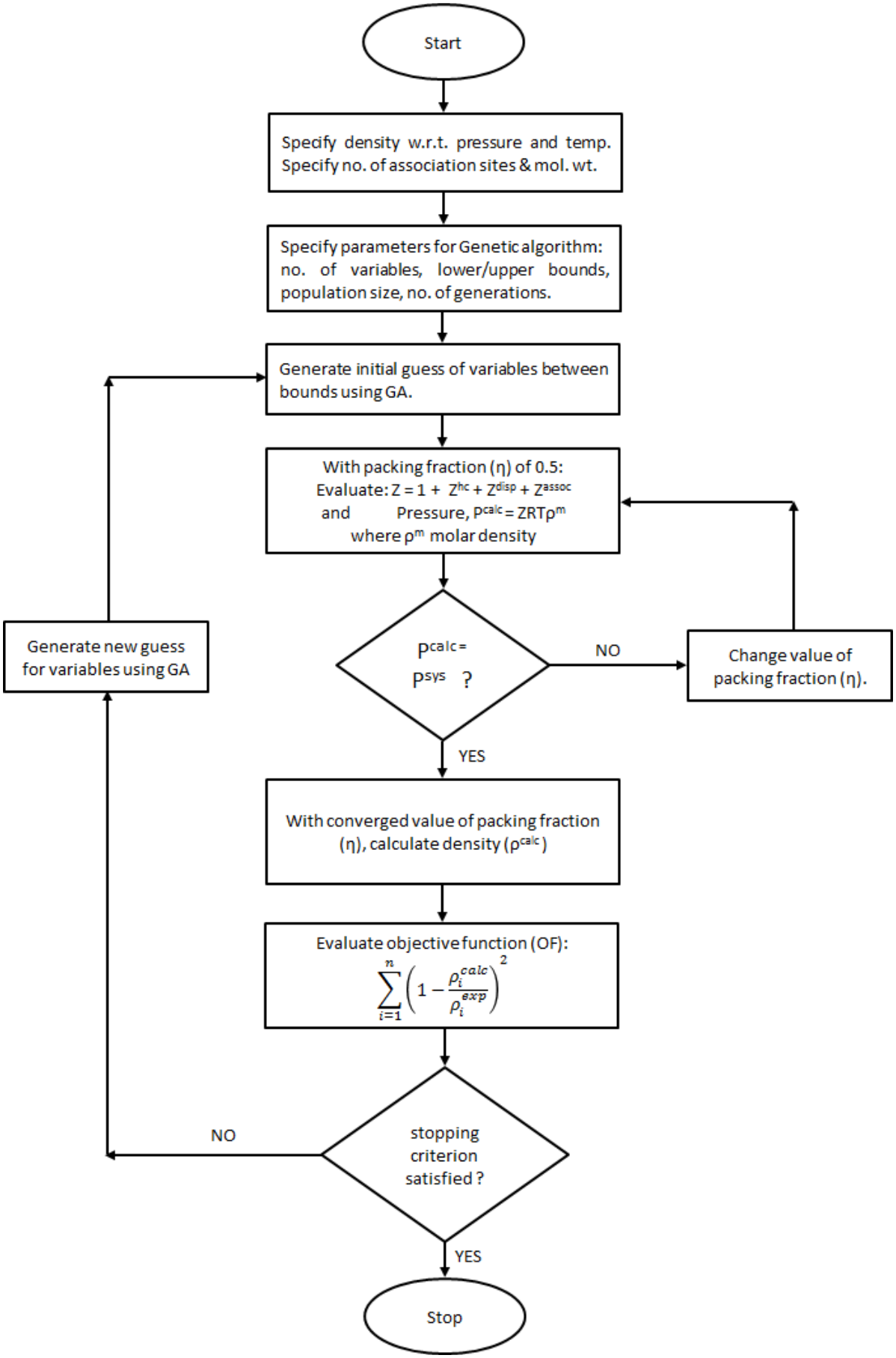

Figure 5.3.: Flow diagram of the algorithm for the estimation of PC-SAFT parameters for pure components (w.r.t.: with respect to and mol. wt.: Molecular weight

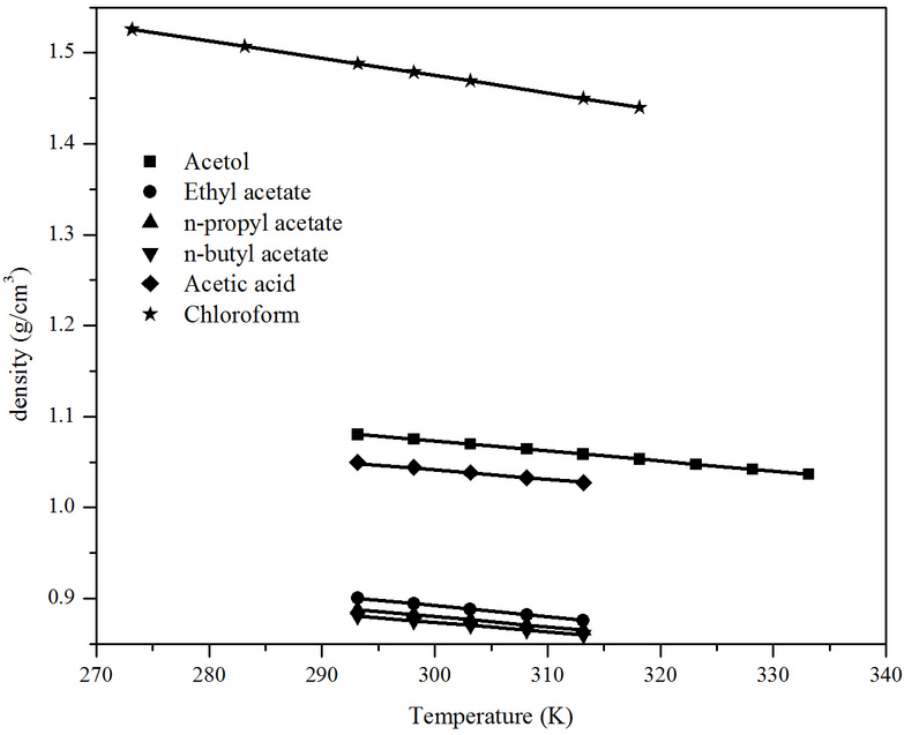

Figure 5.4.: Temperature-density diagrams for components used in this work. Symbols (experimental data) and Solid lines (PC-SAFT regressed lines).

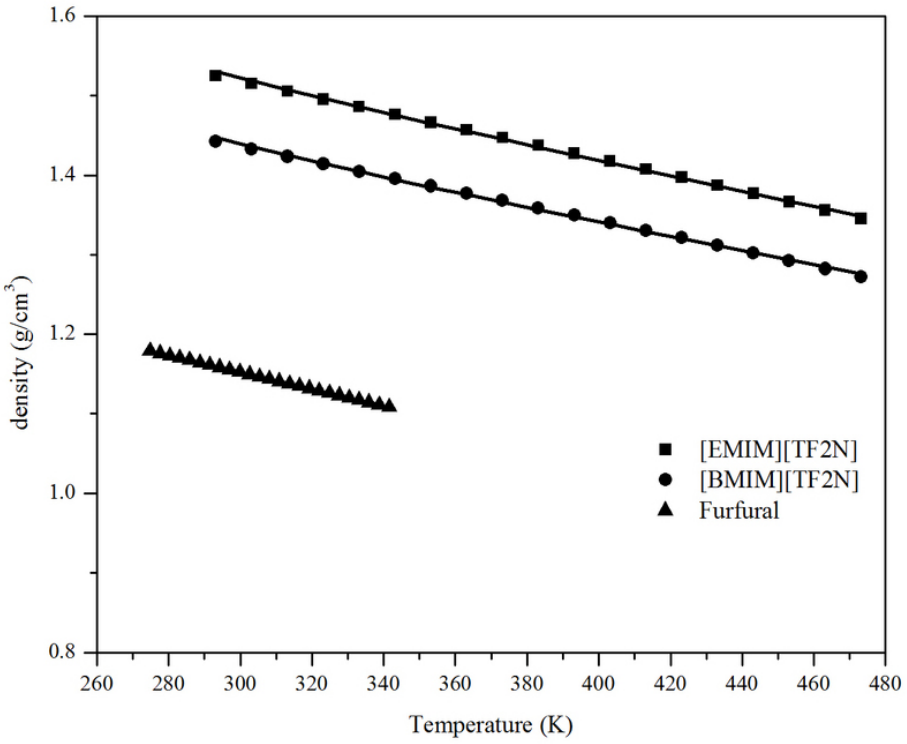

Figure 5.5.: Temperature-density diagrams for components used in this work. Symbols (experimental data) and Solid lines (PC-SAFT regressed lines).

Table 5.1.: Pure Component Parameters of PC-SAFT Equation of State

Compounds	m	σ	ϵ/k_B (K)	κ^{AB}	ϵ^{AB}/k (K)	AAD(%)	refs
Acetic acid [a]	1.3162	3.8419	201.49	0.05	3000.0	0.070	d
Furfural [a]	2.8895	3.4166	256.94	0.0366	2114.1	0.010	d
Acetol [a]	3.0896	3.0974	214.88	0.043922	2419.1	0.010	d
Ethyl acetate [b]	3.7909	3.1953	217.40	-	-	0.004	d
n-propyl acetate [b]	3.9475	3.3453	224.08	-	-	0.003	d
n-butyl acetate [b]	3.9839	3.5103	234.30	-	-	0.003	d
Chloroform [b]	3.0676	3.2263	242.75	-	-	0.008	d
[EMIM][Tf_2N] [a]	5.0016	4.2980	380.28	0.00225 [c]	3450.0 [c]	0.120	d
[BMIM][Tf_2N] [a]	5.4406	4.3648	383.65	0.00225 [c]	3450.0 [c]	0.129	d
Water [a]	1.0656	3.0007	366.51	0.034868	2500.7	-	e

[a] Two association sites

[b] Nonassociating behaviour assumed

[c] [Chan et al., 2012]

[d] This work

[e] [Gross and Sadowski, 2002]

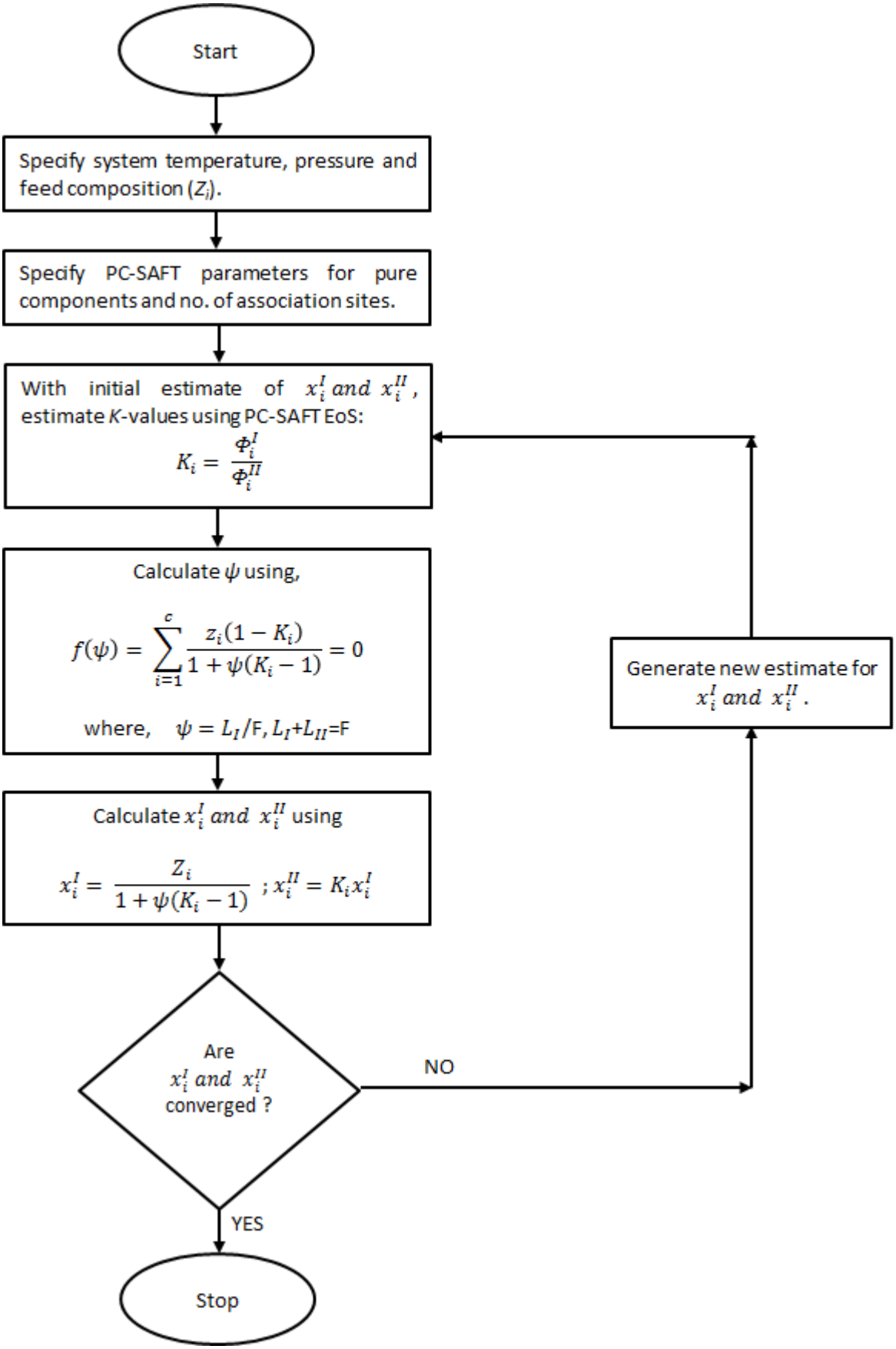

Figure 5.6.: Flow diagram of the algorithm for the prediction of LLE

where *m* refers to the number of tie lines and *c* refers to the number of components. Here, x_{ik}^{l} and $\widehat{x}_{ik}^{l}$ are, respectively, the experimental and predicted values of mole fraction for component *i* for the *k*th tie line in phase *l*.

Tie-Lines predicted by Aspen Plus and Inhouse developed code are reported in Table 5.2 along with experimental data. In case of inhouse developed code, % RMSD between experimental and predicted data were 9.43% and 20.9% for extract and raffinate phases respectively. Whereas from Aspen Plus, %RMSD were 6.53% and 3.76% for extract and raffinate phases respectively. The major difference was in the prediction of ionic liquid composition in raffinate phase by inhouse code. Overall %RSMD was 5.33% and 16.23% from Aspen Plus and Inhouse code respectively. Therefore, inhouse code has to be further upgraded to increase its accuracy at par with Aspen Plus simulator. So, in further work analyses, Aspen Plus simulator was used for LLE prediction by PC-SAFT EoS.

For better prediction, binary interaction parameters (k_{ij}) i.e. between acetic acid-water, water-solvent and solvent-acetic acid can be provided as input in the model. These binary interaction parameters are generally evaluated from experimental binary VLE/LLE data. In our PC-SAFT computation, k_{ij} values for water-solvent and solvent-acetic acid were assumed to be zero. This is necessary as we generally tend to know the interaction between the components of the known system i.e acetic acid and water from which acid is to be extracted from water. In present case, interaction parameter (k_{ij}) between acetic acid and water was evaluated by regressing the available experimental isobaric VLE data at 101.32 kPa [Peng and Lu, 2014]. The estimated value of k_{ij} was -0.111 with %RMSD of 1.37%. The VLE plot clearly shows that the experimental data is well correlated with experimental VLE data(Figure 5.7). With this value of k_{ij}, %RMSD for ternary systems reduces from 5.33% (Table 5.2) to 2.43% (Table 5.3) i.e. a reduction of 54.4%. Figure 5.8 shows the ternary plot of [BMIM][Tf_2N] + acetic acid + water system in which experimental data has been plotted along with PC-SAFT predicted tie lines with k_{ij} = 0 and along with PC-SAFT predicted tie lines with k_{ij} = -0.111. It can be seen from Figure 5.8 that PC-SAFT (with k_{ij}=-0.111) provides quantitatively consistent results as compared with the experimental data. The experimentally observed phase behavior for the ternary systems is also predicted using PC-SAFT. Comparison of the slopes of the tie lines (experimental/predicted) yields good agreement. The PC-SAFT predicted IL mole fractions in aqueous phase were found to be extremely low for all tie-lines which is an important modeling result.

Table 5.2.: Experimental Tie Lines data Vs. PC-SAFT predicted Tie-Lines for the system [BMIM][Tf_2N] (1) - acetic acid (2) - water (3) at T = 298.15 K and p = 0.1 Mpa ($k_{ij} = 0$)

Sl.		**Extract phase**			**Raffinate phase**			**%RMSD**
No.		X_1	X_2	X_3	X_1	X_2	X_3	
1	Exp.	0.6317	0.0335	0.3348	0.0000	0.0156	0.9844	
	PC-SAFT-I	0.5642	0.0421	0.3937	0.0001	0.0023	0.9976	3.75
	PC-SAFT-II	0.5912	0.0186	0.3902	0.3121	0.0246	0.6633	18.51
2	Exp.	0.5917	0.0592	0.3491	0.0000	0.0223	0.9777	
	PC-SAFT-I	0.5250	0.0695	0.4055	0.0001	0.0038	0.9961	3.75
	PC-SAFT-II	0.4718	0.0324	0.4957	0.2643	0.0422	0.6934	17.68
3	Exp.	0.5854	0.0780	0.3366	0.0000	0.0337	0.9663	
	PC-SAFT-I	0.4935	0.0909	0.4156	0.0001	0.0049	0.9950	5.25
	PC-SAFT-II	0.6887	0.308	0.2805	0.2756	0.0569	0.6675	17.41
4	Exp.	0.5541	0.1043	0.3416	0.0000	0.0457	0.9543	
	PC-SAFT-I	0.4520	0.1185	0.4295	0.0001	0.0062	0.9937	5.98
	PC-SAFT-II	0.3594	0.0744	0.5662	0.2648	0.0751	0.6601	20.28
5	Exp.	0.4594	0.1446	0.3960	0.0000	0.0684	0.9316	
	PC-SAFT-I	0.3740	0.1681	0.4579	0.0001	0.0084	0.9915	5.61
	PC-SAFT-II	0.5063	0.0743	0.4194	0.2159	0.1081	0.6700	14.21
6	Exp.	0.4408	0.1620	0.3972	0.0000	0.0881	0.9119	
	PC-SAFT-I	0.3409	0.1885	0.4706	0.0001	0.0093	0.9906	6.89
	PC-SAFT-II	0.4959	0.1571	0.3469	0.0002	0.0994	0.9004	3.12
	Overall RMSD			PC-SAFT-I				**5.33**
	Overall RMSD			PC-SAFT-II				**16.23**

PC-SAFT-I : Aspen PlusV8.8 (Aspen Technology Inc., USA).

PC-SAFT-II: Inhouse code

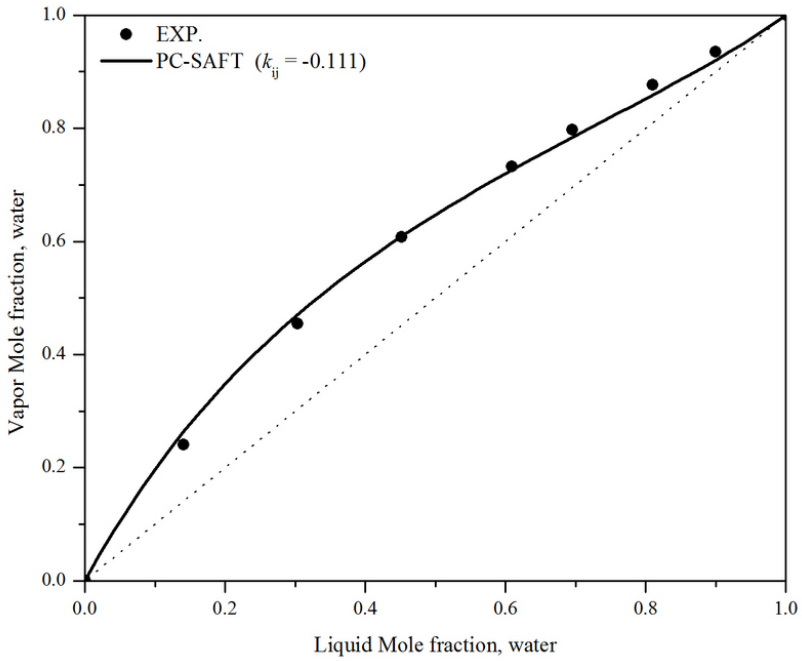

Figure 5.7.: Isobaric VLE plot for acetic acid - water systems. Symbols (experimental data) and Solid lines (PC-SAFT correlated lines; k_{ij} = -0.111).

Table 5.3.: Experimental Vs. PC-SAFT predicted Tie-Lines for the system [BMIM][Tf_2N] (1) - acetic acid (2) - water (3) at T = 298.15 K and p = 0.1 Mpa (k_{ij} : $aceticacid - water = -0.111$)

Sl. No.		**Extract phase**			**Raffinate phase**			**%RMSD**
		X_1	X_2	X_3	X_1	X_2	X_3	
1	Exp.	0.6317	0.0335	0.3348	0.0000	0.0156	0.9844	
	PC-SAFT	0.5888	0.0288	0.3824	0.0001	0.0198	0.9801	2.63
2	Exp.	0.5917	0.0592	0.3491	0.0000	0.0223	0.9777	
	PC-SAFT	0.5668	0.0474	0.3858	0.0002	0.0336	0.9662	1.99
3	Exp.	0.5854	0.0780	0.3366	0.0000	0.0337	0.9663	
	PC-SAFT	0.5472	0.0638	0.3890	0.0002	0.0468	0.9530	2.82
4	Exp.	0.5541	0.1043	0.3416	0.0000	0.0457	0.9543	
	PC-SAFT	0.5223	0.0845	0.3932	0.0003	0.0643	0.9354	2.82
5	Exp.	0.4594	0.1446	0.3960	0.0000	0.0684	0.9316	
	PC-SAFT	0.4808	0.1184	0.4008	0.0007	0.0957	0.9036	2.12
6	Exp.	0.4408	0.1620	0.3972	0.0000	0.0881	0.9119	
	PC-SAFT	0.4578	0.1368	0.4054	0.0011	0.1143	0.8846	2.01
	Overall RMSD							**2.43**

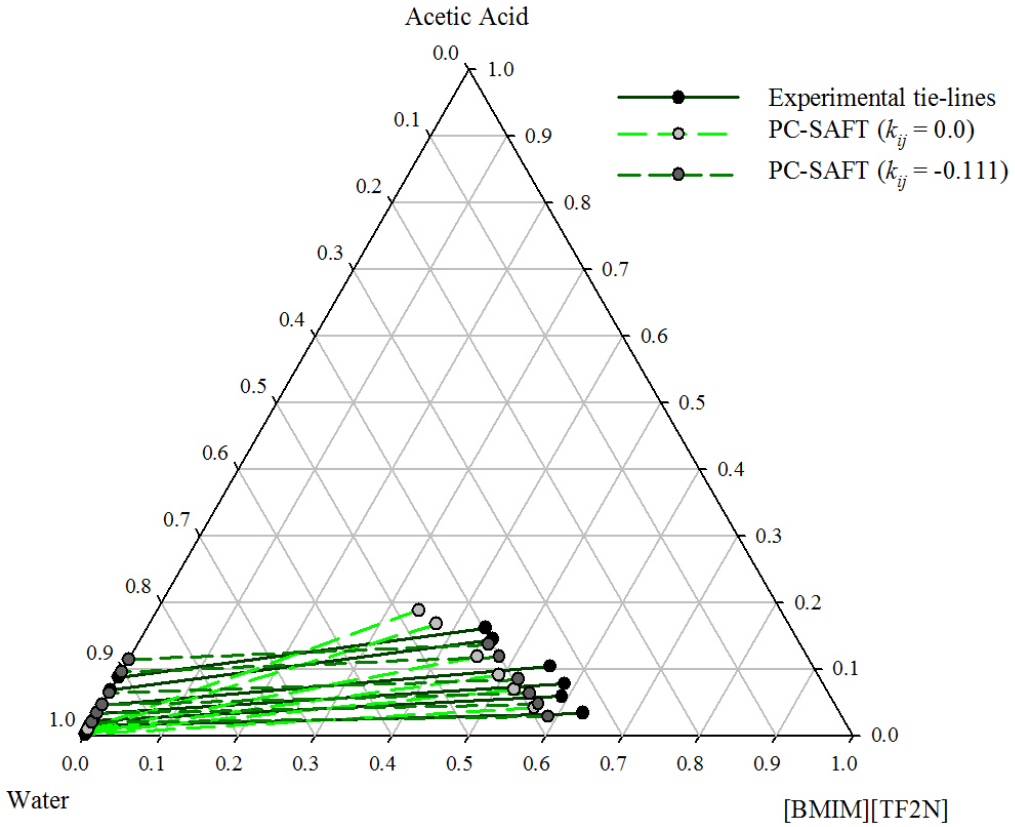

Figure 5.8.: Ternary plot for [BMIM][Tf_2N] (1) + acetic acid (2) + water (3) system at 298.15 K and 1.0 bar.

For [BMIM][Tf_2N] + furfural + water ternary systems, %RMSD is 9.74% with interaction parameters between furfural and water (k_{ij})=0 (Table 5.4). For better prediction, binary interaction parameters (k_{ij}) between furfural and water was only considered; whereas it was kept zero between water-solvent and solvent-furfural. Interaction parameter (k_{ij}) between furfural and water was then evaluated by regressing the available experimental binary LLE data at 101.32 kPa [Stephenson, 1993]. The estimated value of k_{ij} was 0.06 with %RMSD of 2.40%. The binary LLE plot clearly shows that the experimental data is well correlated (Figure 5.9). With this value of k_{ij}, %RMSD for ternary systems reduced from 9.74% (Table 5.4) to 5.30% (Table 5.5), a reduction of 45.6%. Figure 5.10 shows the ternary plot of [BMIM][Tf_2N] + furfural + water system in which experimental data has been plotted along with PC-SAFT predicted tie lines with k_{ij} = 0 and PC-SAFT predicted tie lines with k_{ij} = 0.06. The experimentally observed phase behavior for the ternary system was well predicted by PC-SAFT. Comparison of the slopes of the tie lines (experimental/predicted) yields good agreement.

Table 5.4.: Experimental Tie Lines data Vs. PC-SAFT predicted Tie-Lines for the system [BMIM][Tf_2N] (1) - furfural (2) - water (3) at T = 298.15 K and p = 0.1 Mpa ($k_{ij} = 0$)

Sl. No.		Extract phase			Raffinate phase			%RMSD
		X_1	X_2	X_3	X_1	X_2	X_3	
1	Exp.	0.5653	0.1319	0.3028	0.0004	0.0008	0.9988	
	PC-SAFT	0.4823	0.1123	0.4054	0.0001	0.0012	0.9987	5.45
2	Exp.	0.4617	0.2210	0.3173	0.0002	0.0022	0.9976	
	PC-SAFT	0.3879	0.1859	0.4262	0.0000	0.0022	0.9978	5.56
3	Exp.	0.3400	0.3840	0.2760	0.0002	0.0036	0.9962	
	PC-SAFT	0.2549	0.2883	0.4568	0.0000	0.0042	0.9958	9.05
4	Exp.	0.2873	0.4986	0.2141	0.0000	0.0055	0.9945	
	PC-SAFT	0.1926	0.3362	0.4712	0.0000	0.0056	0.9944	13.00
5	Exp.	0.1913	0.5681	0.2406	0.0000	0.0067	0.9933	
	PC-SAFT	0.1291	0.3850	0.4859	0.0000	0.0078	0.9922	12.75
	Overall RMSD							**9.74**

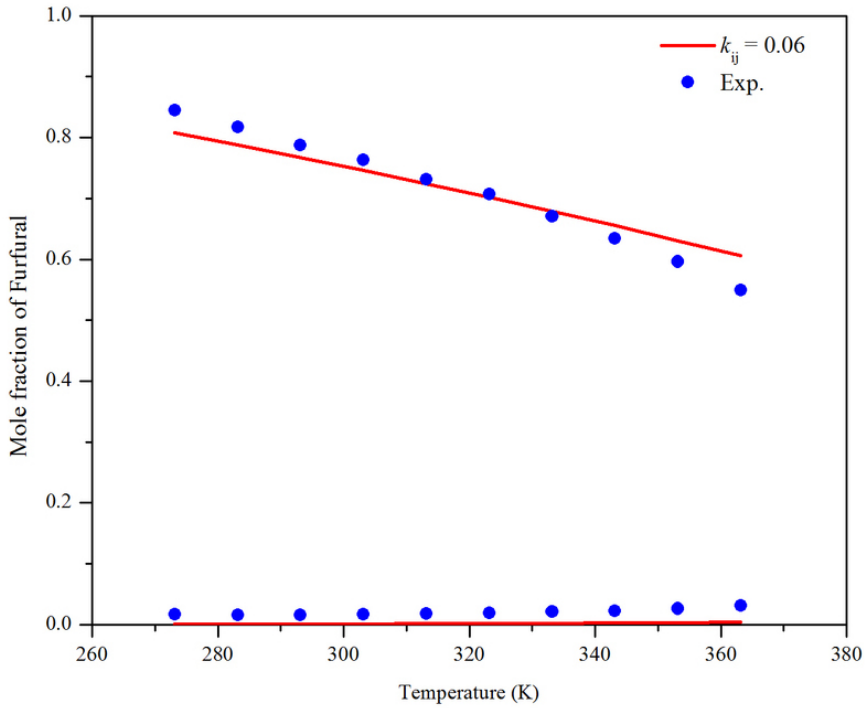

Figure 5.9.: LLE plot for furfural-water binary systems. Symbols (experimental data) and Solid lines (PC-SAFT correlated lines).

Table 5.5.: Experimental Tie Lines data Vs. PC-SAFT predicted Tie-Lines for the system [BMIM][Tf_2N] (1) - furfural (2) - water (3) at T = 298.15 K and p = 0.1 Mpa (k_{ij} : $furfural - water = 0.06$)

Sl. No.		Extract phase X_1	X_2	X_3	Raffinate phase X_1	X_2	X_3	%RMSD
1	Exp.	0.5653	0.1319	0.3028	0.0004	0.0008	0.9988	
	PC-SAFT	0.4977	0.1168	0.3855	0.0000	0.0001	0.9999	4.40
2	Exp.	0.4617	0.2210	0.3173	0.0002	0.0022	0.9976	
	PC-SAFT	0.4136	0.1997	0.3867	0.0000	0.0002	0.9998	3.56
3	Exp.	0.3400	0.3840	0.2760	0.0002	0.0036	0.9962	
	PC-SAFT	0.2916	0.3321	0.3763	0.0000	0.0003	0.9997	5.02
4	Exp.	0.2873	0.4986	0.2141	0.0000	0.0055	0.9945	
	PC-SAFT	0.2313	0.4058	0.3629	0.0000	0.0004	0.9996	7.52
5	Exp.	0.1913	0.5681	0.2406	0.0000	0.0067	0.9933	
	PC-SAFT	0.1650	0.4951	0.3399	0.0000	0.0005	0.9995	5.16
	Overall RMSD							**5.30**

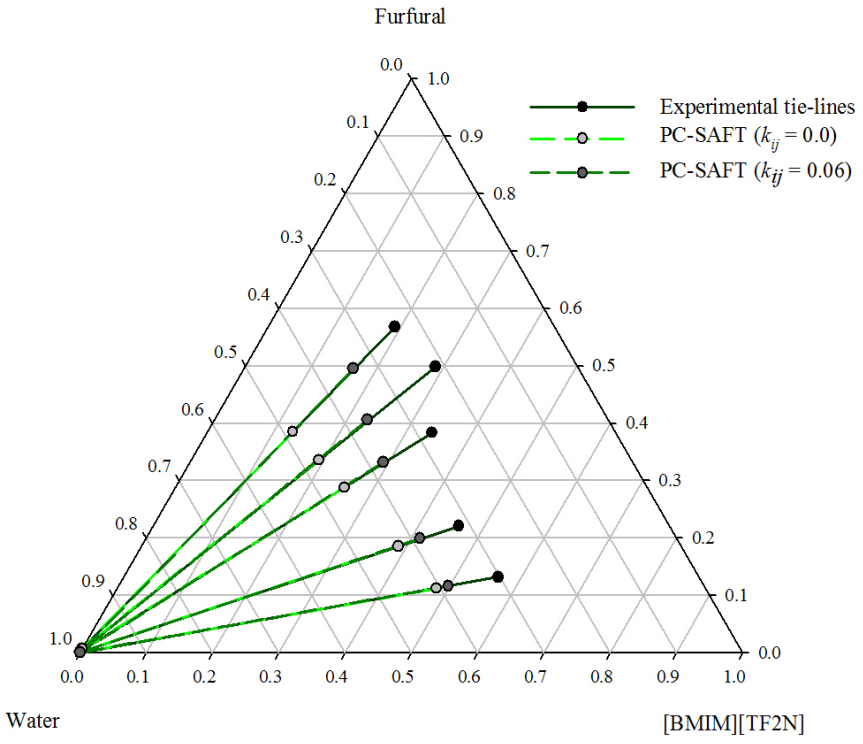

Figure 5.10.: Ternary plot for [BMIM][Tf_2N] (1) + furfural (2) + water (3) system at 298.15 K and 1.0 bar.

For ethyl acetate/*n*-propyl acetate/*n*-butyl acetate/chloroform/[EMIM][Tf_2N]/[BMIM][Tf_2N] + acetol + water ternary systems, %RMSD is in the range of 5-14% (k_{ij} = 0; acetol-water)(Table 5.6). The results shows that % RMSD for ionic liquid based systems, where all components are self-associating, were in the range of 5.5-8.6% which is better than organic solvent based systems which were in the range of 10.7-14.1%. The reason for this deviation is due to the fact that organic solvents (ethyl acetate/*n*-propyl acetate/*n*-butyl acetate/chloroform) are nonassociating in nature but capable of forming hydrogen bonds with water/acetol molecules.

For better prediction, binary interaction parameters (k_{ij}) i.e. between acetol-water can be provided as input in the model. But in this case, binary VLE data for acetol/water is not available. On the contrary, acetol/water is being completely miscible for the entire composition range. This creates a hindrance for the evaluation of binary LLE data. Hence we adopted a trial and error approach in which we optimized the value of binary interaction parameter (k_{ij}) between acetol-water, so that the deviation between the experimental and predicted values is minimized. For this purpose out of 37 tie lines comprising of six systems (Table 5.6), we selected a tie-line (tie-line no. 7, Table No. 3.10) which gave the highest deviation. Since k_{ij} value is directed towards the interaction of acetol-water only, it is devoid of the presence of any third component. As reported in Table 5.7, for k_{ij} = -0.034, the deviation between experimental and predicted values are minimum. Using this value of k_{ij}, VLE diagram for acetol-water system was plotted (Figure 5.11). The VLE diagram revealed that water-acetol system formed an azeotrope at higher water purity. This was an interesting prediction for acetol-water system by PC-SAFT EoS. But, due to lack of experimental data, we could not verify this prediction. So, we used another predictive model, COnductor-like Screening MOdel-Segment Activity Co-efficient (COSMO-SAC), to verify this VLE plot [Lin and Sandler, 2002, Kundu and Banerjee, 2011].

COSMO-SAC is a predictive model which is based on quantum chemical approach and statistical mechanical framework [Lin and Sandler, 2002, Kundu and Banerjee, 2011]. Before applying COSMO-SAC for acetol/water, we used this model for VLE prediction of ethanol/water, acetic acid/water and acetone/water systems for benchmarking the COSMO-SAC model. The reason for selecting ethanol, acetic acid and acetone is due to the fact that acetol is the simplest compound which contains both hydroxyl functional group and ketone functional group (Figure 5.12). Figure 5.13 shows the comparison between COSMO-SAC and experimental VLE plot for these systems.

Table 5.6.: Estimate of deviations in LLE calculation for different ternary systems using PC-SAFT(k_{ij}): acetol-water = 0.0

System	Extract phase(%RMSD)	Raffinate phase(%RMSD)	Overall(%RMSD)
ethyl acetate - acetol - water	10.73	10.78	10.76
n-propyl acetate - acetol - water	7.73	15.30	12.12
n-butyl acetate - acetol - water	10.45	17.08	14.16
chloroform - acetol - water	11.35	13.58	12.51
[EMIM][Tf_2N] - acetol - water	4.57	6.30	5.51
[BMIM][Tf_2N] - acetol - water	6.88	10.08	8.63
Overall RMSD			**11.24**

Table 5.7.: Estimate of deviations in LLE calculation for the single tie-line of *n*-butyl acetate (1) - acetol (2) - water (3) system using different binary interaction parameters (k_{ij}:acetol - water)

k_{ij}	**Extract phase**			**Raffinate phase**			**%RMSD**
	X_1	X_2	X_3	X_1	X_2	X_3	
0.000	0.5976	0.2381	0.1643	0.4161	0.3671	0.2168	20.55
	0.0243	0.3173	0.6584	0.0000	0.0131	0.9868	
-0.040				0.6675	0.2195	0.1130	3.64
				0.0190	0.3252	0.6558	
-0.030				0.5621	0.2783	0.1596	3.51
				0.0126	0.2768	0.7106	
-0.033				0.5999	0.2576	0.1425	1.86
				0.0157	0.2981	0.6862	
-0.034				0.6112	0.2513	0.1375	1.74
				0.0165	0.3034	0.6801	
-0.034				0.6216	0.2455	0.1329	1.84
				0.0171	0.3080	0.6749	

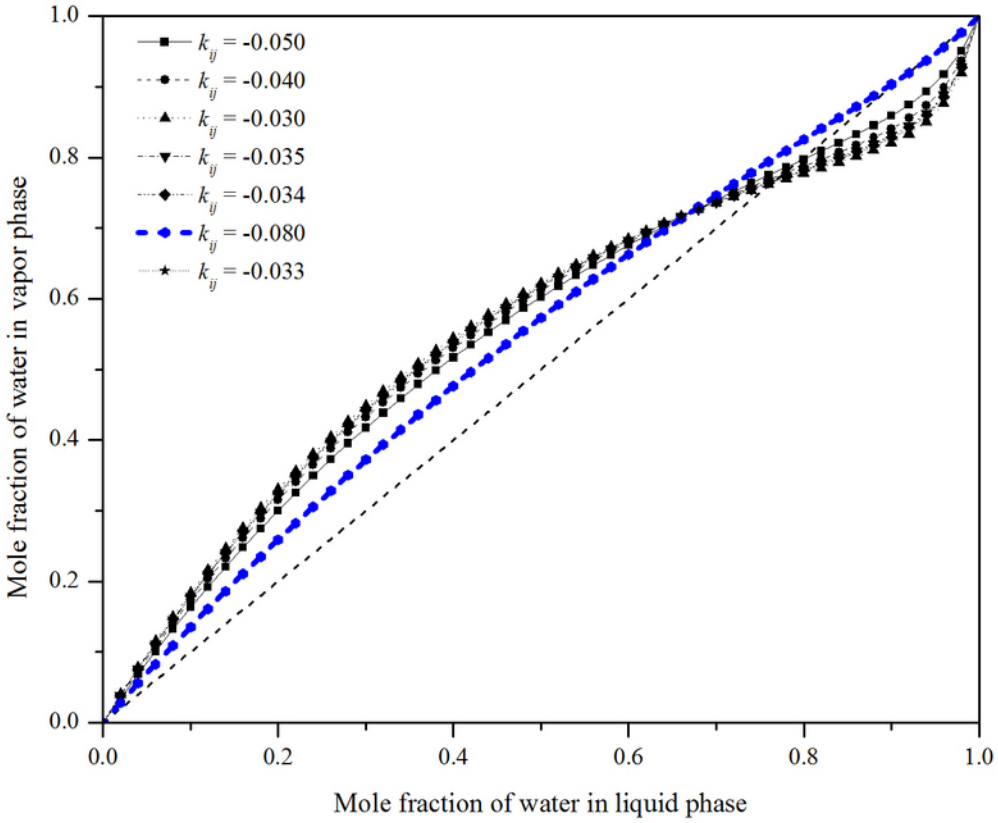

Figure 5.11.: VLE diagram of acetol-water system predicted by PC-SAFT with different values of binary interaction parameters (k_{ij})

The plot revealed that COSMO-SAC was able to correctly predict the VLE for these systems. Using this benchmarking, COSMO-SAC was applied for acetol-water system. Figure 5.14 shows the comparison between COSMO-SAC and PC-SAFT predicted VLE plot for acetol/water system. PC-SAFT prediction has been carried out for two different values of k_{ij}: -0.034 and -0.080. k_{ij} = -0.034 has been selected based on the optimization carried out earlier to minimize the deviation between the experimental and predicted values (Table 5.7). k_{ij} = -0.080 is the minimum value which will prevent the formation of azeotrope between acetol and water (Figure 5.14). It is very much clear from the plot (Figure 5.14) that PC-SAFT prediction of VLE based on two association sites scheme for water and acetol is not in good agreement with COSMO-SAC prediction which does not show an azeotrope formation.

It should be noted that the systems studied in this work are strongly self-associating/cross-associating in nature. Therefore, correct association scheme of a given molecule along with corresponding energy and volume association parameters is necessary for LLE prediction.

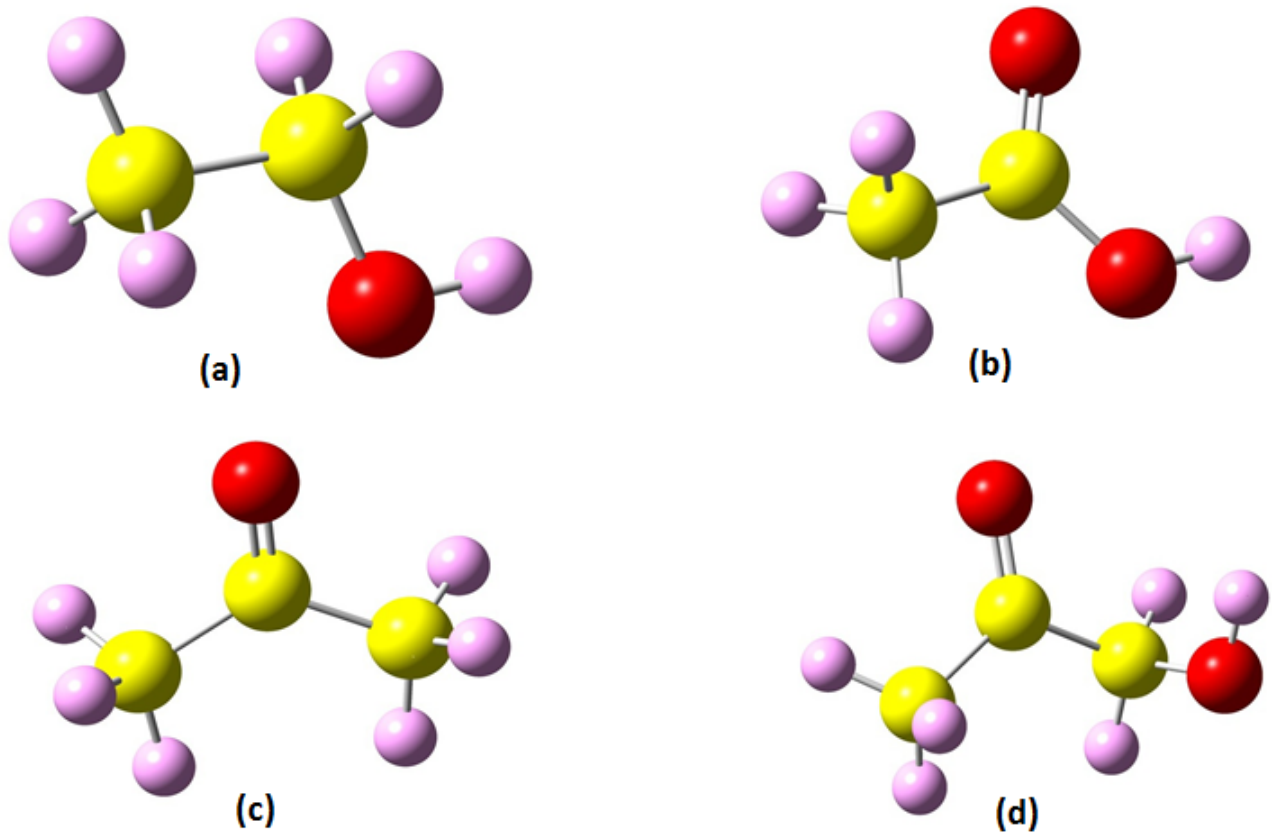

Figure 5.12.: Ball-stick representation of different molecules:(a) ethanol (b) acetic acid (c) acetone (d) acetol

Both experimentally and molecular simulation studies have shown that the average number of hydrogen bonds per water molecule is approximately 3.5 [Guardia et al., 2015]. This is due to the fact that each water molecule can form two hydrogen bonds involving their hydrogen atoms as well as utilizing its two lone pair of electrons on oxygen atom. Therefore, considering water as a self-associating compound with 4-association site will lead us toward proper results. In a recent work, Fouad et al. [Fouad et al., 2016] have studied the alcohol-water binary mixtures considering water as a four-site model and alcohol as a three-site and obtained good agreement with experimental data. In 4C association scheme, we have:

$$\begin{aligned} \Delta^{AA} = \Delta^{AB} = \Delta^{BB} = \Delta^{CC} = \Delta^{CD} = \Delta^{DD} = 0; \\ \Delta^{AC} = \Delta^{AD} = \Delta^{BC} = \Delta^{BD} \neq 0; \\ X^A = X^B = X^C = X^D = \frac{-1 + (1 + 8\rho\Delta)^{1/2}}{4\rho\Delta} \end{aligned} \tag{5.41}$$

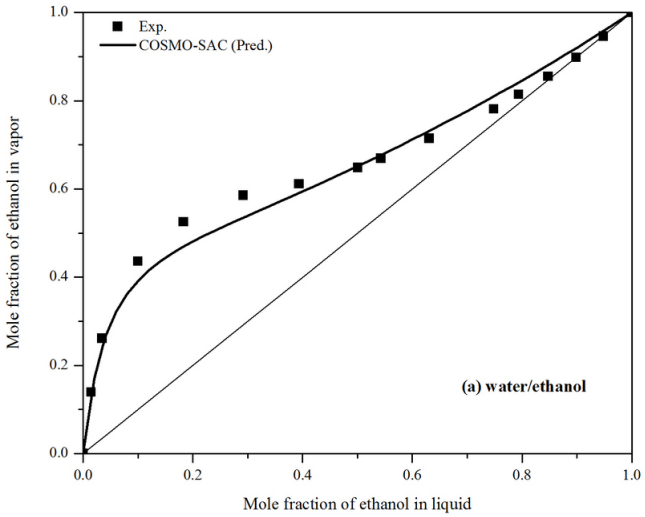

(a)

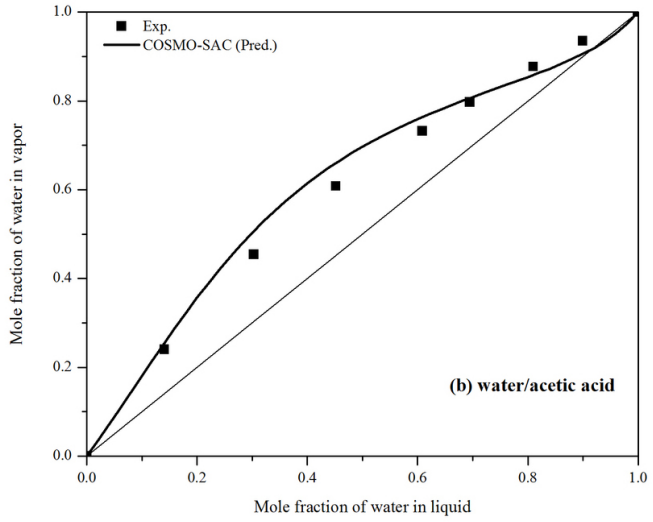

(b)

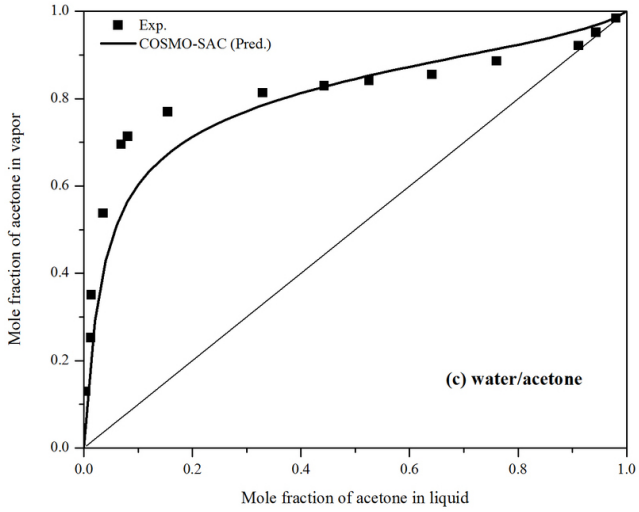

(c)

Figure 5.13.: VLE diagram for (a) water/ethanol (b) water/acetic acid (c) water/acetone at $p = 1.013$ bar

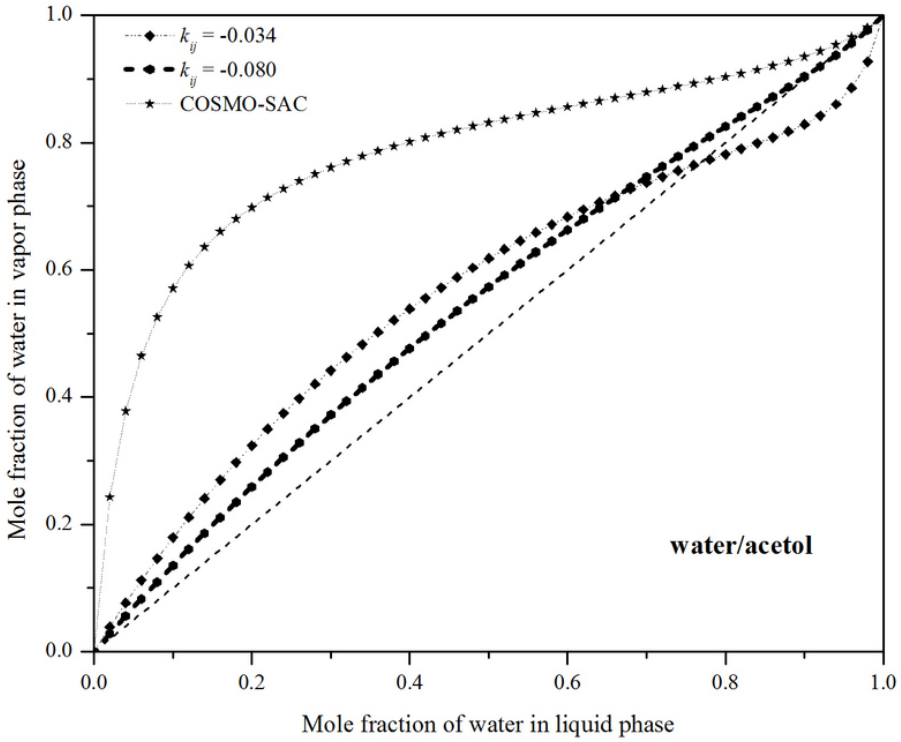

Figure 5.14.: VLE diagram for water/acetol PC-SAFT (k_{ij} = -0.034:-0.080) vs. COSMO-SAC Prediction

In a similar manner, acetol has two oxygen atoms (4 lone pair of electrons) along with one hydroxyl hydrogen. So, acetol can be modeled as compound having four associating site. Based on this, modified PC-SAFT parameters for water and acetol are reported in Table 5.8. On a similar note, ethyl acetate, n-propyl acetate and n-butyl acetate were modeled as compounds having one association site, while the cross-association parameters were taken from literature [Ahmed et al., 2016]. Based on these assumptions, LLE data were predicted by PC-SAFT and are reported in Table 5.9. In case of ethyl acetate system, the %RMSD reduced from 10.76% to 6.25%; for *n*-propyl acetate system it reduced from 12.12% to 5.76% and for *n*-butyl acetate it reduces from 14.16% to 4.55%. The overall %RMSD for all the systems reduced from 12.52% to 5.52%. This gave a 55.9% reduction in RMSD. More interestingly, with these parameters, PC-SAFT predicted VLE agrees well with that of COSMO-SAC prediction (Figure 5.15).

Table 5.8.: Pure Component Parameters of PC-SAFT Equation of State

Compounds	m	σ	ϵ/k_B (K)	κ^{AB}	ϵ^{AB}/k (K)
water [a]	1.0000 [b]	3.144 [b]	220 [b]	0.0454 [b]	1631.6 [b]
acetol [a]	2.78832 [c]	3.14401 [c]	106.7460 [c]	0.986311 [c]	1381.02 [c]
ethyl acetate	3.7909 [c]	3.1953 [c]	217.40 [c]	0.03112 [d]	1637.68 [d]
n-propyl acetate	3.9475 [c]	3.3453 [c]	224.08 [c]	0.03112 [d]	1637.68 [d]
n-butyl acetate	3.9839 [c]	3.5103 [c]	234.30 [c]	0.03112 [d]	1637.68 [d]

[a] Four association site scheme
[b] [Fouad et al., 2016]
[c] This work
[d] [Ahmed et al., 2016]

Table 5.9.: Estimate of deviations in LLE calculation for different ternary systems using PC-SAFT k_{ij} : acetol-water = -0.034

Sl. No.	Extract Phase (%RMSD)	Raffinate Phase (%RMSD)	Overall (%RMSD)	Overall (%RMSD) (with $k_{ij} = 0$)	%Reduction
1	8.55	2.23	6.25	10.76	41.9
2	7.71	2.63	5.76	12.12	52.5
3	5.40	3.51	4.55	14.16	67.9
		Total	5.52	12.52	55.9

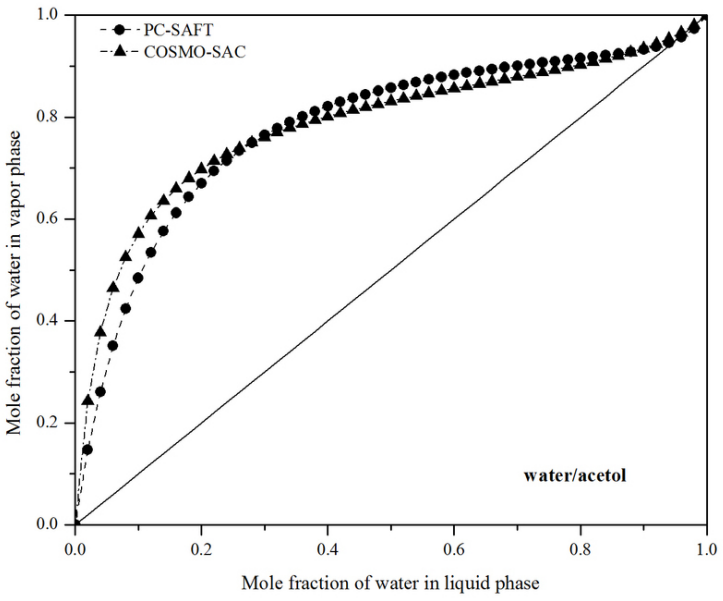

Figure 5.15.: VLE diagram for water/acetol PC-SAFT (modified parameters; k_{ij}=-0.034) vs. COSMO-SAC Predictions

5.4 Conclusions

In this chapter, PC-SAFT EoS was used to model the LLE ternary systems: ethyl acetate/*n*-propyl acetate/*n*-butyl acetate/chloroform/[EMIM][Tf_2N]/[BMIM][Tf_2N] + acetol + water, [BMIM][Tf_2N] + acetic acid + water and [BMIM][Tf_2N] + furfural + water. The binary interaction parameters were determined by fitting the binary VLE data of acetic acid/water and binary LLE data of furfural/water mixtures. In case of ionic liquid based systems where all the components were self-associating in nature, deviation between predicted values and experimental values were in the range of 2.43-8.63% (% RMSD) with 2B association scheme. But for polar solvents, deviation with experimental data were greater than 10.0%. With a proper selection of association site model and coupled with binary interaction parameters (k_{ij}), overall RMSD (%) for acetate solvents based systems reduced from 12.52% to 5.52%, a decrease of 55.9%. This confirms the ability of PC-SAFT to model the extraction behavior of ternary systems based on pure component and binary system data.

Note: PC-SAFT equations and MATLAB Code for estimation of pure components parameters are in **Appendix D**.

REFERENCES

[Abrams and Prausnitz, 1975] Abrams, D. S. and Prausnitz, J. M. (1975). Statistical thermodynamics of liquid mixtures a new expression for the excess gibbs energy of partly or completely miscible systems. *AICHE J.*, 21:116–128.

[Ahmed et al., 2016] Ahmed, S., Ferrando, N., de Hemptinne, J. C., Simonin, J. P., Bernard, O., and Baudouin, O. (2016). A new pc-saft model for pure water, water-hydrocarbons, and water-oxygenates systems and subsequent modeling of vle, vlle, and lle. *J. Chem. Eng. Data*, 61:4178–4190.

[Chan et al., 2012] Chan, Y., Mutelet, F., and Jaubert, J. (2012). Modeling the solubility of carbon dioxide in imidazolium-based ionic liquids with the pc-saft equation of state. *J. Phys. Chem. B*, 116:14375–14388.

[Chapman et al., 1989] Chapman, W., Gubbins, K., Jackson, G., and Radosz, M. (1989). Saft: Equation-of-state solution model for associating fluids. *Fluid Phase Equilibria*, 52:31–38.

[Chapman et al., 1990] Chapman, W., Gubbins, K., Jackson, G., and Radosz, M. (1990). New reference equation of state for associating liquids. *Ind. Eng. Chem. Res.*, 29:1709–1721.

[Clara et al., 2010] Clara, R. A., Marigliano, C. G., Morales, D., and Solimo, H. N. (2010). Density, viscosity, vapor-liquid equilibrium, and excess molar enthalpy of chloroform + methyl tert-butyl ether. *J. Chem. Eng. Data*, 55:5862–5867.

[Fouad et al., 2016] Fouad, W. A., Wang, L., Haghmoradi, A., Asthagiri, D., and Chapman, W. G. (2016). Understanding the thermodynamics of hydrogen bonding in alcohol-containing mixtures:cross-association. *J. Phys. Chem. B*, 120:3388–3402.

[Fredenslund et al., 1975] Fredenslund, A., Jones, R. L., and Prausnitz, J. M. (1975). Group-contribution estimation of activity coefficients in nonideal liquid mixtures. *AIChE J.*, 21:1086–1099.

[Fu and Sandler, 1995] Fu, Y. H. and Sandler, S. (1995). A simplified saft equation of state for associating compounds and mixtures. *Ind. Eng. Chem. Res.*, 34:1897–1909.

[Gross and Sadowski, 2001] Gross, J. and Sadowski, G. (2001). Perturbed-chain saft: An equation of state based on a perturbation theory for chain molecules. *Ind. Eng. Chem. Res.*, 40:1244–1260.

[Gross and Sadowski, 2002] Gross, J. and Sadowski, G. (2002). Application of the perturbed-chain saft equation of state to associating systems. *Ind. Eng. Chem. Res.*, 41:5510–5515.

[Guardia et al., 2015] Guardia, E., Skarmoutsos, I., and Masia, M. (2015). Hydrogen bonding and related properties in liquid water: A car-parrinello molecular dynamics simulation study. *J. Phys. Chem. B*, 119:8926–8938.

[Huang and Radosz, 1990] Huang, S. and Radosz, M. (1990). Equation of state for small, large, polydisperse, and associating molecules. *Ind. Eng. Chem. Res.*, 29:2284–2294.

[Kontogeorgis and Folas, 2010] Kontogeorgis, G. and Folas, G. (2010). *Thermodynamic Models For Industrial Applications: From Classical And Advanced Mixing Rules To Association Theories*. John Wiley & Sons, UK.

[Kontogeorgis et al., 1996] Kontogeorgis, G. M., Voutsas, E. C., Yakoumis, I. V., and Tassios, D. P. (1996). An equation of state for associating fluids. *Industrial & Engineering Chemistry Research*, 35:4310–4318.

[Kundu and Banerjee, 2011] Kundu, D. and Banerjee, T. (2011). Multicomponent vapor-

liquid-liquid equilibrium prediction using an a priori segment based model. *Ind. Eng. Chem. Res.*, 50:14090–14096.

[Lin and Sandler, 2002] Lin, S. T. and Sandler, S. I. (2002). A priori phase equilibrium prediction from a segment contribution solvation model. *Ind. Eng. Chem. Res.*, 41:899–913.

[Peng and Robinson, 1976] Peng, D.-Y. and Robinson, D. B. (1976). A new two-constant equation of state. *Industrial and Engineering Chemistry Fundamentals*, 15:59–64.

[Peng and Lu, 2014] Peng, Y. and Lu, X. J. (2014). Isobaric vapor-liquid equilibria for water + acetic acid + 1-ethyl-3-methylimidazolium diethylphosphate at 101.32 kpa. *Chem. Eng. Data*, 59:250–256.

[Redlich and Kwong, 1949] Redlich, O. and Kwong, J. N. S. (1949). On the thermodynamics of solutions. v. an equation of state. fugacities of gaseous solutions. *Chemical Reviews*, 44:233–244.

[Renon and Prausnitz, 1968] Renon, H. and Prausnitz, J. M. (1968). Local compositions in thermodynamic excess functions for liquid mixtures. *AICHE J.*, 14:135–144.

[Soave, 1972] Soave, G. (1972). Equilibrium constants from a modified redlich-kwong equation of state. *Chem. Eng. Sci.*, 27:1197–1203.

[Stephenson, 1993] Stephenson, R. M. (1993). Mutual solubility of water and aldehydes. *Journal of Chemical & Engineering Data*, 38:630–633.

[Tariq et al., 2010] Tariq, M., Serro, A. P., Mata, J. L., Saramago, B., Esperanc, J. M., Lopes, J. N. C., and Rebelo, L. P. N. (2010). High-temperature surface tension and density measurements of 1-alkyl-3-methylimidazolium bistriflamide ionic liquids. *Fluid Phase Equilibria*, 294:131–138.

[Wei and Sadus, 2000] Wei, Y. and Sadus, R. (2000). Equations of state for the calculation of fluid-phase equilibria. *AiChE J.*, 46:169–196.

[Wertheim, 1984a] Wertheim, M. (1984a). Fluids with highly directional attractive forces.i. statistical thermodynamics. *J Stat Phys*, 35:19–34.

[Wertheim, 1984b] Wertheim, M. (1984b). Fluids with highly directional attractive forces.ii. thermodynamic perturbation theory and integral equations. *J Stat Phys*, 35:35–47.

[Wertheim, 1986a] Wertheim, M. (1986a). Fluids of dimerizing hard spheres, and fluid mixtures of hard spheres and dispheres. *The Journal of Chemical Physics*, 85:2929–2936.

[Wertheim, 1986b] Wertheim, M. (1986b). Fluids with highly directional attractive forces.iii. multiple attraction sites. *J Stat Phys*, 42:459–476.

[Wertheim, 1986c] Wertheim, M. (1986c). Fluids with highly directional attractive forces.iv. equilibrium polymerization. *J Stat Phys*, 42:477–492.

[Wertheim, 1987] Wertheim, M. (1987). Thermodynamic perturbation theory of polymerization. *The Journal of Chemical Physics*, 87:7323–7331.

[Wolbach and Sandler, 1998] Wolbach, J. and Sandler, S. (1998). Using molecular orbital calculations to describe the phase behavoiur of cross-associating mixtures. *Ind. Eng. Chem. Res.*, 37:2917–2928.

CHAPTER 6

Monte Carlo simulation study of the liquid-liquid equilibria

6.1 Introduction

Conventionally phase equilibria data is obtained through laboratory experiments by sampling and analyzing each phase of an equilibrated mixture. An alternative means of generating such data is via molecular simulations especially at conditions which are difficult to obtain in laboratory. It also provides microscopic insight into the properties of liquid mixtures. Advancement of simulation methodologies and computational power have made the study of liquid-liquid phase behavoiur relatively simpler. Compared to vapor-liquid equilibria (VLE), very few studies have been carried out to understand the behavoiur of liquid mixtures through molecular simulation. Keasler et al. have explored the extraction of ethanol from aqueous solution using seven 10-carbon alcohols (decan-1-ol, decan-2-ol, decan-3-ol, decan-4-ol, 2-methylnonan-2-ol (2M2N), 3,7-dimethyloctan-3-ol (37DM3O), and 4-propylheptan-4-ol (4P4H)) [Keasler et al., 2013]. They observed that configurational-bias Monte Carlo (CBMC) simulations [Siepmann and Frenkel, 1992, Mooij et al., 1992, Laso et al., 1992, Martin and Siepmann, 1999] in the Gibbs ensemble [Panagiotopoulos, 1987, Panagiotopoulos et al., 1988] coupled with the Transferable Potentials for Phase Equilibria (TraPPE) [Martin and Siepmann, 1998] force field was effective in predicting extraction abilities of solvents in terms of distribution coefficient and selectivity. Lasich et al. investigated the extraction of light alcohols (methanol, ethanol and propan-2-ol) from aqueous solution using *n*-dodecane as a solvent through GEMC simulations [Lasich et al., 2014]. TraPPE force field was used for alcohols and *n*-dodecane; while Water was modeled with simple point charge (SPC) [Berendsen et al., 1981] and TIP4P [Jorgensen et al., 1983] water models. They observed that SPC and TIP4P water models may be used in conjunction with the TraPPE model for dodecane/methanol/water system whereas simulations were completely in disagreement with the experimental data for the systems containing ethanol and propan-2-ol. Harwood et al. reinvestigated the ternary mixtures of *n*-dodecane, ethanol and water as studied by Lasich et al [Harwood et al., 2016]. They observed that TraPPE-UA force field under predicted the mutual miscibilities for the *n*-dodecane/ethanol mixture and over predicted the upper critical solution temperature by about 15%. For ternary n-dodecane/ethanol/water mixture the simulations correctly predicted the decrease of the ethanol solubility in the *n*-dodecane-rich phase and of *n*-dodecane in the polar phase upon the addition of water.

In summary the above mentioned studies were focussed on the extraction of lighter alcohols

(methanol, ethanol, propan-2-ol). In this chapter, we have investigated the extraction of acetic acid from aqueous solution using three different solvents: ethyl acetate, *n*-butyl acetate and 1-Butyl-3-methylimidazolium bis(trifluoromethylsulfonyl)imide ([BMIM][Tf_2N]) through Gibbs ensemble Monte Carlo approach employing CMBC algorithm. The objective is to check the prediction capability of the existing simulation methodologies and force field parameters in predicting the liquid mixture phase behavoiur.

6.2 Theory and simulation details

6.2.1. Gibbs Ensemble Monte Carlo Simulation (GEMC)

The Gibbs Ensemble Monte Carlo (GEMC) simulation methodology enables the direct calculation of phase coexistence properties of pure components and mixtures from a single simulation [Panagiotopoulos, 1987, Panagiotopoulos et al., 1988]. The basic idea of this methodology is to simulate phase coexistence properties by following the evolution in phase space of a system composed of two distinct regions. The two regions have different densities and compositions and are at thermodynamic equilibrium both internally and with each other. A schematic diagram of the technique is shown in Figure 6.1. Figure 6.1 shows a macroscopic system with two liquid phases (phase I and phase II) in equilibrium at a temperature T. Gibbs ensemble simulations are performed in two separate microscopic regions (boxes) within the bulk phases, away from the interface. Each region is simulated within periodic boundary conditions. The two boxes remain in thermodynamic equilibrium with each other with no physical contact between them. This implies there is no interface between the two boxes and thus the particles does not move from one box to another box through the interface. The first simulation box contains N^I particles in a volume V^I and is chosen from a region deep inside phase I. The second simulation box contains N^{II} particles in volume V^{II} and is chosen from a region deep inside phase II. The thermodynamic requirements for phase coexistence are that each region should be in internal equilibrium, and that temperature, pressure and the chemical potentials of all components should be the same in the two regions. System temperature is specified in advance. The remaining three conditions are satisfied by performing three types of Monte Carlo moves: displacement moves of particles within each phase (for internal equilibrium), fluctuations in the volume of the two phases (for equality of pressure) and transfers of particles between phases

(for equality of chemical potentials of all components). There are two versions of GEMC: NVT-GEMC and NPT-GEMC. In NVT-GEMC, volume change of the simulation boxes are coupled so that total volume of the system remains constant. In NPT-GEMC, volume of each simulation box changes independent of each other so that the boxes are at the same pressure.

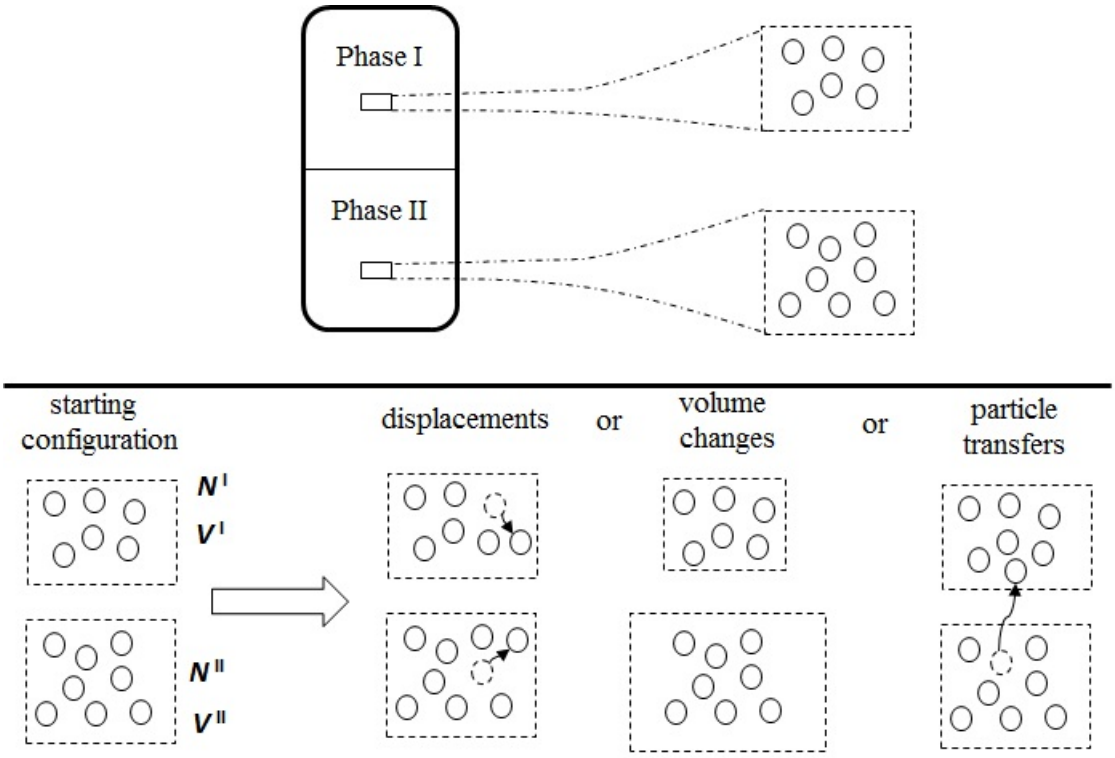

Figure 6.1.: Schematic diagram of the Gibbs ensemble Monte Carlo simulation methodology [Panagiotopoulos, 1987]

(a) Particle displacement move: In this step each box is independent. This step is similar to conventional random displacements of molecules in either of boxes I or II (or both), without a change in the volume or number of molecules in each box. Thus, each box is a system from the canonical ensemble at constant-NVT. For a displacement step internal to one of the regions, the probability of acceptance is the same as for conventional NVT simulations:

$$p_{move} = min[1, exp(-\beta \Delta E)] \tag{6.1}$$

where ΔE is the energy change resulting from the displacement move.

(b) Volume rearrangement move: In NPT-GEMC, to assure a constant pressure criterion, the volume of each box is varied independently and is accepted or rejected with a probability as

given below:

$$p_{volume} = min\left[1, exp\left(-\beta\left[\Delta E^I + \Delta E^{II} - N^I kTln\frac{V^I + \Delta V^I}{V^I} - N^{II} kTln\frac{V^{II} + \Delta V^{II}}{V^{II}} + P(\Delta V^I + \Delta V^{II})\right]\right)\right] \quad (6.2)$$

(c) Particle transfer move: This step consists of the movement of a single molecule from one phase to another phase. The transfer of a molecule from one phase to the other does not take place through an interface. In simulation, one would select a molecule at random from one phase to disappear and appear at a random point in the other phase. The acceptance criterion for particle transfers (from phase I to phase II) is thus given by:

$$p_{transfer} = min\left[1, \frac{N^{II}V^I}{(N^I+1)V^{II}} exp(-\beta\Delta E^I - \beta\Delta E^{II})\right] \quad (6.3)$$

6.2.2. Simulation details

Acetic acid, ethyl acetate, *n*-butyl acetate and 1-Butyl-3-methylimidazolium bis(trifluoromethyl-sulfonyl)imide [BMIM][Tf_2N] were modeled with the TraPPE-UA [Martin and Siepmann, 1998] force field which means that hydrogen atoms bonded to carbon atoms are grouped together to form a single interaction site. The non-bonded portion of the force field for all the components consists of a combination of Lennard-Jones (LJ) 12-6 and Coulomb interactions:

$$U(r_{ij}) = 4\epsilon_{ij}\left[\left(\frac{\sigma_{ij}}{r_{ij}}\right)^{12} - \left(\frac{\sigma_{ij}}{r_{ij}}\right)^{6}\right] + \frac{q_i q_j}{4\pi\epsilon_o r_{ij}} \quad (6.4)$$

where r_{ij}, ϵ_{ij}, σ_{ij}, q_i and q_j are the separation, LJ well depth, LJ diameter and partial charges for interaction sites *i* and *j* respectively. The LJ parameters for unlike interactions were determined with the Lorentz-Berthelot combining rules:

$$\sigma_{ij} = \frac{\sigma_{ii} + \sigma_{jj}}{2} \quad and \quad \epsilon_{ij} = \sqrt{\epsilon_{ii}\epsilon_{jj}} \quad (6.5)$$

In TraPPE-UA force field, interaction sites are connected by bonds of fixed length, while a harmonic potential is used to define the interaction between atoms separated by two bonds:

$$U_{bend} = \frac{k_\theta}{2}\left(\theta - \theta_o\right)^2 \tag{6.6}$$

Here k_θ, θ, and θ_o are the force constant, bending angle and equilibrium bending angle respectively.

For atoms separated by three bonds, a torsion potential of the following form is used for acetic acid

$$U_{torsion} = c_1\left[1 + cos\left(\phi + f_1\right)\right] + c_2\left[1 - cos^2\left(\phi\right)\right] \tag{6.7}$$

where ϕ is the dihedral angle and c_1, c_2, and f_1 are coefficients.

For ethyl acetate and *n*-butyl acetate following cosine form is used:

$$U_{torsion} = c_o + c_1\left[1 + cos\left(\phi\right)\right] + c_2\left[1 - cos\left(2\phi\right)\right] + c_3\left[1 + cos\left(3\phi\right)\right] \tag{6.8}$$

where ϕ is the dihedral angle and c_i are the Fourier constants.

For [BMIM][Tf_2N] following cosine form is used:

$$U_{torsion} = K_\chi\left[1 + cos\left(n\chi - \delta\right)\right] \tag{6.9}$$

TIP4P model [Jorgensen et al., 1983] have been used to describe the water molecules in this study. TIP4P model makes use of four interaction sites: two positively charged hydrogen sites, the oxygen site and a massless charge balancing site at the center of mass of the water molecule. All the atom types are shown in Figure 6.2 and 6.3 along with the force field parameters used in this work as reported in Tables 6.1-6.4.

Gibbs Ensemble Monte Carlo simulation in the isobaric-isothermal ensemble (NPT) as implemented in Monte Carlo for Complex Chemical Systems (MCCCS)-Towhee 7.1.0 code [Martin, 2013] was used to investigate the ternary mixtures. The cubic simulation box with standard periodic boundary conditions was used for all the simulations. LJ interactions were truncated at 10 Å and analytical tail corrections were applied beyond this diatance. The cut-off radius used

in this work was always less than half the box lenght. The Ewald summation technique (Kmax = 5) with tin-foil boundaries were used to calculate the long-range electrostatic interactions.

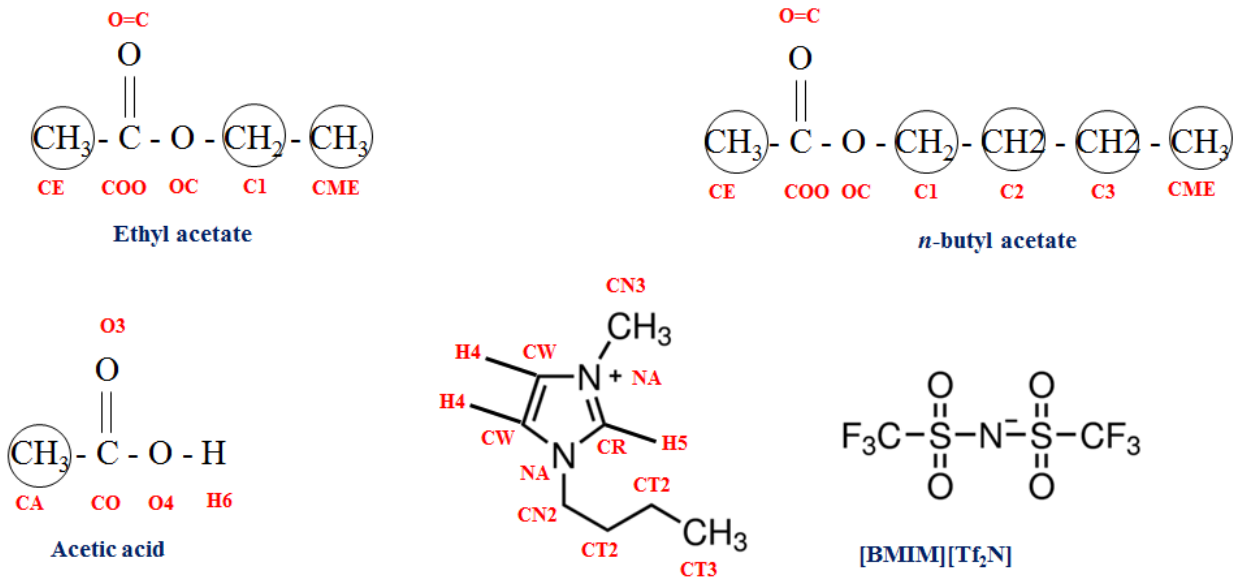

Figure 6.2.: Schematic structure and atom-type notations of molecules used in this work

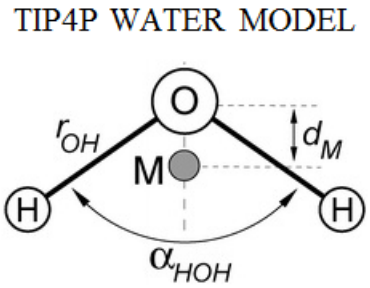

r_{OH} = 0.9572 Å $\quad \alpha_{HOH}$ = 104.52° $\quad q_H$ = +0.52

d_M = 0.1500 Å $\quad \alpha_{HOM}$ = 52.26° $\quad q_M$ = -1.04

σ_O = 3.15 Å $\quad (\varepsilon/k_B)_O$ = 78.02 K

Figure 6.3.: Atom-type notations and force field parameters of TIP4P water model

Table 6.1.: Non-bonded force field parameters of components studied in this work

atoms	σ	ϵ/k_B (K)	charge (e)	atoms	σ	ϵ/k_B (K)	charge (e)
	acetic acid [1]				[BMIM][Tf_2N] [2]		
CA	3.750	98.0	0.12	NA	3.250	85.51	0.015
CO	3.900	41.0	0.42	CR	3.400	43.26	0.000
O3	3.055	80.7	-0.45	CW	3.400	43.26	-0.160
O4	3.038	117.5	-0.46	H5	1.247	15.09	0.150
H6	0.000	0.000	0.37	H4	1.604	15.09	0.200
	ethyl acetate / n-butyl acetate [3]			CN3	3.660	95.56	0.260
CE	3.750	98.0	0.05	CN2	3.820	45.77	0.230
COO	3.900	41.0	0.55	CT2	3.950	45.77	0.050
O=C	3.050	79.0	-0.45	CT3	3.750	95.56	0.000
OC	2.800	55.0	-0.40	CF3	4.472	80.47	-0.095
C1	3.950	46.0	0.25	N	3.250	85.50	-0.272
C2	3.900	46.0	0.00	S	3.564	125.75	0.627
C3	3.900	46.0	0.00	O	2.960	105.62	-0.398
CME	3.750	98.0	0.00				

[1] [Kamath et al., 2004]; [2] [Zhong et al., 2011]; [3] [Kamath et al., 2006]

Table 6.2.: Bonded force field parameters of components studied in this work

Bond	r_o	Bond	r_o
acetic acid [1]		[BMIM][Tf_2N] [2]	
CA-CO	1.520	NA-CR	1.325
CO-O3	1.214	CW-NA	1.378
CO-O4	1.364	CW-CW	1.343
O4-H6	0.970	CW-H4	1.070
acetates [3]		CR-H5	1.070
CE-COO	1.520	NA-CN3	1.500
COO-(O=C)	1.200	NA-CN2	1.490
COO-OC	1.344	CT2-CN2	1.610
OC-C1	1.410	CT2-CT2	1.610
C1-C2	1.540	CT2-CT3	1.610
C2-C3	1.540	CF3-S	2.400
C3-CME	1.540	S-N	1.570
		S-O	1.450

[1] [Kamath et al., 2004]; [2] [Zhong et al., 2011]; [3] [Kamath et al., 2006]

Table 6.3.: Force field parameters (angle) of components studied in this work

angle	$\theta_o(^\circ)$	k_θ/k_B (K)
acetic acid [1]		
CA-CO-O3	126	80600
O3-CO-O4	123	80600
CA-CO-O4	111	70600
CO-O4-H6	107	35200
[BMIM][Tf_2N] [2]		
CW-NA-CR	108.0	68204
NA-CR-NA	109.9	74140
NA-CR-H5	125.7	51506
H4-CW-NA	122.1	51506
H4-CW-CW	130.7	50298
NA-CW-CW	107.1	70216
NA-CN2-CT2	112.2	80476
CW-NA-CN2	125.7	64582
CR-NA-CN2	126.3	64582
CN3-NA-CW	125.7	64582
CN3-NA-CR	126.3	64582

CT2-CT2-CN2		102.2	94158
CT2-CT2-CT2		102.2	94158
CT2-CT2-CT3		104.8	114276
N-S-CF3		105.9	79370
O-S-CF3		103.2	76956
S-N-S		125.2	61564
O-S-O		114.6	75044
N-S-O		112.7	70618
	acetates [3]		
CE-COO-(O=C)		125	62500
(O=C)-COO-OC		125	62500
CE-COO-OC		110	70600
COO-OC-C1		115	62500
OC-C1-C2		112	50300
C1-C2-C3		114	62500
C2-C3-CME		114	62500

[1] [Kamath et al., 2004]; [2] [Zhong et al., 2011]; [3] [Kamath et al., 2006]

Table 6.4.: Force field parameters (dihedral) of components studied in this work

	acetic acid [1]			
dihedral	C_1/k_B (K)	C_2/k_B (K)	$f_1(°)$	
CA-CO-O4-H5	630.0	1562.4	0.0	
O3-CO-O4-H5	630.0	1562.4	180.0	
	acetates [2]			
dihedral	C_0 (K)	C_1 (K)	C_2 (K)	C_3 (K)
CE-COO-(OC)-C1	0.00	2158.0	2098.0	197.3
(O=C)-COO-OC-C1	4716.0	2194.0	2059.0	-153.4
COO-OC-C1-C2	0.00	725.35	163.75	558.2
OC-C1-C2-C3	0.00	176.62	-53.34	769.93
C1-C2-C3-CME	0.00	355.03	-68.19	791.32
	[BMIM][Tf_2N] [3]			
dihedral	n	k (kcal/mol)	$\delta(°)$	
H4-CW-NA-CNx	2	1.5	180	
H4-CW-NA-CR	2	2	180	
CW-CW-NA-CR	2	12	180	
CW-CW-NA-CNx	2	2	180	

NA-CW-CW-H4	2	1.5	180
H4-CW-CW-H4	2	1.5	180
NA-CW-CW-NA	2	12	180
CNx-NA-CR-NA	2	2	180
CNx-NA-CR-H5	2	1.5	180
CW-NA-CR-NA	2	12	180
CW-NA-CR-H5	2	1.5	180
CW-NA-CN2-CT2	1	0.193	0
	2	0.220	180
	3	0.009	0
CR-NA-CN2-CT2	1	0.017	0
	2	0.015	180
	3	-0.212	0
X-CT2-CT2-X	1	-3.5	0
	2	1.6	180
	3	1.6	0

[1] [Clifford et al., 2006]; [2] [Kamath et al., 2006]; [3] [Zhong et al., 2011]

6.3 Results and Discussions

6.3.1. n-butyl acetate + acetic acid + water ternary systems

Isobaric-isothermal (NpT) GEMC simulations were carried out for ternary mixtures of *n*-butyl acetate + acetic acid + water at ambient pressure (p = 101.325 kpa) and at temperature 304.15 K. Number of molecules of *n*-butyl acetate, water and acetic acid were varied between 161-290, 446-542 and 47-144 respectively (Figure 6.4). Number of molecules were selected in such a way so that the overall mole fraction of acetic acid was 0.06 (Case-1 (ba)), 0.11 (Case-2 (ba)), 0.15 (Case-3 (ba)), and 0.17 (Case-4 (ba)). Three simulation box set-up was used for the NPT GEMC of ternary mixtures [Harwood et al., 2016]. Two boxes were used to model the liquid phases (box-1: organic phase; box-3: aqueous phase) and the third box was used as a transfer medium (box-2: transfer medium). Initially, all solvent molecules (*n*-butyl acetate) were placed in box-1 whereas all acetic acid molecules were placed in box-3. Water molecules were equally distributed between the two boxes. During the simulation, volume moves were applied to box-1 and box-3 whereas volume of box-2 was kept constant (box-2 length: $50.0\,\text{Å}$).

Helium molecules (25 nos.) were filled in box-2 and allowed to move in box-2 only. Before attempting the particle transfer move, box-1 and box-3 were equilibrated. During equilibration volume moves (1%), rigid-body center-of-mass translation moves (40%), rotations around the center of mass moves (45%) and CBMC regrowth moves for conformational changes (14%) were applied. Volume moves were equally distributed between box-1 and box-3. Translation moves were equally distributed between all the molecules whereas rotational moves were applied for all the molecules except Helium atoms. CBMC regrowth moves were equally distributed between acetic acid and *n*-butyl acetate. During equilibration, density of the two boxes were observed. Once the two boxes achieved a constant density, particle transfer moves were switched on. During this process, volumes moves (1%), translation moves (27%), rotational moves (27%), CBMC regrowth moves (15%) and CBMC-enabled particle transfer moves (only for acetic acid, water and *n*-butyl acetate) were applied. Transfer of particles were allowed between liquid phase and transfer medium only i.e. between box-1 & box-2 and box-2 & box-3. During the simulation, maximum displacements for translational, rotational, and volume moves were adjusted so to give an acceptable rate of 50%. Simulations were ran for 8,00,000 Monte Carlo Steps (MCS) where a Monte Carlo Step consists of N Monte Carlo Moves, N being the total number of particles in the simulation. Ensemble averages were computed over last 50,000 MCS. For systems consisting of approx. 4000 atoms, 1,00,000 MCS took about 15 days to complete on a single Intel Core i5-3470 processor.

The mole fraction trajectories for the components of the ternary mixture are shown in Figure 6.5 where left panels are for extract phase and right panels are for raffinate phase. Recall that these simulations were initiated with acetic acid molecules in the aqueous phase; *n*-butyl acetate molecules in the extract phase and water molecules equally distributed between the extract phase and raffinate phase. As soon as particle transfer moves are switched on, acetic acid molecules transfers rapidly into extract phase and water molecules transfer from extract phase to raffinate phase (Figure 6.5). In the raffinate phase, the mole fraction of water increases whereas mole fraction of acetic acid is seen to decrease and attain then equilibrium. *n*-butyl acetate molecules is seen to remain in the extract phase. Mole fraction of all the components is seen to achieve equilibrium values in both extract phase and raffinate phase. This is depicted in Case-1 (ba) and Case-3 (ba). In case of Case-2 (ba) and Case-4 (ba), mole fraction of components is also seen to attain equilibrium values.

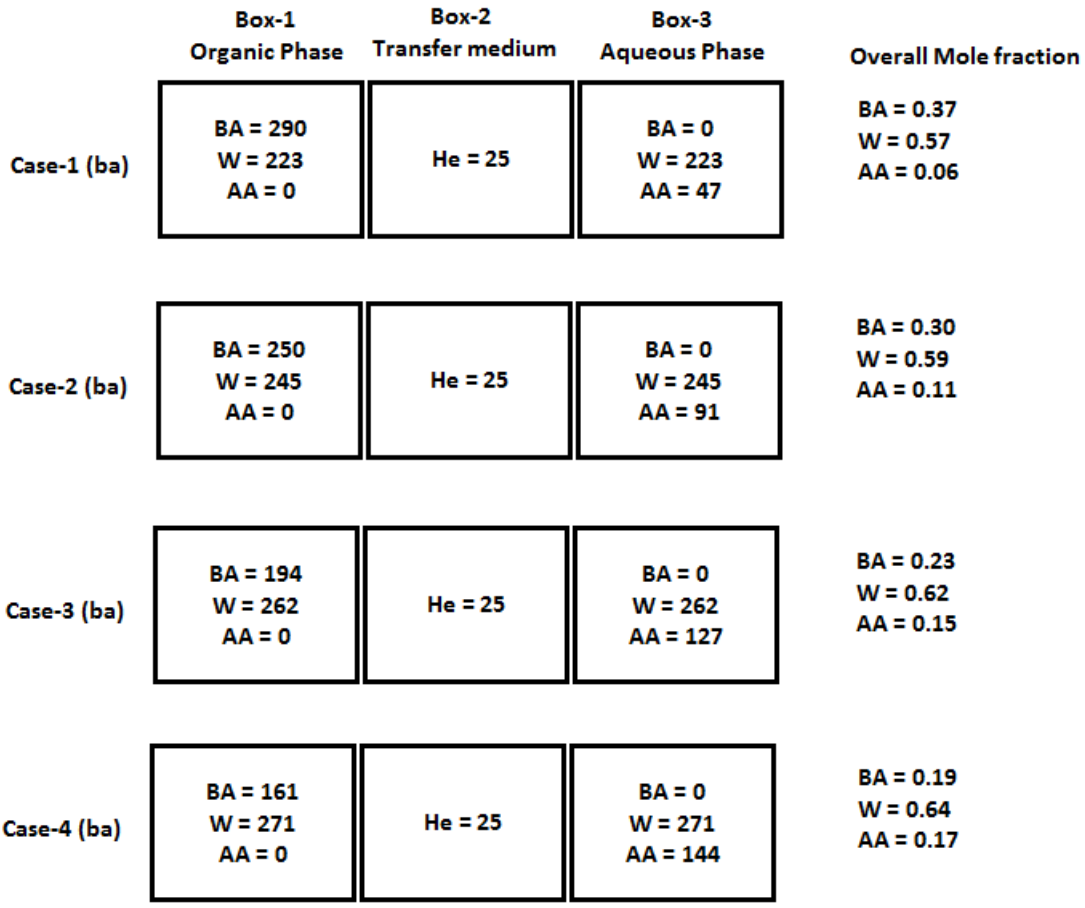

Figure 6.4.: Number of molecules for *n*-butyl acetate + acetic acid + water ternary systems

The ternary plot at 304.15 K and 0.1 MPa is shown in Figure 6.6 with the numerical data listed in Table 6.5 along with experimental data [Wang et al., 2007]. GEMC predcited ternary plot reveals that the *n*-butyl acetate has the potential to extract acetic acid from aqueous solution (Figure 6.6). The slope of GEMC predicted tie-lines were slightly higher in magnitude and more positive as compared to experimental tie-lines. *n*-butyl acetate composition in raffinate phase is close to zero which is in line with experimental observation [Wang et al., 2007]. Slight deviation was observed with respect to water composition in extract phase. The composition of water in extract phase increases with increase of composition of acetic acid in feed which is the same trend as experimental measurements. Again slight deviation was observed in the composition of acetic acid in raffinate phase. The composition of acetic acid in raffinate phase increases with increase of acetic acid composition in feed which is again the same trend as observed in experiments.

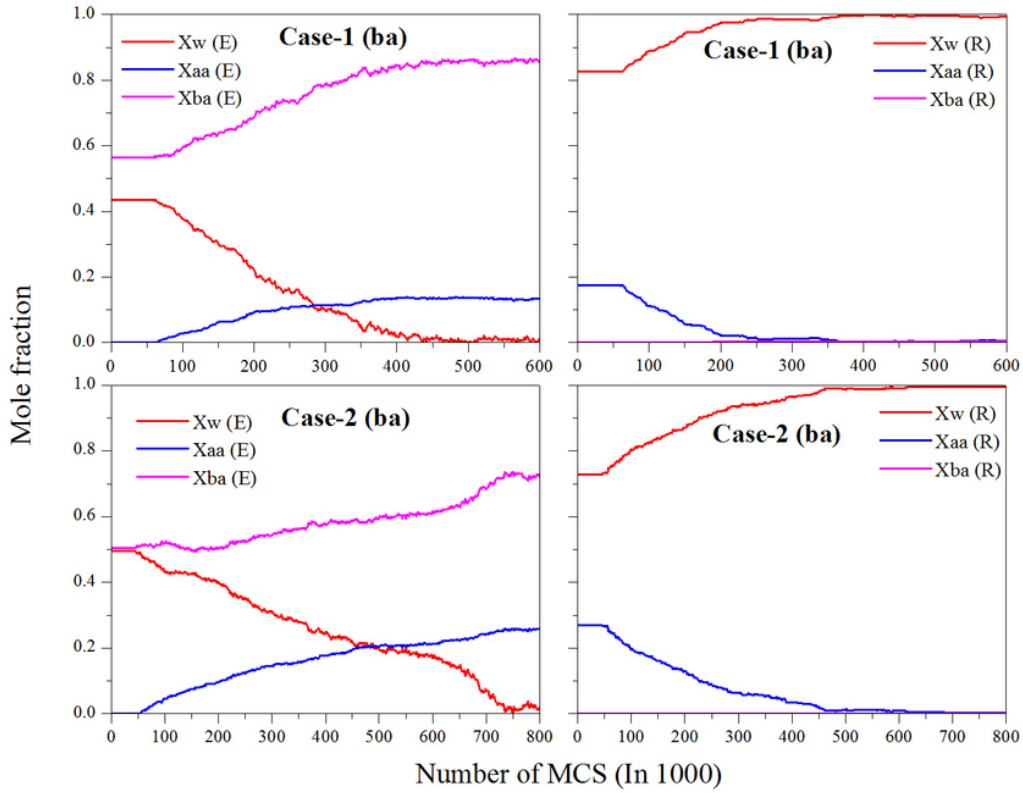

(a)

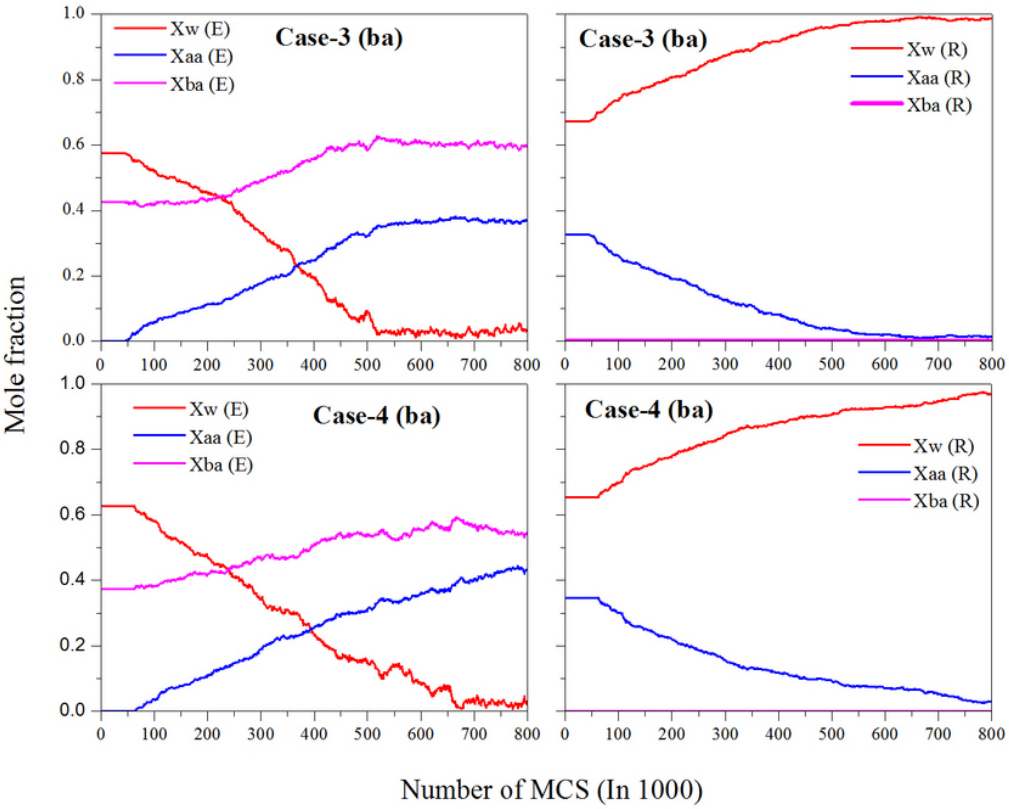

(b)

Figure 6.5.: Trajectories of the mole fraction of components in the *n*-butyl acetate + acetic acid + water ternary systems at T = 304.15 K and p = 0.1 MPa for (a) Case-1 (ba) and Case-2 (ba) and (b) Case-3 (ba) and Case-4 (ba); E=Extract phase and R=Raffinate phase

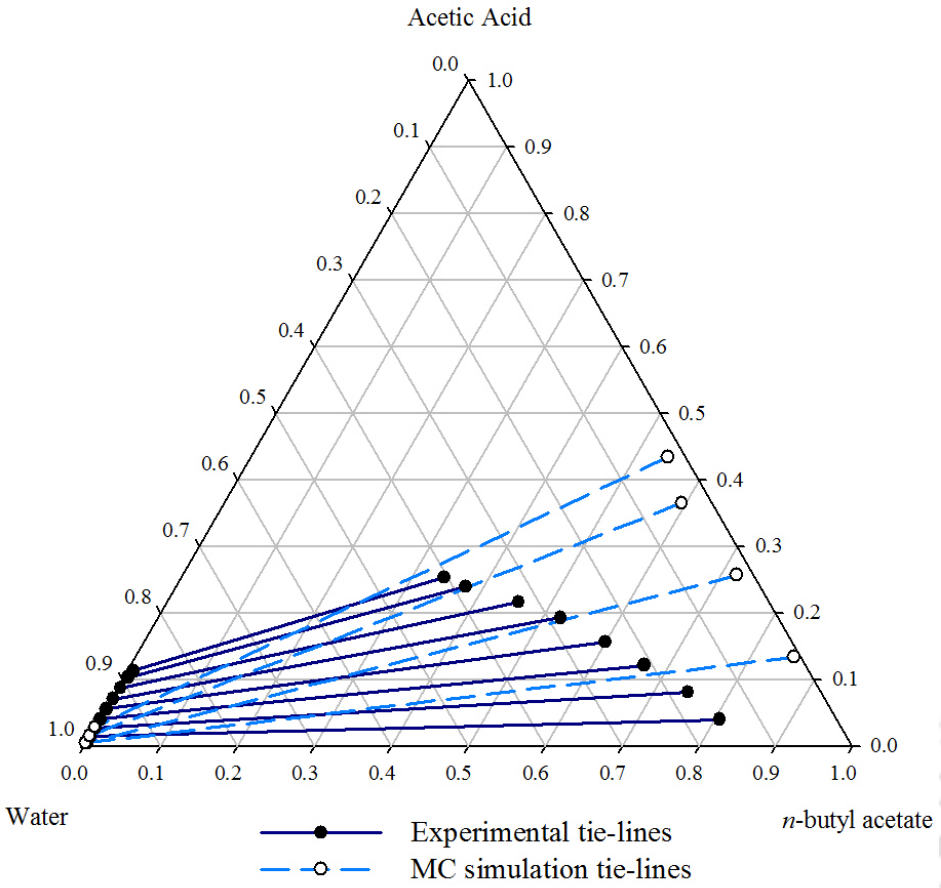

Figure 6.6.: Ternary plot for *n*-butyl acetate + acetic acid + water ternary systems at 304.15 K and 1.0 bar

Table 6.5.: GEMC predicted tie-lines Vs. Experimental tie-lines for *n*-butyl acetate (1) - acetic acid (2) - water (3) at T = 304.15 K and p = 0.1 Mpa

Sl. No.		**Extract phase**			**Raffinate phase**		
		X_1	X_2	X_3	X_1	X_2	X_3
1	Exp.	0.7455	0.0808	0.1737	0.0014	0.0277	0.9709
	GEMC	0.8574	0.1335	0.0091	0.0023	0.0044	0.9933
2	Exp.	0.6003	0.1563	0.2434	0.0023	0.0558	0.9419
	GEMC	0.7210	0.2565	0.0225	0.0000	0.0041	0.9959
3	Exp.	0.4573	0.2166	0.3261	0.0043	0.0869	0.9088
	GEMC	0.5949	0.3656	0.0395	0.0000	0.0149	0.9851
4	Exp.	0.3765	0.2396	0.3839	0.0062	0.1028	0.8910
	GEMC	0.5427	0.4348	0.0225	0.0000	0.0285	0.9715
	Overall % RMSD						**13.92**

From GEMC, Gibbs free energy of transfer was estimated using the following expression [Keasler et al., 2013]:

$$\Delta G_{trans} = -RTln\frac{\rho_{extract}}{\rho_{raffinate}} \tag{6.10}$$

where R is the gas constant, T is the absolute temperature, and $\rho_{extract}$ and $\rho_{raffinate}$ are the number densities of acetic acid or water in extract and raffinate phases, respectively. The Gibbs free energies of transfer for acetic acid and water have been computed from the simulations and are reported in Table 6.6. ΔG values are negative for acetic acid which indicates its preference for *n*-butyl acetate while ΔG values are positive for water which indicates water molecules have no attraction for solvent molecules.

Table 6.6.: Gibbs Free Energies of Transfer for Acetic acid and Water from the Aqueous to the extract Phase (*n*-butyl acetate)

Case	$\Delta G_{trans}(AA)$	$\Delta G_{trans}(W)$
	kJ/mol	kJ/mol
Case-1 (ba)	-7.87	13.66
Case-2 (ba)	-11.38	11.57
Case-3 (ba)	-7.19	9.72
Case-4 (ba)	-5.09	10.62

In summary, GEMC predicted that all acetic acid molecules will be transferred into extract phase while water molecules to raffinate phase. It means in ternary systems, acetic acid has more affinity towards *n*-butyl acetate and has almost no affinity towards water. Therefore, the selected force fields are able to explain the phase behaviour of *n*-butyl acetate + acetic acid + water ternary systems quite well.

6.3.2. ethyl acetate + acetic acid + water ternary systems

Isobaric-isothermal (NpT) GEMC simulations were carried out for ternary mixtures of ethyl acetate + acetic acid + water at ambient pressure (p = 101.325 kpa) and at temperature 298 K. Number of molecules of ethyl acetate, water and acetic acid were varied between 170-310, 580-720 and 50-110 respectively (Figure 6.7). Number of molecules were selected in such a way so that the overall mole fraction of acetic acid was 0.11 (Case-1 (ea)), 0.09 (Case-2 (ea)),

0.05 (Case-3 (ea)), and 0.07 (Case-4 (ea)). Simulation procedure was similar to *n*-butyl acetate based ternary system (section 6.3.1). The mole fraction trajectories for the components of the ternary mixture are shown in Figure 6.7 where left panels are for extract phase and right panels are for raffinate phase. Simulations were initiated with all the acetic acid molecules in the aqueous phase, all the ethyl acetate molecules in the extract phase and water molecules were equally distributed between the extract phase and raffinate phase. As soon as, particle transfer moves are switched on, acetic acid molecules transfers rapidly into extract phase and water molecules transfer rapidly out of extract phase into raffinate phase (Figure 6.8). In raffinate phase, mole fraction of water increases; whereas mole fraction of acetic acid decreases and then attain equilibrium values. Further a portion of ethyl acetate molecules are also transferred into the raffinate phase. To understand the molecules transfer process during the simulation, number of molecules are plotted against MCS and are shown in Figure 6.9 where left panels are for extract phase and right panels are for raffinate phase.

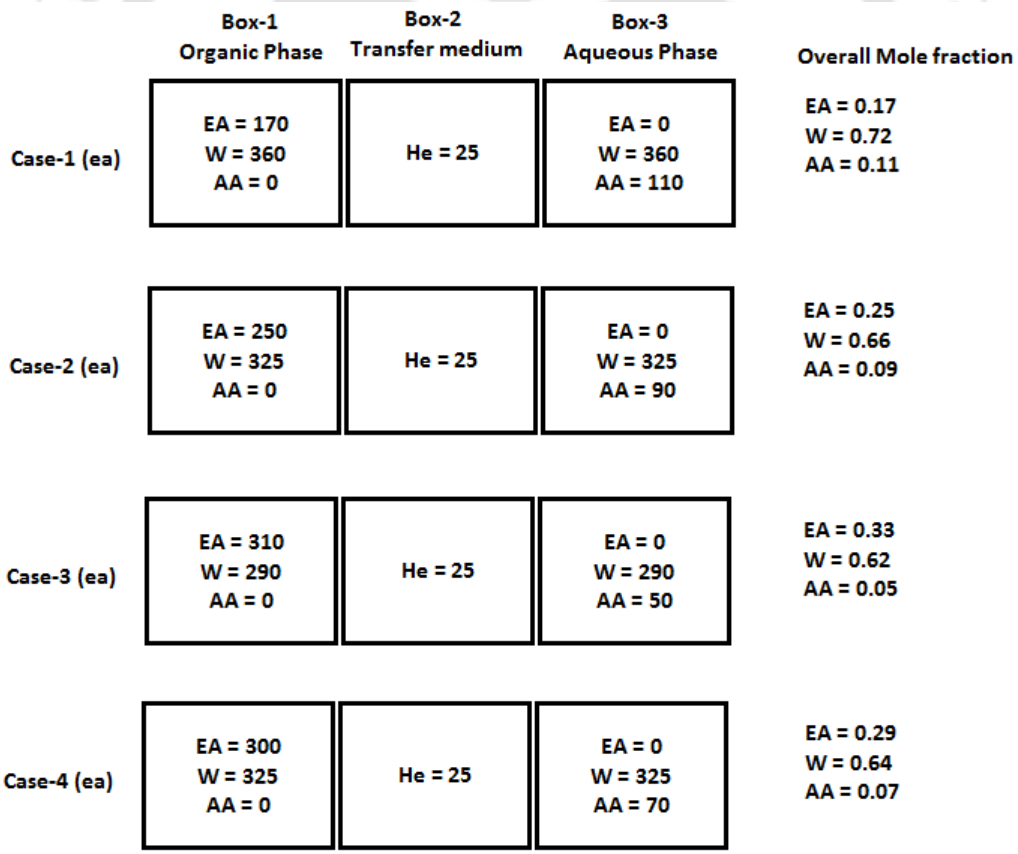

Figure 6.7.: Number of molecules for ethyl acetate + acetic acid + water ternary systems

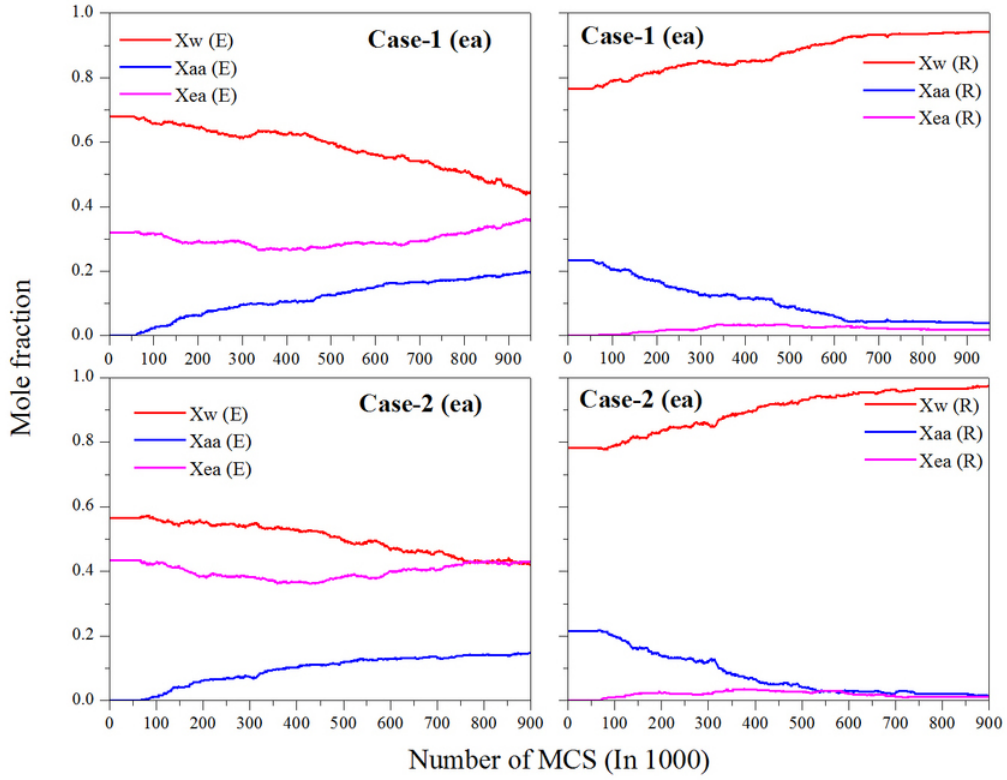

(a)

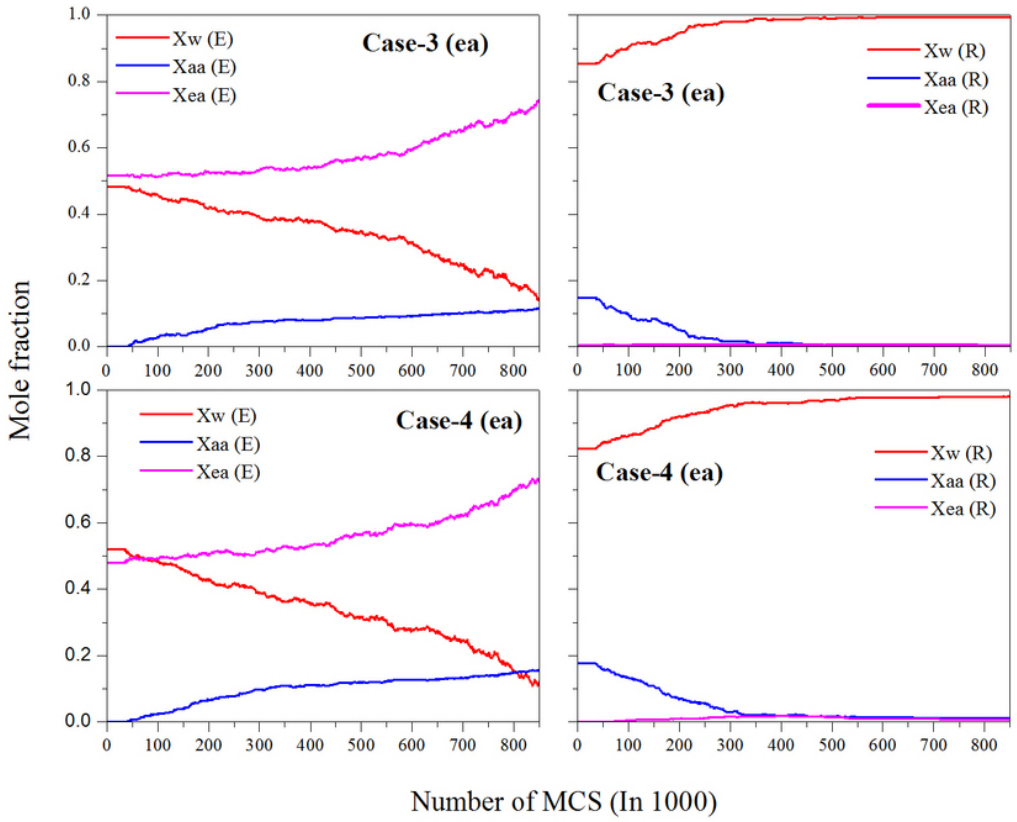

(b)

Figure 6.8.: Trajectories of mole fraction of components in ethyl acetate + acetic acid + water ternary systems at T = 298.15 K and p = 0.1 MPa for (a) Case-1 (ea) and Case-2 (ea) and (b) Case-3 (ea) and Case-4 (ea); E=Extract phase and R=Raffinate phase

In Case-1 (ea), number of molecules of acetic acid in extract phase increased from zero and attained a equilibrium value of 88 in about 7,50,000 MCS; while 22 molecules remained in the raffinate phase. Similarly, number of molecules of ethyl acetate in extract phase decreased from 170 and attained a equilibrium value of 160 in about 7,50,000 MCS while 22 molecules remained in the raffinate phase. However it should be noted that the number of water molecules in both phases have not attained equilibrium value even after 9,50,000 MCS. In extract phase, it decreased from 360 to 200 and in raffinate phase it increased from 360 to 520 in 9,50,000 MCS. In Case-2 (ea), number of molecules of acetic acid in extract phase increased from zero and attained a equilibrium value of 84 while 6 of its molecules remained in the raffinate phase. Similarly, number of molecules of ethyl acetate in extract phase decreased from 250 and attained a equilibrium value of 245; while 5 of its molecules remained in the raffinate phase. On a similar notes the number of water molecules in both phases did not attain equilibrium value even after 9,00,000 MCS. In extract phase, it decreases from 325 to 239 and in raffinate phase it increases from 325 to 411 in 9,00,000 MCS. In Case-3 (ea), number of molecules of acetic acid in extract phase increased from zero and attained a equilibrium value of 48 while 2 molecules remained in the raffinate phase. Similarly, number of molecules of ethyl acetate in extract phase decreased from 310 and attained a equilibrium value of 308 while 2 molecules remained in the raffinate phase. However, the number of water molecules in both phases did not attain equilibrium value even after 8,50,000 MCS. In extract phase, it decreased from 290 to 62 and in raffinate phase increased from 290 to 518 in 8,50,000 MCS. In Case-4 (ea), number of molecules of acetic acid in extract phase increased from zero and attained a equilibrium value of 63 while 7 molecules remained in the raffinate phase. Similarly, number of molecules of ethyl acetate in extract phase decreased from 300 and attained a equilibrium value of 295 while 5 molecules remained in the raffinate phase. But water did not attain equilibrium value in both phases even after 8,50,000 MCS. In extract phase, it decreased from 325 to 46 and in raffinate phase increased from 325 to 604 in 8,50,000 MCS. In all four cases, the acetic acid molecules have not transferred to extract phase as well as few ethyl acetate molecules have transferred from extract phase to raffinate phase; whereas in all cases of *n*-butyl acetate ternary systems almost all acetic acid molecules are transferred to extract phase with no *n*-butyl acetate molecules transferred to raffinate phase. Looking at the decreasing trend of water molecules in the extract phase, it seems that almost all water molecules will be transferred into raffinate.

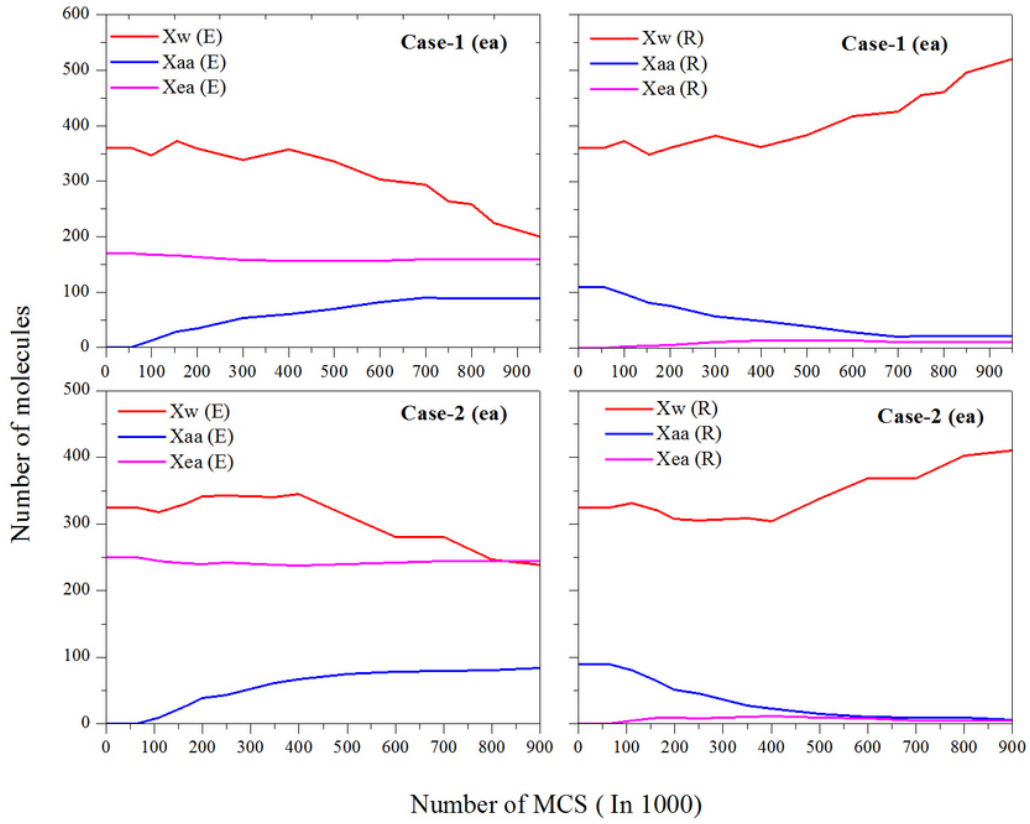

(a)

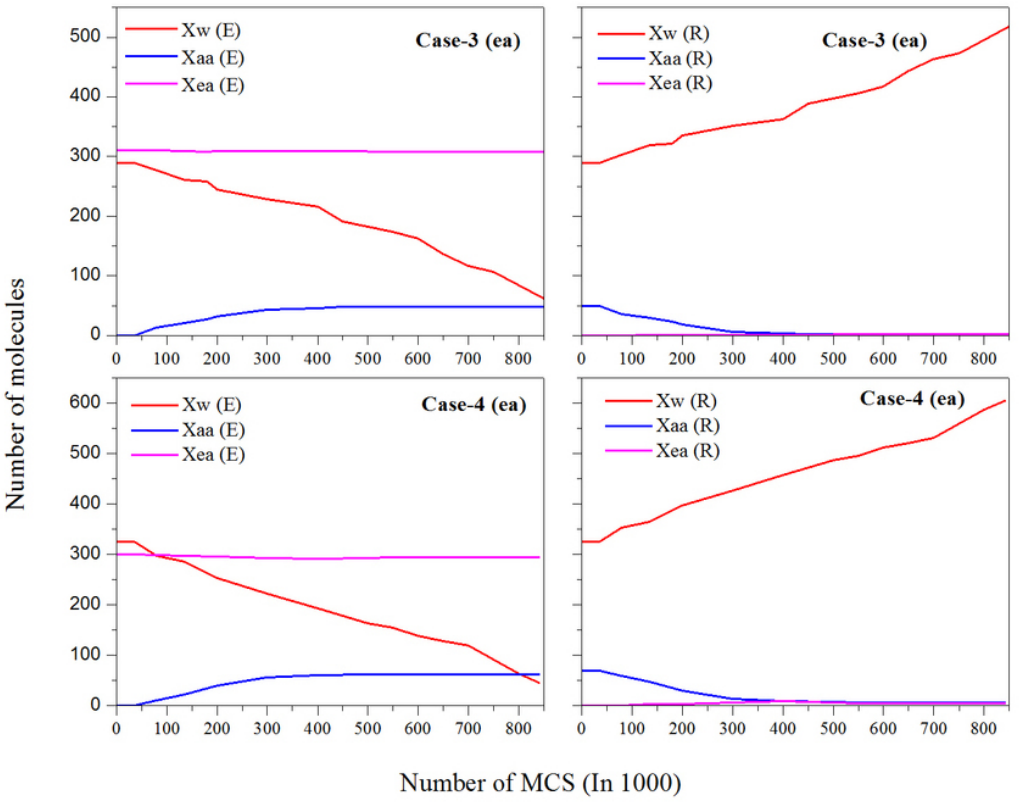

(b)

Figure 6.9.: Trajectories of number of molecules of components in ethyl acetate + acetic acid + water ternary systems at T = 298.15 K and P = 0.10 MPa for (a) Case-1 (ea) and Case-2 (ea) and (b) Case-3 (ea) and Case-4 (ea); E=Extract phase and R=Raffinate phase

Therefore, we carried out two more simulations Case-3r(ea) corresponding to Case-3(ea) and Case-4r(ea) corresponding to Case-4(ea). The difference between present and earlier simulation was that the simulation started with different distribution of initial number of molecules in extract and raffinate phases while the total number of molecules were kept constant (Figure 6.10). In case 3r (ea), extract phase initially contained 310 ethyl acetate, 20 water and 40 acetic acid molecules whereas raffinate phase contained 560 water, 10 acetic acid and zero ethyl acetate molecules. While in case 3 (ea), when water molecules were equally distributed between the two phases, all ethyl acetate molecules were in extract phase and all water molecules were in raffinate phase. After 2,00,000 MCS, almost all acetic acid molecules transferred into extract phase while only one molecule was left behind in raffinate phase. Similarly, only one ethyl acetate was transferred to raffinate phase while six water molecules remained in extract phase. The comparison between case 3 (ea) and case 3r (ea) is shown in Table 6.7. This confirms the observation regarding the final composition of water molecules in both phases.

Table 6.7.: Comparison between Case 3 (ea) and Case 3r (ea)

	Initial molecules		Final molecules	
	Case 3 (ea)	Case 3r (ea)	Case 3 (ea)	Case 3r (ea)
Extract phase				
Ethyl acetate	310	310	309	309
Water	290	20	62	6
Acetic acid	0	40	48	49
Raffinate phase				
Ethyl acetate	0	0	1	1
Water	290	560	518	574
Acetic acid	50	10	2	1

Similarly, the comparison between case 4 (ea) and case 4r (ea) is shown in Table 6.8. Here only three water molecules were left behind in extract phase; while both cases predicted the same mole composition of acetic acid and ethyl acetate in both phases.

The ternary plot for the ternary system at 298.15 K and 0.1 MPa is shown in Figure 6.10 with the numerical data listed in Table 6.9 along with experimental data [Colombo et al., 1999]. GEMC predicted ternary plot revealed that ethyl acetate has the potential to extract acetic acid from aqueous solution (Figure 6.10). The slope of GEMC predicted tie-lines were slightly higher in

magnitude and more positive as compared to experimental tie-lines. Ethyl acetate composition in raffinate phase is close to zero which is in line with experimental observation [Colombo et al., 1999]. Slight deviation was observed in water composition in extract phase and in acetic acid composition in raffinate phase.

Table 6.8.: Comparison between Case 4 (ea) and Case 4r (ea)

	Initial molecules		Final molecules	
	Case 4 (ea)	Case 4r (ea)	Case 4 (ea)	Case 4r (ea)
Extract phase				
Ethyl acetate	300	300	295	298
Water	325	10	46	3
Acetic acid	0	60	63	64
Raffinate phase				
Ethyl acetate	0	0	5	2
Water	325	640	604	647
Acetic acid	70	10	7	6

Table 6.9.: GEMC predicted tie-lines Vs. Experimental tie-lines for ethyl acetate (1) - acetic acid (2) - water (3) at $T = 298.15$ K and $p = 0.1$ Mpa

Sl. No.		**Extract phase**			**Raffinate phase**		
		X_1	X_2	X_3	X_1	X_2	X_3
1	Exp.	0.2953	0.1485	0.5562	0.0441	0.0777	0.8782
	GEMC	0.6275	0.3450	0.0275	0.0135	0.0295	0.9570
2	Exp.	0.4803	0.1242	0.3955	0.0213	0.0462	0.9325
	GEMC	0.7292	0.2500	0.0208	0.0076	0.0092	0.9832
3	Exp.	0.6512	0.0754	0.2734	0.0177	0.0243	0.9580
	GEMC	0.8489	0.1346	0.0165	0.0018	0.0017	0.9965
4	Exp.	0.5630	0.1035	0.3335	0.0190	0.0353	0.9457
	GEMC	0.8164	0.1753	0.0083	0.0030	0.0092	0.9878
	Overall % RMSD						**19.88**

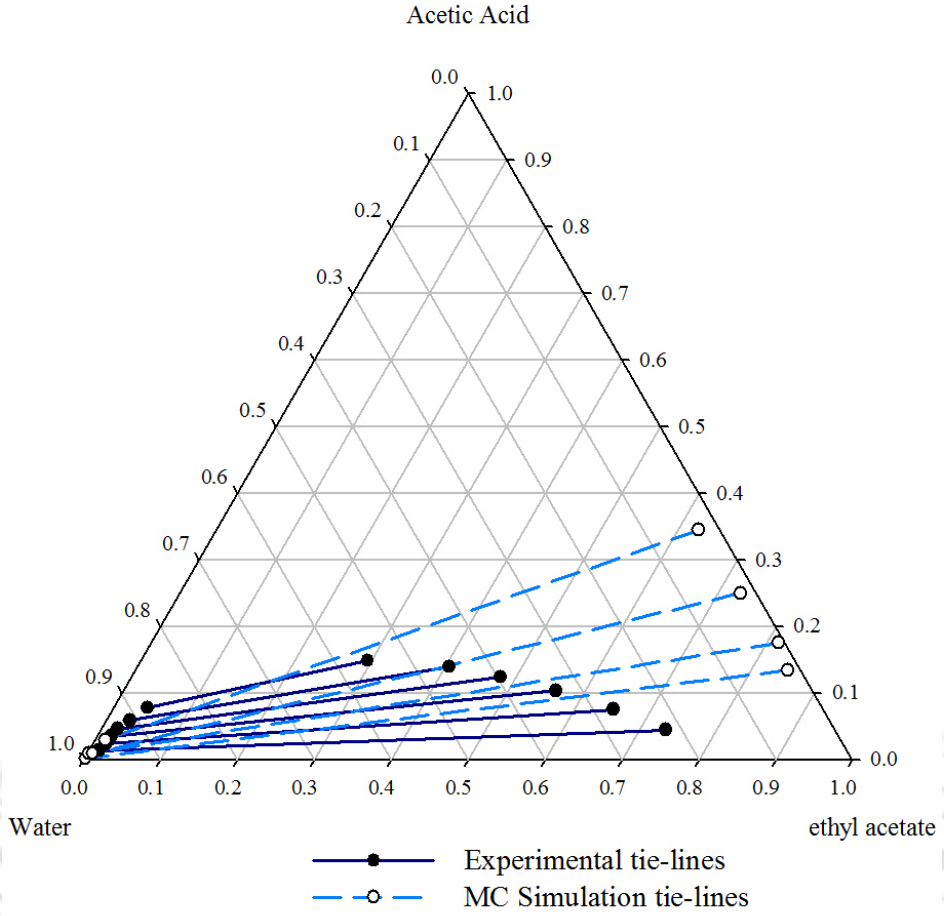

Figure 6.10.: Ternary plot for ethyl acetate + acetic acid + water ternary systems at 298.15 K and 0.1 Mpa

The Gibbs free energies of transfer for acetic acid and water have also been computed from the simulations and are reported in Table 6.10. ΔG values are negative for acetic acid which indicates its preference for ethyl acetate while ΔG values are positive for water which indicates water molecules have no attraction for solvent molecules.

Table 6.10.: Gibbs Free Energies of Transfer for Acetic acid and Water from the Aqueous to the extract Phase (ethyl acetate)

Case	$\Delta G_{trans}(AA)$	$\Delta G_{trans}(W)$
	kJ/mol	kJ/mol
Case-1 (ea)	-3.44	11.46
Case-2 (ea)	-6.54	11.20
Case-3 (ea)	-9.65	11.31
Case-4 (ea)	-5.87	13.32

Similar to *n*-butyl acetate based ternary systems, force fields were able to explain the phase behaviour of ethyl acetate + acetic acid + water ternary systems.

6.3.3. [BMIM][Tf_2N]+ acetic acid + water ternary systems

Isobaric-isothermal (NpT) GEMC simulations were carried out for ternary mixtures of [BMIM]-[Tf_2N] + acetic acid + water at ambient pressure (p = 101.325 kpa) and at temperature 298 K. Number of molecules of [BMIM][Tf_2N], water and acetic acid were varied between 120-125, 400-476 and 25-85 respectively (Figure 6.11). Number of molecules were selected in such a way so that the overall mole fraction of acetic acid was 0.04 (Case-1 (IL)), 0.08 (Case-2 (IL)), 0.12 (Case-3 (IL)), and 0.14 (Case-4 (IL)). Since ionic liquid has slow dynamics, the entire ternary system was first equilibrated at 373 K. The final configuration obtained at 373 K was used as a starting configuration for equilibrating the system at 298.15 K. Also particle transfer move was not attempted on [BMIM][Tf_2N] as ionic liquid is large and hydrophobic. The remaining procedure was similar to *n*-butyl acetate based ternary system (section 6.3.1). Number of molecules trajectories for the components of the ternary mixture are shown in Figure 6.12. Simulations were initiated with acetic acid molecules in the aqueous phase, [BMIM][Tf_2N] molecules in the extract phase and water molecules equally distributed between the extract phase and raffinate phase. As soon as particle transfer moves are switched on, acetic acid molecules transfers rapidly into extract phase and water molecules transfer rapidly out of extract phase into raffinate phase (Figure 6.12). In raffinate phase, number of water molecules increases whereas number of acetic acid molecules decreases and then attain equilibrium condition. While number of molecules of all components have attained equilibrium values in both phases for case-1 (IL) and case-2(IL); on the contrary case-3(IL) and case-4(IL), the equilibrium values did not reach even after 8,00,000 MCS. Therefore, we will not consider case-3(IL) and case-4(IL) in further discussions.

In case-1 (IL), all acetic acid molecules have transferred to extract phase whereas in case-2 (IL) 44 (out of 51) acetic acid molecules are transferred to extract phase after 8,00,000 MCS. In case of water molecules the prediction is in agreement with experimental data. In case-1 (IL), number of molecules of water in extract phase decreased from 238 and then attain a equilibrium value of 120; while case-2 (IL) attains an equilibrium value of 65 starting with

226 molecules. In ethyl acetate and *n*-butyl acetate based ternary systems, MC predicted that the water molecules will be transferred into raffinate phase whereas in [BMIM][Tf_2N] based ternary systems significant amount of water is present in extract phase. Therefore, prediction of water composition is in agreement with experimental data.

The ternary plot for the ternary system at 298.15 K and 0.1 MPa is shown in Figure 6.13 with the numerical data are listed in Table 6.11 along with experimental data. The plot revealed that GEMC prediction for [BMIM][Tf_2N] based ternary system ((%)RMSD = 7.61 %) is better than ethyl acetate and *n*-butyl acetate based ternary systems.

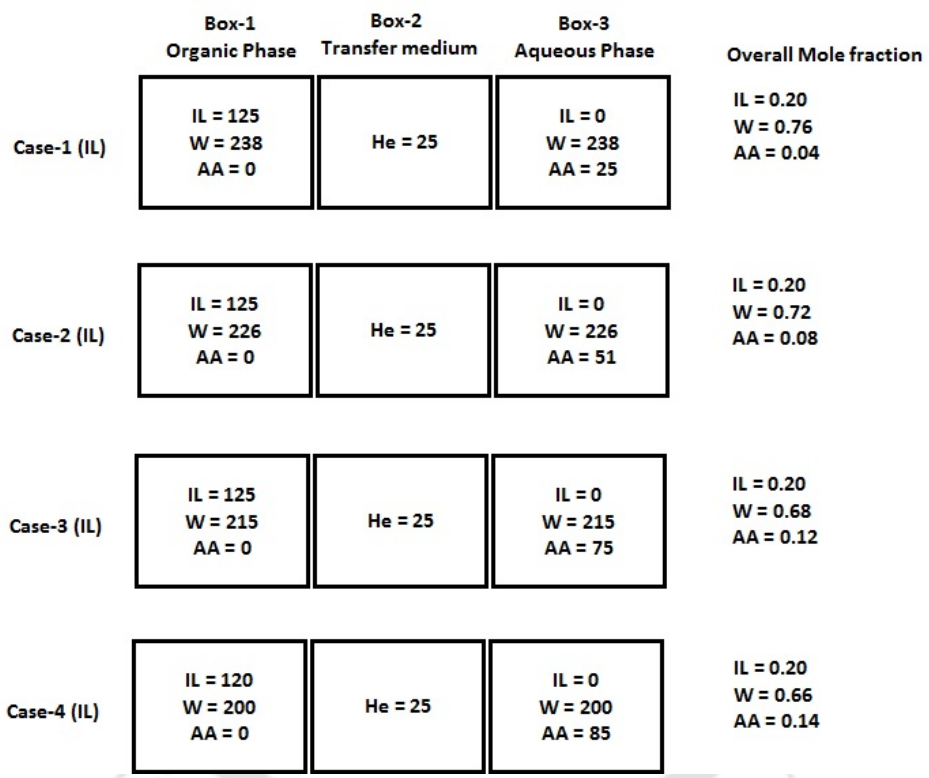

Figure 6.11.: Number of molecules for [BMIM][Tf_2N] + acetic acid + water ternary systems

Table 6.11.: GEMC predicted tie-lines Vs. Experimental tie-lines for [BMIM][Tf_2N] (1) - acetic acid (2) - water (3) at T = 298.15 K and p = 0.1 Mpa

Sl. No.		**Extract phase**			**Raffinate phase**		
		X_1	X_2	X_3	X_1	X_2	X_3
1	Exp.	0.6317	0.0335	0.3348	0.0000	0.0156	0.9844
	GEMC	0.4630	0.0926	0.4444	0.0000	0.0000	1.0000
2	Exp.	0.5917	0.0592	0.3491	0.0000	0.0223	0.9777
	GEMC	0.5342	0.1880	0.2778	0.0000	0.0178	0.9822
	Overall % RMSD						**7.61**

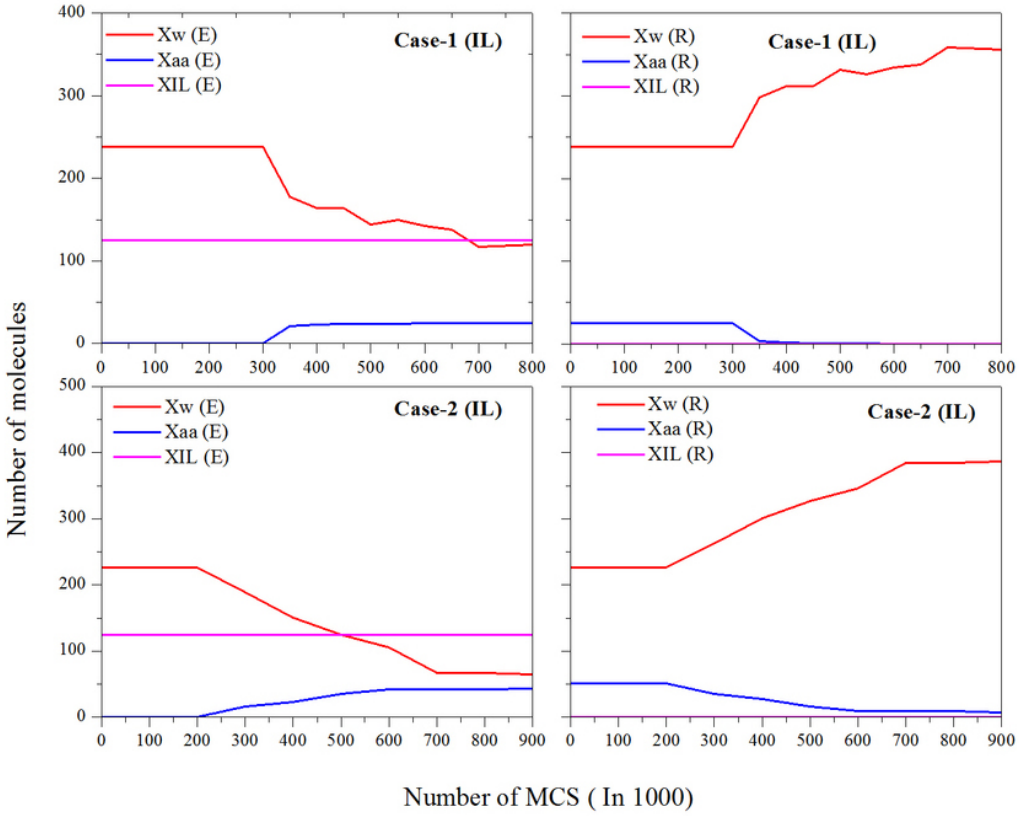

(a)

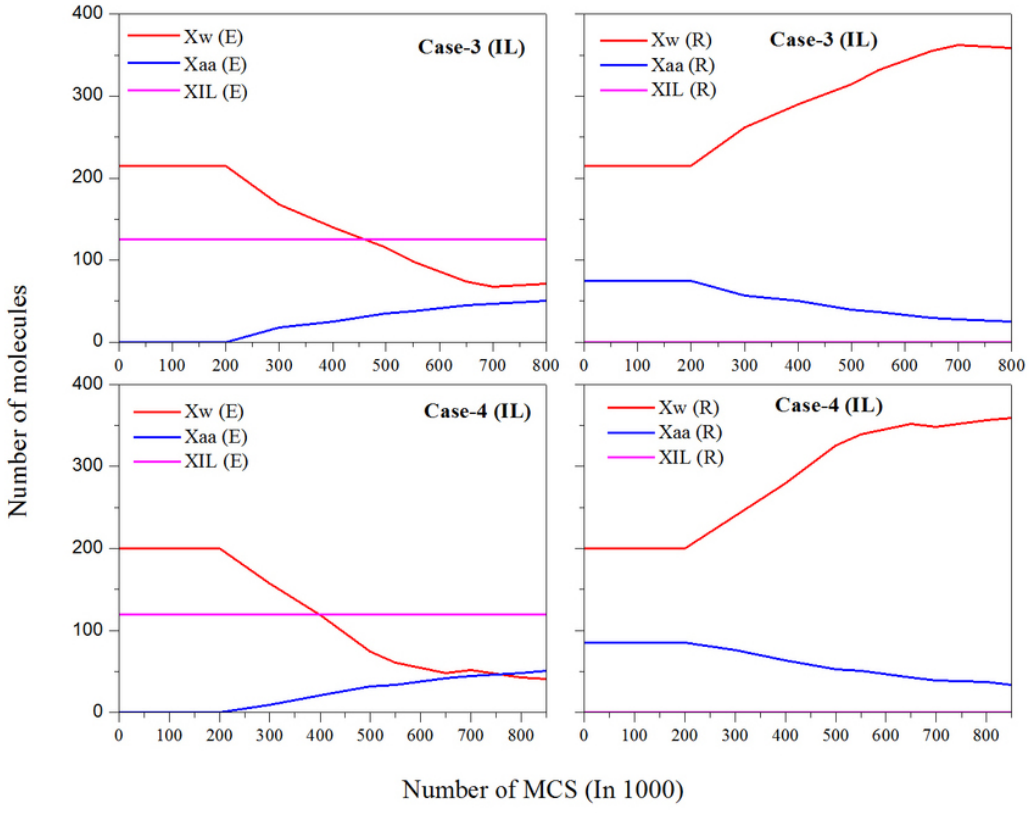

(b)

Figure 6.12.: Trajectories of number of molecules of components in [BMIM][Tf_2N] + acetic acid + water ternary systems at 298.15 K and P = 0.10 MPa for (a) Case-1 (IL) and Case-2 (IL) and (b) Case-3 (IL) and Case-4 (IL)

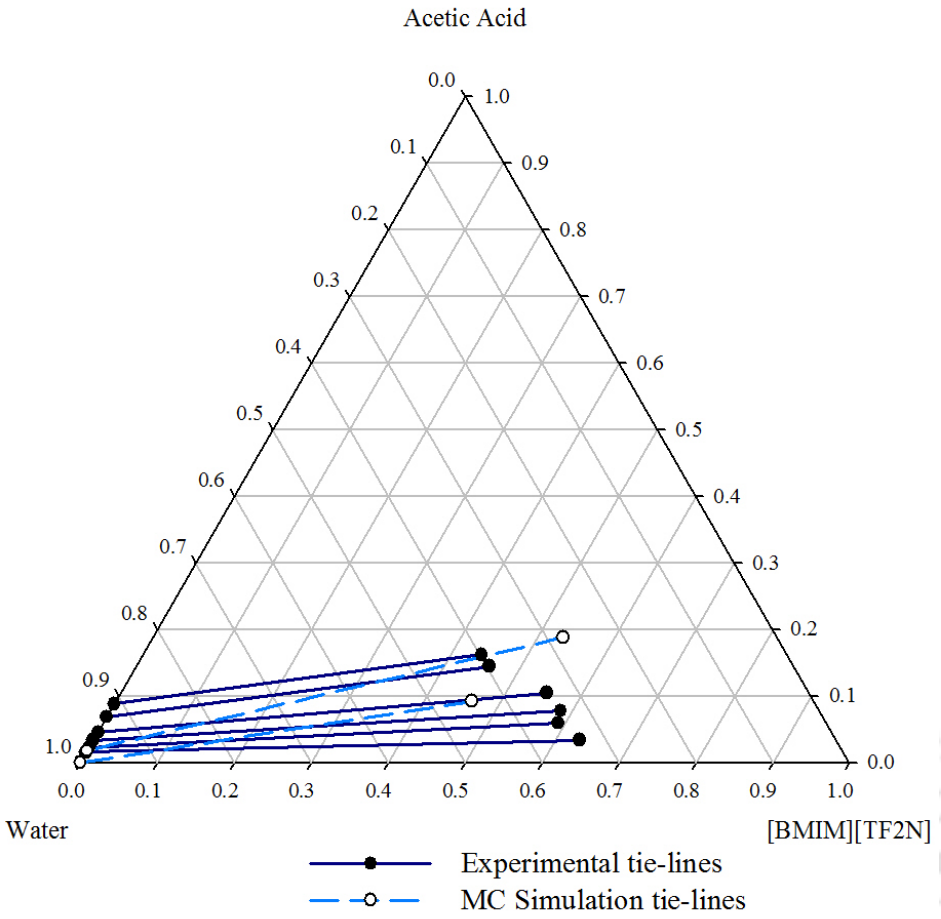

Figure 6.13.: Ternary plot for [BMIM][Tf_2N] + acetic acid + water ternary systems at 298.15 K and 0.1 Mpa

6.4 Conclusions

The Gibbs Ensemble Monte Carlo simulation was used to predict the LLE of ternary systems. For the studied systems, abberation was observed with respect to prediction of composition of acetic acid in raffinate phase and water composition in extract phase for the systems containing ethyl acetate and *n*-butyl acetate. However an excellent agreement was observed for ionic liquid ([BMIM][Tf_2N]) based ternary systems. The Gibbs free energies of transfer for acetic acid for *n*-butyl acetate system was in the range of -5.09 to -11.38 KJ/mol whereas for ethyl acetate based systems it was -3.44 to -9.65 KJ/mol. The Gibbs free energy values indicate both solvents i.e. ethyl acetate and *n*-butyl acetate are equally favourable for acetic acid extraction.

Note: Sample towhee input file and force field file are in **Appendix E.**

REFERENCES

[Berendsen et al., 1981] Berendsen, H., Postma, J., van Gunsteren, W., and Hermans, J. (1981). *Interaction models for water in relation to protein hydration (pp. 331-342) in 'Intermolecular Forces' ed. B. Pullman*. Reidel Publishing Company, Dordrecht.

[Clifford et al., 2006] Clifford, S., Bolton, K., and Ramjugernath, D. (2006). Monte carlo simulation of carboxylic acid phase equilibria. *J Phys Chem B*, 110:21938–21943.

[Colombo et al., 1999] Colombo, A., Battilana, P., Ragaini, V., and Bianchi, C. L. (1999). Liquid-liquid equilibria of the ternary systems water + acetic acid + ethyl acetate and water + acetic acid + isophorone (3,5,5-trimethyl-2-cyclohexen-1-one). *J. Chem. Eng. Data*, 44:35–39.

[Harwood et al., 2016] Harwood, D. B., Peters, C. J., and Siepmann, J. I. (2016). A monte carlo simulation study of the liquid-liquid equilibria for binary dodecane-ethanol and ternary dodecane-ethanol-water mixtures. *Fluid Phase Equilibria*, 407:269–279.

[Jorgensen et al., 1983] Jorgensen, W., Chandrasekhar, J., Madura, J., Impey, R., and Klein, M. (1983). Comparison of simple potential functions for simulation liquid water. *J. Chem. Phys.*, 72:926–935.

[Kamath et al., 2004] Kamath, G., Cao, F., and Potoff, J. (2004). An improved force field for the prediction of the vapor-liquid equilibria for carboxylic acids. *J Phys Chem B*, 108:14130–

14136.

[Kamath et al., 2006] Kamath, G., Robinson, J., and J.J.Potoff (2006). Application of trappe-ua force field for determination of vapor-liquid equilibria of carboxylate esters. *Fluid Phase Equilibria*, 240:46–55.

[Keasler et al., 2013] Keasler, S. J., Lewin, J. L., Siepmann, J. I., Gryska, N. M., Ross, R. B., Schultz, N. E., and Nakamura, M. (2013). Molecular insights for the optimization of solvent-based selective extraction of ethanol from fermentation broths. *AiChE J.*, 59:3065–3070.

[Lasich et al., 2014] Lasich, M., Johansson, E. L., and Ramjugernath, D. (2014). Assessing the ability of force-fields to predict liquid-liquid equilibria of ternary systems of light alcohols + water + dodecane by monte carlo simulation. *Fluid Phase Equilibria*, 368:65–71.

[Laso et al., 1992] Laso, M., DePablo, J., and Suter, U. W. (1992). Simulation of phase equilibria for chain molecules. *J Chem Phys*, 97:2817–2819.

[Martin, 2013] Martin, M. G. (2013). Mcccs towhee: a tool for monte carlo molecular simulation, http://towhee.sourceforge.net. *Mol. Simulat.*, 39:1212–1222.

[Martin and Siepmann, 1999] Martin, M. G. and Siepmann, J. (1999). Novel configurational-bias monte carlo method for branched molecules. transferable potentials for phase equilibria. 2. united-atom description of branched alkanes. *J Phys Chem B*, 103:4508–4517.

[Martin and Siepmann, 1998] Martin, M. G. and Siepmann, J. I. (1998). Transferable potentials for phase equilibria. 1. united-atom description of n-alkanes. *J Phys Chem B*, 102:2569–2577.

[Mooij et al., 1992] Mooij, G., Frenkel, D., and Smit, B. (1992). Direct simulation of phase equilibria of chain molecules. *J Phys Cond Matt*, 4:L255–L259.

[Panagiotopoulos, 1987] Panagiotopoulos, A. (1987). Direct determination of phase coexistence properties of fluids by monte-carlo simulation in a new ensemble. *Mol. Phys.*, 61:813–826.

[Panagiotopoulos et al., 1988] Panagiotopoulos, A., Quirke, N., Stapleton, M., and Tildesley, D. (1988). Phase equilibria by simulation in the gibbs ensemble: alternative derivation, generalization and application to mixture and membrane equilibria. *Mol. Phys.*, 63:527–545.

[Siepmann and Frenkel, 1992] Siepmann, J. I. and Frenkel, D. (1992). Configurational-bias monte carlo. a new sampling scheme for flexible chains. *Mol Phys.*, 75:59–70.

[Wang et al., 2007] Wang, L., Cheng, Y., Xiao, X., and Li, X. (2007). Liquid-liquid equilibria for the ternary systems acetic acid + water + butyl acetate and acetic acid + water + 2-methyl propyl acetate at 304.15 k, 332.15 k, and 366.15 k. *J. Chem. Eng. Data*, 52:1255–1257.

[Zhong et al., 2011] Zhong, X., Liu, Z., and Cao, D. (2011). Improved classical united-atom force field for imidazolium-based ionic liquids: Tetrafluoroborate, hexafluorophosphate, methylsulfate, trifluoromethylsulfonate, acetate, trifluoroacetate, and bis(trifluoromethylsulfonyl)imide. *J Phys Chem B*, 115:10027–10040.

CHAPTER 7

Reactive Force Field Simulation studies on the Combustion Behavior of *n*-Octanol

7.1 Introduction

Petroleum-based liquid fuels such as gasoline and diesel have dominated the transportation sectors in the twentieth century. But the need to reduce the emission of greenhouse gases and the dependency on fossil fuels have motivated researchers across the globe to look for alternative and renewable sources of fuels. Fuels derived from various bio-based feedstocks have attracted great attention in recent decades [Corma et al., 2007, Bozell and Petersen, 2010, Nigam and Singh, 2011]. Oxygen containing biofuels, such as alcohols, have shown considerable promise, because they are renewable and considered to be neutral with regard to net greenhouse gas emissions [Bergthorson and Thomson, 2015, Sarathy et al., 2014, Harvey and Meylemans, 2011, Jin et al., 2011, Kremer et al., 2015, Frassoldati et al., 2010, Shahid and Jamal, 2008, Basha et al., 2009, Borugadda and Goud, 2012, Koberg and Gedanken, 2012, Sarin, 2012, Shahir et al., 2015]. With respect to the current work concerning bio-oil, after a thorough upgradation the potential greener fuels needs to be looked at for combustion phenomena. One of the prominent fuel namely Octanol is selected in final stages to study its combustion behaviour. This was the only fuel where kinetic data for combustion was available. Octanol has generated a considerable amount of interest where recently new pathways were described to obtain *n*-octanol from biomass or bio-oil. Julis et al. [Julis and Leitner, 2012] have discovered a new route for the production of *n*-octanol from carbohydrate feedstock. Starting with furfural and acetone, an overall 73% yield of *n*-octanol was obtained in a step-wise procedure and 54% overall in a one-pot procedure. Akhtar et al. [Akhtar et al., 2015] have engineered a synthetic pathway for the synthesis of *n*-octanol from glucose and fatty acids in Escherichia coli BL21 (DE3) by overexpression of three enzymes (thioesterase, carboxylic acid reductase and aldehyde reductase) and one maturation factor (phosphopantetheinyl transferase).The majority (73%) of the fatty alcohol was localised within the media without a requirement of detergent or solvent overlay.

n-Octanol is found to have better fuel properties as compared to ethanol and *n*-butanol. It has higher energy density (33.7 MJ/L) as compared to ethanol (19.6 MJ/L) and *n*-butanol (29.2 MJ/L). It also has a comparable energy density with petro-diesel (40.3 MJ/L). Another important terminology in compression-ignition (CI) engine is cetane number where a high cetane number indicates a high self-ignition tendency. *n*-octanol has a cetane number (CN) of 39

which is much higher than *n*-butanol (CN $\sim$ 17) and ethanol (CN $\sim$ 11) but slightly less than petro-diesel (CN $\sim$ 45-50). Solubility of fuel in water is another important aspect which has to be considered with regard to its pipeline compatibility. Solubility of *n*-octanol in water is very low $\sim$ 0.59 g/L as compared with ethanol (miscible) and *n*-butanol ($\sim$ 77 g/L). *n*-octanol having vapor pressure of 0.08 mmHg is also much less than ethanol ($\sim$ 55 mmHg) and *n*-butanol ($\sim$ 7 mmHg) but slightly less than petro-diesel ($\sim$ 0.4 mmHg). This makes them safe in terms of storage, handling and transportation. The viscosity of *n*-octanol (4.4 cST 40 °C) is again close to the upper limit of the diesel viscosity range (1.8-5.8 cST 40 °C), while the boiling point of *n*-octanol (195 °C) is at the low end of the diesel boiling curve (180-300 °C). Overall, based on properties, *n*-octanol is a suitable fuel for operation in compression ignition (CI) engines [Akhtar et al., 2015].

Very few studies have been carried out to understand the combustion behaviour of *n*-octanol. Heuser et al. [Heuser et al., 2013] have investigated the effect of *n*-octanol combustion on engine emissions. With *n*-octanol the particulate matter (PM) emissions was found to reduce by a factor of 20 as compared to diesel fuel. However, the slightly lower cetane number with respect to diesel fuel causes minor over-leaning effects in particular at its lowest load. Thus, the hydrocarbon, CO and combustion noise emissions exceed than those of diesel combustion at low load operation. Kerschgens et al. [Kerschgens et al., 2016] also investigated the combustion behaviour of *n*-octanol in diesel engine. While on one side lower soot emissions and nitrogen oxide emissions were obtained, on the other hand the emissions of unburned hydrocarbons and CO were found to be rather high due to the longer ignition delay. To understand the phenomena further Cai et al. [Cai et al., 2015] carried out the chemical kinetic investigation on the oxidation of *n*-octanol. Ignition delay times and stable species concentration profiles were experimentally obtained for *n*-octanol oxidation in a shock tube and a jet stirred reactor, respectively. The oxidation of *n*-octanol was found to be initiated via hydrogen atom abstraction from the fuel by molecular oxygen. *n*-octanol was mainly consumed by the build-up of OH radicals. The fuel's combustion characteristics were then compared to those of n-alkanes and short chain alcohols. The major differences between linear alcohols and alkanes with the same carbon chain length are the presence of the hydroxyl group in alcohols. Thus the hydrogen abstractions by OH and HO_2 radicals were found to play a dominant role in determining ignition delay times.

For a better understanding of *n*-octanol oxidation behavior, knowing its fundamental combus-

tion characteristics is necessary. A detailed investigation on combustion reaction mechanisms can provide important information with respect to the intermediates. However, it becomes a challenge to disentangle the various fundamental combustion steps by experiments and compare the same with kinetic modeling methods. This necessitates the requirement of computational approach to help us widen our sight and provide an efficient way to understand the true nature of the complex combustion reactions. In theory, quantum mechanical (QM) methods can provide accurate reaction pathways and rate constants for individual elementary reaction. However, these methods are computationally expensive in providing the detailed description of complex reactions. Therefore, a number of empirical methods (Molecular dynamics) have been developed in order to reduce the computational cost. Classical molecular dynamics simulations are able to describe systems with thousands of atoms but they fail to describe the processes of bond breaking and bond formation in the chemical reactions. In order to overcome the deficiencies of conventional MD simulations, bond order based reactive force field (ReaxFF) has been developed by Duin et al. [van Duin et al., 2001] as an efficient method for describing chemical reactions. ReaxFF is a first principle based bond-order dependent reactive force field that provides an accurate description of bond breaking and bond formation. Parameters of this force field are derived from QM. Hence, the potential can nearly reproduce the accuracy of the ab initio calculation at much lower computational cost. ReaxFF has seen extensive use over the past 10 years modeling several different types of reactive systems including combustion, catalysis, fuel cells, and nanotubes [van Duin et al., 2001, Chenoweth et al., 2008, Chenoweth et al., 2009, Goddard et al., 2006b, Goddard et al., 2006a, Nielson et al., 2005]. In the present work, MD simulations for *n*-octanol has been carried out by employing the reactive force field (ReaxFF) as implemented in ADF software [http://www.scm.com,]. The ReaxFF force field for C/H/O systems as developed by van Duin et al. [van Duin et al., 2001] has been used to simulate the oxidation of *n*-octanol. This will further elucidate the oxidation pathways of *n*-octanol under representative conditions such as temperatures (3000-4000 K) and equivalence ratios (0.5, 1.0, 2.0).

7.2 Computational Details

ReaxFF is a reactive force field method that uses the concept of bond order to model the interactions in a chemical system. The bond order concept was first implemented by Tersoff [Tersoff, 1988] for silicon. Later on, Brenner [Brenner, 1990] extended the Tersoff potential for carbon and hydrocarbons. Based on bond order concept, ReaxFF ensures smooth transition of bond formation and bond dissociation during chemical reactions. In ReaxFF force field, the general expression for the energy function is:

$$E_{system} = E_{bond} + E_{over} + E_{under} + E_{val} + E_{pen} + E_{tors} + E_{conj} + E_{vdWaals} + E_{Coulomb} \quad (7.1)$$

Where, E_{bond} denotes the bond energy, E_{over} and E_{under} represent the over- and under-coordinated atom in the energy contribution, respectively. Other terms, including E_{val}, E_{pen}, E_{tors}, E_{conj}, $E_{vdWaals}$, and $E_{Coulomb}$ are the valence angle term, penalty energy, torsion energy, conjugation effects to energy, nonbonded van der Waals interaction and Coulomb interaction, respectively.
The ReaxFF potential determines the connectivity of the system based on bond orders calculated from interatomic distances that are updated every time step. The bonded interactions are bond-order dependent while non-bonded interactions are calculated between all atom pairs and are shielded at short interatomic distances to prevent these interactions from becoming excessive. It has been shown that ReaxFF can give good reproduction of all relevant quantum mechanical data, and can provide atomistic descriptions of many complex chemical reactions. The details of ReaxFF with its equations and methodology can be found elsewhere [van Duin et al., 2001, Chenoweth et al., 2008].
In this work, *n*-octanol/O_2 mixtures for a wide range of input conditions were investigated. All the input conditions are listed in Table 7.1. All simulations were performed with fixed number of atoms (N), fixed volume (V) and a fixed temperature (T), known as NVT-MD simulation. In all MD simulations, cubic periodic box of side length 30.0 Å has been considered. These systems were equilibrated via low-temperature (5K) ReaxFF simulations with a time step of 0.1 fs for 50 ps to prevent occurrence of chemical reactions during equilibration. The equilibrated systems were then used in the NVT-MD simulations with time step of 0.1 fs. During all the NVT-MD simulations, the system temperature were controlled via a Berendsen thermostat [Berendsen

et al., 1984] with a 0.5 ps damping constant. The equivalence ratio (Φ) is defined as the ratio of the actual *n*-octanol-to-oxygen ratio to the stoichiometric *n*-octanol-to-oxygen ratio i.e.

$$\text{Equivalence Ratio} = \frac{(\text{n-octanol}/\text{O}_2)_{\text{actual}}}{(\text{n-octanol}/\text{O}_2)_{\text{stoichiometric}}} \tag{7.2}$$

Table 7.1.: Equivalence Ratio, Number of Molecules and Temperature of the studied system

Equivalence Ratio(Φ)	n-octanol/ oxygen	Temperature (K)	Box Size (Å)	Ensemble
0.5	10/240	3000-3500-4000	30 X 30 X 30	NVT
1.0	10/120	2000-2500-3000-3500-4000	30 X 30 X 30	NVT
2.0	10/60	3000-3500-4000	30 X 30 X 30	NVT

The simulation conditions used in this work are not fully equivalent with that of actual reaction conditions. The time scale of the simulation (250 ps) is orders of magnitude shorter than that of the experiment which is 0.7 s. Thus, in the ReaxFF simulations, we increase the temperature from 500-1200 K (as used in experiments) to 3000-4000 K to allow chemical reactions to be observed on the computational affordable time scale. This difference in time and temperature scales between simulation and experiment may certainly affect product distributions. However high temperature used in simulation is known to only influence the reaction rates but not reaction mechanisms. We expect to find a qualitative agreement between the experimental and simulation results as well as various insights related to reaction mechanisms such as initiation step and formation of major products through ReaxFF MD simulations.

7.3 Results and Discussions

7.3.1. Effect of Temperature on the oxidation of n-octanol

Time evolution of potential energy, total number of molecules, *n*-octanol, major intermediate products (C_2H_4 and CH_2O) and main combustion products (CO_2, CO & H_2O) are presented in Figures 7.1-7.7. The simulations were performed at temperatures 3000-4000 K in the interval

of 500 K for a total simulation time of 250 ps. The equivalence ratio was kept as unity and the total number of molecules of octanol and oxygen were taken to be 10 and 120 respectively. The potential energy (Figure 7.1) shows that the system initially gains energy from heating and then start to react. With the oxidation of *n*-octanol molecules, the potential energy finally decreases. It has been observed that the decrease in potential energy is rapid with increase in temperature indicating that a higher temperature accelerates the oxidation of *n*-octanol. Time evolution graphs of total number of molecules (Figure 7.2) and number of *n*-octanol molecules (Figure 7.3) indicate that the reaction proceeds at a faster rate as the temperature increases. Starting with 130 number of molecules, the total number of molecules at the end of 250 ps are 168, 188 and 195 (Figure 7.2). It should be noted that the reaction were conducted in the following regime: (a) an equilibration time from 0-50 ps followed by a (b) production time from 50 to 250 ps. This is the reason that the figures 7.1-7.7 have started from 50 ps, as no reaction takes place during the equilibration time. *n*-Octanol oxidation was found to start at 50.55 ps, 52.7 ps and 63.74 ps for 4000, 3500 and 3000 K respectively. This is then seen to be consumed at 59.82 ps (4000 K), 66.925 ps (3500 K) and 145.7 ps (3000 K) (Figure 7.3). The final products observed from the simulations are CO_2, CO and H_2O (Figures 7.4-7.5).

From the product distribution, CO_2, CO and H_2O begin to increase as the temperature goes up and it reaches a maximum number at 4000 K. As depicted in Figure 7.5, the rate of formation of CO and CO_2 are almost the same at low temperature (3000 K). As temperature increases, the rate of formation of CO was found to be higher than CO_2. The same has been observed in experiments conducted by Cai et al. [Cai et al., 2015] in the jet stirred reactor. The major intermediate products obtained in ReaxFF MD simulations are ethylene followed by formaldehyde which is again the same behavior as reported in experiments [Cai et al., 2015]. Time evolution of major intermediate products, such as ethylene and formaldehyde, are presented in Figure 7.6 and Figure 7.7 respectively. Ethylene molecule reaches a maximum number of 23 at 3500 K while formaldehyde reaches a maximum number of 15 at 3500 K. The C_2H_4 and CH_2O molecules are also observed as major intermediates in the previous studies on the oxidation of *n*-butanol [Sarathy et al., 2009]. The plots indicate that as the temperature increases the number of molecules for both C_2H_4 and CH_2O decreases, indicating the molecules are unstable at high temperature and would convert quickly to final products. This observation is again in line with the experimental data [Cai et al., 2015].

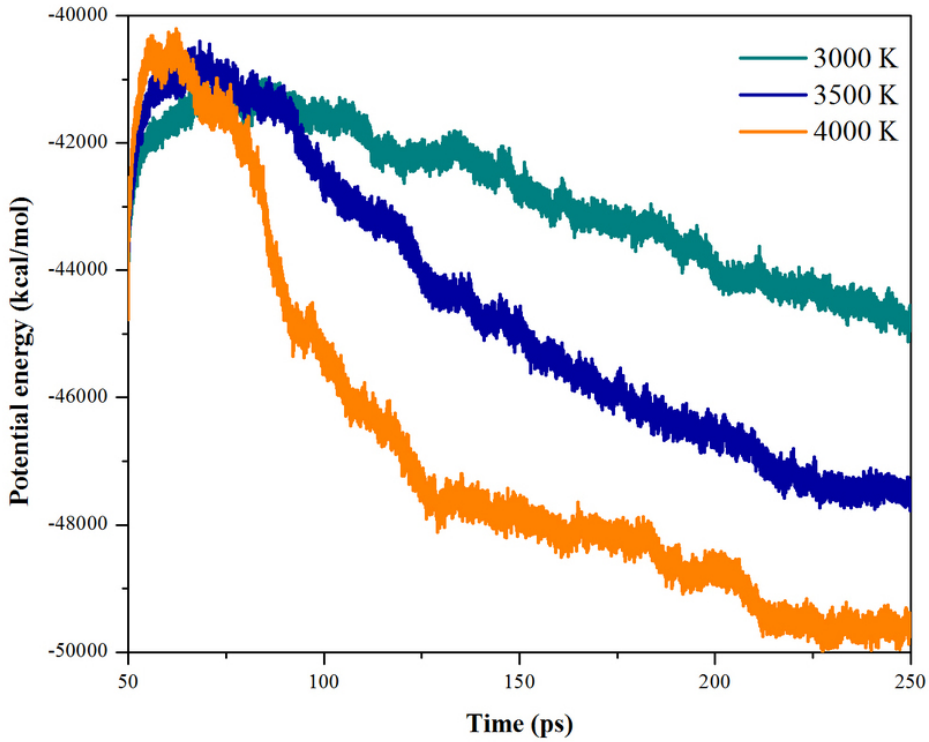

Figure 7.1.: Time evolution of potential energies at temperatures 3000-4000 K (NVT-MD simulation, $\Phi = 1.0$)

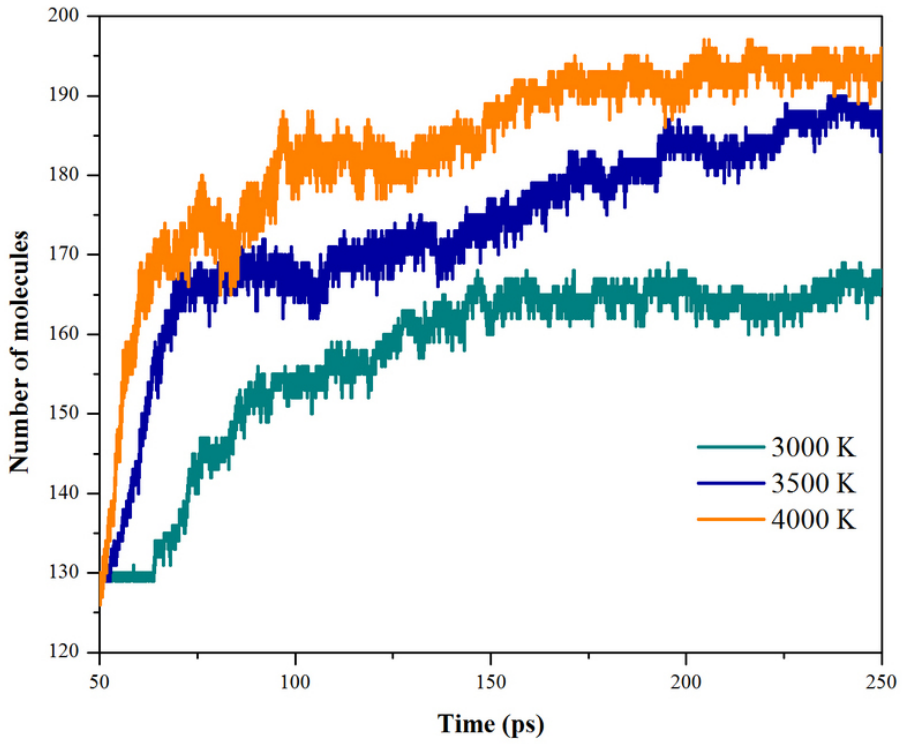

Figure 7.2.: Time evolution of total number of molecules at temperatures 3000-4000 K (NVT-MD simulation, $\Phi = 1.0$)

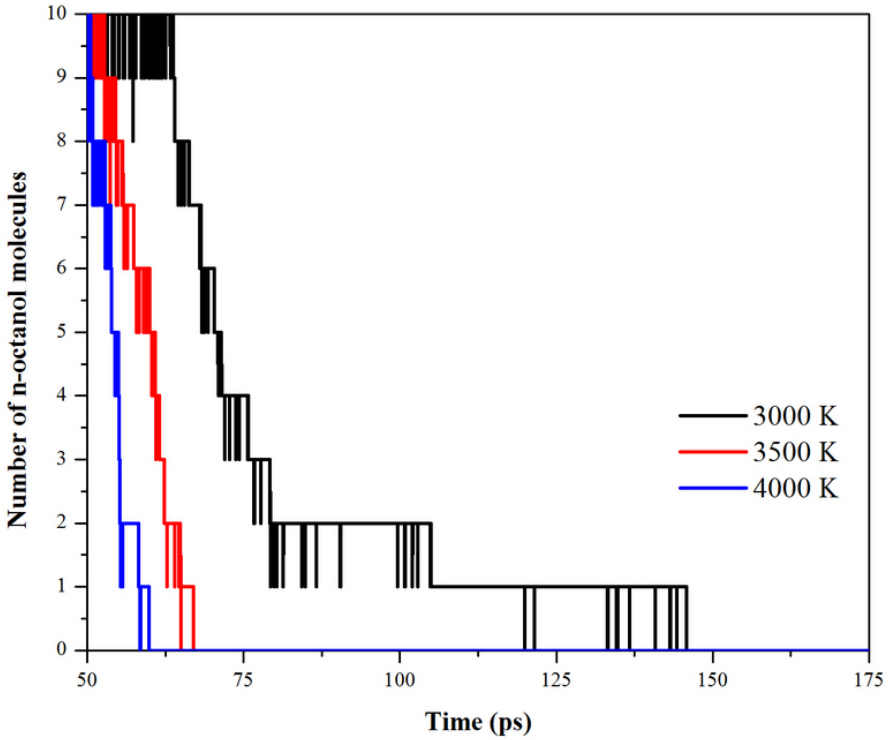

Figure 7.3.: Time evolution of *n*-octanol molecules at temperatures 3000-4000 K (NVT-MD simulation, $\Phi = 1.0$)

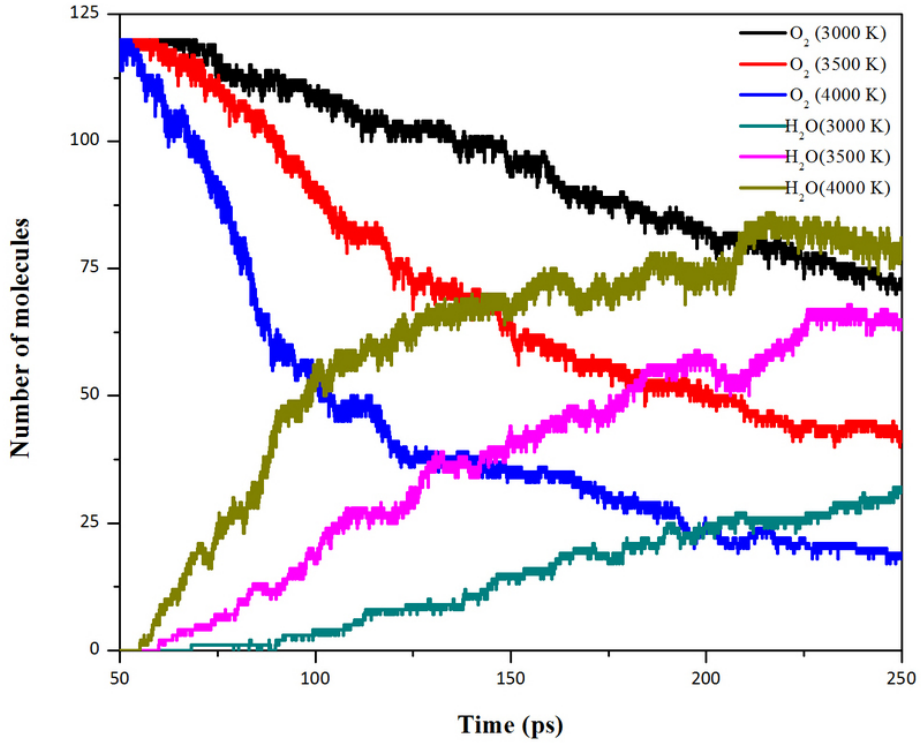

Figure 7.4.: Time evolution of O_2 and H_2O molecules at temperatures 3000-4000 K (NVT-MD simulation, $\Phi = 1.0$)

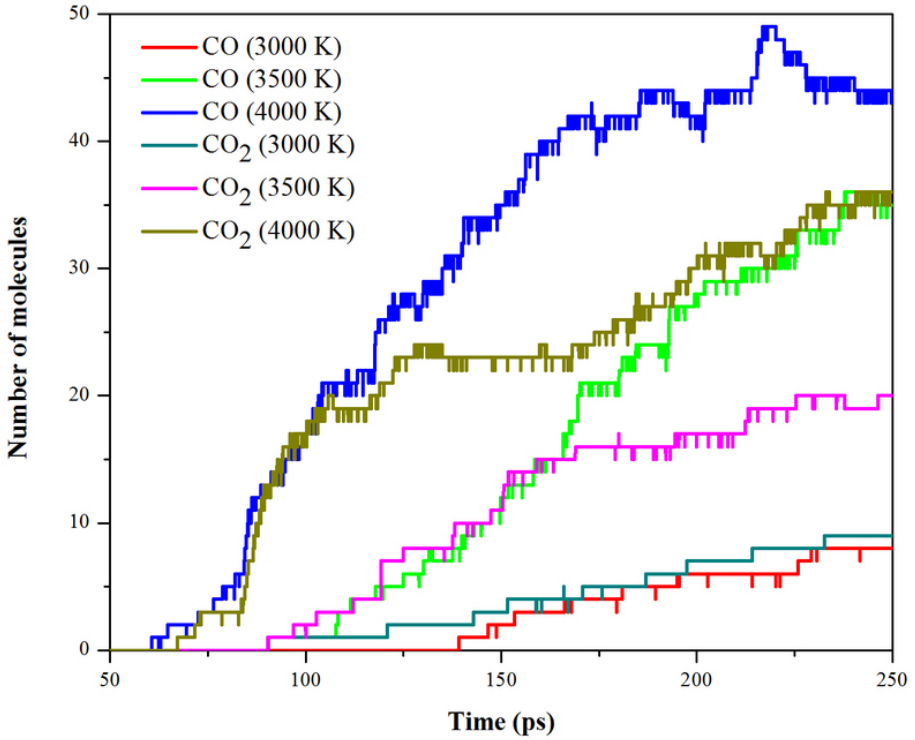

Figure 7.5.: Time evolution of CO and CO_2 molecules at temperatures 3000-4000 K (NVT-MD simulation, $\Phi = 1.0$)

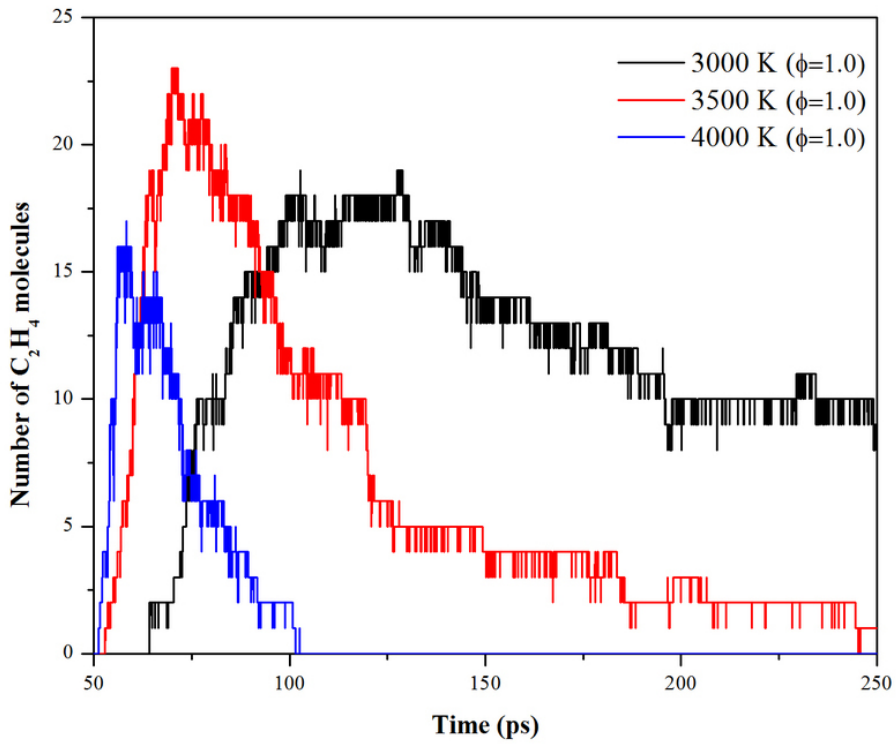

Figure 7.6.: Time evolution of C_2H_4 molecules at temperatures 3000-4000 K (NVT-MD simulation, $\Phi = 1.0$)

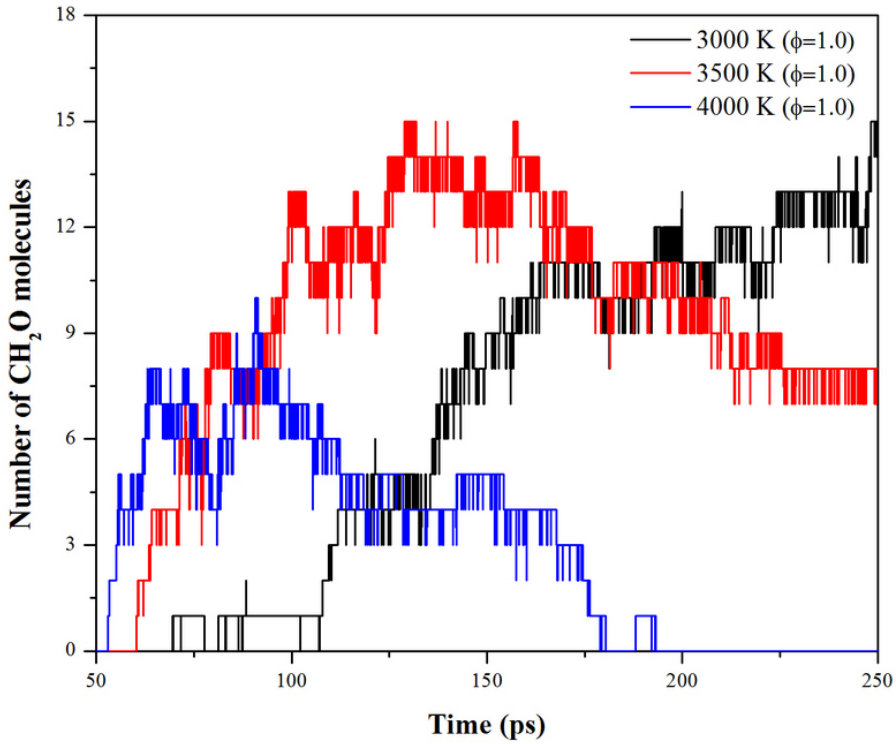

Figure 7.7.: Time evolution of CH_2O molecules at temperatures 3000-4000 K (NVT-MD simulation, $\Phi = 1.0$)

7.3.2. Effect of Equivalence Ratio on the oxidation of n-octanol

The effect of equivalence ratio on *n*-octanol oxidation has been analyzed by performing a series of NVT-MD simulations covering a range of equivalence ratios from 0.5 to 2.0. Water formation profile at 4000 K with different equivalence ratio are presented in Figure 7.8. The rate of water formation is found to be higher at lower equivalence ratio. CO and CO_2 formation at 4000 K with different equivalence ratio are presented in Figure 7.9. At lower equivalence ratio ($\Phi = 0.5$), initially rate of CO formation is higher, however with time due to presence of excess oxygen molecules, CO concentration were found to decrease with corresponding increase in CO_2 concentration. Major intermediate products (CH_2O and C_2H_4), at 4000 K with different equivalence ratio, are presented in Figure 7.10 and Figure 7.11 respectively. In oxygen-rich mixture, the conversion of CH_2O and C_2H_4 to final products is faster whereas in oxygen-lean mixture the residence time was higher. The time required for initiation as well as completion of *n*-octanol molecules oxidation has been determined for each simulation. *n*-octanol oxidation initiation time and completion time at the temperatures 3000-4000 K are depicted in Figure

7.12. It can be visualized that at constant equivalence ratio, reaction initiation time as well as completion time decreases with increase in temperature. This trend is again confirmed for each equivalence ratio.

The effect of equivalence ratio at different temperatures on reaction initiation time and completion time has been depicted in Figure 7.13. At higher temperature (4000 K), reaction initiation time decreases with increase in equivalence ratio whereas reaction completion was found to follow a contrary trend. This suggests that at higher temperature in absence of sufficient oxygen molecules (high equivalence ratio), *n*-octanol oxidation starts with pyrolysis reaction. But once reaction starts, presence of excess oxygen molecules (low equivalence ratio) aids in it for faster completion of *n*-octanol oxidation. At lower temperature (3000 K), the overall trend suggests that reaction initiation time as well as completion time is lower at low equivalence ratio (Φ = 0.5) when compared to high equivalence ratio (Φ = 2.0). The stoichiometric mixture was found to possess the slowest reaction kinetics. This suggest that in presence of excess oxygen molecules, *n*-octanol oxidation starts with H-abstraction mechanism rather than pyrolysis where an increase in the reaction rate leads to a faster completion of reaction.

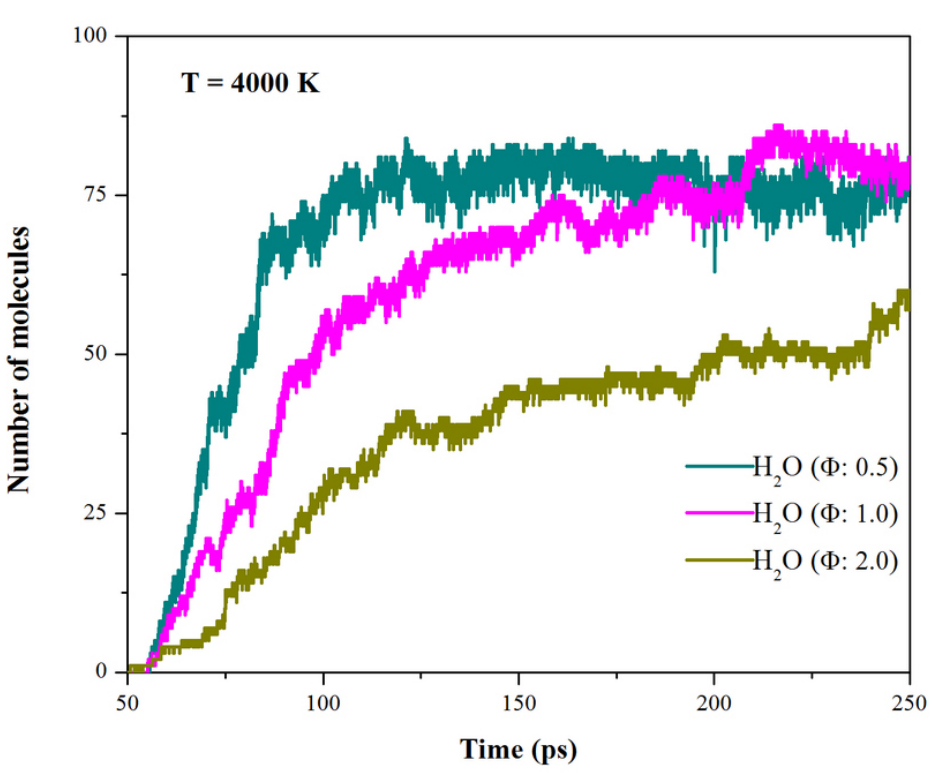

Figure 7.8.: Time evolution of H_2O molecules at 4000 K

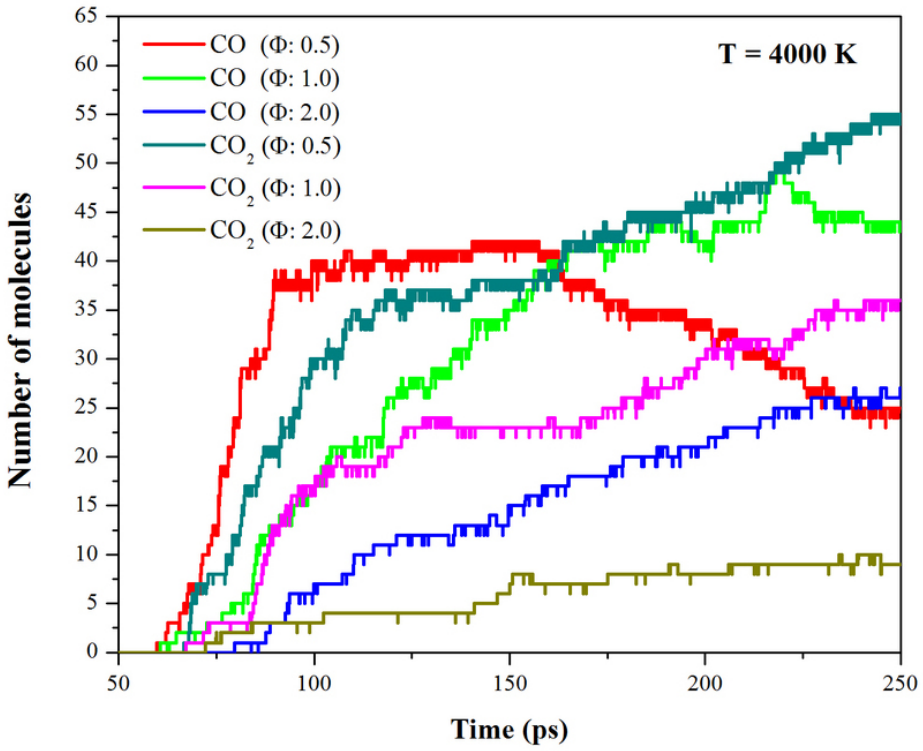

Figure 7.9.: Time evolution of CO and CO_2 molecules at 4000 K

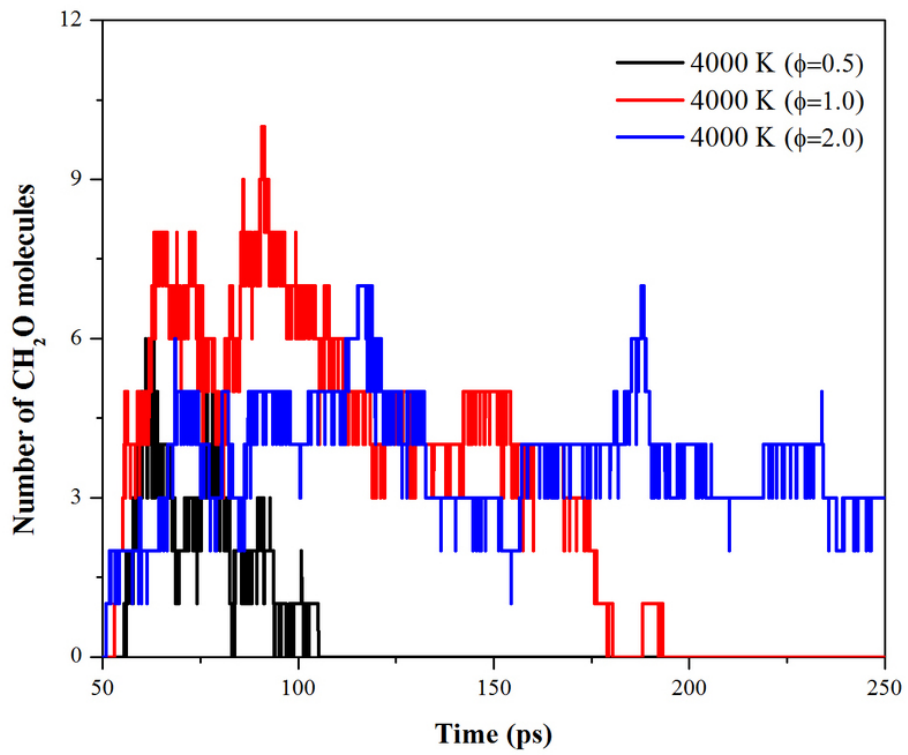

Figure 7.10.: Time evolution of CH_2O molecules at 4000 K

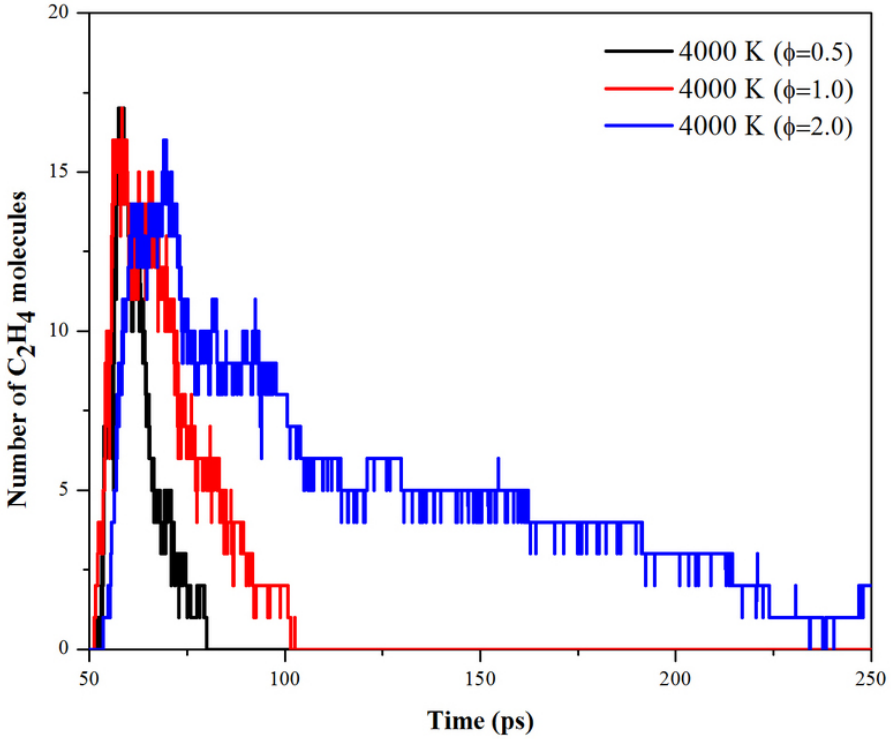

Figure 7.11.: Time evolution of C_2H_4 molecules at 4000 K

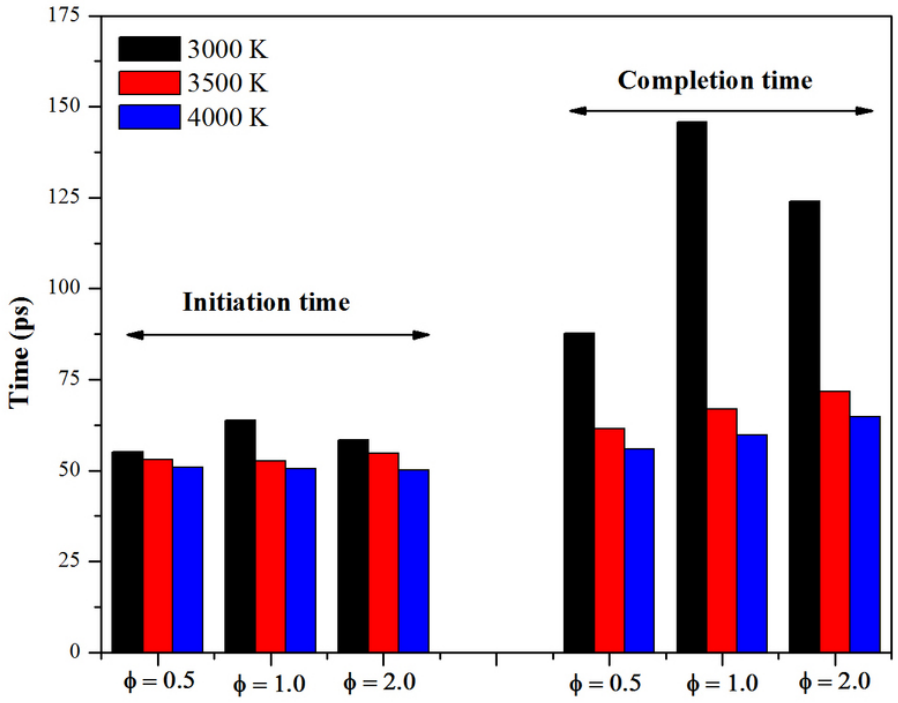

Figure 7.12.: Time evolution of the reaction initiation time and completion time at temperatures 3000-4000 K (NVT-MD simulation)

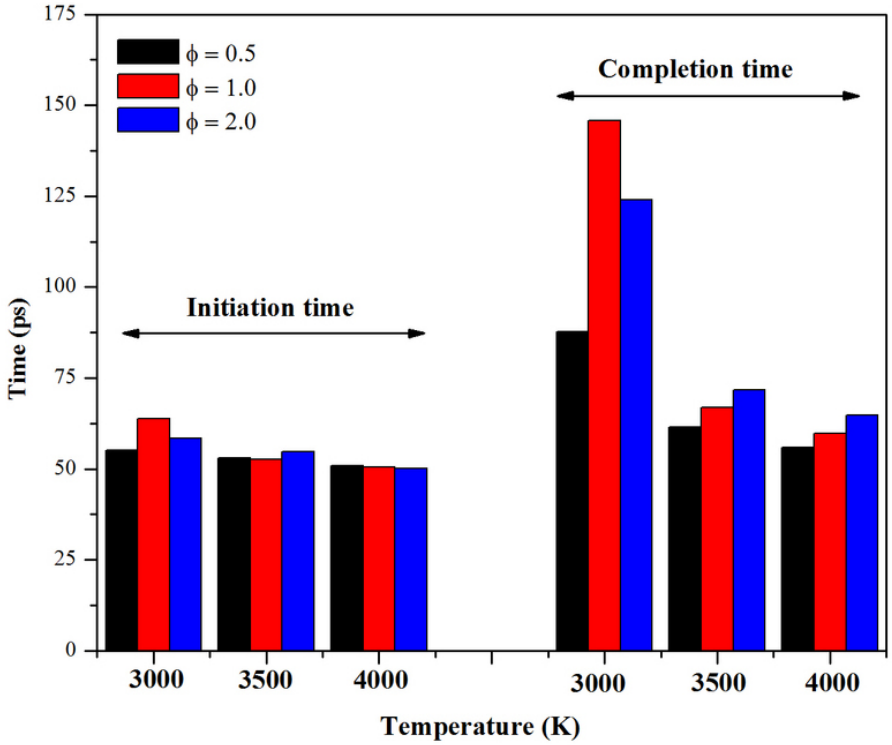

Figure 7.13.: Time evolution of the reaction initiation time and completion time at temperatures 3000-4000 K (NVT-MD simulation)

7.3.3. Proposed Reaction Mechanisms for oxidation of n-octanol

To further investigate the reaction mechanism of *n*-octanol oxidation, a series of NVT-MD simulations were carried out with two different approaches: (a) systems containing a single *n*-octanol molecule and 100 oxygen molecules at 4000 K; and (b) ten *n*-octanol molecules and 120 oxygen molecules with temperature ranging from 2000 K to 4000 K in 500 K intervals. Detailed analysis of *n*-octanol oxidation observed in ReaxFF simulation at 4000 K in approach-(a) is depicted in Figure 7.14 and Figure 7.15. The oxidation of *n*-octanol is initiated by the abstraction of chain end hydrogen by molecular oxygen to form intermediate radicals IM1 and hydroperoxyl (O_2H). In the next step, -H is released from C-7 carbon which leads to formation of IM2. The hydrogen radical quickly reacts with molecular oxygen to form a new hydroperoxyl (O_2H) radical. The IM2 radical then undergoes hemolytic C4-C5 bond cleavage to form IM3 and IM4 radicals. IM3 radical further undergoes hemolytic C2-C3 bond cleavage to form ethylene molecule and IM5 radical. In the following step, hydroperoxyl radical (O_2H) attacks the IM5 radical and form IM6 radical. The O-O bond of IM7 is cleaved to form hydroxyl (-OH)

and IM7 radical. The radical IM7 further undergoes hemolytic C1-C2 bond cleavage to form formaldehyde molecule and IM8 radical. H-atom released by IM8 and another formaldehyde molecule is then formed. The hydrogen radical formed quickly reacts with molecular oxygen and forms a new hydroperoxyl (O_2H) radical. Two hydroperoxyl (O_2H) radicals then combine together and form hydrogen peroxide and releases molecular oxygen.

The hydrogen peroxide is unstable and breaks into two hydroxyl radicals. The IM4 radical which forms by the hemolytic C4-C5 bond cleavage of IM2 remains unreactive so far. After sufficient time, it undergoes C6-C7 bond cleavage and forms another ethylene molecule and IM9 radical. It was observed that hydroxyl radical attacks the ethylene molecule and thus one water molecule along with another IM9 radical is formed. Therefore, System containing single *n*-octanol molecule and 100 oxygen molecules at 4000 K gave detailed mechanism for the formation of major intermediate products (formaldehyde and ethylene apart from hydroxyl and hydroperoxyl radicals) with a water molecule as final product. The above NVT-MD simulation was run for 250 ps during which no carbon monoxide and carbon dioxide was observed. Finally, the intermediate products such as formaldehyde and ethylene underwent oxidation reactions to produce final products such as water, carbon monoxide and carbon dioxide. In comparison to approach-1, it was observed that the initiation reactions of *n*-octanol oxidation in approach-2 were very complex and different. In addition to H-abstraction reactions by oxygen molecules, pyrolysis reactions were observed. The observed reactions are listed in Table 7.2. Reaction mechanisms also revealed that intermediates are mainly consumed by the build-up of hydroxyl and hydroperoxyl radicals. As pointed out by Cai et al. [Cai et al., 2015] which complemented our work, the hydrogen abstractions by OH and HO_2 radicals are found to be important reactions for ignition delay times.

Table 7.2.: Initiation Reactions observed in MD simulations at Φ=1.0 for Temperatures from 2000 to 4000 K

Tempearture (K)	Initiation Reactions
2000	Pyrolysis (C4-C5)
2500	H-abstraction by O_2 from C6
3000	Pyrolysis (C1-C2)
3500	Pyrolysis (C6-C7)
4000	H-abstraction by O_2 from C5

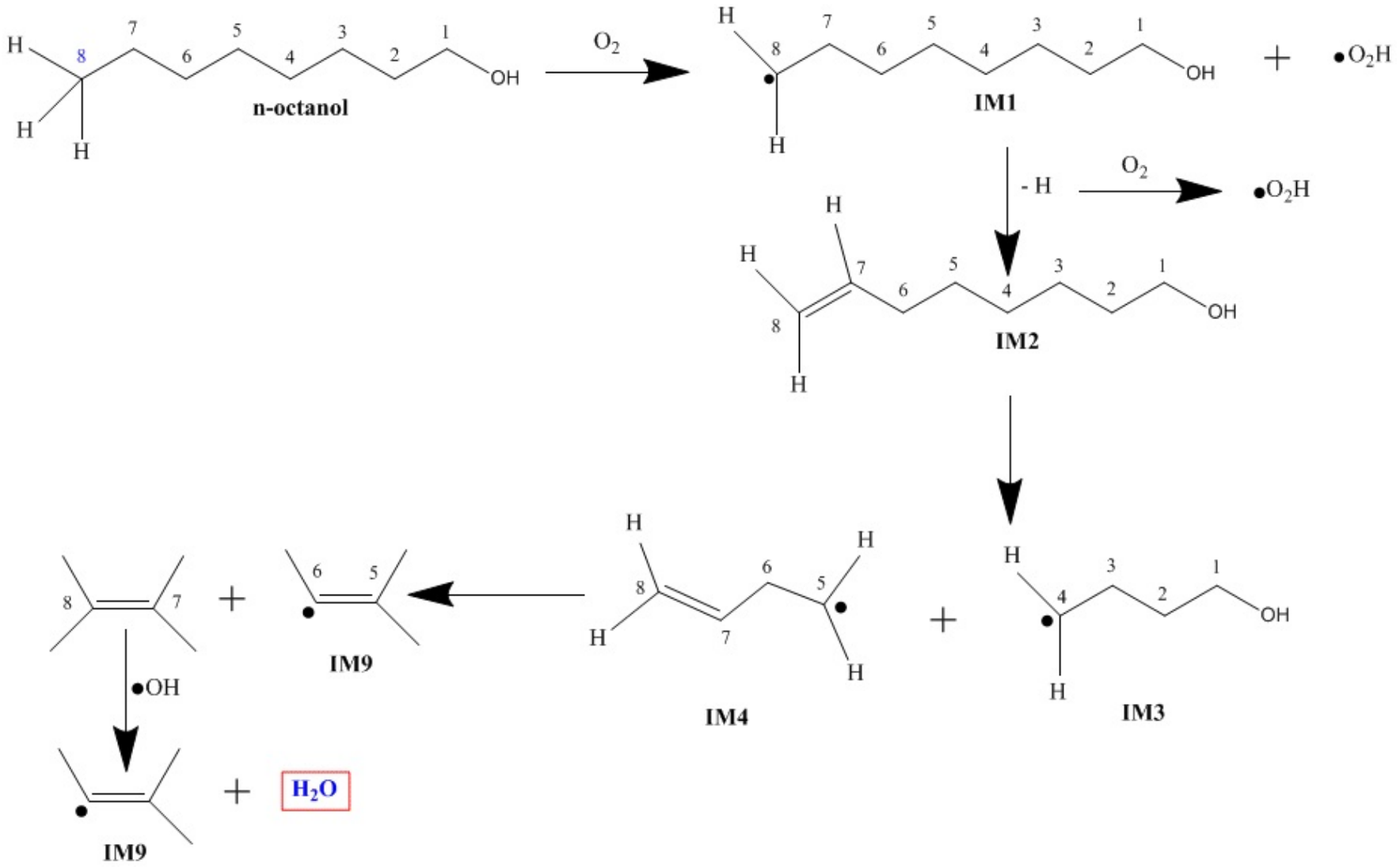

Figure 7.14.: Proposed reaction mechanism as observed during ReaxFF MD simulation of *n*-octanol oxidation

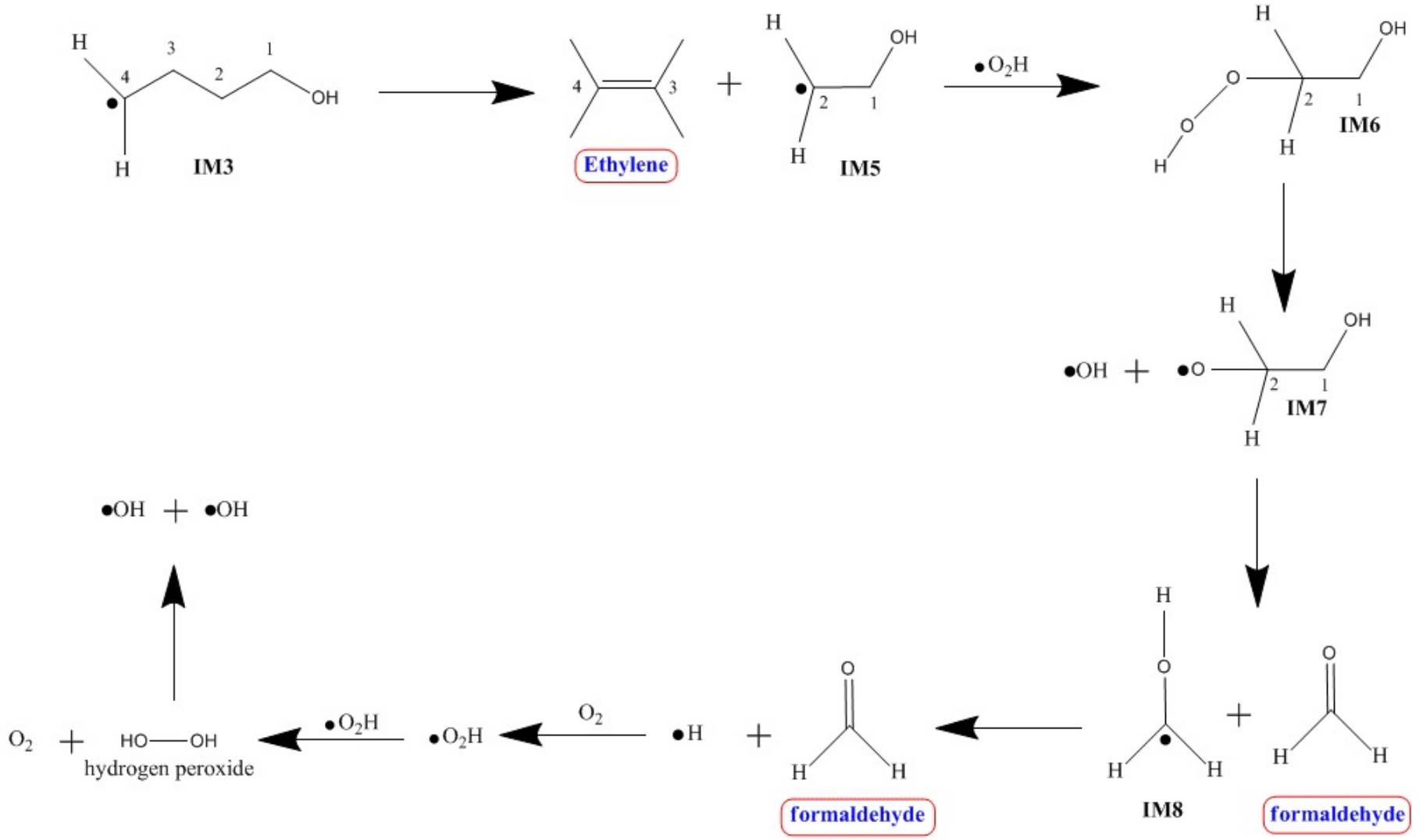

Figure 7.15.: Proposed reaction mechanism as observed during ReaxFF MD simulation of *n*-octanol oxidation

7.3.4. Proposed CO and CO2 formation mechanisms

CO and CO_2 formation mechanism from major intermediates such as formaldehyde and ethylene are presented in Figure 7.16. In one mechanism, oxidation of formaldehyde is initiated by the abstraction of hydrogen by molecular oxygen to form intermediate radical IM1 which is then finally converted to CO with the release of H radical. In another mechanism, formaldehyde undergoes hemolytic C-H bond cleavage to form intermediate radical IM2. IM2 is then converted by hydroxyl radical leading to the formation of radical IM3.This undergoes further hemolytic O-H bond cleavage to form radical IM4. IM4 rearranges and form IM5 which is finally converted to CO_2 with the release of H radical. Similarly, ethylene oxidation is initiated by the attack of hydroxyl radical. In one mechanism, formaldehyde is formed which further undergo oxidation and form either CO or CO_2 as explained above. In another mechanism, ethylene is converted into formaldehyde and CO. As observed, CO is formed from formaldehyde by 2-step mechanisms whereas CO_2 is formed by 5-step mechanism. Similarly, starting with ethylene, CO and formaldehyde is formed. The formaldehyde further converts into CO or CO_2. This explains the reason why the rate of formation of CO is more than CO_2 as observed during ReaxFF MD simulations and experiments. Therefore, CO and CO_2 formation from formaldehyde and ethylene starts with either an attack of molecular oxygen or hydroxyl radical or by hemolytic O-H bond cleavage.

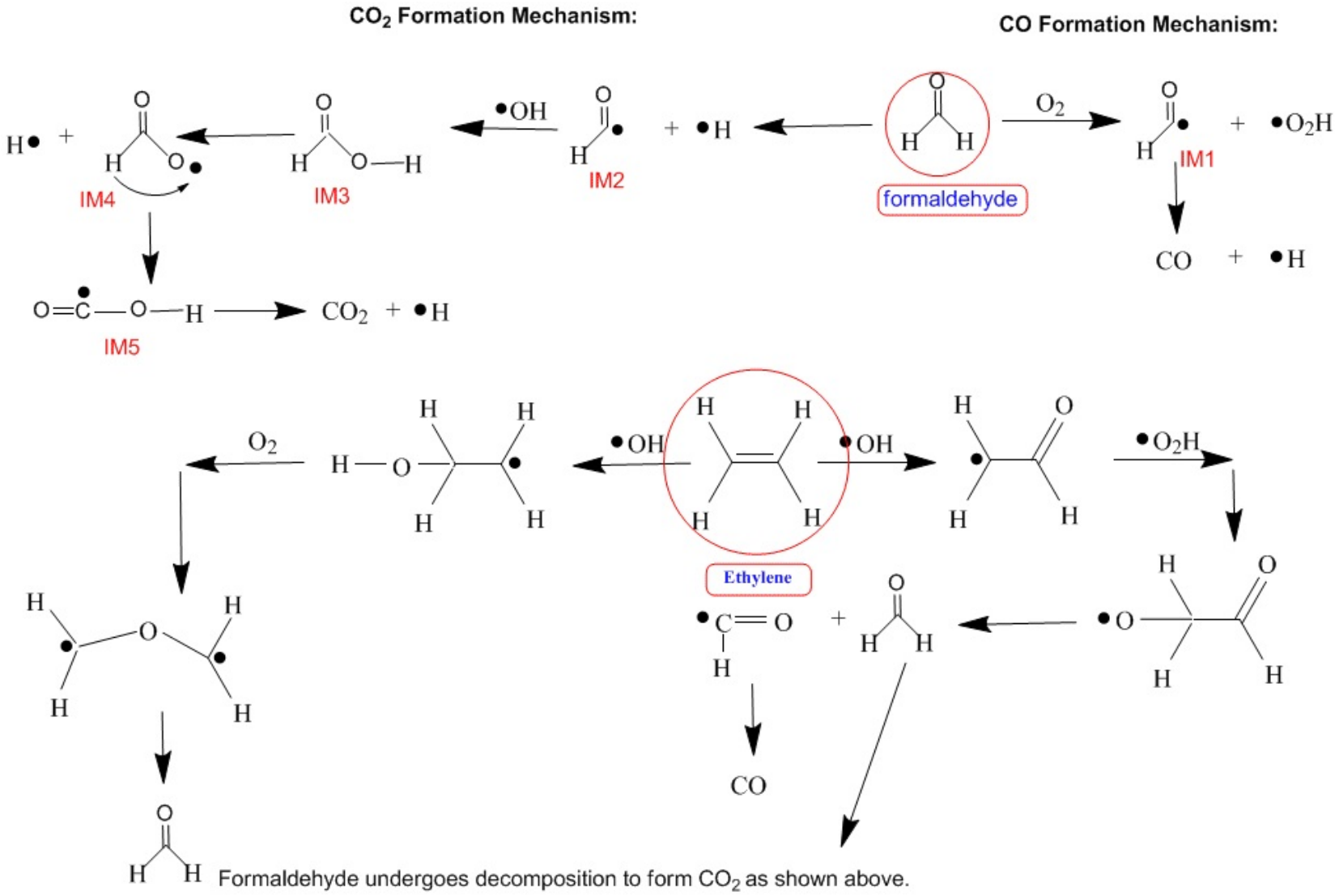

Figure 7.16.: Proposed reaction mechanism for the formation of CO and CO_2 for *n*-octanol oxidation

7.4 Conclusions

In order to understand the combustion characteristics of *n*-octanol, reactive molecular dynamics (ReaxFF MD) simulation of *n*-octanol have been performed at various temperatures (2000 K - 4000 K) with equivalence ratios ranging from 0.5-2.0. From the ReaxFF MD simulations, we have found that the oxidation of *n*-octanol is initiated mainly through two routes, (1) H-abstraction reaction by oxygen molecules and (2) the cleavage of C-C bond. It has been observed that rate of formation of CO and CO_2 are almost similar at low temperature (3000 K). With higher temperature the rate of formation of CO is more than that of CO_2. The major intermediate products found in ReaxFF MD simulations are ethylene followed by formaldehyde. A detailed reaction mechanism has been proposed for the formation of major intermediates (C_2H_4 and CH_2O) and final products (CO and CO_2). Reaction mechanisms reveal that intermediates are mainly consumed by the build-up of hydroxyl and hydroperoxyl radicals. In summary, the present work gives a pathway for understanding the *n*-Octanol combustion as well as intermediate product species distribution.

REFERENCES

[Akhtar et al., 2015] Akhtar, M. K., Dandapani, H., Thiel, K., and Jones, P. R. (2015). Microbial production of 1-octanol: A naturally excreted biofuel with diesel-like properties. *Metabolic Engineering Communications*, 2:1–5.

[Basha et al., 2009] Basha, S. A., Gopal, K. R., and Jebaraj, S. (2009). A review on biodiesel production, combustion, emissions and performance. *Renewable and Sustainable Energy Reviews*, 13:1628–1634.

[Berendsen et al., 1984] Berendsen, H. J. C., Postma, J. P. M., van Gunsteren, W. F., DiNola, A., and Haak, J. R. (1984). Molecular dynamics with coupling to an external bath. *The Journal of Chemical Physics*, 81:3684–3690.

[Bergthorson and Thomson, 2015] Bergthorson, J. M. and Thomson, M. J. (2015). A review of the combustion and emissions properties of advanced transportation biofuels and their impact on existing and future engines. *Renewable and Sustainable Energy Reviews*, 42:1393–1417.

[Borugadda and Goud, 2012] Borugadda, V. B. and Goud, V. V. (2012). Biodiesel production from renewable feedstocks: Status and opportunities. *Renewable and Sustainable Energy Reviews*, 16:4763 – 4784.

[Bozell and Petersen, 2010] Bozell, J. J. and Petersen, G. R. (2010). Technology development

for the production of biobased products from biorefinery carbohydrates-the us department of energys top 10 revisited. *Green Chem.*, 12:539–554.

[Brenner, 1990] Brenner, D. W. (1990). Empirical potential for hydrocarbons for use in simulating the chemical vapor deposition of diamond films. *Phys. Rev. B*, 42:9458–9471.

[Cai et al., 2015] Cai, L., Uygun, Y., Togbe, C., Pitsch, H., Olivier, H., Dagaut, P., and Sarathy, S. M. (2015). An experimental and modeling study of n-octanol combustion. *Proceedings of the Combustion Institute*, 35:419–427.

[Chenoweth et al., 2009] Chenoweth, K., van Duin, A. C. T., Dasgupta, S., and Goddard III, W. A. (2009). Initiation mechanisms and kinetics of pyrolysis and combustion of jp-10 hydrocarbon jet fuel. *The Journal of Physical Chemistry A*, 113:1740–1746.

[Chenoweth et al., 2008] Chenoweth, K., van Duin, A. C. T., and Goddard, W. A. (2008). Reaxff reactive force field for molecular dynamics simulations of hydrocarbon oxidation. *The Journal of Physical Chemistry A*, 112:1040–1053.

[Corma et al., 2007] Corma, A., Iborra, S., and Velty, A. (2007). Chemical routes for the transformation of biomass into chemicals. *Chemical Reviews*, 107:2411–2502.

[Frassoldati et al., 2010] Frassoldati, A., Cuoci, A., Faravelli, T., Niemann, U., Ranzi, E., Seiser, R., and Seshadri, K. (2010). An experimental and kinetic modeling study of n-propanol and iso-propanol combustion. *Combustion and Flame*, 157:2–16.

[Goddard et al., 2006a] Goddard, W. A., Merinov, B., van Duin, A., Jacob, T., Blanco, M., Molinero, V., Jang, S., and Jang, Y. (2006a). Multi-paradigm multi-scale simulations for fuel cell catalysts and membranes. *Molecular Simulation*, 32:251–268.

[Goddard et al., 2006b] Goddard, W. A., van Duin, A., Chenoweth, K., Cheng, M.-J., Pudar, S., Oxgaard, J., Merinov, B., Jang, Y. H., and Persson, P. (2006b). Development of the reaxff reactive force field for mechanistic studies of catalytic selective oxidation processes on bimoo. *Topics in Catalysis*, 38:93.

[Harvey and Meylemans, 2011] Harvey, B. G. and Meylemans, H. A. (2011). The role of butanol in the development of sustainable fuel technologies. *Jour. of Chemical Technology & Biotechnology*, 86:2–9.

[Heuser et al., 2013] Heuser, B., Kremer, F., Pischinger, S., Julis, J., and Leitner, W. (2013). Optimization of diesel combustion and emissions with newly derived biogenic alcohols. In *SAE Technical Paper*. SAE International.

[http://www.scm.com,] http://www.scm.com. Vrije universiteit, amsterdam, the netherlands (2016).

[Jin et al., 2011] Jin, C., Yao, M., Liu, H., fon F. Lee, C., and Ji, J. (2011). Progress in the production and application of n-butanol as a biofuel. *Renewable and Sustainable Energy Reviews*, 15:4080–4106.

[Julis and Leitner, 2012] Julis, J. and Leitner, W. (2012). Synthesis of 1-octanol and 1,1-dioctyl ether from biomass-derived platform chemicals. *Angewandte Chemie International Edition*, 51:8615–8619.

[Kerschgens et al., 2016] Kerschgens, B., Cai, L., Pitsch, H., Heuser, B., and Pischinger, S. (2016). Di-n-buthylether, n-octanol, and n-octane as fuel candidates for diesel engine combustion. *Combustion and Flame*, 163:66–78.

[Koberg and Gedanken, 2012] Koberg, M. and Gedanken, A. (2012). Optimization of biodiesel production from oils, cooking oils, microalgae, and castor and jatropha seeds: probing various heating sources and catalysts. *Energy Environ. Sci.*, 5:7460–7469.

[Kremer et al., 2015] Kremer, F., Blank, L. M., Jones, P. R., and Akhtar, M. K. (2015). A comparison of the microbial production and combustion characteristics of three alcohol biofuels: Ethanol, 1-butanol, and 1-octanol. *Frontiers in Bioengineering and Biotechnology*, 3:112.

[Nielson et al., 2005] Nielson, K. D., van Duin, A. C. T., Oxgaard, J., Deng, W.-Q., and Goddard, W. A. (2005). Development of the reaxff reactive force field for describing transition metal

catalyzed reactions, with application to the initial stages of the catalytic formation of carbon nanotubes. *The Journal of Physical Chemistry A*, 109:493–499.

[Nigam and Singh, 2011] Nigam, P. S. and Singh, A. (2011). Production of liquid biofuels from renewable resources. *Progress in Energy and Combustion Science*, 37:52–68.

[Sarathy et al., 2009] Sarathy, S., Thomson, M., Togbe, C., Dagaut, P., Halter, F., and Mounaim-Rousselle, C. (2009). An experimental and kinetic modeling study of n-butanol combustion. *Combustion and Flame*, 156:852–864.

[Sarathy et al., 2014] Sarathy, S. M., Obwald, P., Hansen, N., and Kohse-Hoinghaus, K. (2014). Alcohol combustion chemistry. *Progress in Energy and Combustion Science*, 44:40–102.

[Sarin, 2012] Sarin, A. (2012). *Biodiesel: Production and Properties*. RSC, UK.

[Shahid and Jamal, 2008] Shahid, E. M. and Jamal, Y. (2008). A review of biodiesel as vehicular fuel. *Renewable and Sustainable Energy Reviews*, 12:2484–2494.

[Shahir et al., 2015] Shahir, V., Jawahar, C., and Suresh, P. (2015). Comparative study of diesel and biodiesel on ci engine with emphasis to emissions-a review. *Renewable and Sustainable Energy Reviews*, 45:686–697.

[Tersoff, 1988] Tersoff, J. (1988). New empirical approach for the structure and energy of covalent systems. *Phys. Rev. B*, 37:6991–7000.

[van Duin et al., 2001] van Duin, A. C. T., Dasgupta, S., Lorant, F., and Goddard, W. A. (2001). Reaxff:a reactive force field for hydrocarbons. *The Journal of Physical Chemistry A*, 105:9396–9409.

CHAPTER 8

Conclusions and Scope for future work

8.1 Research Conclusions

The major conclusions of the studies are discussed below:

Solubility of bio-chemicals in aqueous phase in terms of intermolecular interaction energy using supermolecule approach was theoretically investigated. It was found that the computed interaction energy of the chosen molecules in water predicts the correct trend of the experimentally reported solubility parameters of the corresponding molecules. Thus, this approach can be used for computing the trend of distribution coefficients when experimental data are not available. Localized Molecular Orbital-Energy Decomposition Analysis (LMO-EDA) partitioned the interaction energy into its chemical origins (e.g. electrostatics, exchange-repulsion, polarization and charge transfer) which helped us in understanding the nature of interactions and this can be used to develop force fields for molecular simulations.

In terms of distribution co-efficient, selectivity and solvent loss, ionic liquid, [BMIM][Tf2N], was found to be the best solvent for the extraction of acetic acid, furfural and acetol from aqueous solution.

Liquid-liquid equilibria data for multicomponent systems were correlated by the UNIQUAC and NRTL models. The binary interaction parameters were estimated using the Cuckoo Search algorithm. It has been found that population size of 20 is sufficient to satisfactorily predict the LLE with high accuracy. RMSD results are extremely encouraging, with deviations in phase compositions less than unity for all systems indicating a better fit. The performance of the cuckoo search algorithm was compared against genetic algorithm and particle swarm optimization algorithm. The comparison showed a higher efficiency for the CS algorithm in solving global optimization problems.

PC-SAFT EoS was found to correctly predict the LLE behaviour of polar and associating biochemical LLE ternary systems based on pure component and binary system data only. Prediction was better in mixtures where all the components were associating in nature compared to mixtures consisting of polar components.

Gibbs Ensemble Monte Carlo molecular simulations in isobaric-isothermal (NPT) ensemble with Transferable Potentials for Phase Equilibria (United-Atom) and TIP4P force fields agreed favorably with the experimental data for all the systems over the entire composition range.

Reactive molecular dynamics (ReaxFF MD) simulations gave insights in understanding the re-

action mechanism and product distribution for the combustion for oxygenated fuel.

8.2 Future work

(1) In the present work, solvents were selected for the extraction of various components based on distribution co-efficient and selectivity. Using these solvents, conceptual processes can be developed and the entire process can be optimized in Aspen Plus. Based on optimization, best solvent can be selected and further studies can be carried out for the development of industrial level process.

(2) The success of PC-SAFT EoS depends on the correct assumption of association models of components. However, a clear basis for choosing a certain association scheme for components has not yet been defined, thereby limiting the scope and generality of the equation of state framework. Therefore, Molecular dynamic simulations can be used to evaluate the distribution of hydrogen bonds in various liquid mixtures and general guidelines can be made regarding association schemes for compounds of different natures.

(3) In the present work, Transferable Potentials for Phase Equilibria (United-Atom) and TIP4P force fields were used to study the ternary liquid-liquid behaviour through Gibbs Ensemble Monte Carlo approach. The same study can be carried out with other force fields such as SPC, TIP3P, TIP5P and all atom models to decide which combination is best for LLE study.

(4) Monte Carlo Simulations were carried out with Towhee freeware which runs on a single processor which in turns increase the computational cost of the simulation. Therefore, Molecular dynamics simulation can be used to study the behaviour of liquid mixtures to generate the tie-line data. This can be compared against experimental as well as Monte Carlo Simulation predicted tie line data.

APPENDIX A

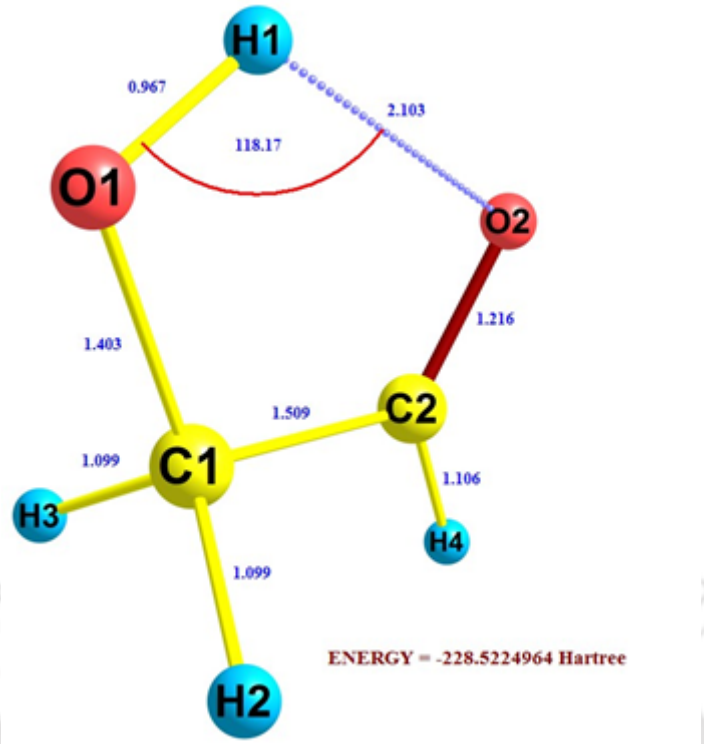

Figure A.1.: Optimized equilibrium geometry of Cis cis (Cc) conformer of glycolaldehyde

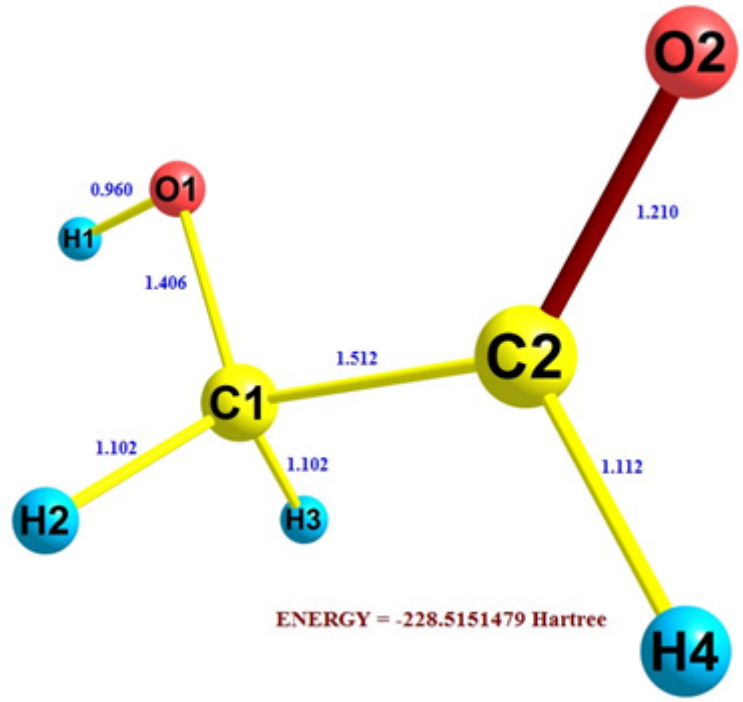

Figure A.2.: Optimized equilibrium geometry of Cis trans (Ct) conformer of glycolaldehyde

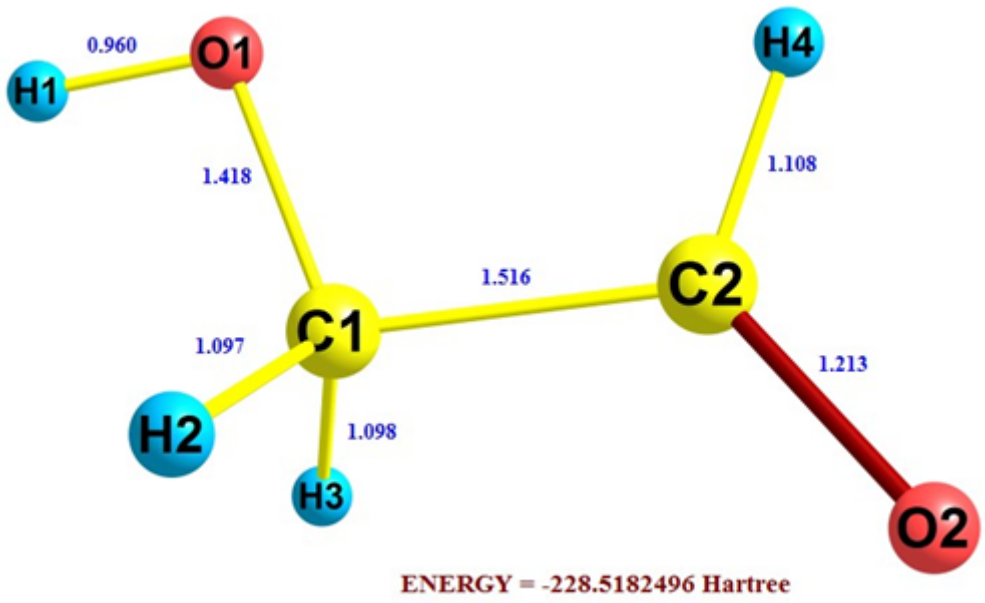

Figure A.3.: Optimized equilibrium geometry of Trans trans (Tt) conformer of glycolaldehyde

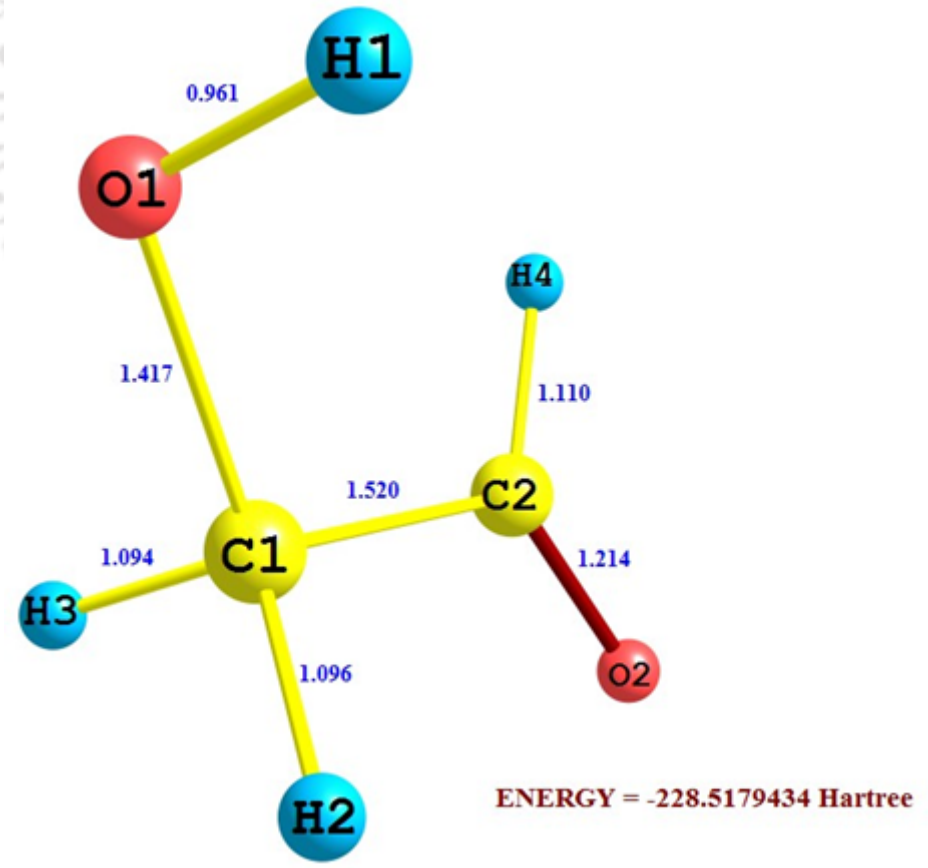

Figure A.4.: Optimized equilibrium geometry of Trans gauche (Tg) conformer of glycolaldehyde

Table A.1.: Calculated Bond length (in Å) of O-H group of Glycolaldehyde and water in isolated state and in complexes

Complex	Group	Bond Length in Isolated	Bond Length in Complex
Cc-1	O-H of Glycolaldehyde	0.967	0.970
	O-H of water	0.960	0.965
Cc-2	O-H of water	0.960	0.965
Cc-3	O-H of water	0.960	0.966
Cc-4	O-H of Glycolaldehyde	0.967	0.969
	O-H of water	0.960	0.961
Ct-1	O-H of water	0.960	0.967
Ct-2	O-H of Glycolaldehyde	0.960	0.967
Ct-3	O-H of water	0.960	0.965
Tt-1	O-H of water	0.960	0.967
Tt-2	O-H of water	0.960	0.965
Tt-3	O-H of Glycolaldehyde	0.960	0.966
Tg-1	O-H of water	0.960	0.966
Tg-2	O-H of water	0.960	0.966

Table A.2.: MP2 Energy (KJ/mol) of Glycolaldehyde and water complexes with respect to Cc-1 complex

	Hartree	KJ/mol	ΔE(KJ/mol)
Cc-1	-304.8103038	-803340	0.0
Cc-2	-304.8059286	-803329	11.5
Cc-3	-304.8069099	-803331	8.9
Cc-4	-304.8062609	-803330	10.7
Ct-1	-304.7993992	-803312	28.7
Ct-2	-304.8019146	-803318	22.1
Ct-3	-304.8024628	-803320	20.7
Tt-1	-304.8015008	-803317	23.2
Tt-2	-304.8027097	-803320	20.0
Tt-3	-304.8050772	-803327	13.8
Tg-1	-304.8014666	-803317	23.3
Tg-2	-304.8031043	-803321	19.0

Table A.3.: Natural charges by Natural Bond Order (NBO) Method for Cis cis (Cc) conformer of glycolaldehyde and water complexes

	Cis cis	Cc-1	Cc-2	Cc-3	Cc-4
C1	-0.051	-0.050	-0.053	-0.057	-0.047
C2	0.524	0.546	0.537	0.526	0.541
H1	0.484	0.509	0.483	0.495	0.518
H2	0.163	0.155	0.167	0.176	0.159
H3	0.163	0.169	0.167	0.176	0.159
H4	0.106	0.094	0.134	0.110	0.097
O1	-0.758	-0.657	-0.757	-0.788	-0.780
O2	-0.631	-0.776	-0.671	-0.633	-0.654
TOTAL	0.000	-0.010	+0.007	+0.006	-0.007
O	-0.911	-0.960	-0.949	-0.948	-0.951
H	0.456	0.500	0.485	0.489	0.469
H	0.456	0.470	0.457	0.453	0.489
TOTAL	0.000	+0.010	-0.007	-0.006	+0.007

Table A.4.: Natural charges by Natural Bond Order (NBO) Method for Cis trans (Ct) conformer of glycolaldehyde and water complexes

	Cis trans	Ct-1	Ct-2	Ct-3
C1	-0.048	-0.050	-0.041	-0.051
C2	0.519	0.533	0.524	0.525
H1	0.458	0.460	0.500	0.471
H2	0.151	0.156	0.147	0.164
H3	0.151	0.156	0.147	0.159
H4	0.086	0.113	0.080	0.095
O1	-0.734	-0.734	-0.773	-0.597
O2	-0.583	-0.623	-0.593	-0.759
TOTAL	0.000	+0.010	-0.010	+0.008
O	-0.911	-0.952	-0.939	-0.952
H	0.456	0.488	0.475	0.487
H	0.456	0.454	0.475	0.458
TOTAL	0.000	-0.010	+0.010	-0.008

Table A.5.: Natural charges by Natural Bond Order (NBO) Method for Trans trans (Tt) conformer of glycolaldehyde and water complexes

	Trans trans	Tt-1	Tt-2	Tt-3
C1	-0.056	-0.056	-0.061	-0.051
C2	0.535	0.551	0.546	0.540
H1	0.466	0.467	0.473	0.507
H2	0.164	0.166	0.166	0.159
H3	0.163	0.165	0.180	0.160
H4	0.107	0.129	0.107	0.102
O1	-0.764	-0.761	-0.790	-0.801
O2	-0.614	-0.651	-0.617	-0.624
TOTAL	0.000	+0.010	+0.005	-0.011
O	-0.911	-0.949	-0.947	-0.940
H	0.456	0.486	0.484	0.475
H	0.456	0.453	0.458	0.475
TOTAL	0.000	-0.010	-0.005	+0.011

Table A.6.: Natural charges by Natural Bond Order (NBO) Method for Trans gauche (Tg) conformer of glycolaldehyde and water complexes

	Trans gauche	Tg-1	Tg-2
C1	-0.057	-0.059	-0.060
C2	0.517	0.533	0.518
H1	0.097	0.122	0.112
H2	0.163	0.166	0.166
H3	0.182	0.185	0.194
H4	0.456	0.457	0.466
O1	-0.751	-0.749	-0.780
O2	-0.606	-0.647	-0.609
TOTAL	0.000	+0.009	+0.006
O	-0.911	-0.949	-0.952
H	0.456	0.486	0.458
H	0.456	0.455	0.487
TOTAL	0.000	-0.009	-0.006

Table A.7.: Results of Localized Molecular Orbital-Energy Decomposition Analysis (LMO-EDA) for Glycolaldehyde and water complexes carried out at the MP2/6-311++G** Level. [All Values are in Kcal/mol]

	ΔE^{ES}	ΔE^{EX}	ΔE^{REP}	ΔE^{POL}	ΔE^{DISP}	$\Delta E(INT)$
Cc-1	-16.67	-17.76	32.23	-4.79	-0.47	-7.46
Cc-2	-8.52	-7.87	13.98	-1.93	0.06	-4.28
Cc-3	-8.51	-8.07	14.41	-1.97	-0.71	-4.85
Cc-4	-11.25	-12.18	21.81	-2.91	-0.53	-5.06
Ct-1	-9.38	-8.99	16.06	-2.38	0.02	-4.67
Ct-2	-10.33	-9.89	17.96	-2.83	-0.38	-5.47
Ct-3	-10.41	-9.85	17.52	-2.27	-0.51	-5.52
Tt-1	-8.62	-8.52	15.22	-2.21	0.05	-4.08
Tt-2	-9.26	-11.34	20.18	-2.25	-1.50	-4.17
Tt-3	-10.43	-9.80	17.82	-2.89	-0.31	-5.61
Tg-1	-8.73	-8.46	15.06	-2.12	0.01	-4.24
Tg-2	-9.71	-10.91	19.40	-2.27	-1.14	-4.63

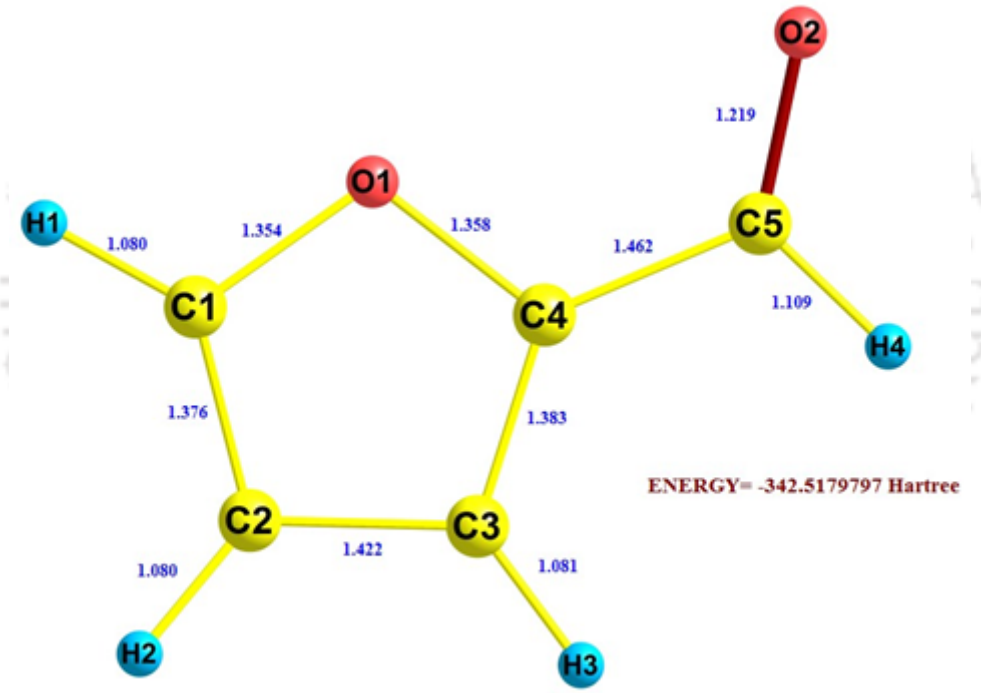

Figure A.5.: Optimized equilibrium geometry of Cis-OO Furfural

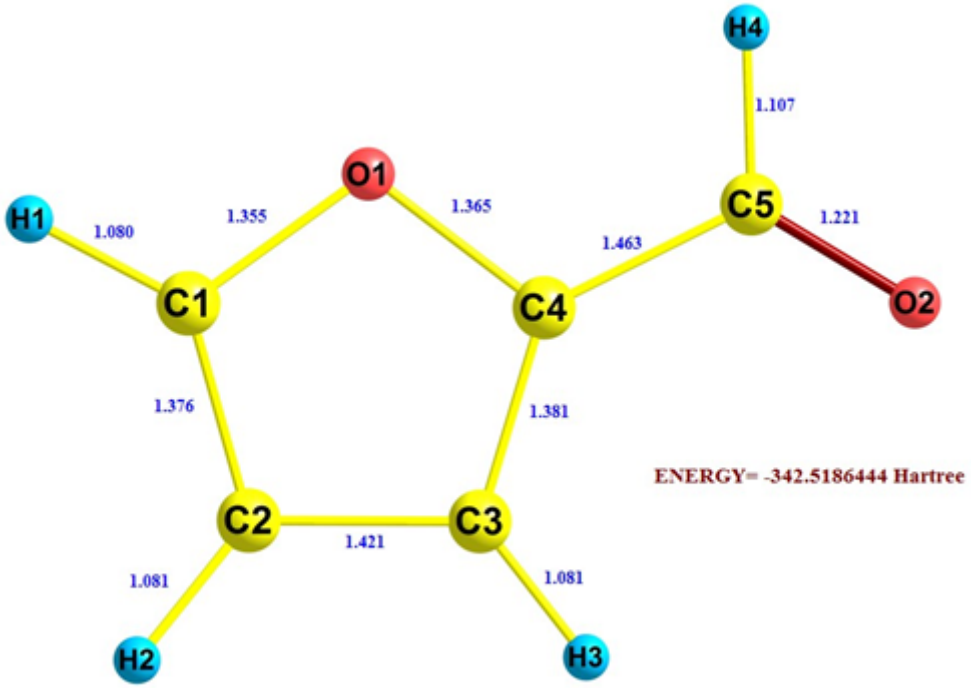

Figure A.6.: Optimized equilibrium geometry of Trans-OO Furfural

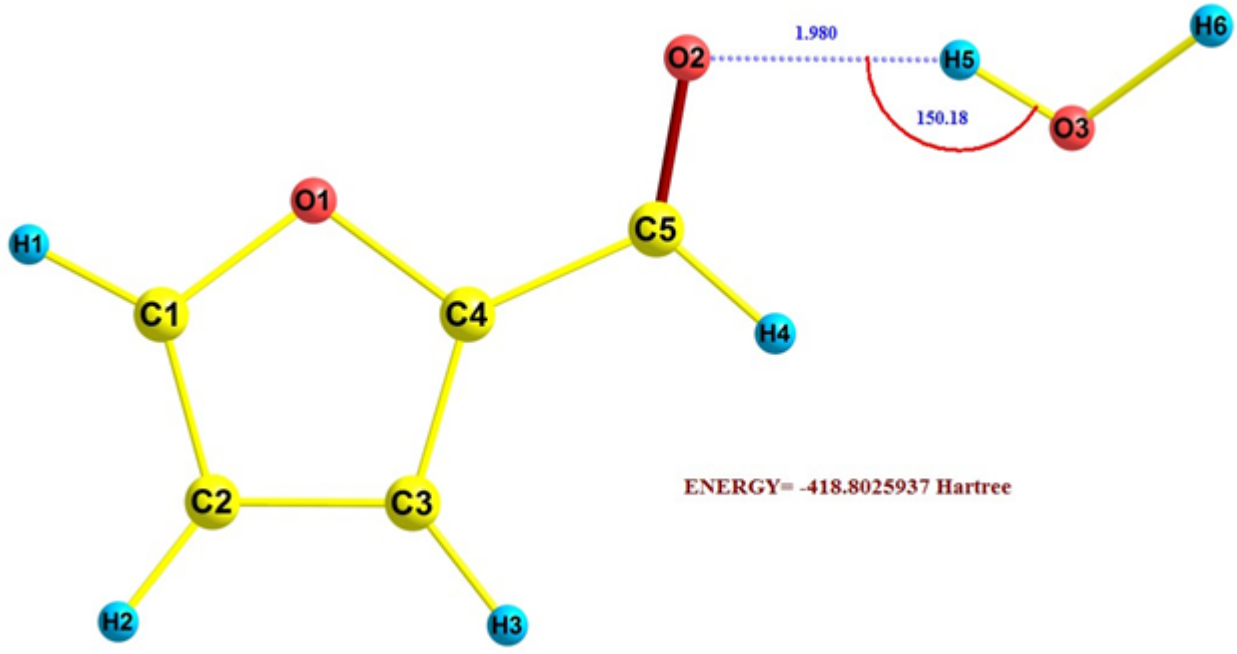

Figure A.7.: Optimized equilibrium geometry of Furfural-water complex FURC-1

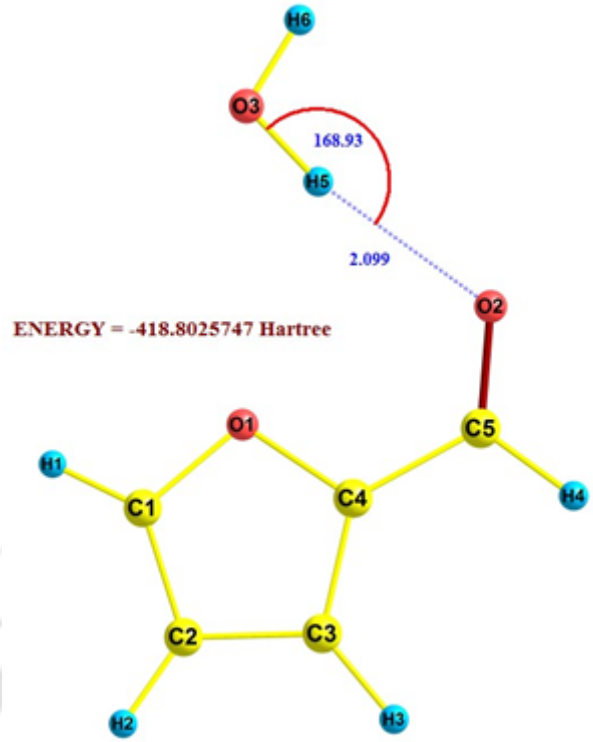

Figure A.8.: Optimized equilibrium geometry of Furfural-water complex FURC-2

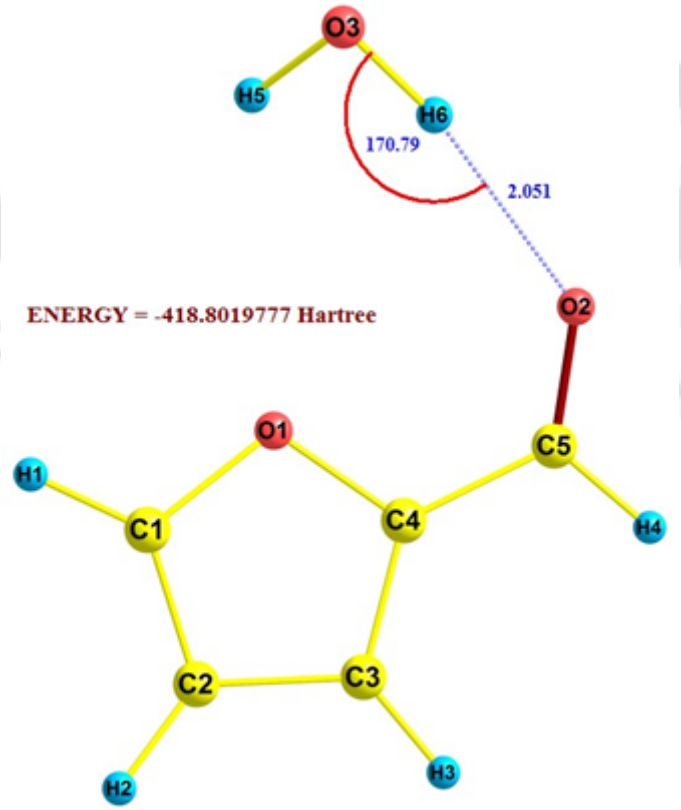

Figure A.9.: Optimized equilibrium geometry of Furfural-water complex FURC-3

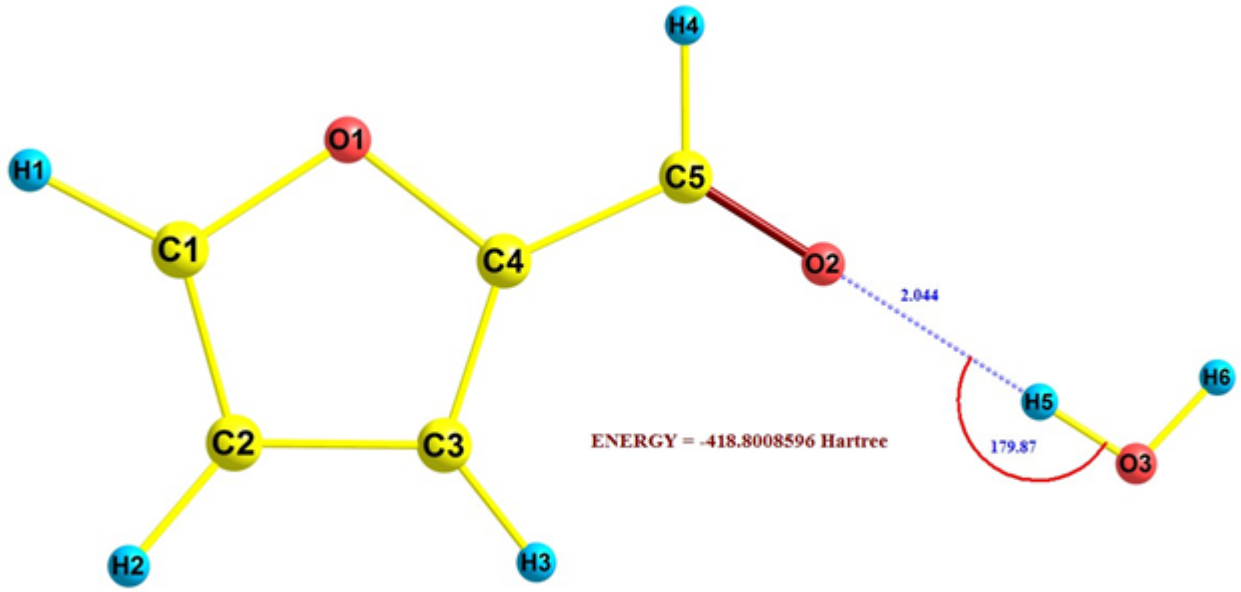

Figure A.10.: Optimized equilibrium geometry of Furfural-water complex FURT-1

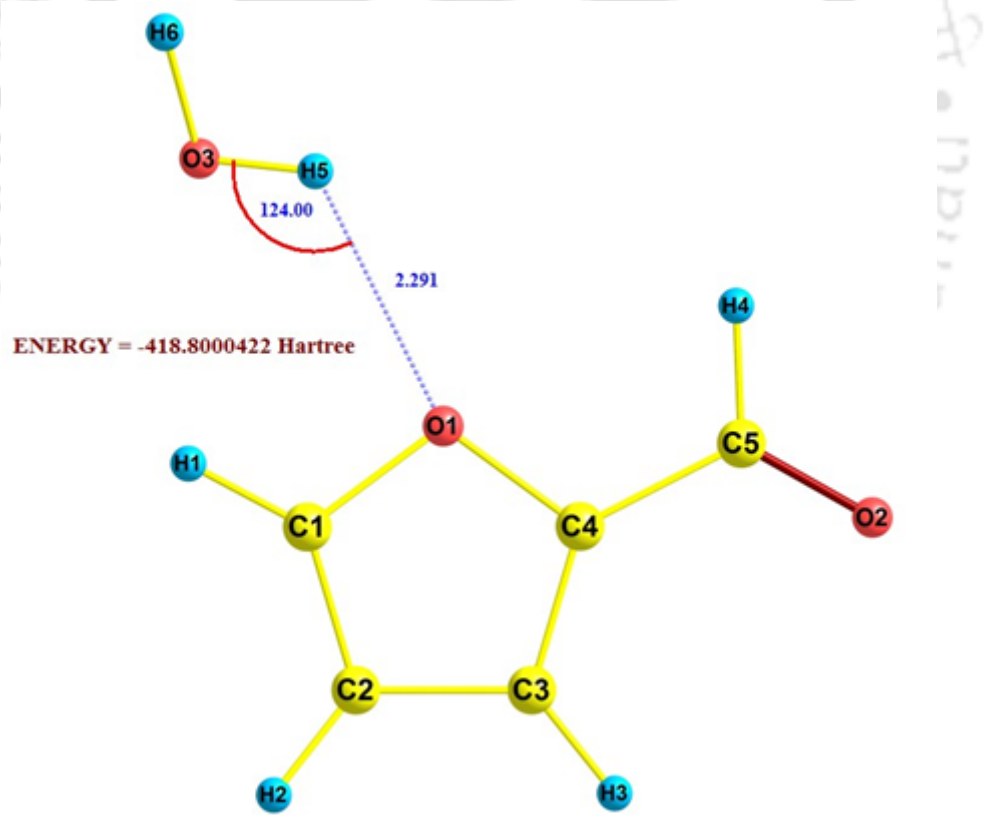

Figure A.11.: Optimized equilibrium geometry of Furfural-water complex FURT-2

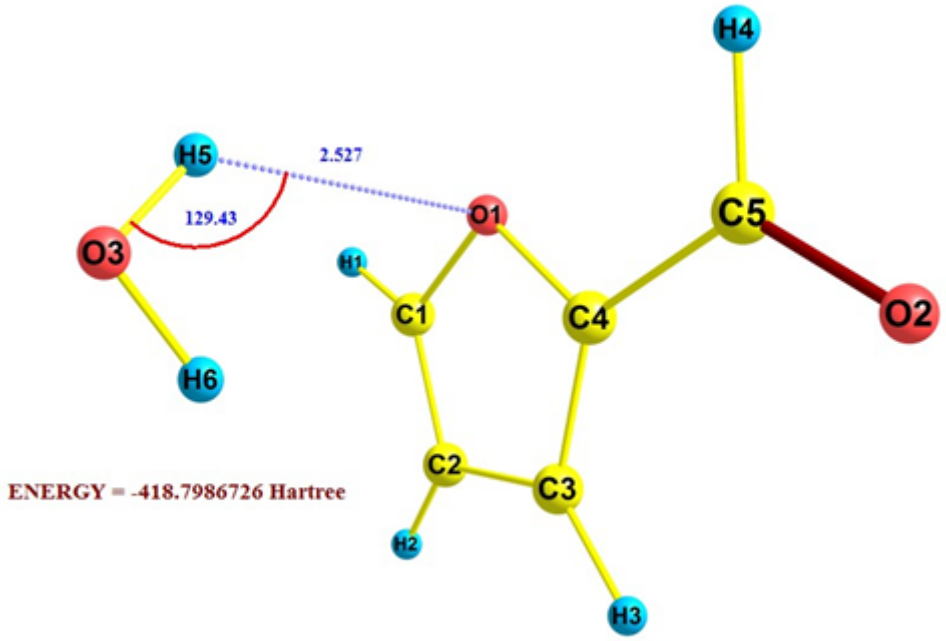

Figure A.12.: Optimized equilibrium geometry of Furfural-water complex FURT-3

Table A.8.: Calculated Bond length (in Å) of O-H group of Furfural and water in isolated state and in complexes

Complex	Group	Bond Length in Isolated	Bond Length in Complex
FURC-1	O-H OF WATER	0.960	0.967
FURC-2	O-H OF WATER	0.960	0.965
FURC-3	O-H OF WATER	0.960	0.965
FURT-1	O-H OF WATER	0.960	0.963
FURT-2	O-H OF WATER	0.960	0.962
FURT-3	O-H OF WATER	0.960	0.961

Table A.9.: MP2 Energy (kJ/mol) of Furfural and water complexes with Respect to FURC-1 complex

COMPLEXES	ΔE (KJ/mol)
FURC-2	0.05
FURC-3	1.60
FURT-1	4.60
FURT-2	6.70
FURT-3	10.30

Table A.10.: Natural Charges by Natural Bond Order (NBO) method for Furfural and water complexes carried out at the MP2/6-311++G** Level

	CIS-OO	FURC-1	FURC-2	FURC-3	TRANS-OO	FURT-1	FURT-2	FURT-3
O1	-0.510	-0.509	-0.512	-0.523	-0.532	-0.530	-0.555	-0.544
C1	0.242	0.249	0.261	0.251	0.228	0.238	0.236	0.226
C2	-0.331	-0.333	-0.337	-0.329	-0.319	-0.321	-0.324	-0.317
C3	-0.204	-0.189	-0.186	-0.186	-0.186	-0.170	-0.176	-0.193
C4	0.185	0.176	0.168	0.173	0.176	0.162	0.168	0.169
C5	0.487	0.497	0.504	0.504	0.494	0.519	0.494	0.491
O2	-0.601	-0.645	-0.642	-0.636	-0.613	-0.661	-0.614	-0.603
H1	0.192	0.192	0.198	0.194	0.190	0.192	0.216	0.195
H2	0.219	0.220	0.220	0.222	0.218	0.220	0.218	0.223
H3	0.216	0.219	0.217	0.219	0.228	0.232	0.228	0.233
H4	0.106	0.133	0.115	0.116	0.116	0.121	0.110	0.119
TOTAL	0.000	0.010	0.006	0.005	0.000	0.003	0.0004	-0.0008
O	-0.911	-0.953	-0.944	-0.942	-0.911	-0.940	-0.932	-0.917
H	0.456	0.489	0.490	0.489	0.456	0.489	0.471	0.458
H	0.456	0.454	0.448	0.448	0.456	0.448	0.460	0.460
TOTAL	0.000	-0.010	-0.006	-0.005	0.000	-0.003	-0.0004	0.0008

Table A.11.: Results of Localized Molecular Orbital-Energy Decomposition Analysis (LMO-EDA) for Furfural- water complexes carried out at the MP2/6-311++G** Level. [All Values are in Kcal/mol]

	ES	EX	REP	POL	DISP	INT
FURC-1	-9.76	-9.45	16.87	-2.52	0.02	-4.84
FURC-2	-7.54	-6.47	11.35	-1.89	-0.18	-4.73
FURC-3	-7.63	-7.31	12.89	-1.89	-0.08	-4.02
FURT-1	-6.29	-4.65	8.23	-1.48	0.35	-3.84
FURT-2	-4.98	-5.20	9.02	-0.92	-0.65	-2.73
FURT-3	-1.84	-4.26	7.13	-0.59	-1.49	-1.05

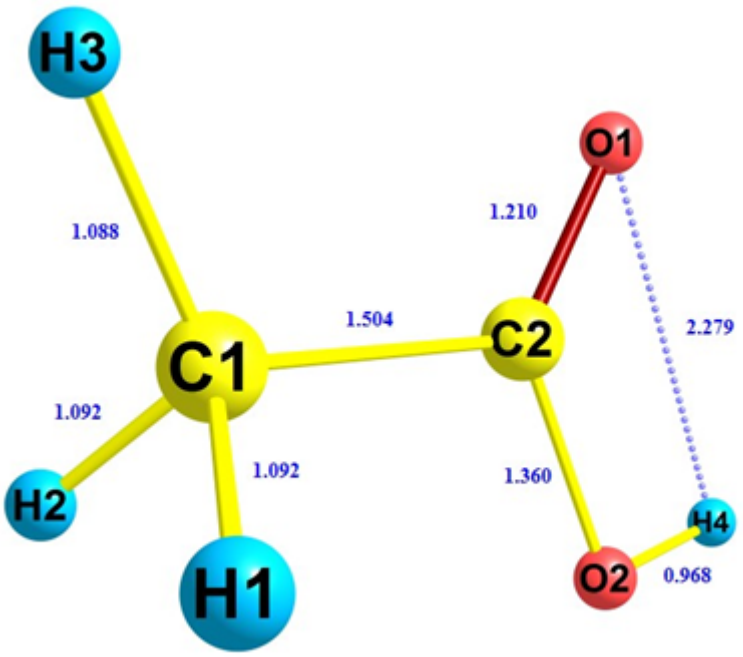

Figure A.13.: Optimized equilibrium geometry of trans-conformer of acetic acid [trans-AA] (Total Energy = -228.5682807 Hartree)

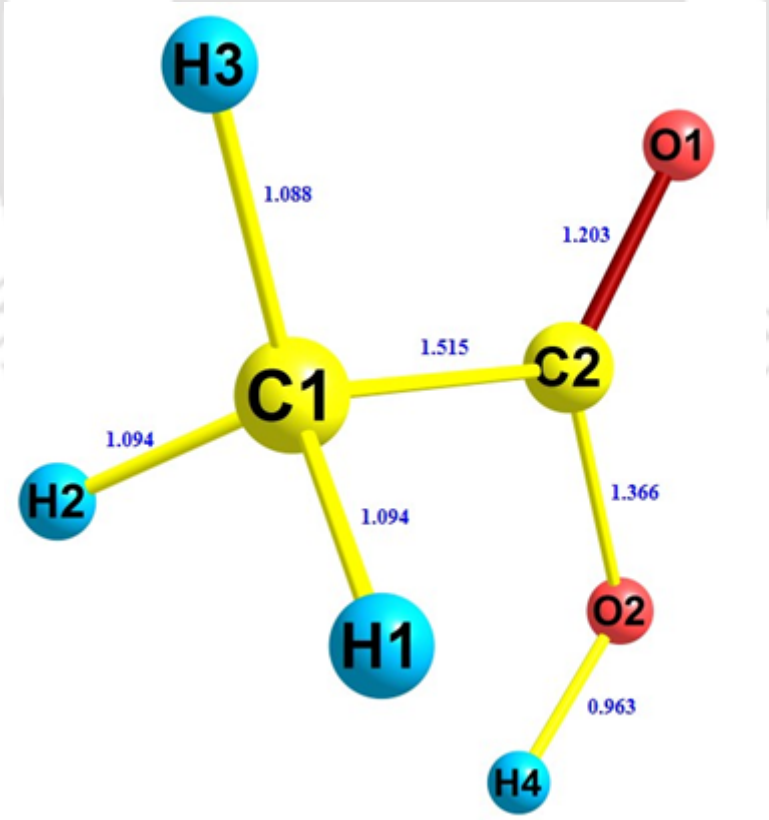

Figure A.14.: Optimized equilibrium geometry of Cis-conformer of acetic acid [Cis-AA] (Total Energy = -228.5586313 Hartree)

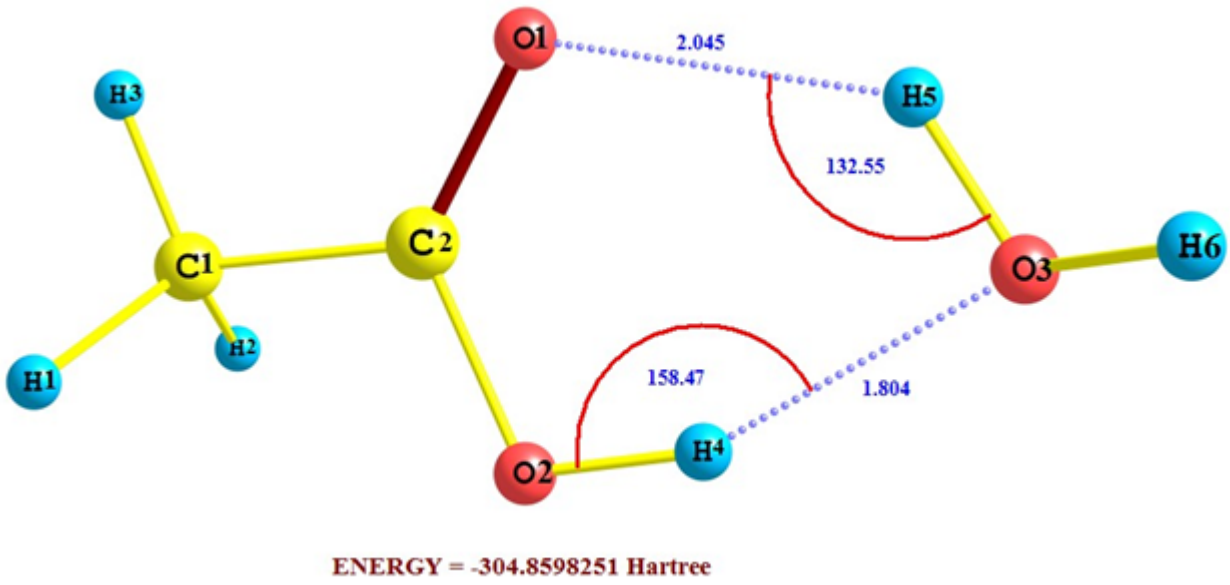

Figure A.15.: Optimized equilibrium geometry of acetic acid-water complex AAT-1

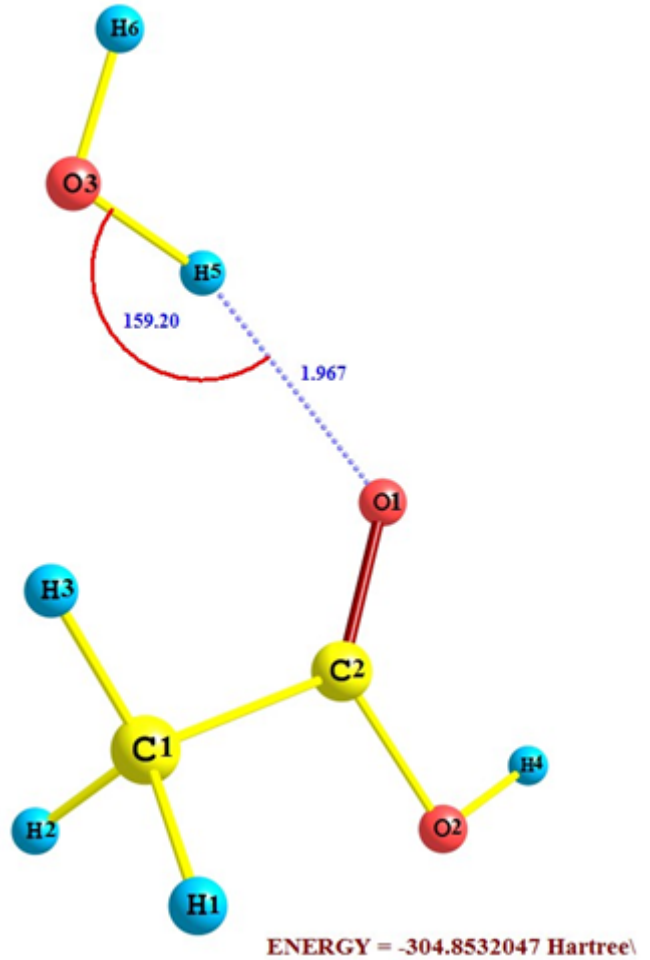

Figure A.16.: Optimized equilibrium geometry of acetic acid-water complex AAT-2

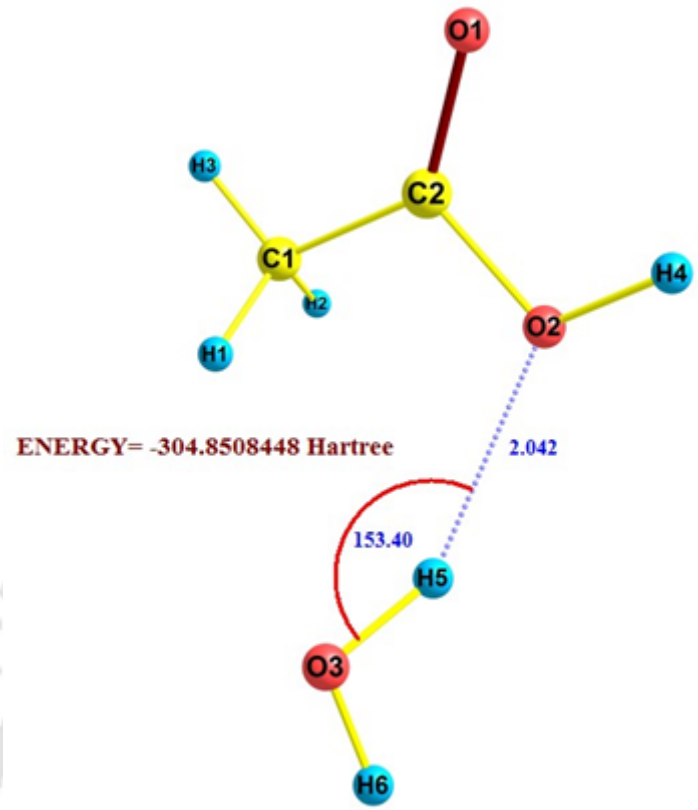

Figure A.17.: Optimized equilibrium geometry of acetic acid-water complex AAT-3

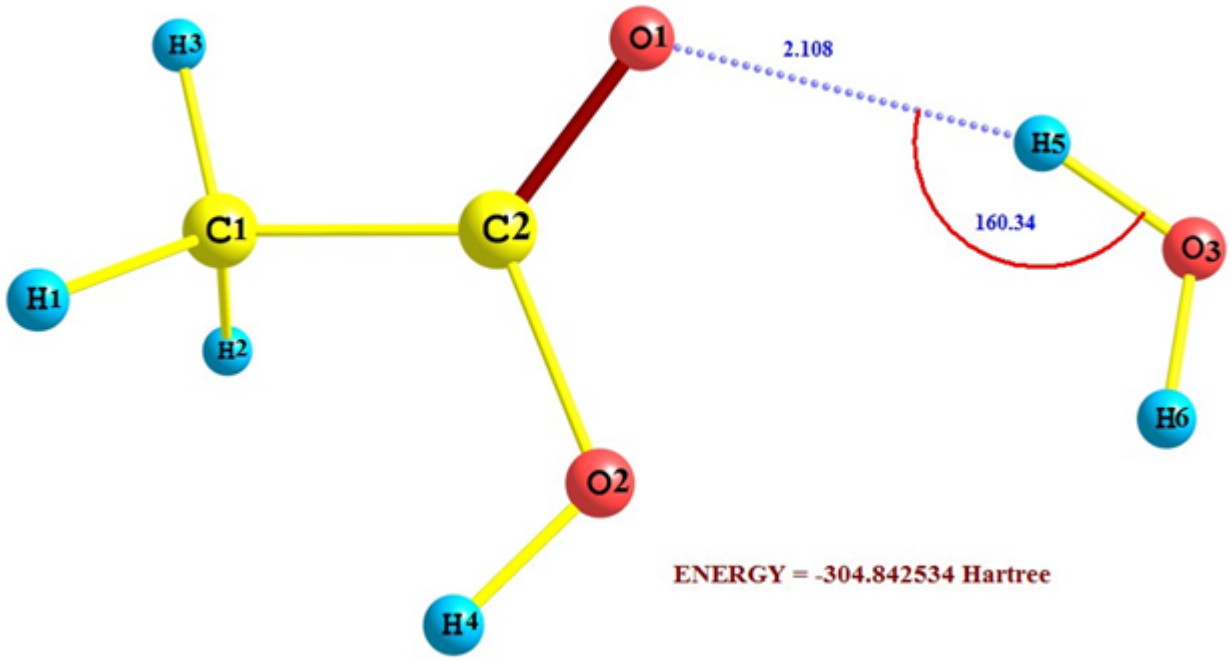

Figure A.18.: Optimized equilibrium geometry of acetic acid-water complex AAC-1

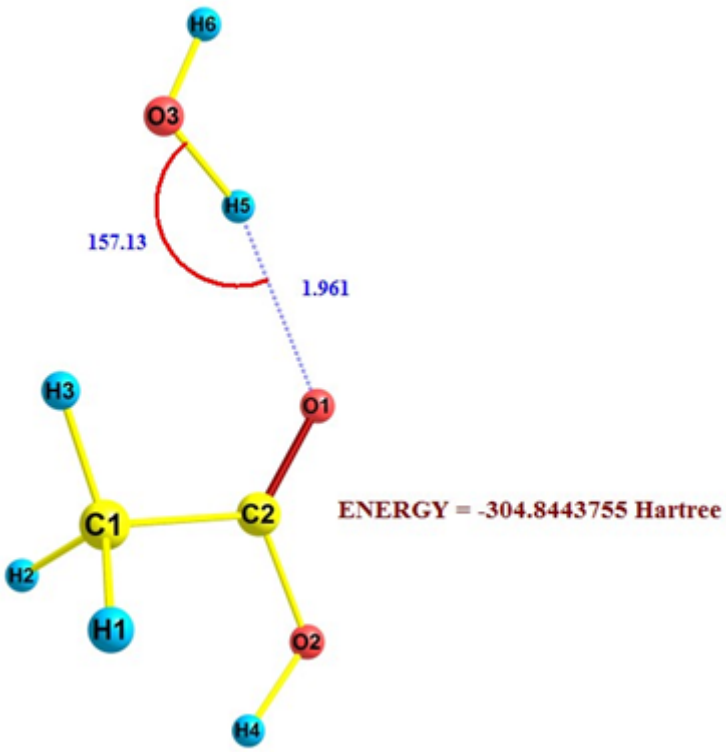

Figure A.19.: Optimized equilibrium geometry of acetic acid-water complex AAC-2

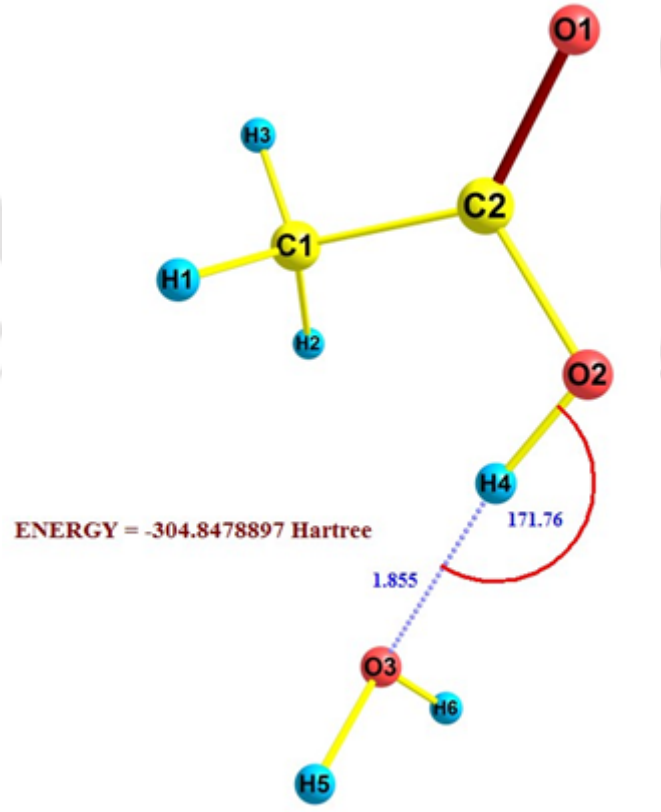

Figure A.20.: Optimized equilibrium geometry of acetic acid-water complex AAC-3

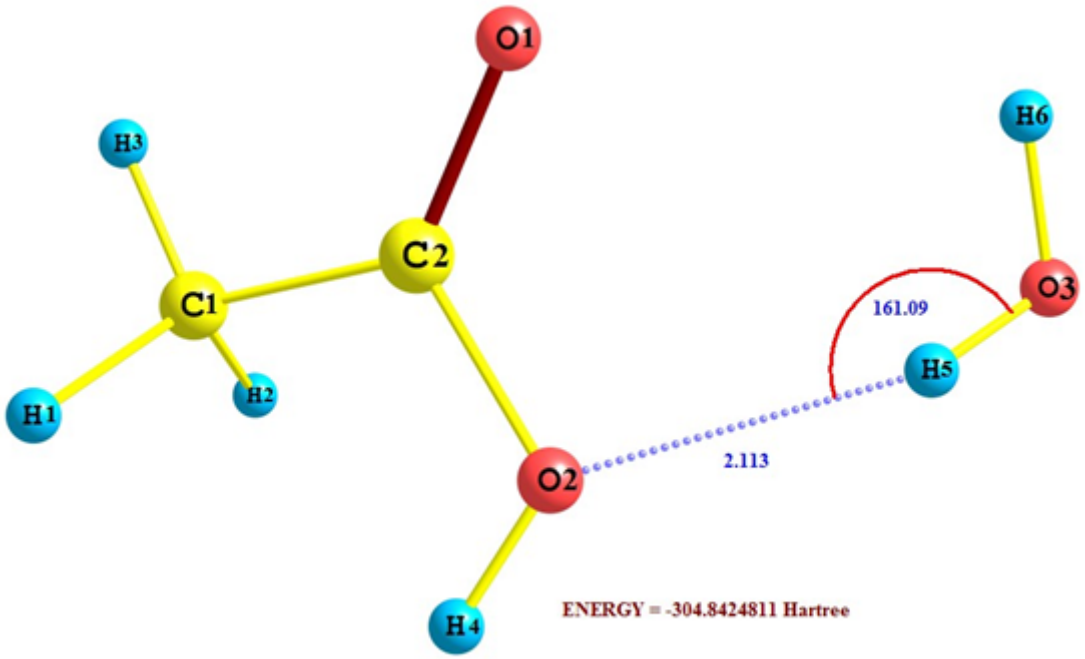

Figure A.21.: Optimized equilibrium geometry of acetic acid-water complex AAC-4

Table A.12.: Calculated Bond length (in Å) of O-H group of acetic acid and water in isolated state and in complexes

Complex	Group	Bond Length in Isolated	Bond Length in Complex
AAC-1	O-H of water	0.960	0.964
AAC-2	O-H of water	0.960	0.967
AAC-3	O-H of Acetic acid	0.963	0.972
AAC-4	O-H of water	0.960	0.962
AAT-1	O-H of water	0.960	0.968
	O-H of Acetic acid	0.968	0.982
AAT-2	O-H of water	0.960	0.969
AAT-3	O-H of water	0.960	0.964

Table A.13.: MP2 Energy (kJ/mol) of Acetic acid and water complexes with Respect to AAT-1 complex

COMPLEX	ΔE (KJ/mol)
AAT-1	0
AAT-2	17.4
AAT-3	23.7
AAC-1	45.6
AAC-2	40.7
AAC-3	31.5
AAC-4	45.7

Table A.14.: Natural Charges by Natural Bond Order (NBO) Analysis of acetic acid-water complexes carried out at the MP2/6-311++G** Level

	TRANS	AAT-1	AAT-2	AAT-3	CIS	AAC-1	AAC-2	AAC-3	AAC-4
C1	-0.618	-0.614	-0.630	-0.631	-0.634	-0.635	-0.646	-0.627	-0.635
H1	0.209	0.208	0.209	0.235	0.199	0.203	0.201	0.199	0.203
H2	0.209	0.209	0.213	0.209	0.199	0.204	0.201	0.199	0.205
H3	0.206	0.203	0.232	0.207	0.219	0.224	0.245	0.209	0.223
C2	0.954	0.972	0.976	0.960	0.940	0.953	0.962	0.944	0.947
O1	-0.692	-0.778	-0.748	-0.681	-0.653	-0.745	-0.695	-0.677	-0.762
O2	-0.759	-0.745	-0.734	-0.790	-0.738	-0.675	-0.731	-0.774	-0.658
H4	0.489	0.533	0.491	0.496	0.468	0.476	0.472	0.512	0.481
TOTAL	0.000	-0.012	0.008	0.004	0.000	0.005	0.009	-0.015	0.004
O3	-0.911	-0.965	-0.955	-0.942	-0.911	-0.942	-0.959	-0.943	-0.939
H5	0.456	0.472	0.454	0.481	0.456	0.452	0.494	0.478	0.474
H6	0.456	0.506	0.492	0.456	0.456	0.484	0.456	0.479	0.461
TOTAL	0.000	0.012	-0.008	-0.004	0.000	-0.005	-0.009	0.015	-0.004

Table A.15.: Results of Localized Molecular Orbital-Energy Decomposition Analysis (LMO-EDA) for Acetic acid-water complexes carried out at the MP2/6-311++G** Level. [All Values are in Kcal/mol]

	ES	EX	REP	POL	DISP	INT
T-1	-20.14	-22.25	40.96	-6.59	-0.42	-8.44
T-2	-10.32	-10.62	18.86	-2.67	-0.28	-5.03
T-3	-7.01	-8.24	14.55	-1.70	-1.00	-3.40
C-1	-7.73	-6.73	11.82	-1.52	-0.08	-4.24
C-2	-11.14	-10.93	19.43	-2.84	-0.21	-5.69
C-3	-12.60	-11.86	21.62	-3.69	-0.40	-6.93
C-4	-7.03	-6.11	10.78	-1.20	-0.31	-3.87

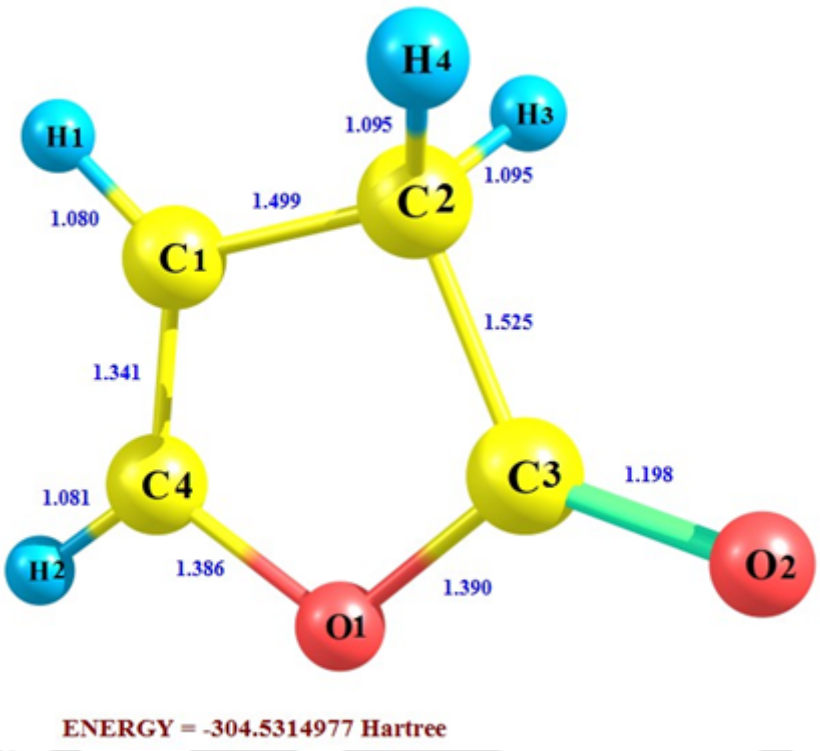

Figure A.22.: Optimized equilibrium geometry of 2(3H)-Furanone

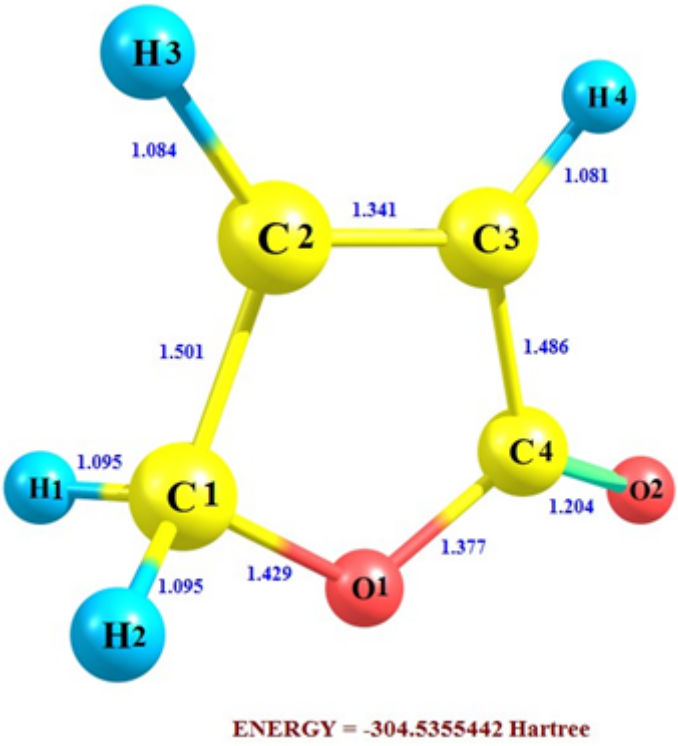

Figure A.23.: Optimized equilibrium geometry of 2(5H)-Furanone

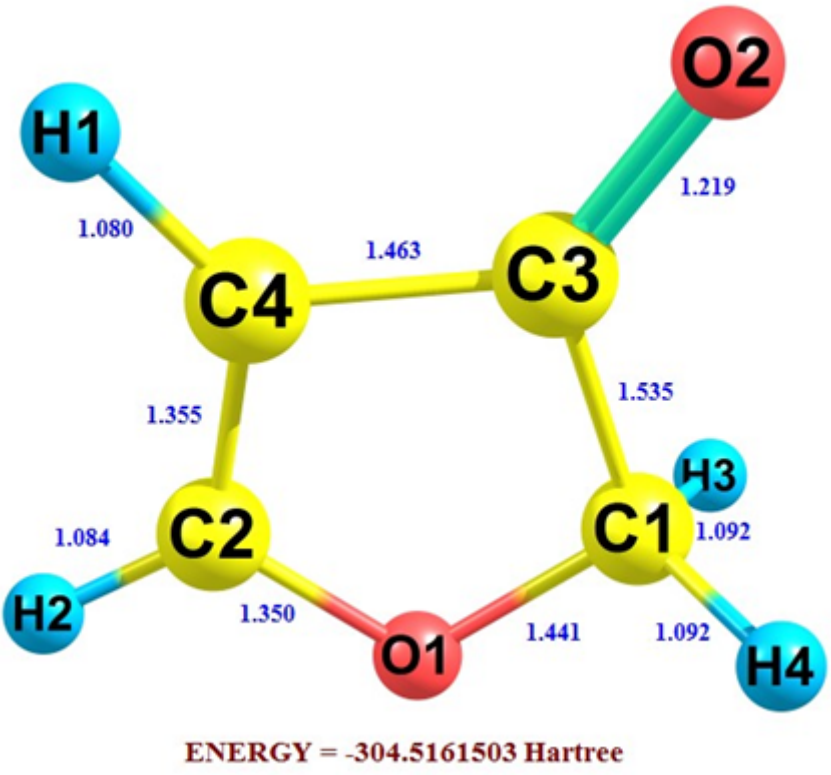

Figure A.24.: Optimized equilibrium geometry of 3(2H)-Furanone

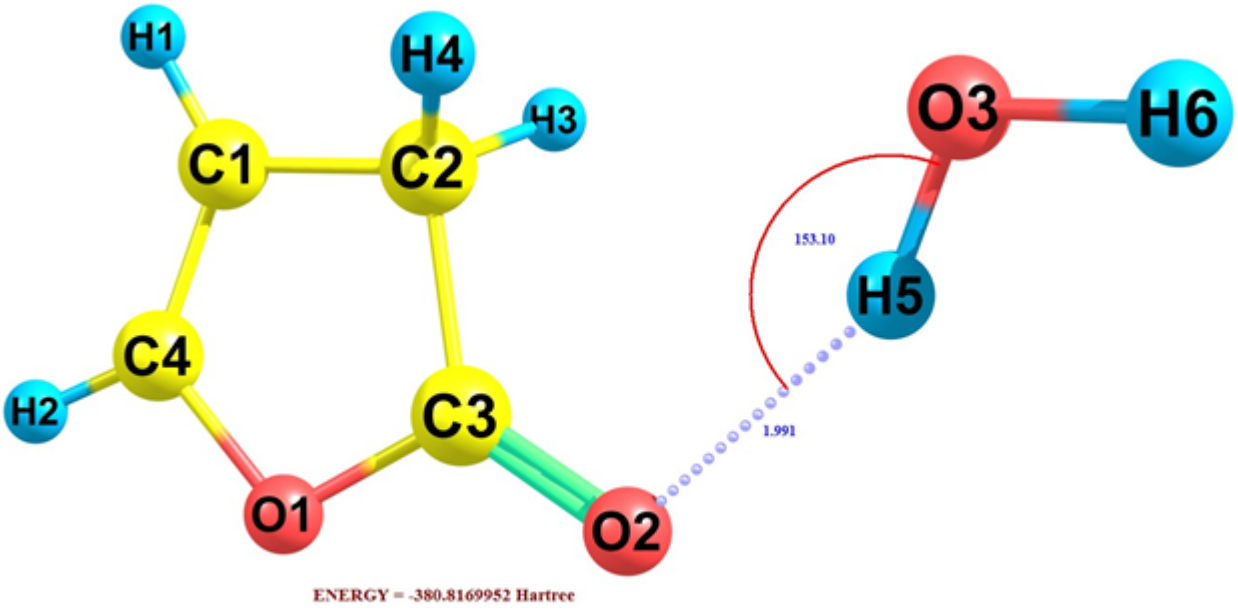

Figure A.25.: Optimized equilibrium geometry of 2(3H)Furanone –water complex [2(3H)FUR-1]

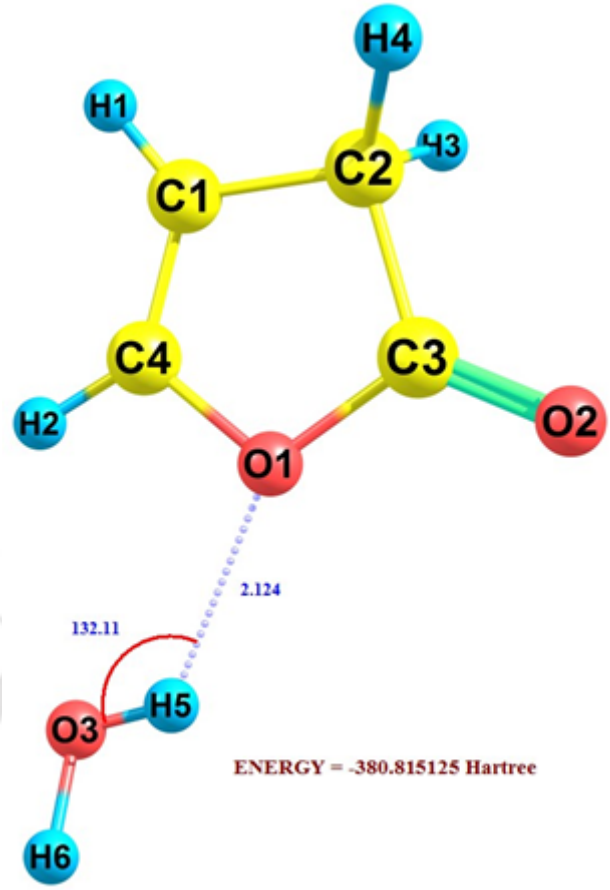

Figure A.26.: Optimized equilibrium geometry of 2(3H)Furanone –water complex [2(3H)FUR-2]

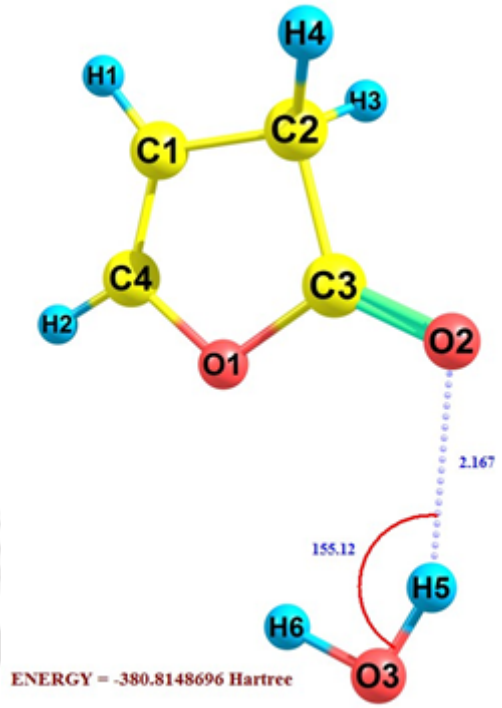

Figure A.27.: Optimized equilibrium geometry of 2(3H)Furanone –water complex [2(3H)FUR-3]

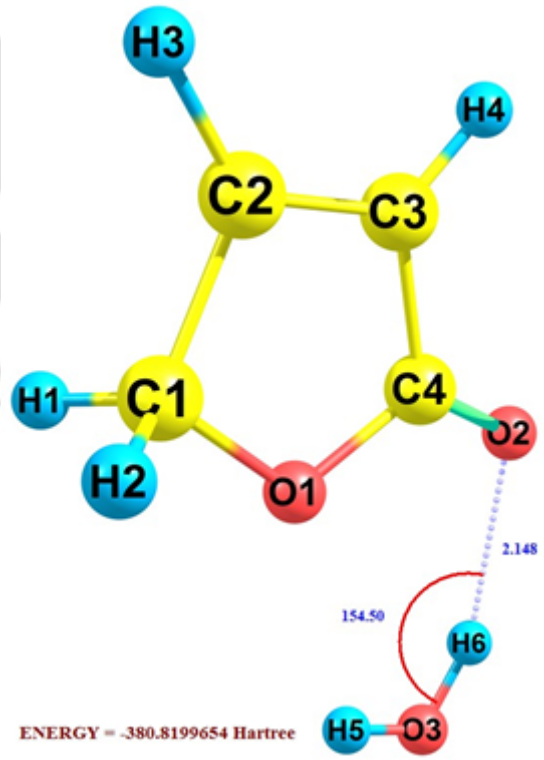

Figure A.28.: Optimized equilibrium geometry of 2(5H)Furanone –water complex [2(5H)FUR-1]

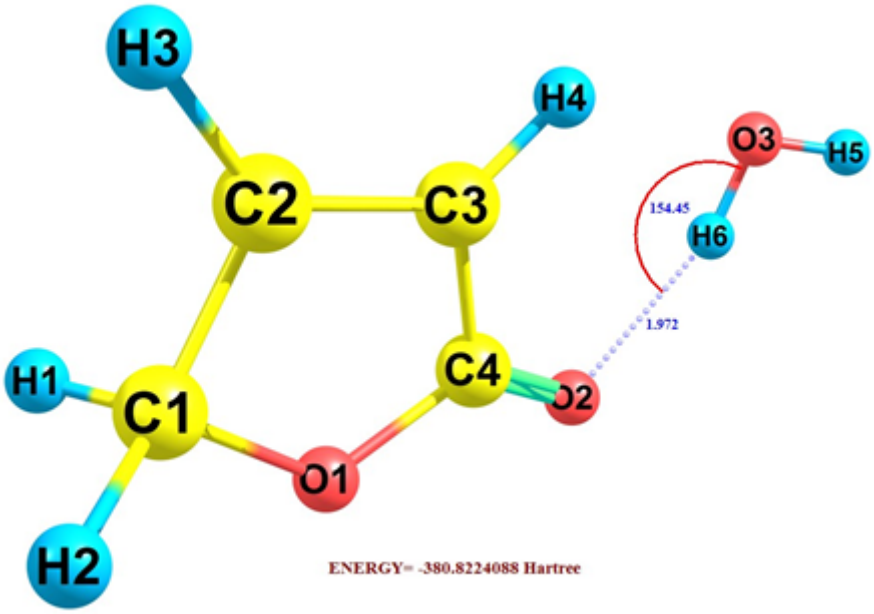

Figure A.29.: Optimized equilibrium geometry of 2(5H)Furanone –water complex [2(5H)FUR-2]

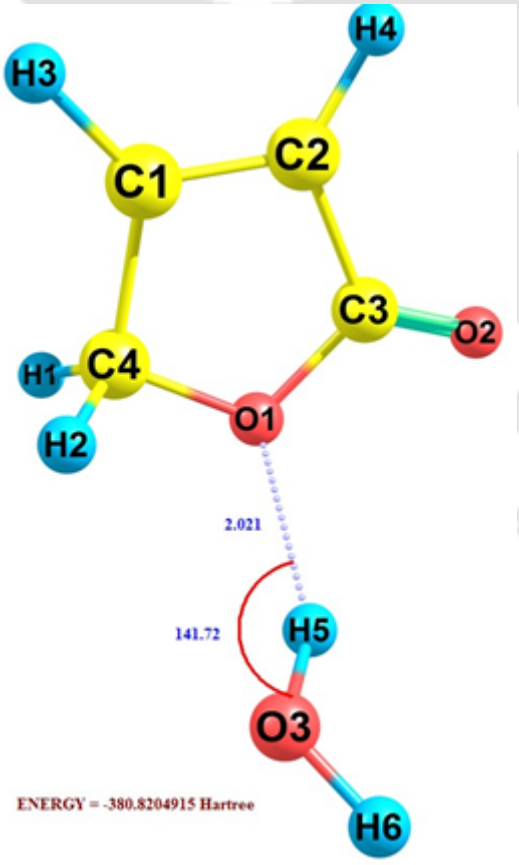

Figure A.30.: Optimized equilibrium geometry of 2(5H)Furanone –water complex [2(5H)FUR-3]

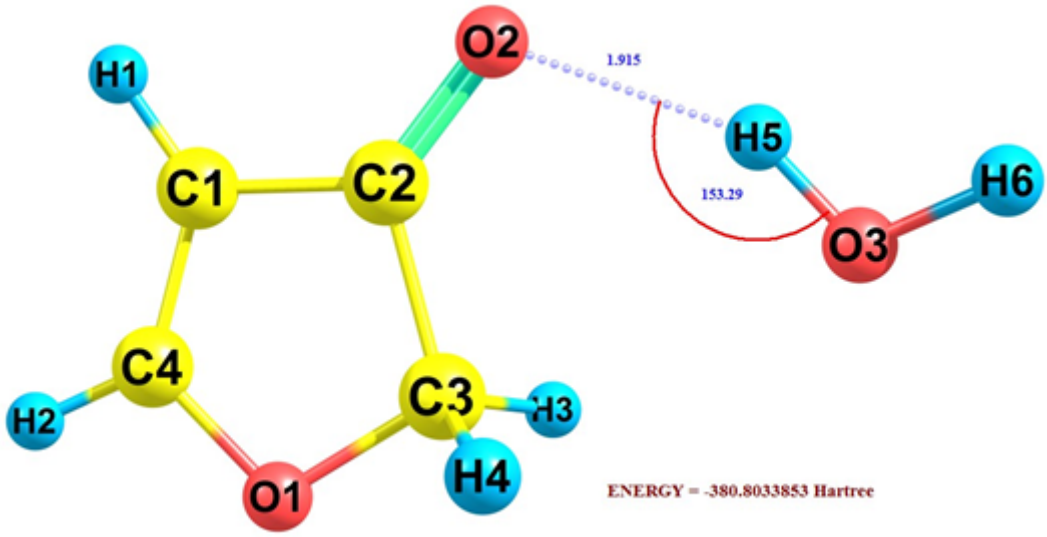

Figure A.31.: Optimized equilibrium geometry of 3(2H)Furanone –water complex [3(2H)FUR-1]

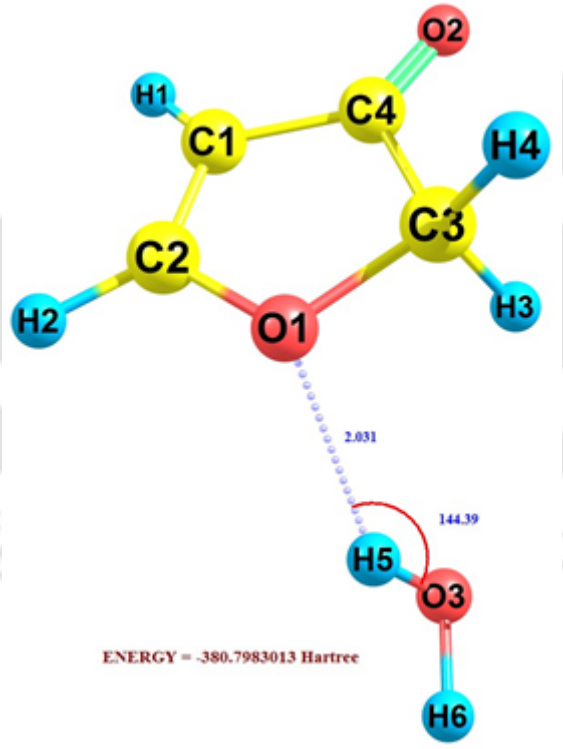

Figure A.32.: Optimized equilibrium geometry of 3(2H)Furanone –water complex [3(2H)FUR-2]

Table A.16.: Calculated Bond length (in Å) of O-H group of furanone and water in isolated state and in complexes

Complex	Group	Bond Length in Isolated	Bond Length in Complex
2(3H)-FUR-1	O-H of water	0.960	0.967
2(3H)-FUR-2	O-H of water	0.960	0.963
2(3H)-FUR-3	O-H of water	0.960	0.963
2(5H)-FUR-1	O-H of water	0.960	0.964
2(5H)-FUR-2	O-H of water	0.960	0.968
2(5H)-FUR-3	O-H of water	0.960	0.964
3(2H)-FUR-1	O-H of water	0.960	0.970
3(2H)-FUR-2	O-H of water	0.960	0.964

Table A.17.: MP2 Energy (kJ/mol) of Furanone and water complexes with Respect to 2(5H)-FUR-2 complex

Complexes	Δ E (KJ/mol)
2(5H)-FUR-2	0
2(3H)-FUR-1	14.3
2(3H)-FUR-2	19.2
2(3H)-FUR-3	19.9
2(5H)-FUR-1	6.4
2(5H)-FUR-3	5.1
3(2H)-FUR-1	50.1
3(2H)-FUR-2	63.5

Table A.18.: Natural Charges by Natural Bond Order (NBO) method for 2(3H)-furanone-water complexes carried out at the MP2/6-311++G** Level.

	2(3H)FURANONE	2(3H)FUR-1	2(3H)FUR-2	2(3H)FUR-3
O1	-0.626	-0.619	-0.656	-0.636
C1	0.966	0.985	0.972	0.977
C2	0.218	0.206	0.216	0.214
C3	-0.479	-0.492	-0.478	-0.480
C4	-0.288	-0.272	-0.288	-0.277
O2	-0.641	-0.685	-0.641	-0.661
H1	0.223	0.233	0.223	0.228
H2	0.223	0.246	0.223	0.228
H3	0.214	0.215	0.215	0.218
H4	0.191	0.192	0.214	0.194
TOTAL	0.000	0.008	0.001	0.005
O	-0.911	-0.955	-0.941	-0.940
H	0.456	0.490	0.481	0.480
H	0.456	0.456	0.458	0.455
TOTAL	0.000	-0.008	-0.001	-0.005

Table A.19.: Natural Charges by Natural Bond Order (NBO) method for 2(5H)-furanone-water complexes carried out at the MP2/6-311++G** Level

	2 (5H) FURANONE	2(5H)FUR-1	2(5H)FUR-2	2(5H)FUR-3
O1	-0.631	-0.642	-0.624	-0.659
C1	0.018	0.017	0.017	0.011
C2	-0.112	-0.101	-0.110	-0.097
C3	0.921	0.931	0.937	0.924
C4	-0.322	-0.325	-0.329	-0.330
O2	-0.655	-0.675	-0.699	-0.655
H1	0.207	0.210	0.208	0.208
H2	0.223	0.228	0.254	0.225
H3	0.175	0.180	0.177	0.200
H4	0.175	0.180	0.177	0.177
TOTAL	0.000	0.004	0.009	0.005
O	-0.911	-0.943	-0.960	-0.946
H	0.456	0.455	0.457	0.484
H	0.456	0.483	0.495	0.458
TOTAL	0.000	-0.004	-0.009	-0.005

Table A.20.: Natural Charges by Natural Bond Order (NBO) method for 3(2H)-furanone-water complexes carried out at the MP2/6-311++G** Level

	3(2H)FURANONE	3(2H)FUR-1	3(2H)FUR-2
O1	-0.609	-0.603	-0.637
C1	-0.046	-0.054	-0.051
C2	0.357	0.375	0.347
C3	0.617	0.633	0.618
C4	-0.459	-0.467	-0.442
O2	-0.657	-0.703	-0.649
H1	0.229	0.230	0.230
H2	0.183	0.184	0.184
H3	0.192	0.212	0.214
H4	0.192	0.206	0.193
TOTAL	0.000	0.013	0.007
O	-0.911	-0.964	-0.939
H	0.456	0.495	0.476
H	0.456	0.456	0.456
TOTAL	0.000	-0.032	-0.007

Table A.21.: Results of Localized Molecular Orbital-Energy Decomposition Analysis (LMO-EDA) for furanone-water complexes carried out at the MP2/6-311++G** Level. [All Values are in Kcal/mol]

	ES	EX	REP	POL	DISP	INT
2(3H)FUR-1	-10.43	-10.49	18.60	-2.59	-0.41	-5.32
2(3H)FUR-2	-7.08	-6.34	11.18	-1.27	-0.62	-4.13
2(3H)FUR-3	-7.12	-6.31	11.02	-1.32	-0.15	-3.88
2(5H)FUR-1	-8.13	-7.07	12.36	-1.52	-0.12	-4.48
2(5H)FUR-2	-11.93	-11.91	21.18	-3.04	-0.38	-6.08
2(5H)FUR-3	-8.28	-8.20	14.6	-1.83	-0.88	-4.59
3(2H)FUR-1	-12.98	-13.83	24.73	-3.6	-0.51	-6.19
3(2H)FUR-2	-6.26	-7.72	13.75	-1.6	-1.16	-2.99

APPENDIX B

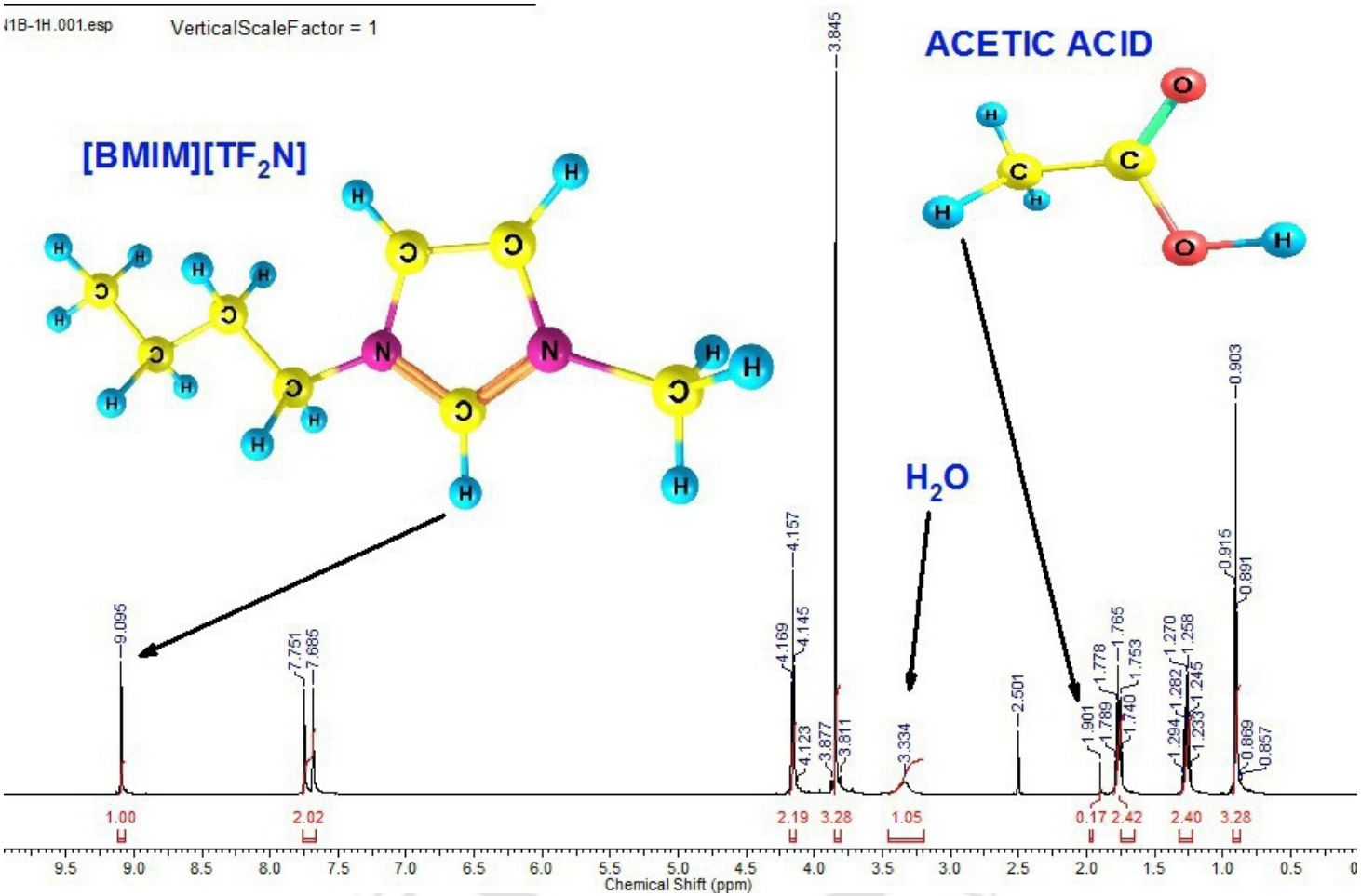

Figure B.1.: 1^{H} NMR spectrum of extract phase of [BMIM][TF_2N]-acetic acid-water system.

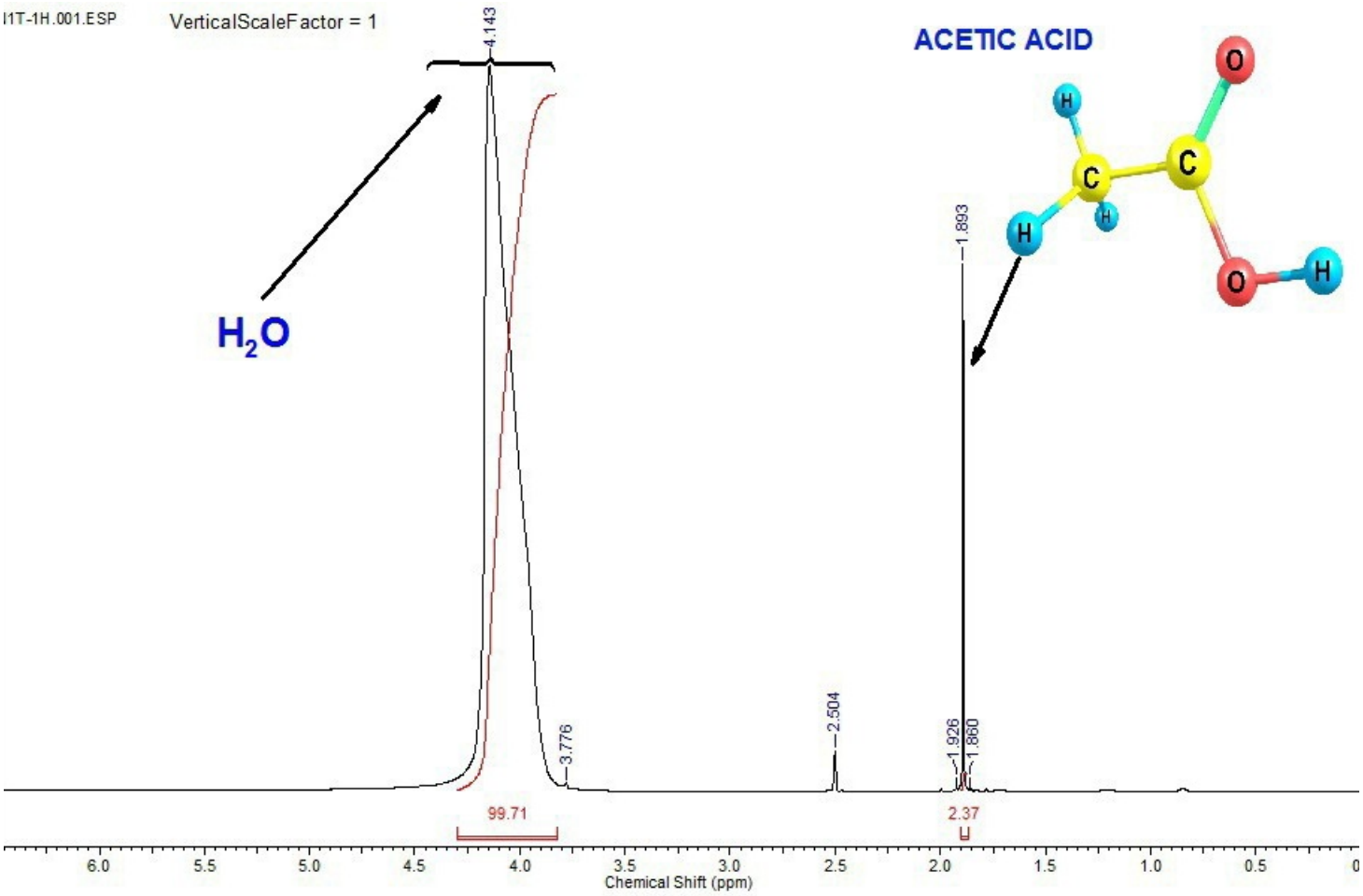

Figure B.2.: 1^{H} NMR spectrum of raffinate phase of [BMIM][TF_2N]-acetic acid-water system.

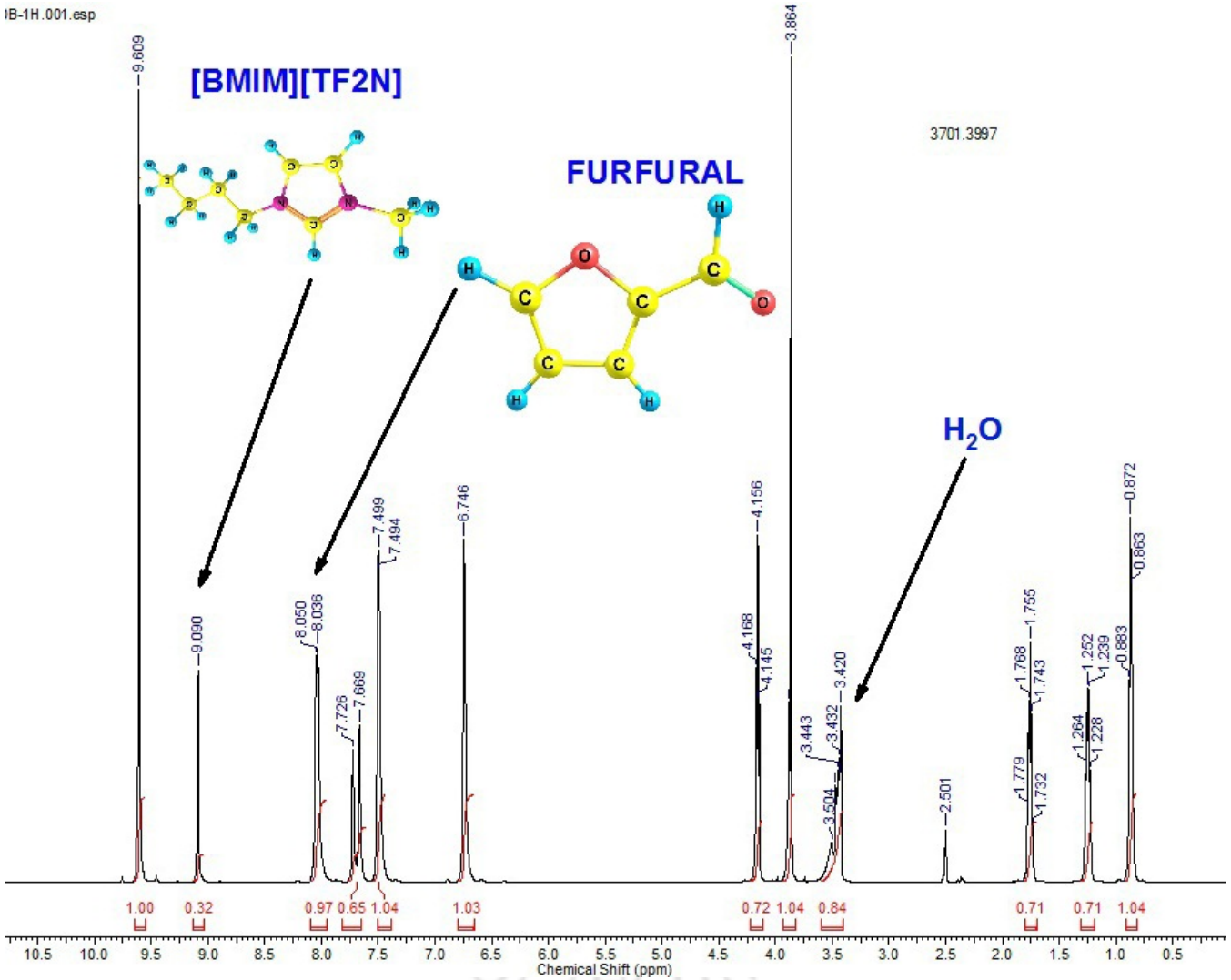

Figure B.3.: 1^{H} NMR spectrum of extract phase of [BMIM][TF_2N]-furfural-water system.

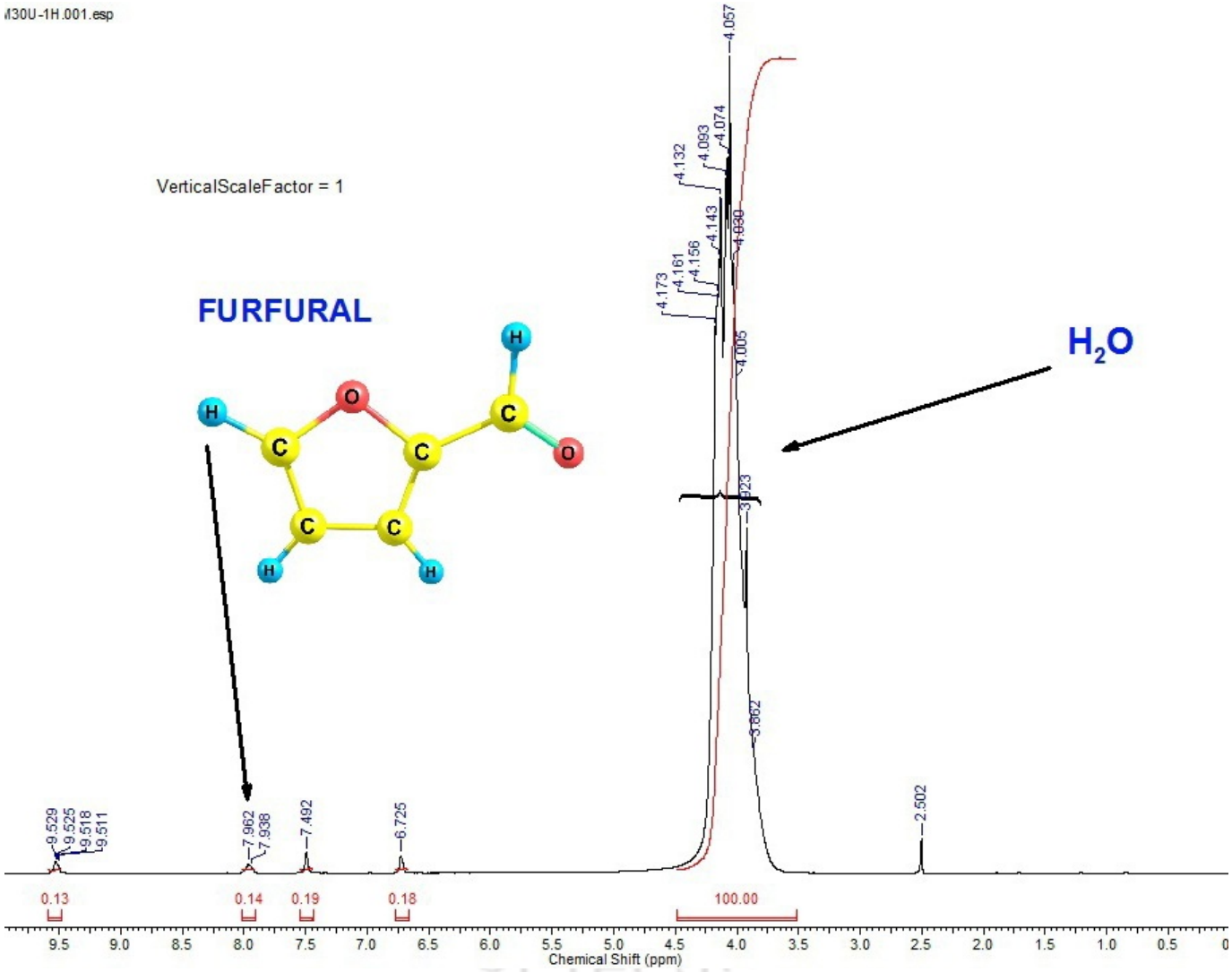

Figure B.4.: 1^{H} NMR spectrum of raffinate phase of [BMIM][TF_2N]-furfural-water system.

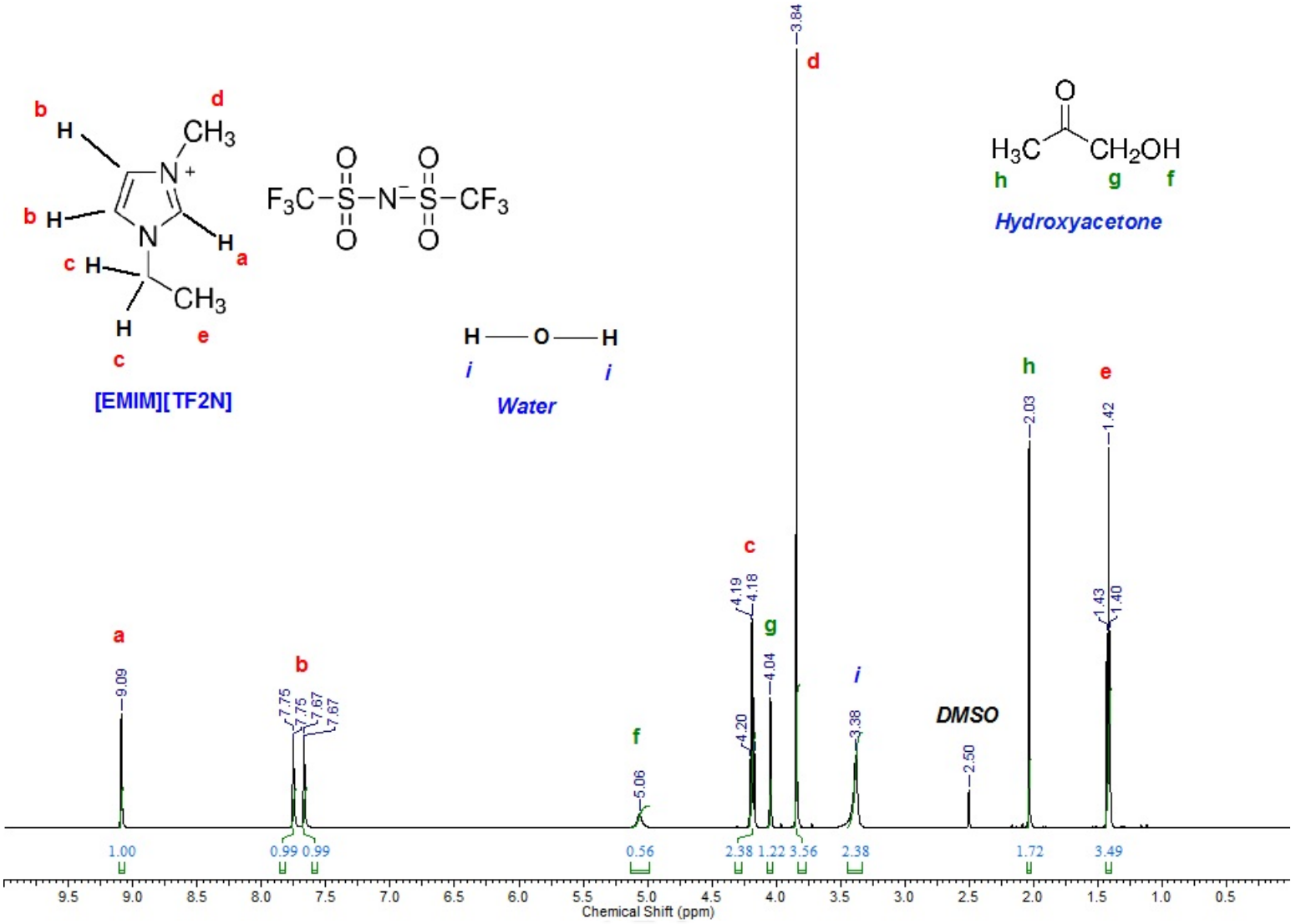

Figure B.5.: 1^{H} NMR spectrum of extract phase of [EMIM][TF_2N]-acetol-water system.

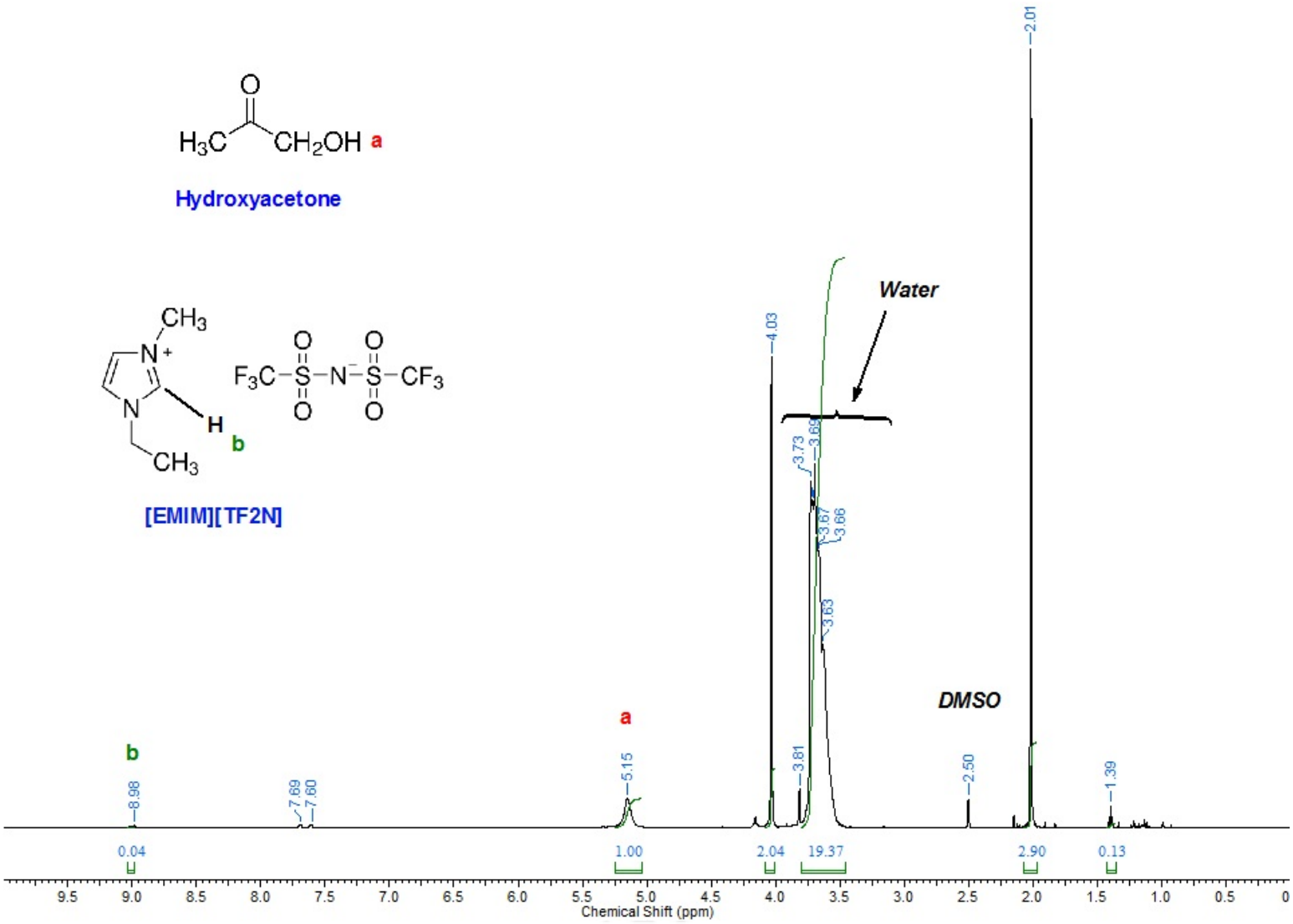

Figure B.6.: 1^{H} NMR spectrum of raffinate phase of [EMIM][TF_2N]-acetol-water system.

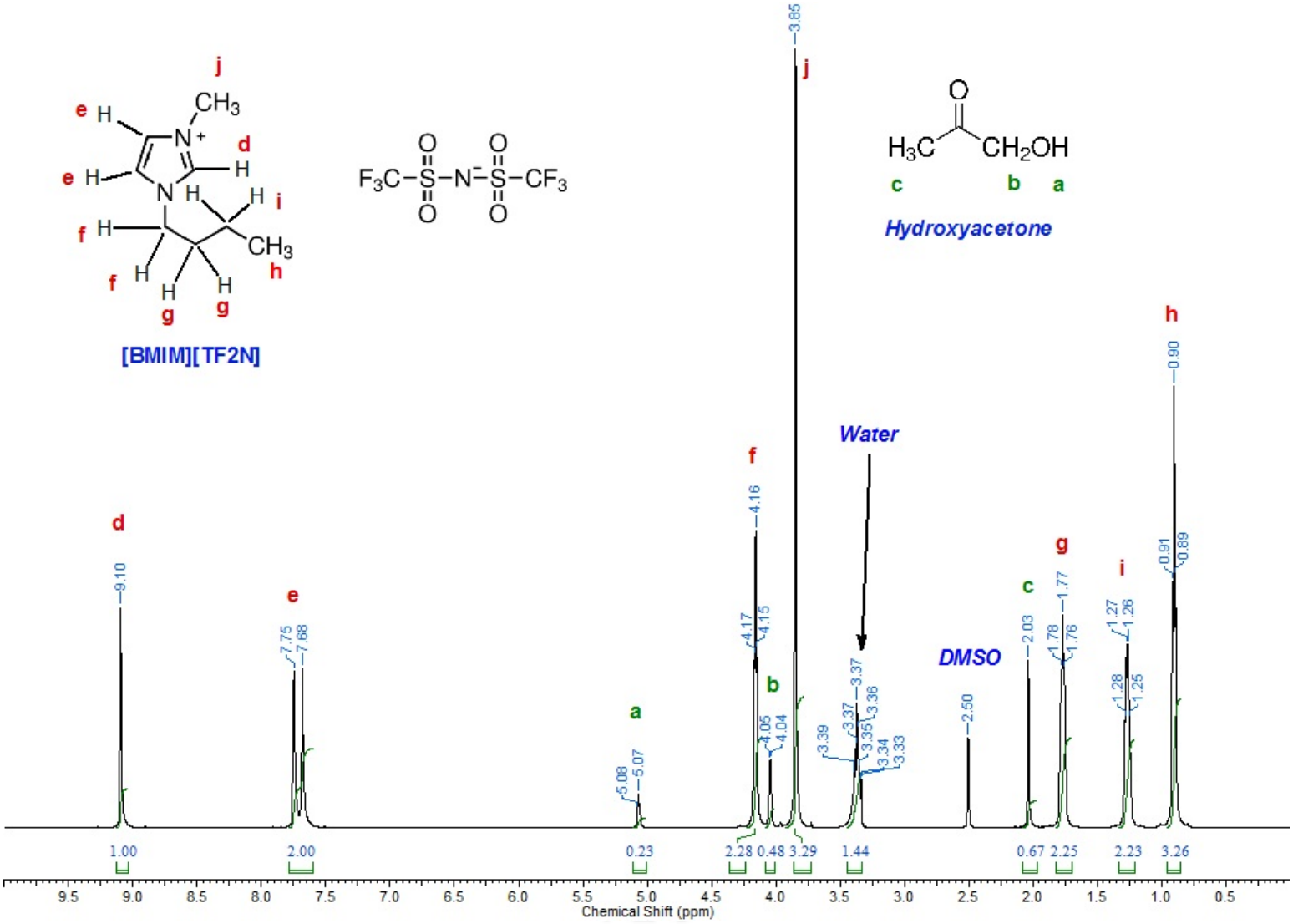

Figure B.7.: ^{1H} NMR spectrum of extract phase of [BMIM][TF_2N]-acetol-water system.

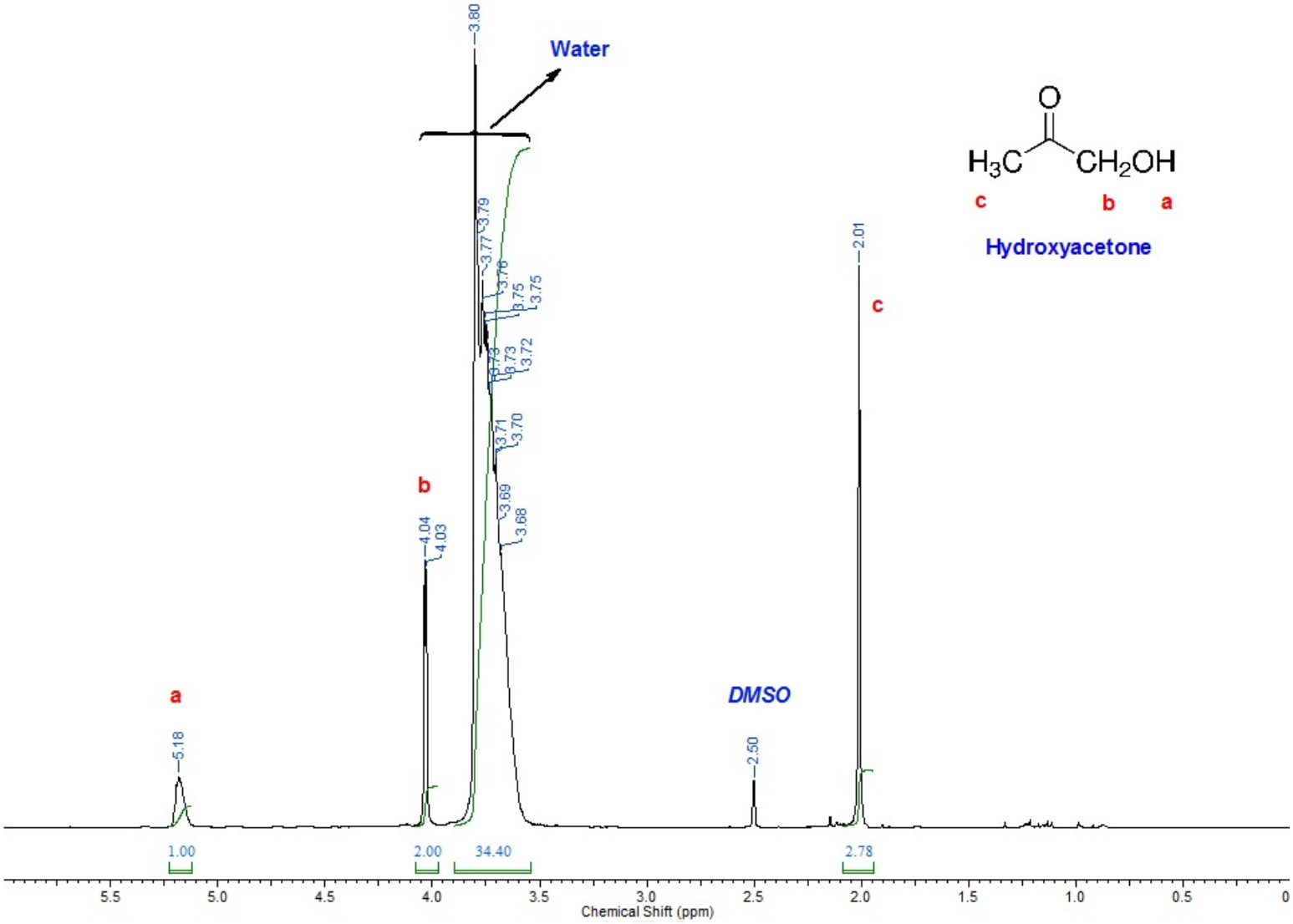

Figure B.8.: ^{1H} NMR spectrum of raffinate phase of [BMIM][TF_2N]-acetol-water system.

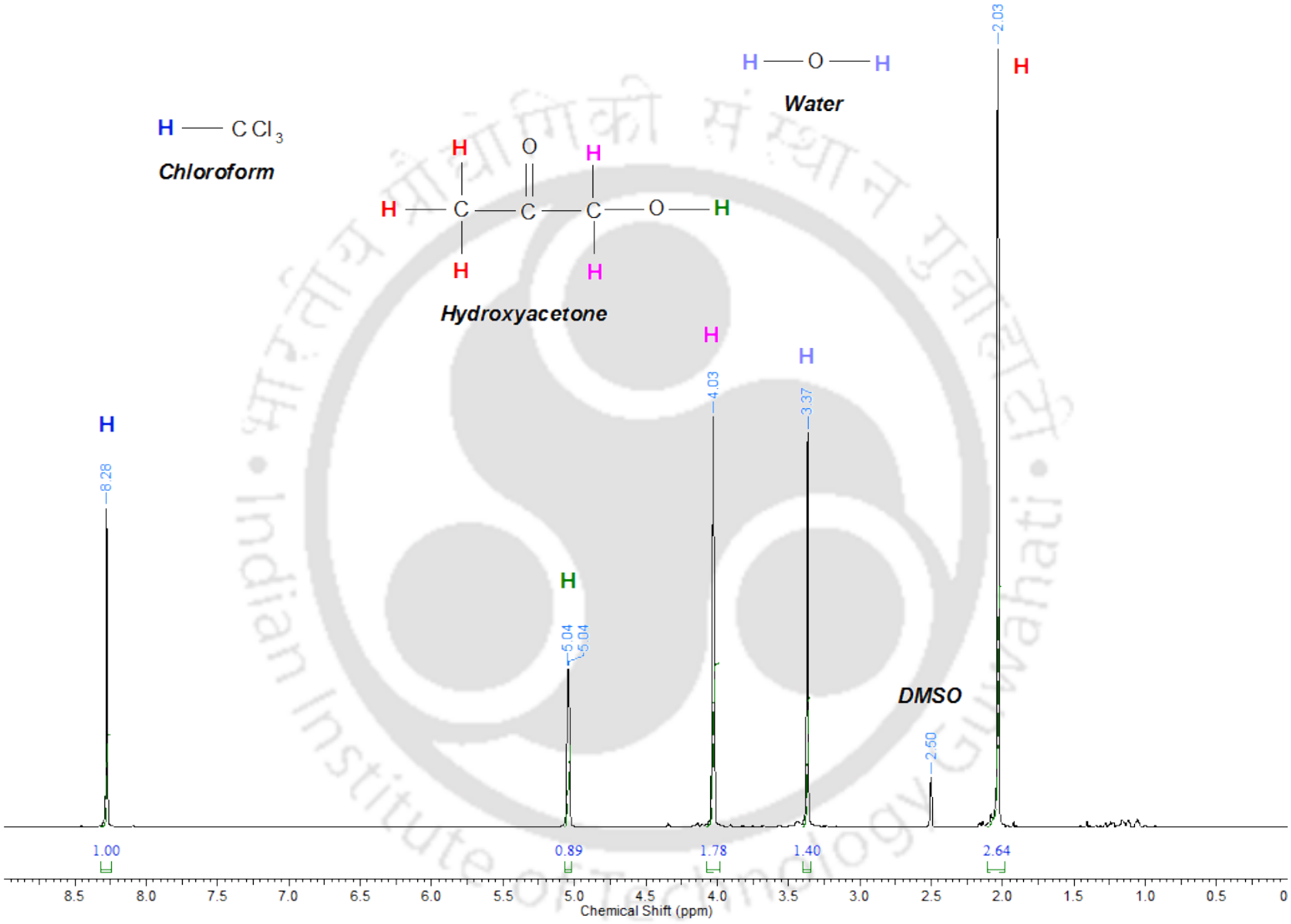

Figure B.9.: 1^{H} NMR spectrum of extract phase of Chloroform-acetol-water system.

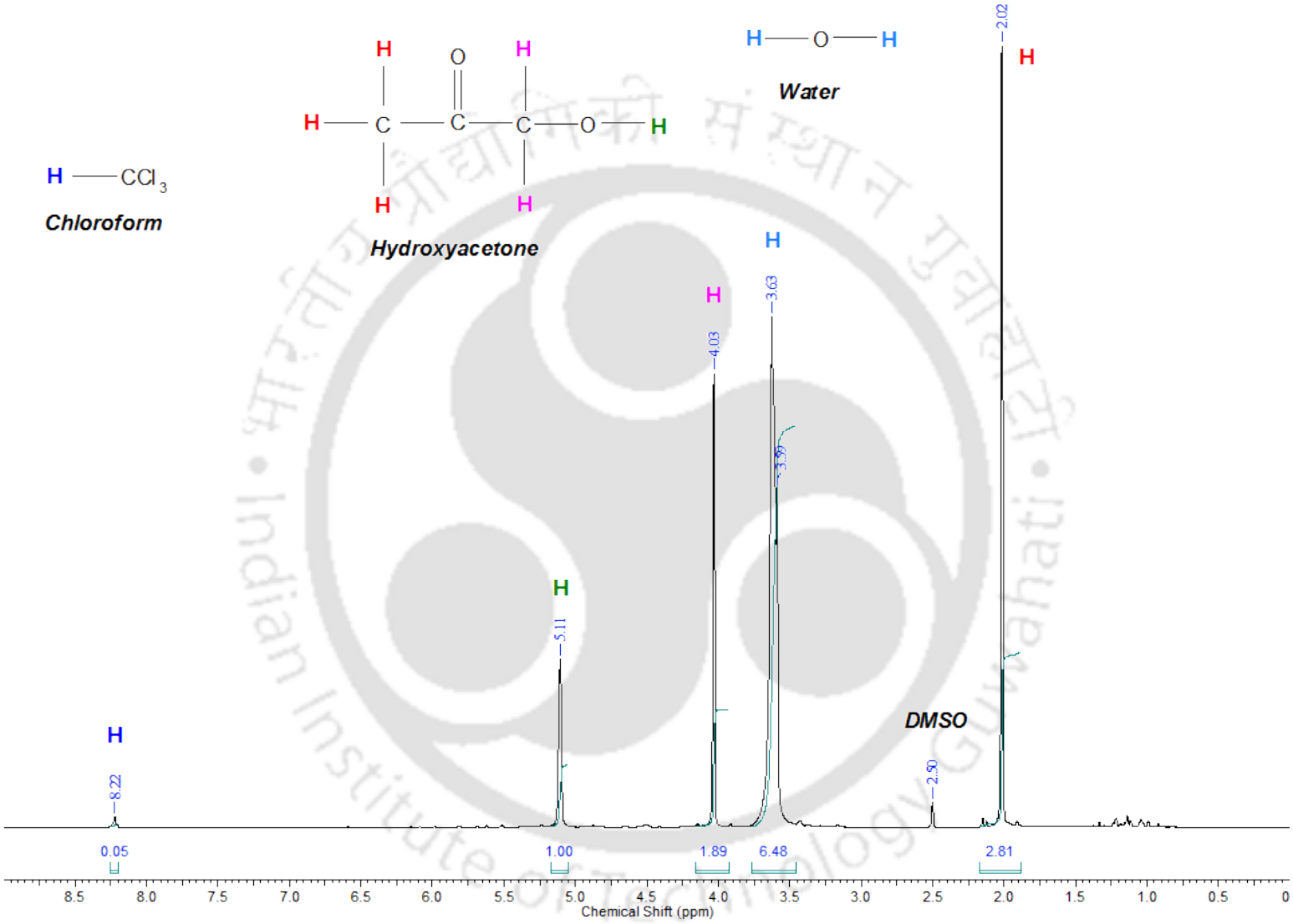

Figure B.10.: 1^{H} NMR spectrum of raffinate phase of Chloroform-acetol-water system.

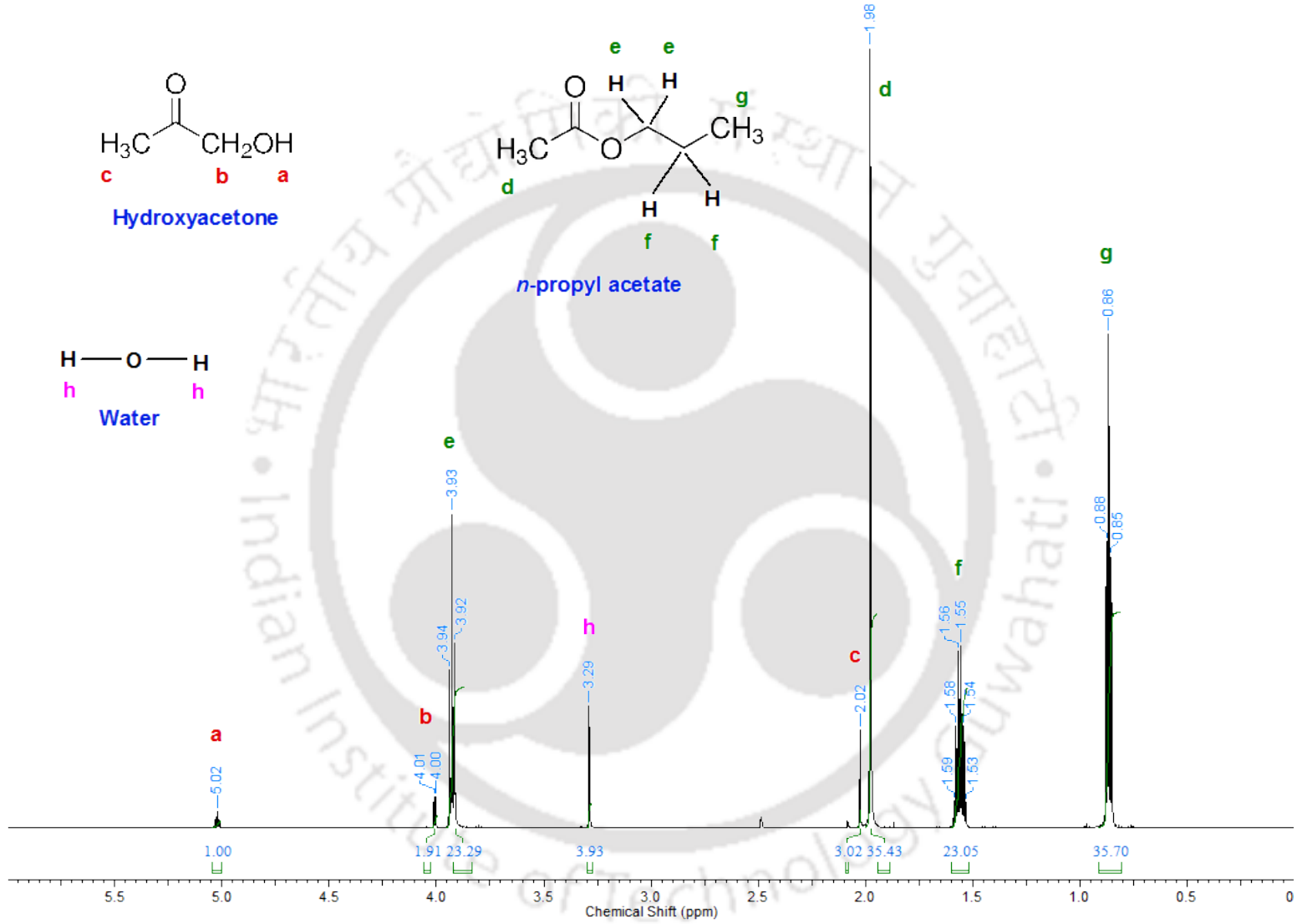

Figure B.11.: 1^{H} NMR spectrum of extract phase of *n*-propyl acetate-acetol-water system.

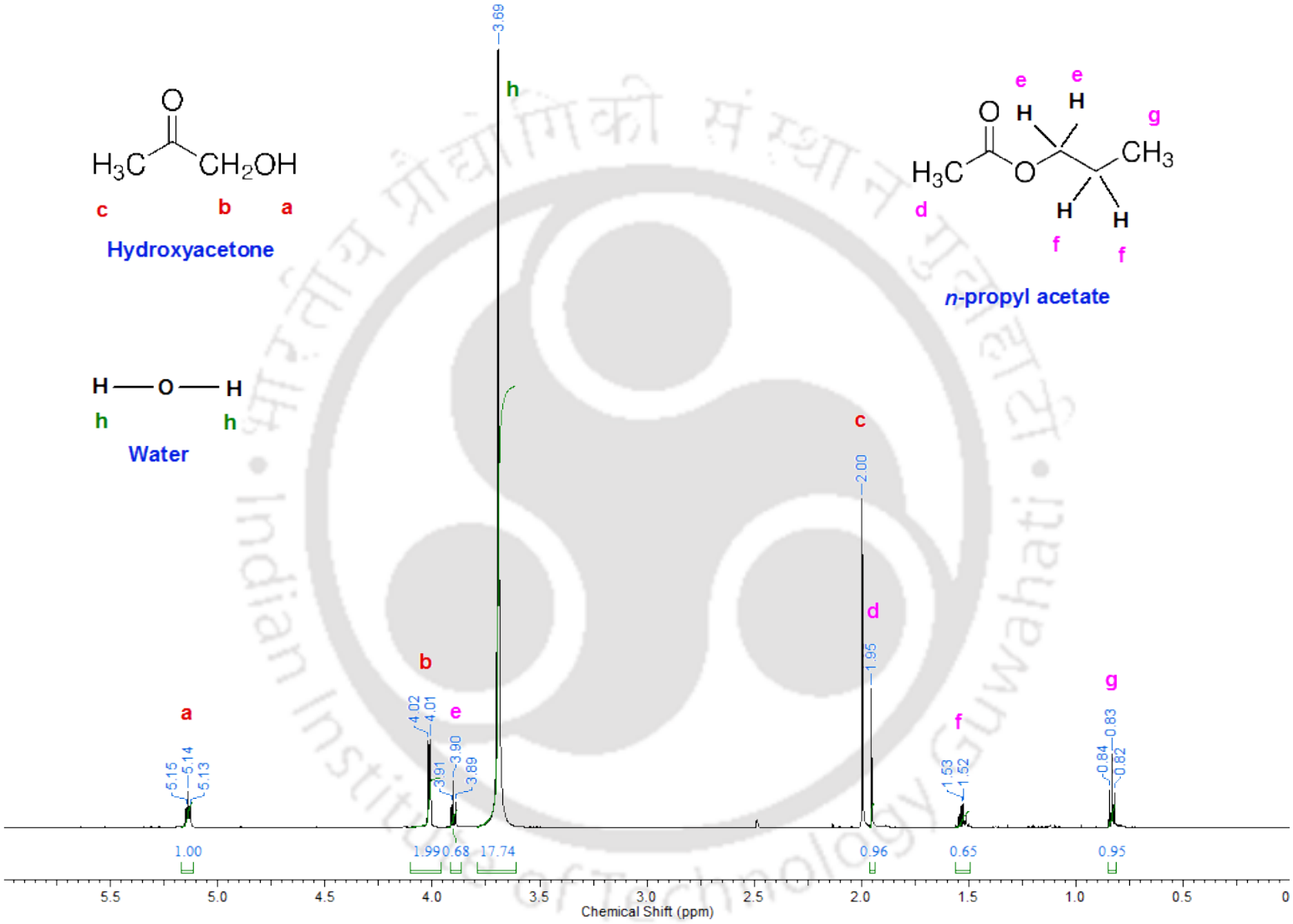

Figure B.12.: 1^{H} NMR spectrum of raffinate phase of *n*-propyl acetate-acetol-water system.

APPENDIX C

Matlab Code for estimation of binary interaction parameters from Cuckoo Search Algorithm:

```
% main.m
for i=1:30
    % THIS CODE WILL CALL THE MAIN FUNCTION "cuckoo_search_new".
    % 30 = NO. OF TRIALS.
    %-------------------------------------------------------------%
    %    6 = NO. OF VARIABLES.
    % -100 = LOWER BOUND
    %  100 = UPPER BOUND
    [bestnest,fmin]=cuckoo_search_new(6,-1000,1000);
    %-------------------------------------------------------------%
    % fmin (value of objective function) DATA WILL BE SAVED
    % IN functionvalue mat FILE.
    functionvalue(i)=fmin;
    %-------------------------------------------------------------%
    % bestnest (value of variables corresponding to fmin)
    % DATA WILL BE SAVED IN variablevalue mat FILE.
    variablevalue(i,:)=bestnest;
    %-------------------------------------------------------------%
    % THE WILL CALL "stubpp" FUNCTION AND CALCULATE FUNCTION
    % VALUE CORRESPONDING TO bestnest AND STORES RMSD VALUE
    % IN RMSD.TXT FILE OF EACH ITERATION.
    stubpp(bestnest);
    %-------------------------------------------------------------%
end

% cuckoo_search_new.m

function [bestnest,fmin]=cuckoo_search_new(nvar,Lb,Ub)
% Number of nests (or different solutions)
n=20;
% Discovery rate of alien eggs/solutions
pa=0.25;
N_IterTotal=1000;
% Lower bounds
Lb=Lb*ones(1,nvar);
% Upper bounds
Ub=Ub*ones(1,nvar);
% Random initial solutions
for i=1:n,
nest(i,:)=Lb+(Ub-Lb).*rand(size(Lb));
end
% Get the current best
fitness=10^10*ones(n,1);
[fmin,bestnest,nest,fitness]=get_best_nest(nest,nest,fitness);
% Starting iterations
for iter=1:N_IterTotal,
    % Generate new solutions (but keep the current best)
     new_nest=get_cuckoos(nest,bestnest,Lb,Ub);
     [fnew,best,nest,fitness]=get_best_nest(nest,new_nest,fitness);
```

```
    % Discovery and randomization
      new_nest=empty_nests(nest,Lb,Ub,pa);
    % Evaluate this set of solutions
      [fnew,best,nest,fitness]=get_best_nest(nest,new_nest,fitness);
    % Find the best objective so far
    if fnew<fmin,
       fmin=fnew;
       bestnest=best;
    end
fileID = fopen('functionvalue.txt','a');
fprintf(fileID,'%5d\t%12.8f\r\n',iter,fmin);
fclose(fileID);
stubp(bestnest);
end
end

% empty_nests.m

% Replace some nests by constructing new solutions/nests
function new_nest=empty_nests(nest,Lb,Ub,pa)
% A fraction of worse nests are discovered with a probability pa
n=size(nest,1);
% Discovered or not -- a status vector
K=rand(size(nest))>pa;
stepsize=rand*(nest(randperm(n),:)-nest(randperm(n),:));
new_nest=nest+stepsize.*K;
for j=1:size(new_nest,1)
    s=new_nest(j,:);
  new_nest(j,:)=simplebounds(s,Lb,Ub);
end
end

% get_best_nest.m

% Find the current best nest
function [fmin,best,nest,fitness]=get_best_nest(nest,newnest,fitness)
% Evaluating all new solutions
for j=1:size(nest,1),
    fnew=stub(newnest(j,:));
    if fnew<=fitness(j),
       fitness(j)=fnew;
       nest(j,:)=newnest(j,:);
    end
end
% Find the current best
[fmin,K]=min(fitness) ;
best=nest(K,:);
end

% get_cuckoos.m

% Get cuckoos by ramdom walk
```

```
function nest=get_cuckoos(nest,best,Lb,Ub)
% Levy flights
n=size(nest,1);
% Levy exponent and coefficient
% For details, see equation (2.21), Page 16 (chapter 2) of the book
% X. S. Yang, Nature-Inspired Metaheuristic Algorithms.
beta=3/2;
sigma=(gamma(1+beta)*sin(pi*beta/2)/(gamma((1+beta)/2)*
       beta*2^((beta-1)/2)))^(1/beta);
for j=1:n,
    s=nest(j,:);
    % This is a simple way of implementing Levy flights
    % For standard random walks, use step=1;
    % Levy flights by Mantegna's algorithm
    u=randn(size(s))*sigma;
    v=randn(size(s));
    step=u./abs(v).^(1/beta);
    % In the next equation, the difference factor (s-best) means that
    % when the solution is the best solution, it remains unchanged.
    stepsize=0.01*step.*(s-best);
    % Here the factor 0.01 comes from the fact that L/100 should the typical
    % step size of walks/flights where L is the typical lenghtscale;
    s=s+stepsize.*randn(size(s));
    % Apply simple bounds/limits
   nest(j,:)=simplebounds(s,Lb,Ub);
end
end
```

```
% lleflash.m

function [f, fstatus] = lleflash(r, q, para, zind, F)
% Single stage (i.e. flash) calculations for LLE
% modified Rachford-Rice formulation - Seader n Henley
% Convergence scheme - Regula falsi method
% zind is the index (the row from which the data needs to be picked
global comps E R
errmsg1 = 'ERROR: The given parameters predict no split !!!!';
eps=1e-4;   % tolerance
eps2 = 1e-3;
comps = 3;
fd=zeros(1,comps)+1;
fstatus = 0;
% data
% Initialization
x = E(zind,:);
y = R(zind,:);
zf = (x + y)/2;
x= x/sum(x);
y = y/sum(y);
zf = zf/sum(zf);
V = F/2;
iterout = 0;
```

```
while (1)
    iterout = iterout + 1;
    V1 = 0.0;
    V2 = F;
    V = V1;
    K = uniquac(r,q,para,x)./uniquac(r,q,para,y);
    for u = 1:1:comps
        if abs(K(u)) < 1e-5
            fstatus = 1;
            break;
        end
    end
    if fstatus == 1
        break;
    end
    f1 = sum(F.*zf.*(1-K)./(1+V.*(K-1)));
    % to compute f2
    V = F;
    f2 = sum(F.*zf.*(1-K)./(1+V.*(K-1)));
    if (f2 <0 & f1 <0) | (f1 > 0 & f2 > 0)
        disp(errmsg1);
        fstatus = 1;
        break;
    end
    iterin = 0;
    while (1)
        iterin = iterin + 1;
        V = (V1 + V2)/2;
        f = sum(F.*zf.*(1-K)./(1+V.*(K-1)));
        if abs(f) < eps
            break;
        elseif iterin > 100 | iterout > 100
            fstatus = 1;
            break;
        elseif f * f1 < 0
            V2 = V;
            f2 = f;
        else
            V1 = V;
            f1 = f;
        end
    end
    x=zf./(1+(V/F).*(K-1));
    y=K.*x;
    oldx = x;
    oldy = y;
    % normalize
    x = x/sum(x);
    y = y/sum(y);
    if norm(abs((oldx-x))) < eps2 & norm(abs((oldy - y))) < eps2
        [zf; x; E(zind,:); y; R(zind,:);  K; V 0 0];
```

```
        break;
    end
end
f = [x; y];% return the estimated tieline
end

%simplebounds.m

% Application of simple constraints
function s=simplebounds(s,Lb,Ub)
% Apply the lower bound
ns_tmp=s;
I=ns_tmp<Lb;
ns_tmp(I)=Lb(I);
% Apply the upper bounds
J=ns_tmp>Ub;
ns_tmp(J)=Ub(J);
% Update this new move
s=ns_tmp;
end

%stub.m

function [val]= stub(x)
global comps E R ;
global f ;
eps=1e-8;
T = 298.15;  % Kelvin
% Exp tieline data - NORMALIZED
% Paste the tielines here. That's all.
% RAFFINATE DATA:
% SOLVENT + MINOR SOLUTE + MAJOR SOLUTE
r=[13.187 2.8569 5.292];
q=[8.357 2.14 4.152];
R= [0.000       0.000    1.000
0.004    0.094    0.902
0.004    0.226    0.770
0.004    0.370    0.626
0.003    0.510    0.487
0.000    0.651    0.349
0.000    0.771    0.229
0.000    0.846    0.154
0.000    0.954    0.046
0.000    1.000    0.000
];
% EXTRACT DATA:
% SOLVENT + MINOR SOLUTE + MAJOR SOLUTE
E = [0.862       0.000    0.138
0.710    0.152    0.138
0.558    0.306    0.136
0.445    0.422    0.133
0.362    0.508    0.130
```

```
0.312    0.563    0.125
0.260    0.627    0.113
0.224    0.679    0.097
0.122    0.836    0.042
0.100    0.900    0.000
];
% THIS para matrix SHOULD BE CONSISTENT in size WITH THE E & R MATRICES
para = [0.0 x(1) x(2); x(3) 0.0 x(4); x(5) x(6) 0.0];%(ternery system)
[m,n] = size(E);
F = 1;
f = [];
error = [];
for X = 1:1:m % take all tielines
    [fres, fstatus] = lleflash(r,q,para, X, F);
    if fstatus == 1
        error = zeros(m,2*n)+1;
        break;
    end
    f = [f ; fres(1,:) fres(2,:)];
    error = [error; E(X,:)-fres(1,:)  R(X,:)-fres(2,:)];
end
val = sum(sum(error.^2));
rmsd = sqrt(val/(2*m*n));
return;
```

```
% stubp.m

function [val]= stubp(x)
global comps E R ;
global f ;
eps=1e-8;
T = 25+273.15;  % Kelvin
% Exp tieline data - NORMALIZED
% Paste the tielines here. That's all.
% RAFFINATE DATA:
% SOLVENT + MINOR SOLUTE + MAJOR SOLUTE
r=[13.187 2.8569 5.292];
q=[8.357 2.14 4.152];
R= [0.000        0.000    1.000
0.004    0.094    0.902
0.004    0.226    0.770
0.004    0.370    0.626
0.003    0.510    0.487
0.000    0.651    0.349
0.000    0.771    0.229
0.000    0.846    0.154
0.000    0.954    0.046
0.000    1.000    0.000
];
% EXTRACT DATA:
% SOLVENT + MINOR SOLUTE + MAJOR SOLUTE
E = [0.862       0.000    0.138
```

```
0.710    0.152    0.138
0.558    0.306    0.136
0.445    0.422    0.133
0.362    0.508    0.130
0.312    0.563    0.125
0.260    0.627    0.113
0.224    0.679    0.097
0.122    0.836    0.042
0.100    0.900    0.000
];
% THIS para matrix SHOULD BE CONSISTENT in size WITH THE E & R MATRICES
para = [0.0 x(1) x(2); x(3) 0.0 x(4); x(5) x(6) 0.0];%(ternary system)
[m,n] = size(E);
F = 1;
f = [];
error = [];
for X = 1:1:m % take all tielines
    [fres, fstatus] = lleflash(r,q,para, X, F);
    if fstatus == 1
        error = zeros(m,2*n)+1;
        break;
    end
    f = [f ; fres(1,:) fres(2,:)];
    error = [error; E(X,:)-fres(1,:)  R(X,:)-fres(2,:)];
end
val = sum(sum(error.^2));
rmsd = sqrt(val/(2*m*n));
disp(f);
disp(error);
disp([val rmsd]);
return;
```

```
% stubpp.m

function [val]= stubpp(x)
global comps E R ;
global f ;
eps=1e-8;
T = 25+273.15;  % Kelvin
% Exp tieline data - NORMALIZED
% Paste the tielines here. That's all.
% RAFFINATE DATA:
% SOLVENT + MINOR SOLUTE + MAJOR SOLUTE
r=[13.187 2.8569 5.292];
q=[8.357 2.14 4.152];
R= [0.000        0.000    1.000
0.004    0.094    0.902
0.004    0.226    0.770
0.004    0.370    0.626
0.003    0.510    0.487
0.000    0.651    0.349
0.000    0.771    0.229
```

```
0.000    0.846    0.154
0.000    0.954    0.046
0.000    1.000    0.000
];
% EXTRACT DATA:
% SOLVENT + MINOR SOLUTE + MAJOR SOLUTE
E = [0.862       0.000    0.138
0.710    0.152    0.138
0.558    0.306    0.136
0.445    0.422    0.133
0.362    0.508    0.130
0.312    0.563    0.125
0.260    0.627    0.113
0.224    0.679    0.097
0.122    0.836    0.042
0.100    0.900    0.000
];
% THIS para matrix SHOULD BE CONSISTENT in size WITH THE E & R MATRICES
para = [0.0 x(1) x(2); x(3) 0.0 x(4); x(5) x(6) 0.0]; %(ternery system)
[m,n] = size(E);
F = 1;
f = [];
error = [];
for X = 1:1:m % take all tielines
    [fres, fstatus] = lleflash(r,q,para, X, F);
    if fstatus == 1
        error = zeros(m,2*n)+1;
        break;
    end
    f = [f ; fres(1,:) fres(2,:)];
    error = [error; E(X,:)-fres(1,:)  R(X,:)-fres(2,:)];
end
val = sum(sum(error.^2));
rmsd = sqrt(val/(2*m*n));
fileID1 = fopen('rmsd.txt','a');
fprintf(fileID1,' %12.8f\r\n',rmsd);
fclose(fileID1);
disp(f);
disp(error);
disp([val rmsd]);
return;
```

```
% uniquac.m

function gamma = uniquac(r, q, para, x)
% returns gamma (activity coefficient)
global comps E R
T = 298.15;
z = 10;
sigxr=0;
sigxq=0;
sigxl=0;
```

```
l=zeros(1,comps);
phi=zeros(1,comps);
theta=zeros(1,comps);
ell=zeros(1,comps);
tau=zeros(comps);
sigthtau=zeros(1,comps);
sigter=zeros(1,comps);
lngammac=zeros(1,comps);
lngammar=zeros(1,comps);
for i=1:1:comps
    sigxr=sigxr+x(i)*r(i);
    sigxq=sigxq+x(i)*q(i);
end
for i=1:1:comps
    phi(i)=x(i)*r(i)/sigxr;
    theta(i)=x(i)*q(i)/sigxq;
    ell(i)=(z/2)*(r(i)-q(i))-(r(i)-1);
end
for i=1:1:comps
    for j=1:1:comps
%         tau(i,j)=exp(-para(i,j)/(8.314*T));
        tau(i,j)=exp(-para(i,j)/(T));
% tau(i,j)=exp(-para(i,j));
    end
end
for i=1:1:comps
    sigxl=sigxl+x(i)*ell(i);
end
for i=1:1:comps
    for j=1:1:comps
        sigthtau(i)=sigthtau(i)+theta(j)*tau(j,i);
    end
end
for i=1:1:comps
    for j=1:1:comps
        sigter(i)=sigter(i)+theta(j)*tau(i,j)/sigthtau(j);
    end
end
for i=1:1:comps
    lngammac(i)=log(r(i)/sigxr) + (z/2)*q(i)*log(q(i)*sigxr/(r(i)*sigxq))
                + ell(i) - (r(i)/sigxr)*sigxl;
    lngammar(i)=q(i)*(1-log(sigthtau(i))-sigter(i));
end
lngamma = lngammac + lngammar;
for i=1:1:comps
    gamma(i)=exp(lngamma(i));
end
```

APPENDIX D

Hard-chain contribution

Hard-chain contribution to compressibility factor is given by

$$Z^{hc} = \bar{m}Z^{hs} - \sum_i x_i(m_i - 1)(g_{ii}^{hs})^{-1}\rho\frac{\partial g_{ii}^{hs}}{\partial\rho} \tag{D.1}$$

where:

x_i is the mole fraction of chains of component *i*

m_i is the number of segments in a chain of component *i*

ρ is the total number density of molecules.

The mean segment number in the mixture is defined as:

$$\bar{m} = \sum_i x_i m_i \tag{D.2}$$

Z^{hs} is the contribution of the hard-sphere fluid given by

$$Z^{hs} = \frac{\xi_3}{1-\xi_3} + \frac{3\xi_1\xi_2}{\xi_0(1-\xi_3)^2} + \frac{3{\xi_2}^3 - \xi_3{\xi_2}^3}{\xi_0(1-\xi_3)^3} \tag{D.3}$$

The radial pair distribution function for the hard-sphere fluid is given by:

$$g_{ij}^{hs}(d_{ij}) = \frac{1}{(1-\xi_3)} + \left(\frac{d_i d_j}{d_i + d_j}\right)\frac{3\xi_2}{(1-\xi_3)^2} + \left(\frac{d_i d_j}{d_i + d_j}\right)^2\frac{2\xi_2^2}{(1-\xi_3)^3} \tag{D.4}$$

and ξ_n is defined as:

$$\xi_n = \frac{\pi}{6}\rho\sum_i x_i m_i d_i^n \qquad\qquad n = \{0,1,2,3\} \tag{D.5}$$

The temperature-dependent segment diameter is obtained as:

$$d_i(T) = \sigma_i\left[1 - 0.12\exp\left(\frac{-3\varepsilon_i}{kT}\right)\right] \tag{D.6}$$

where σ_i is the temperature-independent segment diameter and ϵ_i/k is the depth of the pair-potential.

$$\rho\frac{\partial g_{ij}^{hs}}{\partial\rho}=\frac{\xi_3}{\left(1-\xi_3\right)^2}+\left(\frac{d_id_j}{d_i+d_j}\right)\left(\frac{3\xi_2}{\left(1-\xi_3\right)^2}+\frac{6\xi_2\xi_3}{\left(1-\xi_3\right)^3}\right)+\left(\frac{d_id_j}{d_i+d_j}\right)^2\left(\frac{4\xi_2^2}{\left(1-\xi_3\right)^3}+\frac{6\xi_2^2\xi_3}{\left(1-\xi_3\right)^4}\right) \tag{D.7}$$

Dispersion contribution

The dispersion contribution to compressibility factor is given by

$$Z^{disp}=-2\pi\rho\frac{\partial(\eta I_1)}{\partial\eta}\overline{m^2\varepsilon\sigma^3}-\pi\rho\bar{m}\left[C_1\frac{\partial(\eta I_2)}{\partial\eta}+C_2\eta I_2\right]\overline{m^2\varepsilon^2\sigma^3} \tag{D.8}$$

where

$$\frac{\partial(\eta I_1)}{\partial\eta}=\sum_{i=0}^{6}a_i(\bar{m})(i+1)\eta^i \tag{D.9}$$

$$\frac{\partial(\eta I_2)}{\partial\eta}=\sum_{i=0}^{6}b_i(\bar{m})(i+1)\eta^i \tag{D.10}$$

$$C_1=\left[1+\bar{m}\left(\frac{8\eta-2\eta^2}{\left(1-\eta\right)^4}\right)+(1-\bar{m})\left(\frac{20\eta-27\eta^2+12\eta^3-2\eta^4}{\left[(1-\eta)(2-\eta)\right]^2}\right)\right]^{-1} \tag{D.11}$$

$$C_2=-C_1^2\left[\bar{m}\left(\frac{-4\eta^2+20\eta+8}{\left(1-\eta\right)^5}\right)+(1-\bar{m})\left(\frac{2\eta^3+12\eta^2-48\eta+40}{\left[(1-\eta)(2-\eta)\right]^3}\right)\right] \tag{D.12}$$

$$\overline{m^2\varepsilon\sigma^3}=\sum_i\sum_j x_ix_jm_im_j\left(\frac{\varepsilon_{ij}}{kT}\right)\sigma_{ij}^3 \tag{D.13}$$

$$\overline{m^2\varepsilon^2\sigma^3}=\sum_i\sum_j x_ix_jm_im_j\left(\frac{\varepsilon_{ij}}{kT}\right)^2\sigma_{ij}^3 \tag{D.14}$$

The power series I_1 and I_2 depend only on density and segment number according to:

$$I_1(\eta, \bar{m}) = \sum_{i=0}^{6} a_i(\bar{m})\eta^i \tag{D.15}$$

$$I_2(\eta, \bar{m}) = \sum_{i=0}^{6} b_i(\bar{m})\eta^i \tag{D.16}$$

where the coefficients a_i(m) and b_i(m) are functions of the segment number according to:

$$a_i(\bar{m}) = a_{oi} + \frac{\bar{m}-1}{\bar{m}}a_{1i} + \frac{\bar{m}-1}{\bar{m}}\frac{\bar{m}-2}{\bar{m}}a_{2i} \tag{D.17}$$

$$b_i(\bar{m}) = b_{oi} + \frac{\bar{m}-1}{\bar{m}}b_{1i} + \frac{\bar{m}-1}{\bar{m}}\frac{\bar{m}-2}{\bar{m}}b_{2i} \tag{D.18}$$

a_{oi},a_{1i},a_{2i},b_{oi},b_{1i} and b_{2i} are universal model constants.

Conventional combining rules are employed to determine the parameters for a pair of unlike segments:

$$\sigma_{ij} = \frac{(\sigma_i + \sigma_j)}{2} \tag{D.19}$$

$$\varepsilon_{ij} = \sqrt{\varepsilon_i \varepsilon_j}(1 - k_{ij}) \tag{D.20}$$

Association contribution

The association contribution to compressibility factor is given by

$$Z^{assoc} = \sum_i x_i \rho \sum_A \left[\frac{1}{X^{Ai}} - \frac{1}{2}\right]\frac{\partial X^{A_i}}{\partial \rho} \tag{D.21}$$

where X^{Ai} is the fraction of molecules *i* that are not bonded at the association site A, which is written as

$$X^{A_i} = \left(1 + \rho \sum_j x_j \sum_{B_j}^{nsites} X^{Bj}\Delta^{A_i B_j}\right)^{-1} \tag{D.22}$$

with

$$\Delta^{A_i B_j} = g_{ij}^{hs}(d_{ij}).\kappa^{A_i B_j}.d_{ij}^3\left[exp\left[\frac{\varepsilon^{A_i B_j}}{kT}\right] - 1\right] \tag{D.23}$$

where $\Delta^{A_i B_j}$ is the association strength between two sites A and B belonging to two different molecules *i* and *j*.

Fugacity Coefficient

The fugacity coefficient is related to the residual chemical potential according to

$$\ln \phi_k = \frac{\mu_k^{res}(T,V)}{kT} - \ln Z \tag{D.24}$$

The chemical potential can be obtained from

$$\frac{\mu_k^{res}(T,V)}{kT} = \tilde{a}^{res} + (Z-1) + \left(\frac{\partial \tilde{a}^{res}}{\partial x_k}\right)_{T,V,x_{i\neq k}} - \sum_{j=1}^{N}\left[x_j\left(\frac{\partial \tilde{a}^{res}}{\partial x_j}\right)_{T,V,x_{i\neq j}}\right] \tag{D.25}$$

with

$$\xi_{n,xk} = \frac{\partial \xi_n}{\partial x_k} = \frac{\pi}{6}\rho m_k (d_k)^n \qquad n \in \{0,1,2,3\} \tag{D.26}$$

Hard-chain contribution

$$\left(\frac{\partial \tilde{a}^{hc}}{\partial x_k}\right) = m_k \tilde{a}^{hs} + \bar{m}\left(\frac{\partial \tilde{a}^{hs}}{\partial x_k}\right)_{T,\rho,x_{j\neq k}} - \sum_i x_i (m_i - 1)(g_{ii}^{hs})^{-1}\left(\frac{\partial g_{ii}^{hs}}{\partial x_k}\right)_{T,\rho,x_{j\neq k}} \tag{D.27}$$

$$\left(\frac{\partial \tilde{a}^{hs}}{\partial x_k}\right) = -\frac{\xi_{o,x_k}}{\xi_o}\tilde{a}^{hs} + \frac{1}{\xi_0}\left[\begin{array}{l} \frac{3(\xi_{1,x_k}\xi_2 + \xi_1\xi_{2,x_k})}{(1-\xi_3)} + \frac{3\xi_1\xi_2\xi_{3,x_k}}{(1-\xi_3)^2} + \frac{3\xi_2^2\xi_{2,x_k}}{\xi_3(1-\xi_3)^2} + \\ \frac{\xi_2^3\xi_{3,x_k}(3\xi_3-1)}{\xi_3^2(1-\xi_3)^3} + \\ \left(\frac{3\xi_2^2\xi_{2,x_k}\xi_3 - 2\xi_2^3\xi_{3,x_k}}{\xi_3^3} - \xi_{0,x_k}\right)\ln(1-\xi_3) \\ + \left(\xi_0 - \frac{\xi_2^3}{\xi_3^2}\right) d\frac{\xi_{3,x_k}}{(1-\xi_3)} \end{array}\right] \tag{D.28}$$

$$\frac{\partial g_{ij}^{hs}}{\partial x_k} = \frac{\xi_{3,x_k}}{(1-\xi_3)^2} + \left(\frac{d_i d_j}{d_i + d_j}\right)\left(\frac{3\xi_{2,x_k}}{(1-\xi_3)^2} + \frac{6\xi_2\xi_{3,x_k}}{(1-\xi_3)^3}\right) + \left(\frac{d_i d_j}{d_i + d_j}\right)^2\left(\frac{4\xi_2\xi_{2,x_k}}{(1-\xi_3)^3} + \frac{6\xi_2^2\xi_{3,x_k}}{(1-\xi_3)^4}\right) \tag{D.29}$$

Dispersion contribution

$$\frac{\partial \tilde{a}^{disp}}{\partial x_k} = -2\pi\rho\left[I_{1,x_k}\overline{m^2\varepsilon\sigma^3} + I_1\left(\overline{m^2\varepsilon\sigma^3}\right)_{x_k}\right] - \pi\rho\left\{\left[m_k C_1 I_2 + \bar{m}C_{1,x_k}I_2 + \bar{m}C_1 I_{2,x_k}\right]m^2\varepsilon^2\sigma^3\right\} - \pi\rho\bar{m}C_1 I_2(\overline{m^2\varepsilon^2\sigma^3})_{x_k} \tag{D.30}$$

with

$$\left(\overline{m^2\varepsilon\sigma^3}\right)_{x_k} = 2m_k\sum_j x_j m_j\left(\frac{\varepsilon_{kj}}{kT}\right)\sigma_{kj}^3 \tag{D.31}$$

$$\left(\overline{m^2\varepsilon^2\sigma^3}\right)_{x_k} = 2m_k\sum_j x_j m_j\left(\frac{\varepsilon_{kj}}{kT}\right)^2\sigma_{kj}^3 \tag{D.32}$$

$$C_{1,xk} = C_2\xi_{3,xk} - C_1^2\left[m_k\left(\frac{8\eta - 2\eta^2}{(1-\eta)^4}\right)\right] + C_1^2 m_k\left(\frac{20\eta - 27\eta^2 + 12\eta^3 - 2\eta^4}{[(1-\eta)(2-\eta)]^2}\right) \tag{D.33}$$

$$I_{1,xk} = \sum_{i=0}^{6}\left[a_i(\bar{m})i\xi_{3,xk}\eta^{i-1} + a_{i,xk}\eta^i\right] \tag{D.34}$$

$$I_{2,xk} = \sum_{i=0}^{6}\left[b_i(\bar{m})i\xi_{3,xk}\eta^{i-1} + b_{i,xk}\eta^i\right] \tag{D.35}$$

$$a_{i,xk} = \frac{m_k}{\bar{m}^2} a_{1i} + \frac{m_k}{\bar{m}^2}\left(3 - \frac{4}{\bar{m}}\right) a_{2i} \tag{D.36}$$

$$b_{i,xk} = \frac{m_k}{\bar{m}^2} b_{1i} + \frac{m_k}{\bar{m}^2}\left(3 - \frac{4}{\bar{m}}\right) b_{2i} \tag{D.37}$$

Matlab Code for estimation of PC-SAFT parameters of pure components:

```
% rn.m
for i=1:100
    main
    e1=x(1);
    e2=x(2);
    e3=x(3);
    e4=x(4);
    e5=x(5);
    aad=AAD;
   aadvap=AADVP;
filename='IL1.xlsx';
fileExist = exist(filename,'file');
if fileExist==0
 header = {'i', 'e1 ','e2','e3','e4','e5','aad','aadvp'};
xlswrite(filename,header);
else
% Read in your xls file to a cell array (input)
[~,~,input] = xlsread(filename);
% This is a cell array of the new line you want to add
new_data = {i,e1,e2,e3,e4,e5,aad,aadvap};
 % Concatinate your new data to the bottom of input
output = cat(1,input,new_data);
xlswrite(filename,output); % Write to the new excel file.
end
end


% main.m
clear
```

```
clc

% Number of variables.
   nvars = 5;
% Lower bound
   LB = [1.00   1.00   200   .00500   1000];
% Upper bound
   UB = [15   7.00   450   .10   4500];
options = gaoptimset('Generations',500,'Populationsize',100,
          'StallGenLimit',100,'TolFun',1e-6,'Display','iter');
[x,fval] = ga(@myfun,nvars,[],[],[],[],LB,UB,[],options);
disp(x);
fprintf('\n\n')


% myfun.m
function f2=myfun(E)
M=2;  % No. of association site.
%       Specify System pressure and density.
%       Temp(K)      Pressure(Pa)    Density(kg/m3)
TPV=[278.15      100000   910.8
283.15   100000   907.8
288.15   100000   904.9
293.15   100000   901.9
298.15   100000   899
303.15   100000   896.1
308.15   100000   893.3
313.15   100000   890.4
318.15   100000   887.6
323.15   100000   884.8
328.15   100000   882
333.15   100000   879.2
338.15   100000   876.4
343.15   100000   873.7
348.15   100000   870.9
353.15   100000   868.1
358.15   100000   865.3
363.15   100000   862.6
];
mw=549.9;            %molecular weight of pure substance
[R,C]=size(TPV);  % R = No. of rows; C = No. of columns in TPV matrix.
for i=1:R
```

```
 D(i)=TPV(i,3);                  %density, in kg/m^3
 MD(i)=(D(i)*10^(3))/mw;     %Molar density, in mol/m^3
end
% saving temp, press and molar density in different variables.
for i=1:R
   t(i) =TPV(i,1);          % Tempertaure, in kelvin.
   P1(i)=TPV(i,2);          % Pressure, in pa.
   YL(i)=MD(i);            % Molar density of liquid, in mol/m^3.
 end
% Parameters to be evaluated.
 m=E(1);
 sigma=E(2)*10^-10;                % m
 ebyk=E(3);                        % K
 kab=E(4);                        % K
 epln=E(5);
for i=1:R
   rowL(i)=6.022*10^23*YL(i); % Liquid density, in molecule/m^3.
   d(i)=sigma*(1-0.12*(exp(-(3*ebyk)/t(i))));  % diameter, in m.
 etaLexp(i)=(pi/6)*rowL(i)*m*d(i)^3; % eta based on experimental data.
end
for i=1:R
   etaL(i)=0.5;
   for k=1:1000
   etaL1(i)=etaL(i)-etaL(i)*10^-5;
   rowLc(i)=(6/pi)*etaL(i)*(m*d(i)^3)^-1;
   ZHCLc(i)=feval(@hardchain,rowLc(i),t(i),m,sigma,ebyk);
   ZDISPLc(i)=feval(@dispersion,rowLc(i),t(i),m,sigma,ebyk);
   ZASLc(i)=feval(@assoc,rowLc(i),t(i),m,sigma,ebyk,kab,epln,M);
   ZLc(i)=1+ZHCLc(i)+ZDISPLc(i)+ZASLc(i);
   YLc(i)=rowLc(i)/(6.022*10^23);
   PLc(i)=(ZLc(i)*(8.314*t(i)*YLc(i)));          % Pressure calculation.
   rowLc1(i)=(6/pi)*etaL1(i)*(m*d(i)^3)^-1;
   ZHCLc1(i)=feval(@hardchain,rowLc1(i),t(i),m,sigma,ebyk);
   ZDISPLc1(i)=feval(@dispersion,rowLc1(i),t(i),m,sigma,ebyk);
   ZASLc1(i)=feval(@assoc,rowLc1(i),t(i),m,sigma,ebyk,kab,epln,M);
   ZLc1(i)=1+ZHCLc1(i)+ZDISPLc1(i)+ZASLc1(i);
   YLc1(i)=rowLc1(i)/(6.022*10^23);
   PLc1(i)=(ZLc1(i)*(8.314*t(i)*YLc1(i)));        % Pressure calculation.
   PLdiff(i)=P1(i)-PLc(i);
   PLdiff1(i)=P1(i)-PLc1(i);
   dpdx(i)=(PLdiff1(i)-PLdiff(i))/(etaL1(i)-etaL(i));
```

```
   etaL(i)=etaL(i)-(PLdiff(i)/dpdx(i));
   if abs((P1(i)-PLc(i))/P1(i))*100<=0.01 && etaL(i)>0 && PLc(i)>0
    etafinal(i)=etaL(i);
    etaLexp(i);
    rowLcf(i)=(6/pi)*etafinal(i)*(m*d(i)^3)^-1;
    YLc(i)=rowLcf(i)/(6.022*10^23);
    break,
   end
  end
  end
%converting molar density into density
  for i=1:R
    Dc(i)=(YLc(i)*mw)/10^(3);
  end
 format long e;
 Ddif(1,:)=YLc./YL;
 x(1,:)=ones(1,R);
 Y1(1,:)=Ddif(1,:);
 y1=(x(1,:)-Y1(1,:));
 Y=Y1;
 %Objective function.
  err=x-Y;
  err1=err.^2;
  err2=sum(err1);
  err3=sum(err2');
  f2=err3;
 %AAD calculation.
  err4=sum(sum(abs(err)));
  AAD=err4*100/R;
 %AAD for vap pr
  Pdif(1,:)=PLc./P1;
  perr=x-Pdif;
  perr1=sum(abs(perr));
  aadvp=perr1*100/R;
 %AAD for density
  ddif(1,:)=Dc./D;
   derr=x-ddif;
  derr1=sum(abs(derr));
  aadd=derr1*100/R;
 % These commands transfer the mentioned variables in to main programme.
  assignin('base','AAD',AAD);
```

```
assignin('base','AADVP',aadvp);
 assignin('base','AADd',aadd);
 assignin('base','P_pred',PLc');
 assignin('base','Rho_pre',Dc');
 subplot(2,1,1)
 plot(t,PLc,'r',t,P1,'*');
 subplot(2,1,2)
 plot(t,D,'*',t,Dc,'r');


% hardchain.m

function ZHC=hardchain(row,t,m,sigma,ebyk)
d=sigma*[1-0.12*(exp(-(3*ebyk)/t))];
eta=((pi/6)*row*m*d^3);
ZHC=(m*(4*eta-2*eta^2)/(1-eta)^3)-((m-1)*(5*eta-2*eta^2))/((1-eta)*(2-eta));


% dispersion.m

function ZDISP=dispersion(row,t,m,sigma,ebyk)
d=sigma*[1-0.12*(exp(-(3*ebyk)/t))];
eta=((pi/6)*row*m*d^3);
Acoeff=[0.9105631445 -0.3084016918 -0.0906148351;
0.6361281449 0.1860531159 0.4527842806;
2.6861347891 -2.5030047259 0.5962700728;
 -26.5473624910 21.4197936290 -1.7241829131;
97.759208784 -65.255885330 -4.130211253;
 -159.59154087 83.318680481 13.77663187;
91.297774084 -33.746922930 -8.672847037];
Bcoeff=[0.7240946941 -0.5755498075 0.0976883116;
2.2382791861 0.6995095521 -0.2557574982;
-4.002584949485 3.8925673390 -9.1558561530;
-21.003576815 -17.215471648 20.642075974;
26.855641363 192.67226447 -38.804430052;
206.55133841 -161.82646165 93.626774077;
-355.60235612 -165.20769346 -29.666905585];
for i=1:7
    am(i)=Acoeff(i,1)+((m-1)/m)*Acoeff(i,2)+((m-1)*(m-2)/m^2)*Acoeff(i,3);
    bm(i)=Bcoeff(i,1)+((m-1)/m)*Bcoeff(i,2)+((m-1)*(m-2)/m^2)*Bcoeff(i,3);
end
for i=1:7
```

```
    I1(i)=am(i)*eta^(i-1);
    I2(i)=bm(i)*eta^(i-1);
end
I1=sum(I1);
I2=sum(I2);
% derivation wrt m %.............
for i=1:7
    delI1(i)=am(i)*i*eta^(i-1); %derivation of eta*I1 wrt eta == k1
    delI2(i)=bm(i)*i*eta^(i-1);  %derivation of eta*I2 wrt eta == k2
end
delI1=sum(delI1);
delI2=sum(delI2);
C1=(1+[m*(8*eta-2*eta^2)/(1-eta)^4]+((1-m)*(20*eta-27*eta^2+
   12*eta^3-2*eta^4)/[(1-eta)*(2-eta)]^2))^-1;
uC2s1=-4*eta^2+20*eta+8;
uC2s2=2*eta^3+12*eta^2-48*eta+40;
lC2s1=(1-eta)^5;
lC2s2=[(1-eta)*(2-eta)]^3;
C2=-(C1)^2*[m*uC2s1/lC2s1+(1-m)*uC2s2/lC2s2];
ZDISP=[-2*pi*row*delI1*(m^2*(ebyk/t)*sigma^3)
      -pi*row*m*(C1*delI2+C2*eta*I2)*(m^2*(ebyk/t)^2*sigma^3)];


% assoc.m
function ZAS=assoc(row,t,m,sigma,ebyk,kab,epln,M)
d=sigma*[1-0.12*(exp(-(3*ebyk)/t))];
eta=((pi/6)*row*m*d^3);
% Radial distribution function
g=(1-(eta/2))/(1-eta)^3;
del=g*(exp(epln/t)-1)*(kab*d^3);
Nav=6.023*10^23;
XA=zeros(1,M);
for i=1:M
   XA(i)=[-1+sqrt(1+4*row*del)]/(2*row*del);
end
delg=(1/row)*(eta/2)*(5-2*eta)/(1-eta)^4;
deldel=delg*(exp(epln/t)-1)*(kab*d^3);
Nav=6.023*10^23;
fordelXAU1=2*row*del*[(1/2)*((1+4*row*del)^-0.5)]*(4*del+4*row*deldel);
fordelXAU2=[-1+sqrt(1+4*row*del)]*[2*del+2*row*deldel];
fordelXAL=(2*row*del)^2;
%row=row/Nav;
```

```
delXA=(fordelXAU1-fordelXAU2)/fordelXAL;
%delXA=delXA*Nav;
ZAS1=0;
for i=1:M
ZAS1=ZAS1+row*[(1/XA(i))-(1/2)]*delXA;
end
ZAS=ZAS1;


% pred.m
M=2;  % No. of association site.
%       Specify System pressure and density.
%       Temp(K)     Pressure(Pa)    Density(g/cm3)
TPV=[
298.15   51720000          1.47169
303.14   51720000          1.46716
308.09   51720000          1.46274
313.15   51720000          1.45807
318.14   51720000          1.45364
323.14   51720000          1.44979
328.20   51720000          1.44511
];
mw=419.36;              %molecular weight of pure substance
  [R,C]=size(TPV);  % R = No. of rows; C = No. of columns in TPV matrix.
  for i=1:R
      D(i)=TPV(i,3);                %density, in kg/m^3
      MD(i)=(D(i)*10^(6))/mw;     %Molar density, in mol/m^3
  end
 % saving temp, press and molar density in different variables.
 for i=1:R
            t(i) =TPV(i,1);          % Tempertaure, in kelvin.
            P1(i)=TPV(i,2);          % Pressure, in pa.
            YL(i)=MD(i);            % Molar density of liquid, in mol/m^3.
 end
% Parameters to be evaluated.
    m=6.7516;
     sigma=3.9954*10^-10;                 % m
     ebyk=297.6781;                         % K
     epln=3450;                           % K
     kab=0.00225;
 for i=1:R
  rowL(i)=6.022*10^23*YL(i);  % Liquid density, in molecule/m^3.
```

```
  d(i)=sigma*(1-0.12*(exp(-(3*ebyk)/t(i))));  % diameter, in m.
  etaLexp(i)=(pi/6)*rowL(i)*m*d(i)^3; % eta based on experimental data.
end
for i=1:R
    etaL(i)=0.5;
    for k=1:1000
   etaL1(i)=etaL(i)-etaL(i)*10^-5;
   rowLc(i)=(6/pi)*etaL(i)*(m*d(i)^3)^-1;
   ZHCLc(i)=feval(@hardchain,rowLc(i),t(i),m,sigma,ebyk);
   ZDISPLc(i)=feval(@dispersion,rowLc(i),t(i),m,sigma,ebyk);
   ZASLc(i)=feval(@assoc,rowLc(i),t(i),m,sigma,ebyk,kab,epln,M);
   ZLc(i)=1+ZHCLc(i)+ZDISPLc(i)+ZASLc(i);
   YLc(i)=rowLc(i)/(6.022*10^23);
   PLc(i)=(ZLc(i)*(8.314*t(i)*YLc(i)));          % Pressure calculation.
   rowLc1(i)=(6/pi)*etaL1(i)*(m*d(i)^3)^-1;
   ZHCLc1(i)=feval(@hardchain,rowLc1(i),t(i),m,sigma,ebyk);
   ZDISPLc1(i)=feval(@dispersion,rowLc1(i),t(i),m,sigma,ebyk);
   ZASLc1(i)=feval(@assoc,rowLc1(i),t(i),m,sigma,ebyk,kab,epln,M);
   ZLc1(i)=1+ZHCLc1(i)+ZDISPLc1(i)+ZASLc1(i);
   YLc1(i)=rowLc1(i)/(6.022*10^23);
   PLc1(i)=(ZLc1(i)*(8.314*t(i)*YLc1(i)));       % Pressure calculation.
   PLdiff(i)=P1(i)-PLc(i);
   PLdiff1(i)=P1(i)-PLc1(i);
   dpdx(i)=(PLdiff1(i)-PLdiff(i))/(etaL1(i)-etaL(i));
   etaL(i)=etaL(i)-(PLdiff(i)/dpdx(i));
if abs((P1(i)-PLc(i))/P1(i))*100<=0.01 && etaL(i)>0 && PLc(i)>0
   etafinal(i)=etaL(i);
   etaLexp(i);
   rowLcf(i)=(6/pi)*etafinal(i)*(m*d(i)^3)^-1;
   YLc(i)=rowLcf(i)/(6.022*10^23);
   break,
  end
  end
  end
%converting molar density into density
  for i=1:R
   Dc(i)=(YLc(i)*mw)/10^(6);
 end
 format long e;
 Ddif(1,:)=YLc./YL;
    x(1,:)=ones(1,R);
```

```
Y1(1,:)=Ddif(1,:);
y1=(x(1,:)-Y1(1,:));
Y=Y1;
%Objective function.
err=x-Y;
err1=err.^2;
err2=sum(err1);
err3=sum(err2');
f2=err3;
%AAD calculation.
err4=sum(sum(abs(err)));
AAD=err4*100/R;
%AAD for vap pr
Pdif(1,:)=PLc./P1;
perr=x-Pdif;
perr1=sum(abs(perr));
aadvp=perr1*100/R;
%AAD for density
ddif(1,:)=Dc./D;
derr=x-ddif;
derr1=sum(abs(derr));
aadd=derr1*100/R;
% These commands transfer the mentioned variables in to main programme.
assignin('base','AAD',AAD);
assignin('base','AADVP',aadvp);
assignin('base','AADd',aadd);
assignin('base','P_pred',PLc');
assignin('base','Rho_pre',Dc');
subplot(2,1,1)
 plot(t,PLc,'r',t,P1,'*');
 subplot(2,1,2)
 plot(t,D,'*',t,Dc,'r');
```

APPENDIX E

Sample input file for running ternary LLE system ([BMIM] + [Tf_2N] + Water + Acetic Acid + Helium):

```
inputformat
'Towhee'
ensemble
'npt'
temperature
373.15
pressure
101.325
nmolty
5
nmolectyp
125 125 476 25 25
numboxes
3
stepstyle
'cycles'
nstep
40000
printfreq
1000
blocksize
1000
moviefreq
1000
backupfreq
1000
runoutput
'full'
pdb_output_freq
1000
loutdft
.false.
loutlammps
.true.
pressurefreq
20
trmaxdispfreq
10
volmaxdispfreq
10
potentialstyle
'internal'
ffnumber
4
ff_filename
/home/anand/Documents/anand/ternary/wateracidil/towhee_ff_zhong2011
/home/anand/Documents/anand/ternary/wateracidil/towhee_ff_TIP4P
/home/anand/Documents/anand/ternary/wateracidil/towhee_ff_TraPPE-ace
/home/anand/Documents/anand/ternary/wateracidil/towhee_ff_HE
```

classical_potential
'Lennard-Jones'
classical_mixrule
'Lorentz-Berthelot'
lshift
.false.
ltailc
.true.
rmin
1.0
rcut
10.0
rcutin
10.0
electrostatic_form
'coulomb'
coulombstyle
'ewald_fixed_kmax'
kalp
5.6
kmax
5
dielect
1
linit
.true.
initboxtype
'dimensions'
initstyle
'full cbmc' 'full cbmc' 'full cbmc' 'full cbmc' 'full cbmc'
'full cbmc' 'full cbmc' 'full cbmc' 'full cbmc' 'full cbmc'
'full cbmc' 'full cbmc' 'full cbmc' 'full cbmc' 'full cbmc'
initlattice
'simple cubic' 'simple cubic' 'simple cubic' 'simple cubic' 'simple cubic'
'simple cubic' 'simple cubic' 'simple cubic' 'simple cubic' 'simple cubic'
'simple cubic' 'simple cubic' 'simple cubic' 'simple cubic' 'simple cubic'
initmol
125 125 238 0 0
0 0 0 0 25
0 0 238 25 0
inix iniy iniz
8 8 8
7 7 7
7 7 7
hmatrix
60.0 00.0 00.0
00.0 60.0 00.0
00.0 00.0 60.0
50.0 00.0 00.0
00.0 50.0 00.0
00.0 00.0 50.0

30.0 00.0 00.0
00.0 30.0 00.0
00.0 00.0 30.0
pmvol
0.03
pmvlpr
0.5 0.0 1.0
rmvol
0.1
tavol
0.5
pmcb
0.20
pmcbmt
0.0 0.5 0.0 1.0 0.0
pmall
0.0 0.0 0.0 0.0 0.0
pmpivot
0.30
pmpivmt
1.0 0.0 0.0 0.0 0.0
pmtracm
0.70
pmtcmt
0.20 0.40 0.60 0.80 1.00
rmtrac
0.5
tatrac
0.5
pmrotate
1.00
pmromt
0.25 0.50 0.75 1.00 0.00
rmrot
0.05
tarot
0.5
#bmim
input_style
'basic connectivity map'
nunit
13
nmaxcbmc
13
lpdbnames
F
forcefield
'towhee_ff_zhong2011'
charge_assignment
'manual'
unit ntype qqatom

1 'NA' 0.0150
vibration
3
2 5 7
improper torsion
0
unit ntype qqatom
2 'CR' 0.000
vibration
3
1 3 13
improper torsion
0
unit ntype qqatom
3 'NA' 0.0150
vibration
3
2 4 6
improper torsion
0
unit ntype qqatom
4 'CW' -0.1600
vibration
3
3 5 12
improper torsion
0
unit ntype qqatom
5 'CW' -0.1600
vibration
3
1 4 11
improper torsion
0
unit ntype qqatom
6 'CN3' 0.2600
vibration
1
3
improper torsion
0
unit ntype qqatom
7 'CN2' 0.2300
vibration
2
1 8
improper torsion
0
unit ntype qqatom
8 'CT2' 0.050
vibration

```
2
7 9
improper torsion
0
unit ntype qqatom
9 'CT2' 0.000
vibration
2
8 10
improper torsion
0
unit ntype qqatom
10 'CT3' 0.0000
vibration
1
9
improper torsion
0
unit ntype qqatom
11 'H4' 0.2
vibration
1
5
improper torsion
0
unit ntype qqatom
12 'H4' 0.2
vibration
1
4
improper torsion
0
unit ntype qqatom
13 'H5' 0.15
vibration
1
2
improper torsion
0
#TraPPE TF2N
input_style
'basic connectivity map'
nunit
9
nmaxcbmc
9
lpdbnames
F
forcefield
'towhee_ff_zhong2011'
charge_assignment
```

’manual’
unit ntype qqatom
1 ’CF3’ -0.095
vibration
1
2
improper torsion
0
unit ntype qqatom
2 ’S’ 0.627
vibration
4
1 3 4 5
improper torsion
0
unit ntype qqatom
3 ’O’ -0.398
vibration
1
2
improper torsion
0
unit ntype qqatom
4 ’O’ -0.398
vibration
1
2
improper torsion
0
unit ntype qqatom
5 ’N’ -0.272
vibration
2
2 6
improper torsion
0
unit ntype qqatom
6 ’S’ 0.627
vibration
4
5 7 8 9
improper torsion
0
unit ntype qqatom
7 ’O’ -0.398
vibration
1
6
improper torsion
0
unit ntype qqatom

8 'O' -0.398
vibration
1
6
improper torsion
0
unit ntype qqatom
9 'CF3' -0.095
vibration
1
6
improper torsion
0
water-TIP4P
input_style
'basic connectivity map'
nunit
4
nmaxcbmc
4
lpdbnames
F
forcefield
'TIP4P'
charge_assignment
'manual'
unit ntype qqatom
1 'HW' 0.52
vibration
1
2
improper torsion
0
unit ntype qqatom
2 'OW' 0.0
vibration
3
1 3 4
improper torsion
0
unit ntype qqatom
3 'M' -1.04
vibration
1
2
improper torsion
0
unit ntype qqatom
4 'HW' 0.52
vibration
1

```
2
improper torsion
0
# acetic acid
input_style
'basic connectivity map'
nunit
5
nmaxcbmc
5
lpdbnames
F
forcefield
'TraPPE-UA'
charge_assignment
'manual'
unit ntype qqatom
1 'CH31' 0.12
vibration
1
2
improper torsion
0
unit ntype qqatom
2 'C2' 0.42
vibration
3
1 3 4
improper torsion
0
unit ntype qqatom
3 'O3' -0.45
vibration
1
2
improper torsion
0
unit ntype qqatom
4 'O4' -0.46
vibration
2
2 5
improper torsion
0
unit ntype qqatom
5 'H6' 0.37
vibration
1
4
improper torsion
0
```

```
# Helium
input_style
'basic connectivity map'
nunit
1
nmaxcbmc
1
lpdbnames
F
forcefield
'TraPPE-UA'
charge_assignment
'manual'
unit ntype qqatom
1 'He' 0
vibration
0
improper torsion
0
```

Sample force field file for water [TIP4P]:

```
towhee_ff Version
15
Number of Nonbonded Types
3
Potential Type
Lennard-Jones
Classical Mixrule
LB or Geometric
Atom Type Number
1
Nonbond Coefficients
0.0000000000E+00
0.0000000000E+00
0.0000000000E+00
0.0000000000E+00
Mass
0.1007900000E+01
Element
H
Bond Pattern
s
Base Charge
0.0000000000E+00
Polarizability
0.1000000000E+01
Force Field Name
TIP4P
Atom Names
HW
```

HW
HW
HW
Atom Type Number
2
Nonbond Coefficients
0.3153577942E+01
0.7801954036E+02
0.0000000000E+00
0.0000000000E+00
Mass
0.1599900000E+02
Element
O
Bond Pattern
sp3
Base Charge
0.0000000000E+00
Polarizability
0.1000000000E+01
Force Field Name
TIP4P
Atom Names
OW
OW
OW
OW
Atom Type Number
3
Nonbond Coefficients
0.0000000000E+00
0.0000000000E+00
0.0000000000E+00
0.0000000000E+00
Mass
0.0000000000E+00
Element

Bond Pattern
s
Base Charge
0.0000000000E+00
Polarizability
0.1000000000E+01
Force Field Name
TIP4P
Atom Names
M
M
M
M

Number of Bonded Terms
2
Bond Type Number
1
Bond Style
1
Bond Coefficients
0.9572000000E+00
Vibration Order
wild
Force Field Name
TIP4P
Number of Atoms with Same Parameters
1
Atom Names
OW HW
Bond Type Number
2
Bond Style
1
Bond Coefficients
0.1500000000E+00
Vibration Order
wild
Force Field Name
TIP4P
Number of Atoms with Same Parameters
1
Atom Names
OW M
Number of Angle Terms
2
Angle Type Number
1
Angle Style
0
Angle Coefficients
0.1045200000E+03
0.1000000000E-04
Angle Order
wild
Force Field Name
TIP4P
Number of Atoms with Same Parameters
1
Atom Names
HW OW HW
Angle Type Number
2
Angle Style
0

Angle Coefficients
0.5226000000E+02
0.1000000000E-04
Angle Order
wild
Force Field Name
TIP4P
Number of Atoms with Same Parameters
1
Atom Names
M OW HW
Number of Torsion Terms
0
Number of Improper Terms
0
Number of Angle-Angle Terms
0
Number of One-Five Types
0
Number of Bond Increments
0

APPENDIX F

List of Publications

In Refereed Journals:

(1) **Anand Bharti**, Tamal Banerjee. Enhancement of bio-oil derived chemicals in aqueous phase using Ionic Liquids: Experimental and COSMO-SAC predictions using a modified hydrogen bonding expression. **Fluid Phase Equilibria 400 (2015), 27-37**.

(2) **Anand Bharti**, Tamal Banerjee. Solubility prediction of bio-oil derived chemicals in aqueous media by Localized Molecular Orbital-Energy Decomposition Analysis (LMO-EDA) and COSMO-RS predictions. **Computational and Theoretical Chemistry 1067 (2015), 48-59**.

(3) **Anand Bharti**, Prerna, Tamal Banerjee. Applicability of Cuckoo Search Algorithm for the Prediction of Multicomponent Liquid-Liquid Equilibria for Imidazolium and Phosphonium Based Ionic Liquids. **Ind. Eng. Chem. Res. 54 (2015), 12393-12407**.

(4) **Anand Bharti**, Tamal Banerjee. Reactive force field simulation studies on the combustion behavior of *n*-octanol. **Fuel Processing Technology 152 (2016), 132-139**.

(5) **Anand Bharti**, Rupesh Verma, Prerna, Sarvesh Namdeo, Abhigyan Malviya, Tamal Banerjee, Stanley I. Sandler. Liquid-Liquid Equilibria and PC-SAFT modeling of Organic solvents/Ionic Liquids – Hydroxyacetone – Water Mixtures. (Under review in Fluid Phase Equilibria).

(6) **Anand Bharti**, Abhigyan Malviya, Tamal Banerjee, A Monte Carlo simulation study of the liquid-liquid equilibria for ternary ethyl acetate/n-butyl acetate/ [BMIM] [Tf2N]-acetic acid-water mixtures. (Manuscript under preparation).

Books:

(1) **Anand Bharti**, Debashis Kundu, Dharamashi Rabari, Tamal Banerjee. Phase Equilibria in Ionic Liquid Facilitated Liquid–Liquid Extractions (2017). **CRC Press (ISBN 978-1-49876948-8)**.